Non-canonical roles of Oligoadenylate Synthetase 1 during viral and bacterial infections

by

Joseph Perez

Bachelor of Sciences, University of Puerto Rico at Cayey, 2015

Submitted to the Graduate Faculty of

School of Medicine in partial fulfillment

of the requirements for the degree of

Doctor of Philosophy

University of Pittsburgh

2020

UNIVERSITY OF PITTSBURGH

SCHOOL OF MEDICINE

This dissertation was presented

by

Joseph Perez

It was defended on

August 3, 2020

and approved by

Neal A. DeLuca, Ph.D.
Professor, Microbiology & Molecular Genetics

Jeffrey Brodsky, Ph.D.
Professor, Biological Sciences

Greg M. Delgoffe, PhD
Associate Professor, Immunology

John V. Williams, M.D.
Member
Molecular Virology & Microbiology

Dissertation Director:
Saumendra N. Sarkar, Ph.D.
Associate Professor, Molecular Virology & Microbiology

Non-canonical roles of Oligoadenylate Synthetase 1 during viral and bacterial infections

Joseph Perez, PhD

University of Pittsburgh, 2020

Interferons inhibit growth of several intracellular pathogens, including virus and bacteria, through the expression of interferon stimulated genes (ISGs). We have found that a specific isoform of one such ISG, Oligoadenylate Synthetase 1 (OAS1) enhances translation of a select set of mRNAs, thereby increases the steady state and induced levels of specific proteins with antiviral and antibacterial properties. This OAS1 isoform (OAS1 P46) in humans is generated due to an alternative splice acceptor site at the C-terminus of OAS1 gene. The SNP rs10774671 at this site has been associated with disease severity to West Nile Virus (WNV) and *Mycobacterium tuberculosis*. We show that human OAS1-KO cells have lower basal levels of cGAS protein and can be rescued by OAS1 P46 expression, independent of its enzyme activity. Inducible expression of OAS1 P46 in cGAS-KO cells does not suppress WNV replication, suggesting that the antiviral activity of OAS1 is mediated through cGAS. We also have established functional equivalence between OAS1 P46 and a mouse ortholog, Oas1b (no enzyme activity), which similarly affects WNV susceptibility. Through RNA-protein crosslinking experiments we have identified target mRNAs that bind to OAS1 and Oas1b. We have demonstrated increased sensitivity of WNV in OAS1/Oas1b RNA binding mutants. To define the antibacterial activity of OAS1, we screened OAS1-deficient THP1 cells for bacterial growth using the intracellular bacteria *Listeria monocytogenes* and *Francisella novicida* as model bacterial pathogens. Inducible expression of OAS1 P46 WT and enzymatically inactive mutant rescued this antibacterial activity of OAS1 in OAS1-KO cells. Further investigation of OAS1-KO cells indicated defective type II IFN signaling due to the reduced expression of IRF1. Like cGAS, OAS1 bound to IRF1 mRNA and enhanced

protein synthesis of IRF1. Inducible expression of OAS1 P46 in IRF1-KO cells did not inhibit bacterial growth suggesting that antibacterial activity of OAS1 is mediated through IRF1. Lastly, we found that Oas1b knock-in (Oas1b-KI) mice showed improved survival with *L. monocytogenes* or *F. novicida* as compared to WT mice. These findings suggest a new mechanism of OAS1 in which it binds to target mRNAs, enhances the translation of these RNAs and limits virus and bacterial infections.

Table of Contents

List of Tables

List of Figures

Preface

The road to obtaining my Ph.D. has come with many challenges, hard work and discipline. However, none of these would have been possible without the support of many who have contributed to my development as a successful scientist. First, I would like to acknowledge my mentor Dr. Saumen Sarkar. His patience, wisdom, dedication and support have molded me into the scientist I am today, and for that I am forever grateful. I would also like to thank all present and past members of the Sarkar Lab. Not only were they excellent peers who I could have fruitful discussions with about Science and my work, along the way they became close friends with who I could share my life experiences with. Having been away from family and friends, the Sarkar Lab was truly my family away from home and I never felt lonely while in Pittsburgh.

I would also like to thank my committee members, Greg, Jeff, Neal and John. I greatly appreciate your time, effort, guidance and contribution to my project and development. With your suggestions and critiques, I have been able to drive this project forward and stand where I am today.

The work presented here would have not been possible without the input and contribution of several collaborators. Foremost, I would like to acknowledge several members present and past of the Sarkar Lab, including Aru, Kevin, Lulu, Munesh, Nidhi and Rashmi. Their support and teachings are something I will never forget. I would like to thank Solomon, Frank and Dr. Ram Savan for assistance collecting samples from polysome profiling and for always being available to discuss my analysis. I would also like to thank Dr. Maninjay Atianand for teaching our lab how to perform RNA immunoprecipitation analysis and for providing additional technical and intellectual help. I would also like to thank Thomas and Dr. Veit Hornung for several materials, cell lines and

fruitful discussions provided throughout the years. Lastly, I would like to thank Sharmila and Dr. Michael Diamond for assistance with mouse experiments and intellectual contribution to my work.

This journey would not be possible without the special contribution of several friends and family. To my close childhood and college friends, Alejandro, Christian, Eduardo, Ricardo and Joe, I am grateful for always keeping in touch. To Hong, Felix and Manoj, I thank you for the friendships we have developed in Pittsburgh. To my loving family, there is so much I would like to say. My mom Lorna, I thank you for your unconditional love, support and guidance. I know I could always count on you to make me feel better and also make me great food when you visit! To my father Joseph, your words of encouragement, praise and support always pushed me to work harder. The level of interest you showed in my studies and work, is something I have always appreciated, and I would never get tired of answering all your questions! My little brother Gabriel, our strong bond has no limits in addition to the love and support we share for each other. Even from afar we could share hobbies and fun chats together, which definitely kept my morale up. You have seen my career grow up to this point and now it is my turn to watch you grow. And know that I am already so very proud of you. I would like to extend my gratitude to my extended family. To Myriam my second mom, since the time me and your daughter have started dating you have watched my grow and mature, but you have also counseled and comforted me when I have needed it and for this, I am thankful. To my second brother Josue and my wonderful sister Leira, I thank you for your kindness and unconditional support. Lastly, I would like to thank my grandparents. To “abuelo” Cheo thanks for your love and always wanting to make sure I am OK. To “abuela” Norma, although we did not get to spend much time together, I know you loved me very much and for that I am thankful. To “abuela” Cloty, thanks for the amazing food growing up and your loving nature, I will never forget our time watching game shows together. I especially want to thank

‘abuelo’ Rafi, he always was so supportive, caring and looked after my well-being. I know you were always so proud of my achievements and I wish you could share the completion of my thesis with me. I dedicate my work in your memory. There is so many more family I would like to thank, but it would never end! Just know that you all have a special place in my heart, and I thank you for all your support.

Finally, I would like to thank my loving and beautiful wife Myrielis. You are my best friend and mean everything to me. Your unconditional love, support and praise have pushed me to become the person I am today. We both know the extent of hard work and I know that our choices will establish a wonderful and fruitful future together. Your ability to cheer me up, make me laugh and caring nature have truly been essential in this path I have taken. Through ups and downs, your support has always propelled me forward and I am eternally grateful to have you in my life.

Symbols and Abbreviations

AF	Alexa Fluor
ASC	Apoptosis-associated Speck-like protein with CARD domain
BMDM	Bone Marrow Derived Macrophages
CARD	Caspase Recruitment Domain
CFU	Colony Forming Units
CRISPR/Cas9	Clustered Regularly Interspaced Short Palindromic Repeats/CRISPR-associated protein 9
CXCL	Chemokine C-X-C motif Ligand
DADA	D75A/D77A
DAMPs	Damage-associated Molecular Patterns
dATP	Deoxyadenosine triphosphate
DKO	Double Knock-out
E. coli	*Escherichia coli*
ELISA	Enzyme Linked Immunosorbent Assay
FBS	Fetal Bovine Serum
FFU	Focus Forming Units
GBP	Guanylate-binding Proteins
hTERT	Human Telomerase Reverse Transcriptase
IF	Immunofluorescence
IFN	Interferon
IFNAR	Interferon-Alpha/Beta Receptor
IFNGR	Interferon-Gamma Receptor
IFNα	Interferon-Alpha
IFNβ	Interferon-Beta
IFNγ	Interferon-Gamma
IL	Interleukin

Ind.	Inducible
IP	Immunoprecipitation
IRF	Interferon Regulatory Factors
ISG	Interferon Stimulated Gene
JAK	Janus Kinase
KLD	Kinase, Ligase and DpnI enzyme mix
KI	Knock-in
KO	Knock-out
MHC	Major Histocompatibility Complex
MOI	Multiplicity of Infection
NEB	New England BioLabs
NLR	Nucleotide-binding oligomerization domain (NOD) protein like receptor
PAMP	Pathogen-associated Molecular Pattern
PBS	Phosphate-buffered saline
Pen-Strep	Penicillin-Streptomycin
PFU	Plaque Forming Units
p(I):p(C)	Polyinosinic:polycytidylic acid
PRR	Pattern Recognition Receptor
RT-qPCR	Reverse Transcriptase Quantitative Polymerase Chain Reaction
RIG-I	Retinoic acid-inducible Gene I
RLR	RIG-I-like Receptor
RFLP	Restriction Fragment Length Polymorphism
Rpm	Revolutions per minute
SILAC	Stable Isotope Labeling by/with Amino acids in Cell culture
SOC	Super Optimal broth with Catabolite repression
STAT	Signal Transducer and Activator of Transcription
STING	Stimulator of Interferon Genes
TGF-β	Transform Growth Factor beta
TLRs	Toll-like Receptors
TNFα	Tumor Necrosis Factor alpha

U/ml	Units/ml
WB	Western Blot
WCL	Whole Cell Lysate
WNV	West Nile Virus
WNV-KUN	West Nile Virus Kunjin Strain
WNV-NY	West Nile Virus New York 1999 Strain
WT	Wild Type

1.0 Introduction

On a daily basis the human body is exposed to a vast number of microbial pathogens, many of which are capable of causing disease. Fortunately, higher organisms have developed a sophisticated defense system comprised of cellular and chemical networks that together orchestrate protection against invading microorganisms. The existence of microbial protection has been recorded since ancient times, examples of this include noticeable protection against pathogen re-exposure during plagues, followed by practices over 3 centuries ago of exposure to pathogen agents in order to develop an acquired immunity (1, 2). In order for the immune system to fight off infections it must recognize and respond to microbial agents, target invaders for destruction and minimize spread by inducing cellular death. There is a large diversity of microorganisms and it is logical to conclude that they infect their host through a variety of distinct mechanism and vary greatly in composition. This thought led Charles Janeway Jr. to propose the existence of various receptors expressed on immune cells, which detect distinct pathogens and are known today as PRRs (3). These PRRs are located on cellular and endosomal membranes or in the cytosol and upon recognition of PAMPs induce downstream signaling pathways that lead to the expression of proinflammatory cytokines required to control infection (4, 5). As alluded previously, different microorganisms are detected by different receptors, mostly dependent on infection routes of the pathogen, and illicit distinct signaling responses. Innate immune responses to bacterial infection mostly rely on the recognition of bacterial ligands by TLRs and NLRs leading to the induction of pro-inflammatory cytokines and antibacterial gene expression (6). Additionally, bacterial nucleic acids can lead to the activation of cGAS-STING pathways and promote IFN signaling (7). During viral infection, intracellular TLRs and cytosolic nucleic acid sensors detect viral genetic material

and initiate cellular innate immune responses. Signaling by these receptors results in the activation of transcription factors, such as NF-κB and IRF-3, required for the production of type I interferons (8). Interferons, through JAK-STAT signaling, promote the expression of hundreds of IFN stimulated genes with profound antiviral effects (9).

Among these ISGs exist the Oligoadenylate Synthetase (OAS) family proteins, a group of type I IFN inducible proteins that bind viral dsRNA, and through their Nucleotidyltransferase (NTase) domain, and synthesize 2'-5' oligoadenylates (2-5(A)). These 2-5(A) molecules cause activation of a latent RNase, RNase L through dimerization (10). In addition to multiple antiviral effects (11), OAS proteins have been associated to defense against intracellular bacteria such as *Mycobacterium tuberculosis* (12). There are 4 human OAS-family proteins, 3 of them which are enzymatically active (OAS1, OAS2 and OAS3), and one (OASL) which is enzymatically inactive but confers antiviral protection by enhancing RIG-I signaling (13). Additionally, mice have a variety of OAS homologs, some that are also enzymatically inactive (11, 14). The biological significance of these enzymatically inactive OAS proteins lays in their ability to confer antiviral protection, as seen in OASL and protection against WNV infection by the human OAS1 mouse homolog Oas1b (15, 16). Recent studies have shown that OAS3 is necessary and sufficient for the activation of RNase L, yet overexpression of OAS1 or OAS2 can reduce virus susceptibility (17), suggesting that non-canonical functions exist for both enzymatically active and inactive members of the OAS family proteins. The non-canonical role of OAS1 during viral and bacterial infection has yet to be defined and these unique mechanisms of OAS1 will be explained in this dissertation.

1.1 Innate Immune Signaling

Innate Immunity is an evolutionarily conserved system characterized by a number of non-specific responses to foreign invasion in order to protect the host from infections. It ranges from the most basic physiological barriers of defense, such as: mucosal membranes, acidic environments and chemical mediators, to more complex immune systems reliant on cellular and molecular responses. Cellular responses are mediated through specialized myeloid and lymphoid sensors and effector cells, which become active during tissue damage, infection or stress (18). During infection, macrophages, neutrophils and dendritic cells can engulf and destroy pathogens by phagocytosis followed by processing and presentation of antigens by macrophages and dendritic cells to lymphoid cells, serving as a bridge between innate and adaptive immunity. However, the clearance of infection is not limited to phagocytosis, there are number of innate defense mechanisms that are stimulated upon recognition of PAMPs. These include production of pro-inflammatory cytokines (e.g. TNFα, IL-1, IL6), chemokine secretion (e.g. CXCL proteins) and chemotaxis of other immune cells, pathogen clearance by the Complement system and lysis by antimicrobial peptides (e.g. Lysosomes) among other mechanisms (19–22).

Specific PAMPs are recognized by a distinct variety of PRRs to elicit signaling cascades, and of these receptors first described were TLRs. Parallels between cytokine mediated NF-κB activation and signaling of Toll proteins in *Drosophila* and the discovery of TLR4 as the receptor for LPS (23, 24) suggested that other TLRs could be responsible for recognition of PAMPs of microbial and viral origin (5). After years of extensive research, understanding of the TLR family has become clear and TLRs have been well characterized in mammalian hosts. Humans express 10 TLR proteins (TLRs 1-10), while mice express 11 TLR proteins (TLRs 1-9 and TLRs 11-12)

and what is common between mammalian species is the distribution of TLRs in the cell. Human TLRs expressed on the cell surface include TLR1, TLR2, TLR4, TLR5, TLR6 and TLR10 and mostly bind to PAMPs of bacterial origin (e.g. lipopolysaccharides, lipoproteins and proteins). Intracellular TLRs, found in endosomes, include TLR3, TLR7, TLR8 and TLR9 and bind to DNA or RNA derived from virus, bacteria or self-nucleic acids from damaged cells (regularly not found in cytosol) (25).

TLRs are type I integral membrane receptors consisting of a N-terminal ligand recognition domain, transmembrane helix and a C-terminal signaling domain located in the cytosol (26). The N-terminal domain consists of leucine-rich repeats (LRR), a motif found on several proteins of animals, plants and microorganisms. Once TLRs have bound to their ligand (summarized in Fig. 1), the C-terminal domains of receptors come close together allowing the signaling domains, known as Toll IL-1 receptor domains (TIR), to interact and form dimers. Dimeric receptors recruit TIR domain-containing adaptor proteins such as MyD88 and TRIF, which activate transcription factors and promote gene expression. MyD88 mediates downstream signaling pathways of all TLR proteins, with the exception of TLR3, and consists of a TIR domain and death domain. MyD88 interacts with TLRs through TIR and the death domain interacts with the death domain of IL-1 receptor-associated kinase-4 (IRAK-4) forming a complex that recruits IRAK-1 and IRAK-2, resulting phosphorylation of IRAK proteins (27). TNF receptor-associated factor 6 (TRAF6) is recruited and activated by IRAK-1 forming a complex that dissociates from the receptor and associates to TGF-β-activated kinase 1 (TAK1) and TAK1-binding proteins (TABs)(28). The TRAF6, TAK1 and TAB complex moves to the cytosol and is polyubiquitinated with K63-ubiquitin chains by E2 ubiquitin ligases Ubc13/Uev1A inducing TRAF6 activation, which then promotes IκB Kinase (IKK) complex phosphorylation and activation of NF-κB (29, 30). The IKK

complex is composed of two catalytic subunits (IKKα and IKKβ) and one regulator subunit NF-κB essential modulator (NEMO)/IKKγ. NF-κB subunits share a Rel homology domain, required for DNA binding and dimerization, and NF-κB is tightly regulated by IκB (inhibitor of NF-κB), which masks nuclear localization signals found in NF-κB family proteins (31, 32). Activation of IKK complex leads to the phosphorylation of IκB, which then becomes poly-ubiquitinated by E3 ubiquitin ligases and degraded in the proteasome, therefore releasing NF-κB and allowing NF-κB heterodimer translocation into the nucleus (33). Once in the nucleus, NF-κB promotes transcription of genes involved in inflammatory responses (e.g. TNF, IL-1, INOS, ICAM), proliferation (e.g. Cyclins, MYC, CDK) and survival among others (34, 35). TRAF6 also promotes down-stream activation of the transcription factor activator protein 1 (AP-1). AP-1 is a heterodimer assembled by basic region leucine zipper (bZIP) domains in Fos and Jun (proto-oncogene) family protein subunits (36). AP-1 is activated by mitogen-activated protein kinases (MAPK), specifically MAPKs p38, the extracellular signal-related kinase (ERK) and Jun N-terminal kinase (JNK), all serine/threonine kinases that influence the phosphorylation and activation of multiple transcription factors (37).

Similar to NF-κB signaling, TAK1 is responsible for activating mitogen-activated protein kinases (MAPKs) signaling cascades leading to the activation and translocation of AP-1 to the nucleus (38). Once in the nucleus, AP-1 promotes expression of genes regulating proliferation, differentiation and apoptosis (39, 40). Similar to cell surface TLRs, intracellular TLR 7, 8 and 9 also lead to the activation of TRAF6 and MAPK pathways promoting NF-κB and AP-1, translocation to the nucleus and enhance transcription of target genes. In addition to MyD88, the adaptor protein TIR-domain-containing adapter-inducing IFNβ (TRIF) also regulates signaling of TLRs, specifically TLR3 and TLR4 (41, 42). TRIF recruits TNF receptor-associated factor 3

(TRAF3), which becomes active after K63-polyubiquitination by the E3 ubiquitin-protein ligase HECTD3 and activated TRAF3 promotes activation of TANK-binding kinase 1 (TBK1) and IKKε (43–45). TBK1 and IKKε kinase phosphorylate IRF3, which forms homodimers, translocates to the nucleus and promotes type I IFN expression (46). In addition to TLRs, there are several other PRRs that work to detect cytosolic genetic material of viral, microbial or self-origin, including NLRs, cGAS, and RIG-I like receptors (RLRs).

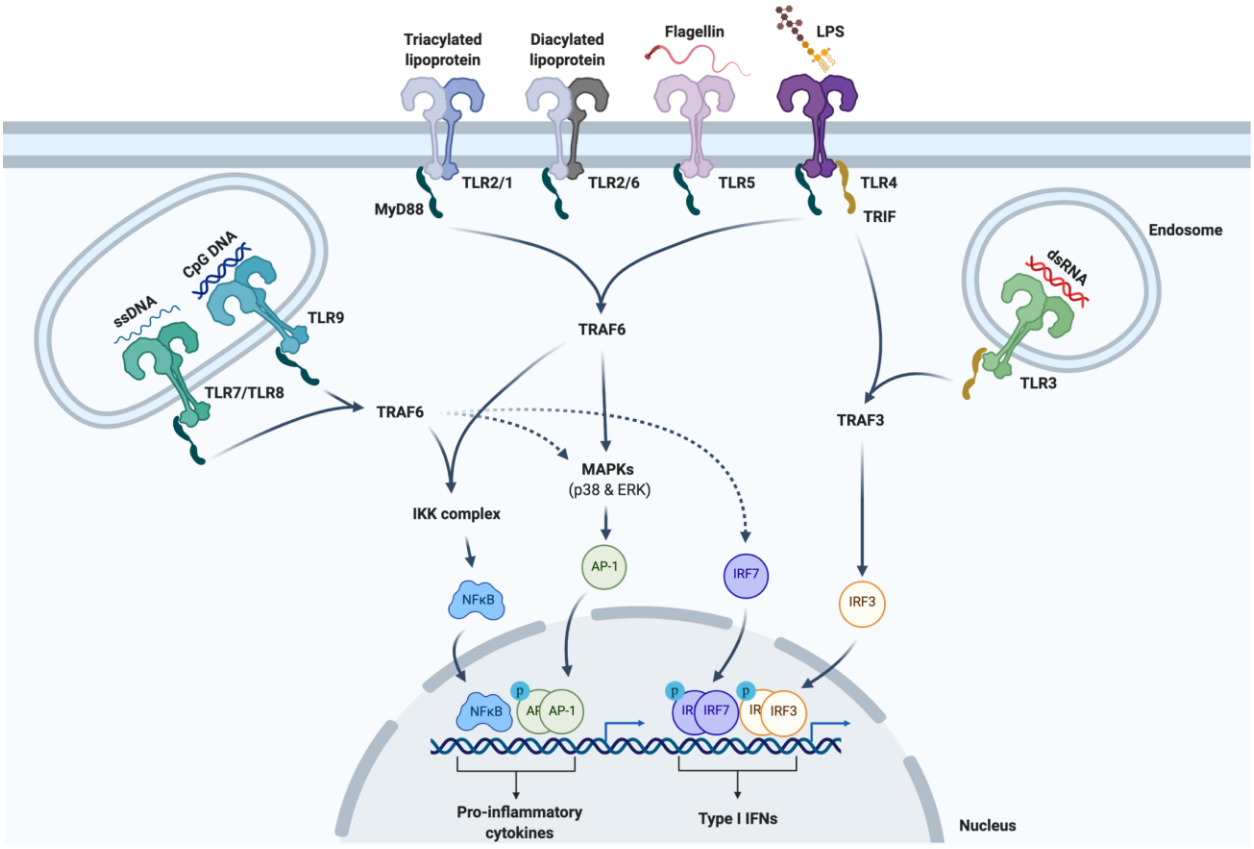

Figure 1. TLR Signaling in human cells.
Schematic of TLR signaling of cell surface and intracellular receptors in human cells. Once TLRs bind PAMPs associated to extracellular or intracellular pathogens, they recruit adaptor proteins and induce signaling cascades leading to the activation of transcription factors, which promote gene expression of pro-inflammatory cytokines and type I IFNs.

1.1.1 Recognition of cytosolic DNA and RNA

In addition to TLRs which detect PAMPs in endosomes, there are several cytoplasmic sensors of nucleic acids that elicit innate immune responses to pathogen invasion or host cellular damage. Among these are NLRs, a family of proteins that form part of intracellular multiprotein complexes called inflammasomes. These inflammasome structures mediate inflammatory and cell death pathways. The NLR family is divided into a variety of subfamilies, differing in their N-terminus, and there are several non-NLR proteins (AIM2, Pyrin and IFI16), which can also form inflammasomes (reviewed in (47)). Inflammasome structures consist of a sensor protein (NLR, AIM2, Pyrin), ASC adaptor protein, and pro-caspase1 (or pro-caspase11 in non-canonical inflammasomes) effector protein (48). Upon activation, pro-caspase1 is cleaved into caspase1 and active caspase1 processes the conversion of pro-IL-1β and pro-IL-18 into IL-1β and IL-18 respectively, followed by their secretion. Additionally, caspase1 also triggers pyroptosis through GasderminD limiting the spread of infectious agents to other cells (49). In addition to NLRs, cGAS and RLRs are well characterized sensors of cytosolic DNA and RNA respectively, which promote inflammatory gene and IFN expression (Fig. 2). In response to DNA of viral, bacterial or self-origin, cGAS synthesizes 2'-3'-cyclic guanosine monophosphate-adenosine monophosphate (cGAMP) a second messenger responsible for activating Stimulator of IFN genes (STING). STING resides in the endoplasmic reticulum (ER) and upon activation promotes NF-κB and TBK1-mediated activation of IRF3. In response to viral dsRNA, RLRs interacts with and activates Mitochondrial antiviral-signaling protein (MAVS), followed by oligomerization of MAVS on the mitochondrial surface. MAVS then activates TRAF3 (similar to TLR3 signaling) and TRAF6 leading to activation of IRF3 and NF-κB respectively.

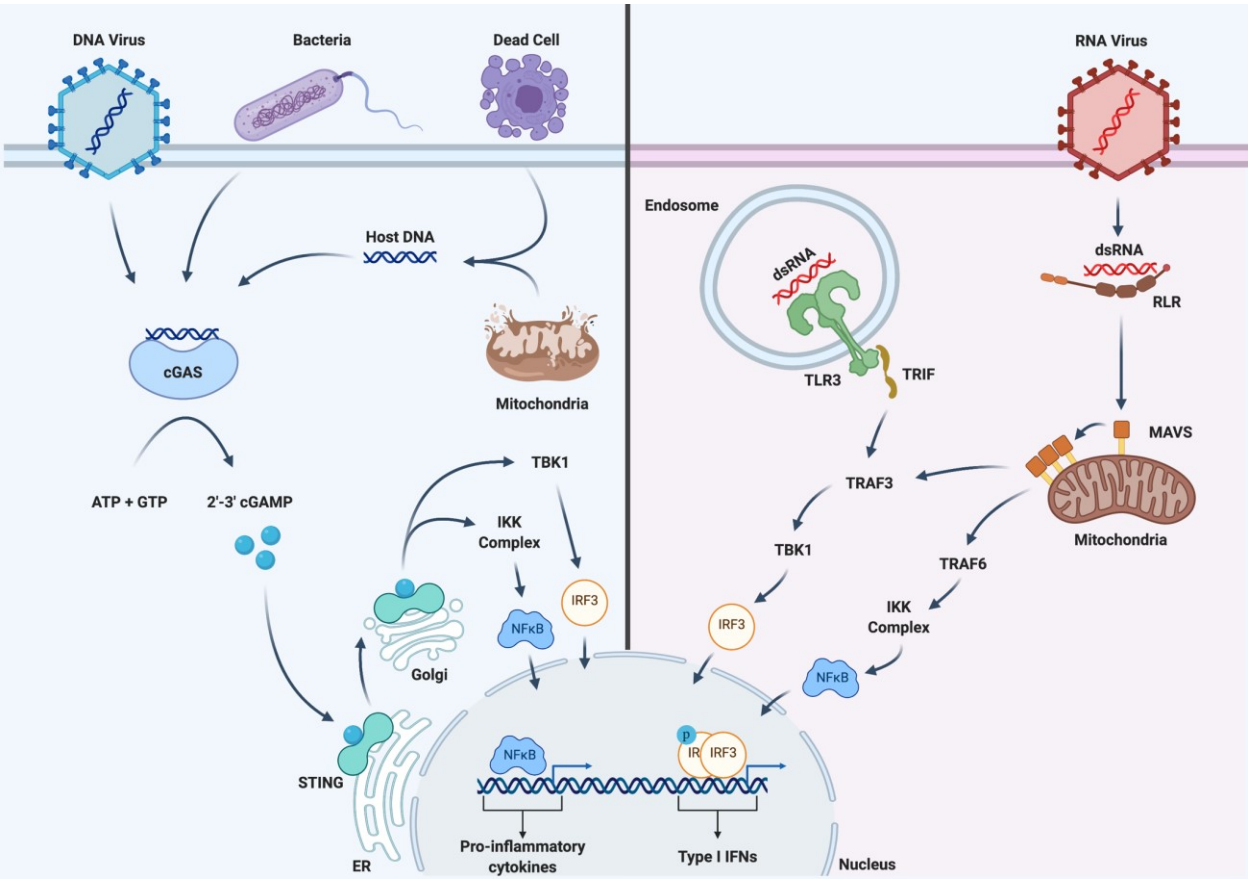

Figure 2. Sensing of cytosolic DNA and RNA in human cells.
Schematic of innate immune response to cytosolic DNA (left) and RNA (right) in human cells. Cytosolic DNA of viral, bacterial or host origin is sensed in the cytosol by cGAS, which converts ATP and GTP to 2'-3'-cGAMP. cGAMP then activates STING signaling pathway. Cytosolic RNA of viral origin is sensed by RLRs, which activate MAVS signaling pathway. Both pathways lead to the activation of transcription factors that promote transcription of pro-inflammatory cytokines and type I IFNs.

1.1.1.1 RNA Sensors

RLRs are intracellular PRRs crucial for detecting cytosolic RNA of invading RNA viruses. These receptors are a family of DExD/H box RNA helicases and include: RIG-I, melanoma differentiation association gene 5 (MDA5) and laboratory of genetics and physiology 2 (LGP2) protein (50). The structure of these RLRs are quite similar, they share a central DExD/H box RNA helicase core required for RNA binding, a C-terminal harboring a repressor domain involved in autoregulation, and in the case of RIG-I and MDA5 a N-terminal CARD signaling domain (51).

Although LGP2 lacks N-terminal CARD domains, it binds tightly to dsRNA and works as a negative or positive regulator of RIG-I and MDA5 signaling (52, 53).

RIG-I was the first RLR to be characterized in the induction of IFN in response to RNA virus infection or p(I):p(C) transfection. RIG-I mediated IFN expression was shown to be alternative to TLR3 signaling and the CARD domain of RIG-I was shown to be a crucial interface between dsRNA sensing and downstream signaling (54). Prior to the engagement of dsRNA, RIG-I remains in a folded inactivated state in which CARD domains are associated to the helicase domain of RIG-I and are not available for signaling (55). RIG-I, through its helicase and C-terminal domain, monitors the 5' end of RNA and is activated upon recognition of free non-capped diphosphate or triphosphate groups on RNA (56, 57). Additionally, methylation of the 2'-hydroxyl group of the 5'-terminal nucleotide of endogenous RNA and is crucial for distinguishing self RNA and repressing RIG-I activation, and the absence of methylation at this group aids in recognition of foreign RNA by RIG-I (58, 59). Upon association of dsRNA with the helicase domain of RIG-I, RIG-I undergoes a conformational change that exposes the CARD domains of RIG-I, which then become K63 poly-ubiquitinated by the E3 ligase tripartite motif-containing 25 (TRIM25)(60). Once poly-ubiquitinated, RIG-I oligomerizes through its CARD domains, which promotes interactions with MAVS adaptor protein (61, 62). Contrary to RIG-I, MDA5 remains in an open state and upon interaction with longer dsRNAs forms filamentous oligomers increasing the affinity to the RNA ligand (63, 64). Similar to RIG-I, the CARD domains on oligomerized MDA5 proteins are K63 poly-ubiquitinated and active oligomers interact with the CARD domains of MAVS, however the mechanism of MDA5 K63 poly-ubiquitinated remains unclear (65).

MAVS was identified as a meditator of RLR dependent activation of IFNβ by IRF3 and NF-κB signaling pathways (66). It was also shown that MAVS contained N-terminal CARD

domains and a C-terminal transmembrane domain, which targets MAVS to mitochondrial membranes, both crucial for the signaling activity of MAVS (67). Additionally, MAVS contains several TRAF-interacting motifs (TIMs), two in the proline-rich region and one near the C-terminal transmembrane domain, and crystal structures of MAVS interacting with TRAF proteins have been characterized (68–70). Once MAVS interacts with RIG-I or MDA5, MAVS proteins cluster together on the mitochondrial surface becoming activate, which then promotes the recruitment of TRAF proteins (Fig. 2) and assembly of a multiprotein complex required for signaling and IFN induction (71, 72). Once recruited, TRAF3 protein complex leads to the induction of type I IFNs mediated by TBK1, IKKε, and TRAF6, which promotes NF-κB signaling leading to the transcription of inflammatory genes.

1.1.1.2 DNA Sensors

As previously discussed, TLRs found in endosomal compartments are capable of recognizing single-stranded or unmethylated CpG DNA and through MyD88 signaling pathways elicit inflammatory gene and IFN expression. However studies in MyD88 and TRIF KO cells evidently showed that TLR independent pathways of IFN expression existed in response to cytosolic DNA and must be related to cytosolic protein sensors to DNA (73) . Extensive research to identify which proteins could be responsible for sensing DNA in the cytosol identified the adaptor protein STING as a crucial mediator of antiviral activity in response to cytosolic DNA. STING was shown to activate both NF-κB and IRF3 signaling pathways, however it was clear that it did not directly interact with DNA, and STING alone was not sufficient for induction of IFNs (74, 75). The discovery of bacterial cyclic di-nucleotides as a mediator of STING activation

confirmed the existence of proteins up-stream of STING that regulated DNA sensing pathways to induce type I IFN signaling (76–78).

cGAS structure is quite similar to that of OAS1 It contains a NTase core and a unique zinc-binding site conserved throughout cGAS orthologues (79, 80). cGAS interacts with dsDNA through two binding sites and can bind shorter or longer DNA molecules based on specific amino acid (a.a.) residues at these binding sites. The cGAS enzymatic activity is also regulated by the dsDNA length, which has been seen to be different in human and mouse cGAS (81, 82). After engaging with DNA, cGAS becomes active and catalyzes the conversion of GTP and ATP into the second messenger cGAMP, which then binds to STING in the ER and promotes the formation of STING oligomers (83). STING consists of a cytosolic domain, required for ligand binding and interaction of TBK1 and IRF3 through its C-terminal tail, and transmembrane domains that anchor STING to the ER. When STING binds cGAMP, there is a 180º rotation of the ligand-binding domain allowing STING oligomers to tightly pack side to side, followed by trafficking through ER-Golgi intermediate compartments to the Golgi apparatus (82). Once translocated to the Golgi, STING physically interacts with TBK1, through a conserved PLPLRT/SD motif in the C-terminal tail of STING, and becomes phosphorylated by TBK1 resulting in recruitment of IRF3 to the C-terminal tail of STING and subsequent phosphorylation and activation by TBK1 (84, 85). Additionally, STING has been show to activate the IKK complex, through TRAF6 and TAK1 signaling, resulting in activation of NF-κB (86, 87). Once activate, IRF3 and NF-κB translocate to the nucleus and promote transcription of IFNs and pro-inflammatory cytokines respectively (Fig. 2).

1.1.2 Interferon Signaling

The discovery of IFNs dates back to the 1950s. Studies of chick chorioallantois membranes in nutrient fluid highlighted the released a novel factor in response to heat killed influenza. Since this factor had the capability of "interfering" with the replication of live virus, it was termed Interferon (88). Approximately 20 years after its discovery, IFNα, IFNβ and IFNγ were successfully purified, analyzed and characterized (89–91). As of today, several human IFNs have been identified and characterized, listed in Fig. 3, and are grouped as Type I, II and III IFNs based on sequence homology and receptor binding (92, 93). Type II IFNs are specific to immune cells while Type I IFNs are expressed by most nucleated cells. Type I and III IFNs are induced downstream of RNA and DNA sensing signaling pathways. Type II IFNs are predominantly secreted by activated T cells and NK cells in response to mitogen or cytokine (IL-12, IL-15, IL-18 and type I IFN) stimulation (94). All IFN receptors consist of two subunits, which come together upon ligand interaction and relay signaling through JAK-STAT pathways (Fig. 3). The subunits of IFN receptors consist of N-terminal ligand domains, a transmembrane domain and cytosolic domain. The subunits of type I IFN receptors are characterized by alpha and beta chains respectively and are termed Interferon alpha/beta receptor alpha or beta chain (IFNAR1 and IFNAR2). The receptors of type III IFNs are composed of Interleukin 28 receptor alpha (IL28RA or more recently known as IFNλR1) and Interleukin 10 receptor beta (IL10RB), which also functions in IL-10 signal transduction (95). Type II IFN receptors consist of two subunits made of alpha and beta chains (IFNGR1 and IFNGR2 respectively), however these receptors work in a four-chain complex in which IFNGR1 homodimers first interact with ligand facilitating IFNGR2

dimer association. Structures of IFNs and their receptors are listed and reviewed by Pestka et al. 2004 (96).

All IFNs share similar signaling and induction of ISGs through JAK-STAT signaling pathways. However, distinct Janus kinases that associate to the different classes of IFN receptors can lead to the formation of hetero or homo dimers of STAT proteins leading to the activation of select promoters (Fig. 3). IFN binding promotes interaction between receptor subunits, which brings receptor-associated Janus kinases JAK1 and TYK2 in close proximity to allow cross phosphorylation of the receptors (at tyrosine residues) leading to the recruitment of STAT1 and STAT2 proteins followed by their phosphorylation at specific tyrosine residues and dimerization (97, 98). STAT1 and STAT2 heterodimer then recruits IRF9 and together form the ISGF3 transcription factor complex. ISGF3 translocates to the nucleus and binds to IFN-stimulated response elements (ISREs) in the promoter regions of ISGs. STAT1 homodimers activated downstream of IFNGR activation are sufficient to induce the transcription of several ISGs by binding to the interferon gamma activated sequence (GAS) in the promoters of said ISGs. Together IFNs play crucial immunoregulatory roles including modulation of cells involved in innate and adaptive immunity, inflammation, regulation of tumor growth, antimicrobials defense and antiviral activity. During viral infections, IFNs lead to the expression of several ISGs, for example OAS, PKR, IFITs and MX1 after type I stimulation and IRF1, CXCL10, GBPs and MHC related proteins after type II stimulation. The goal of these proteins is to disrupt viral replication, by targeting viral nucleic acids for degradation or inactivation of viral proteins, enhancing MHC function of antigen presenting cells (APCs) and the induction of chemokines needed for the recruitment of immune cells responsible for clearing virus infected cells (reviewed in (99–101)).

In response to bacterial infections, type I IFNs can be protective or detrimental to the host and this outcome is reliant on bacterial replication and virulence factors (reviewed in (7, 102). Similarly IFNγ plays a crucial role during microbial infections and was validated by observations of increased pathogenicity to intracellular bacterial in mice with deficiencies in several proteins of the IFNγ signaling pathway (103). Some examples of IFNγ mediated antimicrobial immunity include expression of GBPs known to disrupt bacterial membranes or bacteria containing vacuoles, regulation of cytotoxic T cells and stimulation of autophagy (104–106). Type III IFNs share similarities to Type I IFNs in their signaling pathway, however immunoregulatory functions seem to be confined to epithelial and mucosal structures during viral and bacterial infections (107, 108). Overall IFN are responsible for conferring antiviral or antimicrobial resistance through the regulation of immune cells and expression of ISGs.

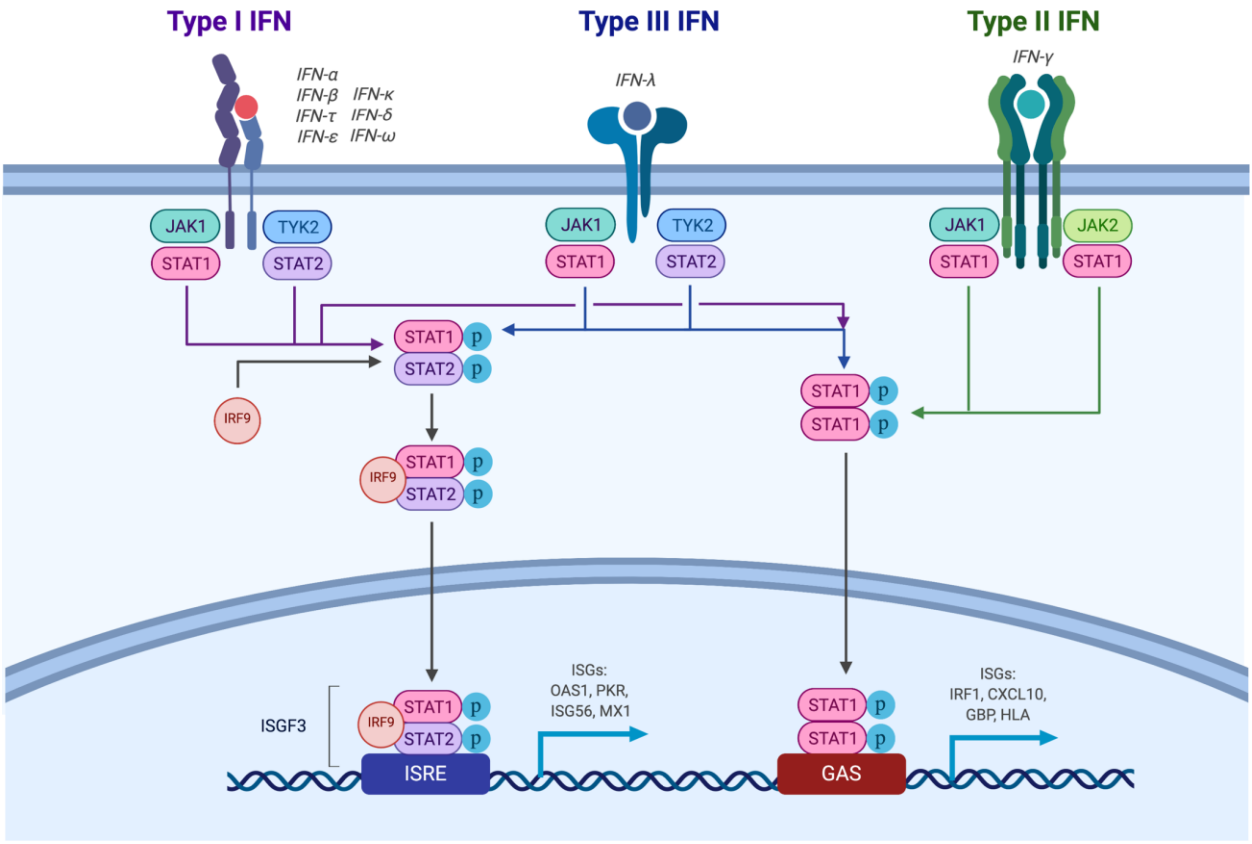

Figure 3. Type I, II and III IFN signaling
Schematic of IFN signaling pathway following IFN engagement to respective receptors. Once IFN receptors become active they recruit JAK and STAT signaling proteins leading to the phosphorylation and dimerization of STAT proteins, followed by interactions with IRF9 during type I IFN signaling, and translocation to the nucleus. STAT homo or hetero dimers in complex with IRF9 bind to target promoters and induce expression of IFN stimulated genes.

1.1.3 Interferon Regulatory Factors

IRFs are a family of transcription factors that play crucial immunoregulatory roles in cell development and differentiation (109–112), oncogenesis (113, 114) and infection (115). Many IRF proteins are constitutively expressed and function in regulating IFN signaling pathways in response to viral or microbial infections (for example IRF3, IRF7 and IRF9). Several are IFN inducible and function in tumor suppression, lymphocyte development and intracellular infections. The expression and function of human IRF1-9 are summarized in Table 1. The structure of human

IRFs are quite similar, they share N-terminal DNA binding domains, nuclear localization sequences, signal-responding domains, C-terminal interferon association domains (which allow interactions with other IRFs) (Fig. 4). Additionally, for multiple IRFs there are activation or repressor domains at their C-terminus (116, 117). IRF proteins exist in the cytosol as monomers, but when phosphorylated in the signal responding domains by serine/threonine kinases undergo conformational changes to form dimeric structures and translocate to the nucleus to promote transcription. IRFs involved in type I IFN induction bind to the positive regulatory domains (PRDs) I and III of the IFNβ promoter and PRD-LE of the IFNα promoter, through their DNA binding domains, and induce transcription of these genes (118). Different from other IRFs, IRF9 works together with STAT1/STAT2 heterodimers during IFN signaling. It forms a complex referred to as ISGF3, which translocates to the nucleus and binds to ISRE in the promoter of several ISGs. Together IRFs are key regulators of inflammation, cellular development and differentiation, infection and in some cases progression of cancer.

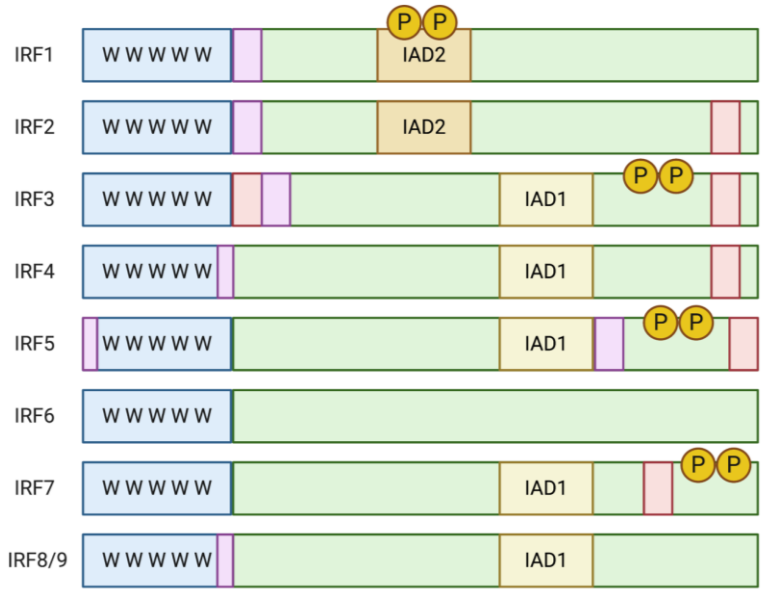

Figure 4. Structure of IRF family proteins
IRF proteins are composed of a N-terminal DNA binding domain (blue) contain tryptophan (W) repeats and a C-terminal regulatory domain (green). Type I (yellow) and type II (orange) interferon association domains are found within the regulatory domain. Several IRFs contain nuclear localization domains (purple) and some harbor repressor

domains (red). The activity of IRF1, 3, 5 and 7 is dependent on phosphorylation. Figure was adapted from Lohoff and Mak 2005 (119).

Table 1. Summary of Interferon Regulatory Factors

IRF	Expression	Function	Reference
IRF1	Inducible expression, highest with IFNγ, in most cell types	Induction of antiviral and antimicrobial ISGs, type I IFN induction, regulation of immune cell function and differentiation, inflammasome activation and tumor suppression	(104, 120), (118), (121–123), (124, 125), (113, 126)
IRF2	Constitutive and Inducible expression in various cell types	Antagonism of IRF1 driven transcription, regulation of immune cell development and pro- or anti- oncogenic roles in Cancer	(127), (128, 129), (113, 130)
IRF3	Constitutive expression in most cell types	TLR dependent and independent induction of type I IFNs,	(131, 132)
IRF4	Constitutive expression in B cells, Macrophages and DC, inducible expression in T cells	Negative regulation of pro-inflammatory cytokines by TLR signaling, regulates differentiation and development of various plasma and lymphocyte cells, promotes tumor growth in several cancers	(133), (134), (113, 135)
IRF5	Inducible expression in several myeloid cells and B cells	Induction of pro-inflammatory cytokines and type I IFNs, roles in DNA damage mediated apoptosis, tumor suppressor	(136, 137), (132, 138), (113, 138)
IRF6	Constitutive expression in epidermal cells	Regulates epidermal cell development and differentiation, tumor suppressor	(139–141), (113, 142)
IRF7	Constitutive expression in macrophages and plasmacytoid dendritic cells (pDCs), and inducible in other cell types	TLR dependent and independent induction of type I IFNs, tumor suppressor	(132, 143), (113, 144)
IRF8	Constitutive expression in B cells and DCs, inducible in Macrophages and T cells	Type I IFN induction, regulates myeloid and lymphocyte differentiation, regulation of apoptosis and tumor suppressor	(145), (146, 147), (113, 148)
IRF9	Constitutive and inducible expression in most cell types	Promotes transcription of type I ISGs (as part of the ISGF3 complex), regulates induction of p53 tumor suppressor protein	(149, 150), (113, 151, 152)

1.1.4 Interferon Stimulated Genes

ISGs are simply defined as genes that are transcriptionally induced downstream of IFN signaling. Once IFNs are induced, following infection or recognition of self-nucleic acids, they bind to their receptors and through JAK-STAT signaling promote activation of transcription factors, which translocate to the nucleus and regulate ISG expression. As early as the 1980s it was found that treatment of cells with IFN lead to gene expression of several proteins that were not found in un-treated cells and inhibition of active translation by actinomycin D in IFN treated cells resulted in decreased levels of these IFN inducible proteins (153, 154). These data represent some of the earliest findings of ISGs and proposed that the antiviral state of IFN signaling may be mediated by the existence of these IFN inducible proteins. As of today, hundreds of genes have been identified as IFN inducible by microarray and transcriptome analysis in diverse mammalian species (155, 156). Although the role of ISGs was first described in the context of antiviral activity, ISGs have proven to be quite diverse and have been shown to regulate apoptosis, induce cytokine secretion, promote chemotaxis and cell adhesion, and provide antimicrobial immunity (155, 157–159).

In response to virus infection, viral nucleic acids lead to the induction of IFN and subsequently the expression of multiple ISGs, which directly affect virus replication (160, 161). There are several conventional ISGs known to suppress viral replication by degrading virus genetic material and inhibiting viral protein synthesis. The antiviral activity of OAS proteins involves binding to dsRNA, synthesize 2'-5' oligoadenylate links and activate the endoribonuclease RNase L. RNase L exists as inactive monomers and upon binding 2'-5' oligoadenylates forms active dimeric structures that targets and cleave viral RNA, therefore inhibiting viral protein synthesis (162, 163). Protein Kinase R (PKR) is an ISG that inhibits the spread of virus by suppressing

protein synthesis. PKR is a serine/threonine kinase that becomes active when bound to dsRNA and phosphorylates the eukaryotic initiation factor 2 (eIF2) alpha subunit, which leads to global translational arrest and consequently inhibition of viral protein synthesis (164). Similar to OAS1 and PKR, the Double -stranded RNA-specific adenosine deaminase ADAR exhibits its antiviral activity by binding to virus dsRNA. ADAR edits dsRNA by catalyzing the conversion of adenosine to inosine, which destabilizes the RNA and suppresses RNA virus replication (165). IFITs are a family of IFN inducible cytosolic proteins with direct or indirect antiviral mechanisms reviewed in (164, 166). IFIT1 and 2 can inhibit protein translation by binding to eukaryotic initiation factor 3, therefore inhibiting formation of the translational initiation complex. Additionally, both IFIT1 and 2 can directly bind to and sequester viral RNA therefore limiting viral replication. IFIT1 specifically binds to RNAs lacking 2'-O-methylation at their 5' cap or RNAs bearing a 5' triphosphate group and IFIT2 can bind to AU rich RNAs. IFIT3 is known to form a large protein complex with IFIT1 and 2 and this interaction is needed for IFIT1 antiviral activity by sequestering RNA. Additionally, IFIT3 itself can promote antiviral activity by enhancing MAVS signaling by functioning as an adaptor between MAVS and TBK1 (167). Human MX proteins 1 and 2 are dynamin-like GTPases with broad antiviral activity depending on the species of virus. MX1 interferes with influenza ribonucleoproteins therefore affecting viral transcription and mRNA translation and MX2 has been shown to inhibit nuclear import of HIV DNA and therefore integration of DNA into the host genome (168–170). Viperin is an example of an ISG capable of restricting a variety of DNA and RNA viruses by interacting with both viral and host proteins (171, 172). Similar to RNase L, Zinc-finger antiviral protein (ZAP) restrict RNA virus replication by targeting RNA for degradation. ZAP binds to CG-rich sequences on viral RNA through its N-

terminal domains. This interaction interferes with the assembly of the translation initiation complex and ZAP recruits RNA processing proteins, which degrade viral RNA (173).

ISG15 is di-ubiquitin like protein that is significantly induced during viral infection, however the mechanisms of its antiviral activity remain unclear. Mice deficient in ISG15 are susceptible to influenza and herpes virus, confirming the ISG15 indeed confers antiviral immunity (174). Evidence suggests that ISG15 may disrupt viral and host protein interactions required for replication and can prevent release of viral particles through post-translational modification (ISGylation) of both viral and host proteins (160, 175). Some studies have reported that ISG15 promotes secretion of IFNγ and IL10 secretion, suggesting potential immunomodulatory roles of ISG15 (176). Immunomodulation in the host is also carried out by many other ISGs, several which enhance the transcription of other ISGs, for example IRFs. IRF1 is an IFNγ stimulated ISG, which also acts as a modulator of type I IFNs, tumor suppressor genes and of cytokines and chemokines required for immune cell development (120). Additionally, ISGs can lead to the secretion of several immunomodulatory cytokines including IL-12, IFNγ and TNFα. Early studies have shown that IFNβ is capable of inducing IL-12 in antigen presenting cells leading to subsequent induction and secretion of IFNγ. IFNγ then regulates the activation and differentiation of T cells and potentiates the effects of IL-12 on APCs (177–181).

ISGs also play crucial roles in cell chemotaxis and development, for example chemokines that recruit myeloid and lymphocytes to the sites of infection and MHC proteins, which help bridge innate and adaptive immunity. CXCL9, 10 and 11 are all examples of IFNγ inducible chemokines secreted mostly by monocytes, endothelial cells and fibroblasts. These chemokines bind to their receptor, CXCR3, on the surface of other monocytes, T cells, natural killer (NK) cells and DCs promoting cellular chemotaxis and proliferation (182, 183). Both type I and type II IFNs are

important modulators of MHC class I and II expression, which is required for antigen presentation and activation of adaptive immune cells in response to pathogen infection or cancer progression to mediate regulatory and cytotoxic roles (184–187).

There are several antiviral ISGs that function to inhibit viral entry and uncoating, block nuclear import and prevent assembly of virus particles. Nuclear receptor coactivator 7 (NCOA7) is an ISG that can inhibit entry of influenza A and hepatitis C virus into the cytosol by regulating endosomal physiology preventing viral fusion with endosomal membranes and release of nucleic acids into the cytosol (188). The IFN-induced transmembrane (IFITM) family of proteins can also inhibit entry of several enveloped viruses (Influenza A, flaviviruses, filoviruses and coronaviruses) and have also been shown to traffic virus particles to lysosomes for degradation (155, 166, 189). The ISG tripartite motif-containing protein 5 alpha (Trim5α) is an E3 ubiquitin ligase that works post viral entry but can restrict retroviral replication by targeting viral capsids and inducing transcription of inflammatory cytokines mediated by TAK1 signaling (190). A PRYSPRY domain in the C-terminus of Trim5α can recognize the HIV-1 capsid forming a hexagonal lattice structure, which is targeted for degradation by the proteasome (191, 192). The apolipoprotein B mRNA-editing enzyme catalytic polypeptide-like protein family (APOBEC) are DNA cytosine deaminases that function in the restriction of DNA pathogens and retroviruses. APOBEC3 for example inhibits viral gene expression and replication by catalyzing the deamination of cytosine to uracil in ssDNA resulting in G to A hypermutations in retroviral cDNA (193).

Some ISGs are capable of restricting virus by directly binding viral proteins. During HIV assembly and trafficking, the transmembrane protein Tetherin anchors virion particles to membranes inhibiting their release from infected cells and limits the spread of the virus throughout the host (194). 2’-3’ cyclic nucleotide 3’-phosphodiesterase (CNP) is another ISG that targets viral proteins

directly, specifically CNP can bind to the major structural protein Gag of HIV inhibiting particle assembly (195).

IFNs also induce or potentiate the effects of several intracellular DNA and RNA sensors. IFI16 is one ISG that has been well characterized as a sensor of cytosolic DNA. Additionally, IFI16 plays a role in suppressing the transcription of human cytomegalovirus (HMCV) DNA polymerase, therefore inhibiting DNA replication (196). IFI16 has also been shown to repress herpes simplex virus 1 (HSV-1) gene expression by modulating histone modifications (196, 197). In addition to IFI16, many of these intracellular receptors are expressed at lower levels under basal conditions to maintain cellular homeostasis and avoid inflammatory damage. However, during infection the expression of many PRRs, for example RIG-I, MDA5, IFI16 and cGAS, are enhanced by IFN stimulation in order to sensitize cells to pathogen detection and therefore enhance antimicrobial or antiviral activity (157, 158, 198). On the other hand there are ISGs, such as suppressor of cytokine signaling (SOCS) proteins, which act as inhibitors of TLR and JAK-STAT signaling pathways, that desensitize cells in order to maintain immune balance (199).

As described previously, the antiviral role of ISGs have been extensively studied, however their role during bacterial infection remains uncertain. Several ISGs that function in antiviral immunity have also been shown to inhibit replication of bacteria, for example ISG15 and Viperin. ISG15 promotes IL-6 and IL-8 secretion required for restricting *L. monocytogenes* infection (200). Viperin is another example of an antiviral ISG known to restrict bacterial infections. Viperin expression is also upregulated during bacterial infection and can restrict *L. monocytogenes* and *Shigella flexneri*. For *S. flexneri* specifically, viperin has been shown to restrict entry into host cells (201).

Many ISGs that work against bacterial infections function by disrupting bacterial or endosomal compartments harboring bacteria. This exposes bacterial ligands to intracellular receptors, which promote IFN signaling and inflammasome activation. These pathways regulate cytokine secretion needed for the recruitment and activation of cells essential for bacterial killing. Additionally, bacterial infection can lead to the transcription of apoptotic ISGs, including Caspase and Fas proteins. Caspase-4 is both IFNα and IFNγ inducible and has been shown to promote inflammasome activation in response to infection with Gram-negative bacteria (202, 203). IRF1 regulates the transcription of several GBPs required for bacterial killing and inflammasome activation. Cells infected with the intracellular pathogens *Listeria monocytogenes* or *Fransicella novicida* lead to the induction of IRF1 followed by GBP expression. GBPs are responsible for disrupting bacterial membranes, which releases bacterial DNA into the cytosol and activate AIM2 inflammasomes (124, 204). GBPs also provide protection against intracellular parasitic infections, for example *Toxoplasma gondii*, and several viruses. The susceptibility to several pathogens to different GBP knock-out mice is reviewed in (104). In addition to inflammasome activation, GBPs can re-route phagosomes harboring intracellular pathogens to lysosomal degradation, enhance formation of reactive oxygen species and promote autophagy (205–207).

Overall antimicrobial and antiviral ISGs may vary in function depending on the class of pathogen detected in the host and exhibit broad activities in order to clear infection. Therefore, it is crucial to study the broad spectrum of ISGs and their functions to understand the mechanisms underlying host-pathogen interactions and develop effective antimicrobial or antiviral therapies. This dissertation describes a novel role of the ISG OAS1 in restricting the replication of viral and bacterial pathogens by an RNase L independent mechanism.

1.2 Oligoadenylate Synthetases

The OAS family proteins are a group of IFN inducible proteins first described to inhibit viral replication by activation of RNase L, a global suppressor of translation. The discovery of OAS proteins began with the observation that IFN lead to the activation of proteins, which in response to dsRNA inhibited cellular translation, therefore limiting translation of viral genes and replication (208). The ability to suppress translation was later attributed to a dsRNA dependent protein kinase known as PKR and a low molecular weight (LMW) inhibitor found in cell extracts of dsRNA treated cells (209, 210). The LMW inhibitor was identified as 2'-5' oligoadenylates that are linked through 2'-5' phosphodiester bonds and the enzyme (OAS) responsible for their synthesis was purified from mouse cells (211, 212). During the same period of time that OAS enzyme was discovered it was apparent that synthesis of 2'-5' oligoadenylates lead to the activation of an endonuclease responsible for the degradation of cellular and viral RNAs. It wasn't until a few years later that this RNase was successfully cloned and analyzed (213–215). Today we know this endonuclease as RNase L, which exists as inactive monomers in the cytosol and comes together in a dimeric structure upon binding to 2'-5' oligoadenylates, thus becoming active and leads to RNA cleavage (162, 216, 217). Once OAS enzyme was discovered, it did not take long before both mouse and human OAS was purified, revealing the existence of two forms of OAS (218–220). Through cDNA expression and sequencing, two forms of OAS (42kd and 46kd) were identified and characterized revealing a difference specifically at the C-terminus of these proteins, which was elongated in the larger variant (221, 222). In addition to these variants of OAS, the existence of two larger forms of OAS (69kd and 100kd) were discovered by monoclonal antibodies designed to identify OAS, revealing that several forms of OAS exist and share a homologous primary structure (223). Characterization of these larger OAS proteins revealed that they

synthesize 2'-5' oligoadenylates varying in length under different cellular conditions (dsRNA concentration and pH for example) and additionally Northern blot hybridization assays revealed that probes designated to recognize OAS mRNA did not work on mRNAs from the larger OAS variants. This suggested that these larger OAS proteins are translated from mRNAs that were transcribed from another set of genes (223–225).

Currently these OAS variants capable of synthesizing 2'-5' oligoadenylates are known as OAS1, OAS2 and OAS3 and share similar structural and functional domains. They all share a NTase domain, required for binding dsRNA and catalyzing 2'-5' oligoadenylate synthesis from ATP, and one, two or three OAS domains on OAS1, OAS2 and OAS3 respectively. In addition to OAS1-3 an enzymatically inactive variant of OAS exists, called OASL, which shares the same OAS domain as the other family members but does not contain a NTase domain, instead it has two ubiquitin-like domains at its C-terminus that mediate antiviral activity by enhancing RIG-I signaling (226, 227). Similar to humans, mouse genomes encode several OAS family proteins, some which are enzymatically active and others inactive (14). However, antiviral functions have been attributed to enzymatically inactive members of the OAS family, for example OASL antiviral activity and flavivirus resistance by the mouse ortholog to human OAS1 (Oas1b) (228, 229). These findings indicate that there are several antiviral mechanisms that are yet to be discovered for members of the OAS family, which is further implied by the discovery that OAS3 is sufficient and necessary for the activation of RNase L (17). However, overexpression of OAS1 and OAS2 still confers antiviral resistance, suggesting that RNase L independent mechanisms of antiviral activity exists for these proteins.

1.2.1 OAS Structure and Function

The human OAS family is a group of IFN inducible proteins consisting of OAS1, OAS2, OAS3 and the enzymatically inactive OASL protein. Through in situ hybridization, *OAS1-3* genes were mapped to a 130kb region on chromosome 12 (12q24.1) and *OASL* was mapped in proximity to the *OAS1-3* gene cluster on chromosome 12q24.2 and are approximately 1Mb apart (225, 230, 231). In mice the OAS family has been mapped to the murine chromosome 5F. Murine *Oas2* and *Oas3* genes share very similar exon and intron structures to human *OAS2* and *OAS3* genes, however there are 8 *Oas1* genes in mice, presumably originating from gene duplication, and are all transcriptionally active after IFN treatment (14, 232). For *OASL* there are two variants in mice, *Oasl1* which shares 74% identity to human OASL and *Oasl2* which shares 49% identity and most likely originated from gene duplication of *Oasl1* (14). All human and mouse *OAS* genes share a high degree of identity in their first 5 exons, suggesting that the OAS family has originated from a common ancestral gene, which has been proposed by Kumar et al. 2000 (233). The positioning of both human and mouse OAS family members in their respective genomes is summarized in Fig. 5, along with their enzymatic activity and potential mechanisms of antiviral functions.

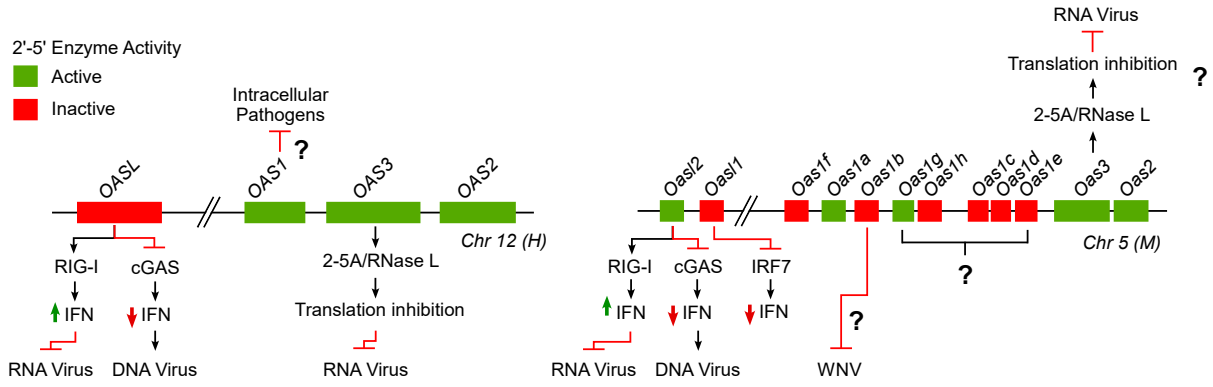

Figure 5. Genomic structure of human and mouse OAS gene family
Schematic of human (left) and mouse (right) *OAS* genes and known antiviral functions. Genes encoding enzymatically active proteins are labeled in green and genes encoding inactive proteins are labeled in red.

All members of the OAS family with the ability to synthesize 2'-5' oligoadenylates share an OAS domain containing NTase domains within them, allowing for binding to RNA substrate and processing of ATP into 2'-5' oligoadenylates through specific catalytic residues (discussed below). On the other hand, the catalytically inactive member of the OAS family, OASL, contains an OAS-like domain with mutations at key residues that abolish its catalytic function and a unique C-terminal domain containing ubiquitin-like sequences. OAS2 and OAS3 contain one and two inactive OAS-like domains respectively in addition to the catalytically active domain, the domain structure of all human OAS proteins is summarized in Fig. 6.

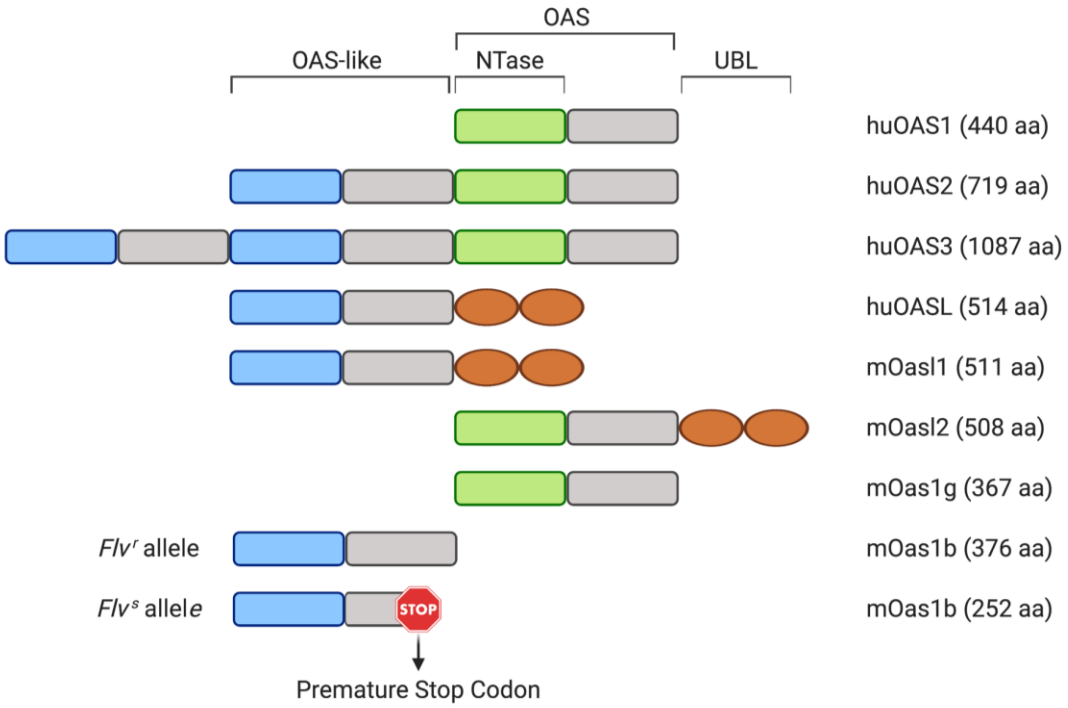

Figure 6. OAS protein domains
Schematic of protein domains found in OAS family members. OAS-like domains are colored in blue and gray, OAS domains, containing the active NTase domain, are colored in green and gray and ubiquitin-like (UBL) domains are identified as orange ovals.

OAS proteins belong to a NTase superfamily and one key feature of this polymerase family is the presence of a catalytic triad composed of aspartic or glutamic acids required for coordination

between magnesium ions and nucleotides in order to catalyze the nucleotide polymerization (234). Structural comparison between DNA polymerase β and OAS2 revealed three aspartate residues that formed part of a catalytic triad similar to that of the polymerase, which is conserved among OAS family proteins. Mutagenesis of the residues in the catalytic triad to alanine resulted in impaired synthetase activity (235). Crystal structure analysis of porcine OAS1 confirmed the presence of this catalytic triad formed by three aspartate residues D74, D76 and D147 on different beta strands and similar to OAS2 mutations of these residues to alanine abolished catalytic activity (236). Additionally, analysis of the crystal structure of porcine OAS1 also revealed a key serine residue (S62), which interacts with phosphate on ATP and several arginine and lysine residues (R38, K41, K59E, R194, R198 and K203) required for RNA binding. Association with RNA promotes conformational changes of OAS proteins required for efficient enzyme activity.

OASL is devoid of enzyme activity due to a threonine residue present at the third carboxyl acid of the catalytic triad instead of aspartate, but shares the same RNA binding residues as OAS1, which are required for binding dsRNA and enhancing RIG-I signaling (13, 237). During RNA virus infection OASL is induced and binds to RIG-I mimicking polyubiquitin and enhancing RIG-I sensitivity to the RNA ligand, leading to more IFN production (238). However, during DNA virus infection OASL instead downregulates IFN production allowing replication of DNA viruses. Ghosh et al. 2018 demonstrated that OASL-deficient cells showed increased levels of IFN and lower viral titers for DNA viruses, and that cGAS-mediated IFN induction was needed for restricting virus in OASL-deficient cells. OASL was shown to bind directly to cGAS resulting in inhibition of cGAMP production, serving as a negative feedback-regulator of cGAS mediated immunity, therefore maintaining cellular homeostasis (239). Different to the oligonucleotides synthesized by polymerases (3’-5’ phosphodiester links), OAS proteins upon binding dsRNA

synthesize 2'-5' oligoadenylate links that vary in length. OAS1, OAS2 and OAS3 function as tetramers, dimers or monomers respectively, which synthesize trimeric or hexameric, tetrameric and dimeric 2'-5' oligoadenylates respectively (235, 236, 240, 241). However it has been reported that OAS3 is more sensitive to dsRNA ligand as compared to OAS1 and were shown to synthesize longer 2'-5' oligoadenylates with trimeric structures needed for RNase L activation (242).

Recent studies by Li et al. 2016, revealed that OAS3 was sufficient for the activation of RNase L in response to viral infection. OAS1- and OAS2-deficient cells were still capable of activating RNase L and degrading ribosomal RNA (rRNA), however this phenotype was completely abolished in OAS3-deficient cells, similar to RNAse L-deficient cells, suggesting that RNAse L activation can be mediated by OAS3 alone (17). Although OAS1 and OAS2 are not strictly required for activating RNase L, overexpression of these proteins reduced susceptibility to viral infections. For example, OAS1 is known to play roles in host defense against WNV, dengue virus (DENV), EMCV and has also been shown to provide antimicrobial defense against intracellular bacteria such as *M. tuberculosis* (243–246). The existence of antiviral roles independent of RNase L in both catalytically active and inactive members of the human OAS family is mirrored in mouse OAS proteins. The exon and intronic structure of mouse *Oas2* and *Oas3* is identical to human *OAS2* and *OAS3* and the amino acid sequences of these exons share a high degree of homology, suggesting that these proteins in mice are functionally equivalent to their human counterparts (14). There have been two *OASL* orthologs identified in mice: *Oasl1* which is enzymatically inactive and *Oasl2* which is active. *Oasl2* contains two aspartate residues, which allows it to exhibit OAS enzyme activity, however studies in bone marrow derived macrophages (BMDMs) from *Oasl2*-deficient mice revealed reduced RIG-I signaling, resulting in enhanced viral replication. (13). In response to DNA virus infection, *Oasl2* shares similar functions as human

OASL. *Oasl2*-deficient mice, infected with several DNA viruses, showed higher levels of IFN production resulting in reduced viral replication (239). Together these data suggest that *Oasl2* works as the functional equivalent to human OASL. Different to the other murine OAS proteins, there are eight *Oas1* genes closely related to human *OAS1*, several which are enzymatically active and the rest inactive. Sequence analysis of all murine *Oas1* genes revealed a high degree of homology between the first five exons of each gene with human *OAS1* exons 1-5 and differ in their C-terminal amino acid residues (Fig. 7).

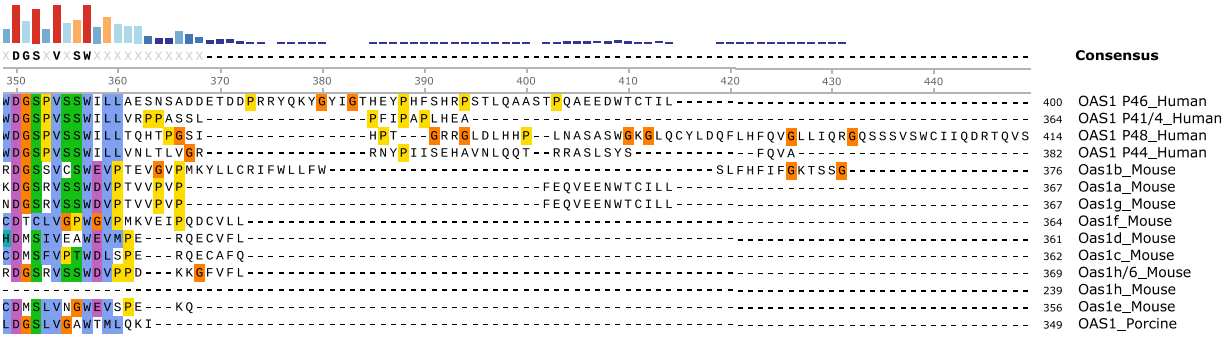

Figure 7. OAS C-terminal Sequences
Protein sequence analysis of the C-terminal domain of human OAS1 isoforms and murine Oas1 proteins. Protein sequences were aligned using Clustal Omega and compared to the consensus sequence. Full sequence alignment is available in Appendix A.

Among all the murine Oas1 proteins, only Oas1a and Oas1g are capable of synthesizing 2'-5' oligoadenylates, however studies show that Oas1b and Oas1d are capable of inhibiting Oas1 synthetase activity in response to p(I):p(C), suggesting potential negative feedback roles among murine Oas1 proteins (247, 248). The inactive Oas1 proteins (b-f, h) are still capable of binding dsRNA, but the function of these proteins are still not completely clear (247, 249). Oas1b however was mapped to a flavivirus resistance gene and full length Oas1b confers antiviral resistance against WNV (248). The susceptibility to flavivirus infection is observed in many common laboratory strain mice as compared to several populations of wild *Mus musculus domesticus* mice

(subspecies of house mice), which are resistant to viral infection, and the alleles that determine susceptibility and resistance were designated as *Flv*^{s} and *Flv*^{r} (250). The gene responsible for the flavivirus phenotype was mapped to *Oas1b* by a positional cloning strategy. Mice susceptible to infection encoded a C-terminal truncated variant of Oas1b as compared to resistant mouse strains, which encode full length Oas1b (Fig. 6) (228). Additionally, the *Flv*^{r} phenotype was restored in flavivirus susceptible mouse strains by genetic knock-in with *Oas1b* capable of expressing full length Oas1b, confirming that this phenotype is mediated by Oas1b alone (251). WNV are sensitive to RNA degradation by RNase L, however it is clear that deficiency in the enzymatically inactive Oas1b protein is detrimental to mouse survival (252, 253). In humans, a single nucleotide polymorphism (SNP) in human OAS1 has also shown susceptibility or resistance to flavivirus infection (discussed below). These studies suggest that although Oas1b lacks enzymatic activity, it could be the functional equivalent to OAS1 and their antiviral activity is independent of RNase L (243, 254).

1.2.2 Oligoadenylate Synthetase 1

OAS1 is the smallest of the human OAS family proteins with only one catalytically active OAS domain in its protein structure (Fig. 6). The catalytic domain of OAS proteins was first characterized by Sarkar et al. 1998 by comparing structural models for OAS2 with DNA polymerase β, which identified a potential catalytic triad of aspartate residues in a highly conserved region found in OAS1, OAS2 and OAS3 (235). The presence of this catalytic triad was confirmed in OAS1 by analysis of the crystal structure of porcine OAS1 by Hartmann et al. 2003 (236). This crystal structure revealed a short N-terminal, followed by the large catalytic domain of OAS proteins and a helix-loop linker domain, which connects the catalytic domain to the large C-

terminal domain of OAS1. Additionally, characterization of the crystal structure of porcine OAS1 identified several residues required for catalytic activity and RNA binding (236). The crystal structure of human OAS1 bound to dsRNA was characterized by Donovan et al. 2013 providing more insight into the conformational changes and functionality of OAS1 (Fig.8). The first two aspartate residues of the catalytic triad are found on the catalytic domain of OAS1 while the third residue is found at the C-terminal domain. These residues come together after dsRNA has bound to OAS1, inducing a conformational change that exposes the negatively charged pocket of the OAS1 monomer to the ATP ligand (Fig.8A-B). RNA binding is crucial for the activation of OAS1 and mutation of the lysine and arginine required for RNA binding to negatively charged amino acid residues greatly effects activation and function of OAS1 (Fig. 8C left). For optimal binding to ATP, two Mg^{+2} ions are required to bridge the catalytic triad of OAS1 to the ATP ligand and catalytic activity is abolished my mutating aspartate to alanine (Fig.8C right).

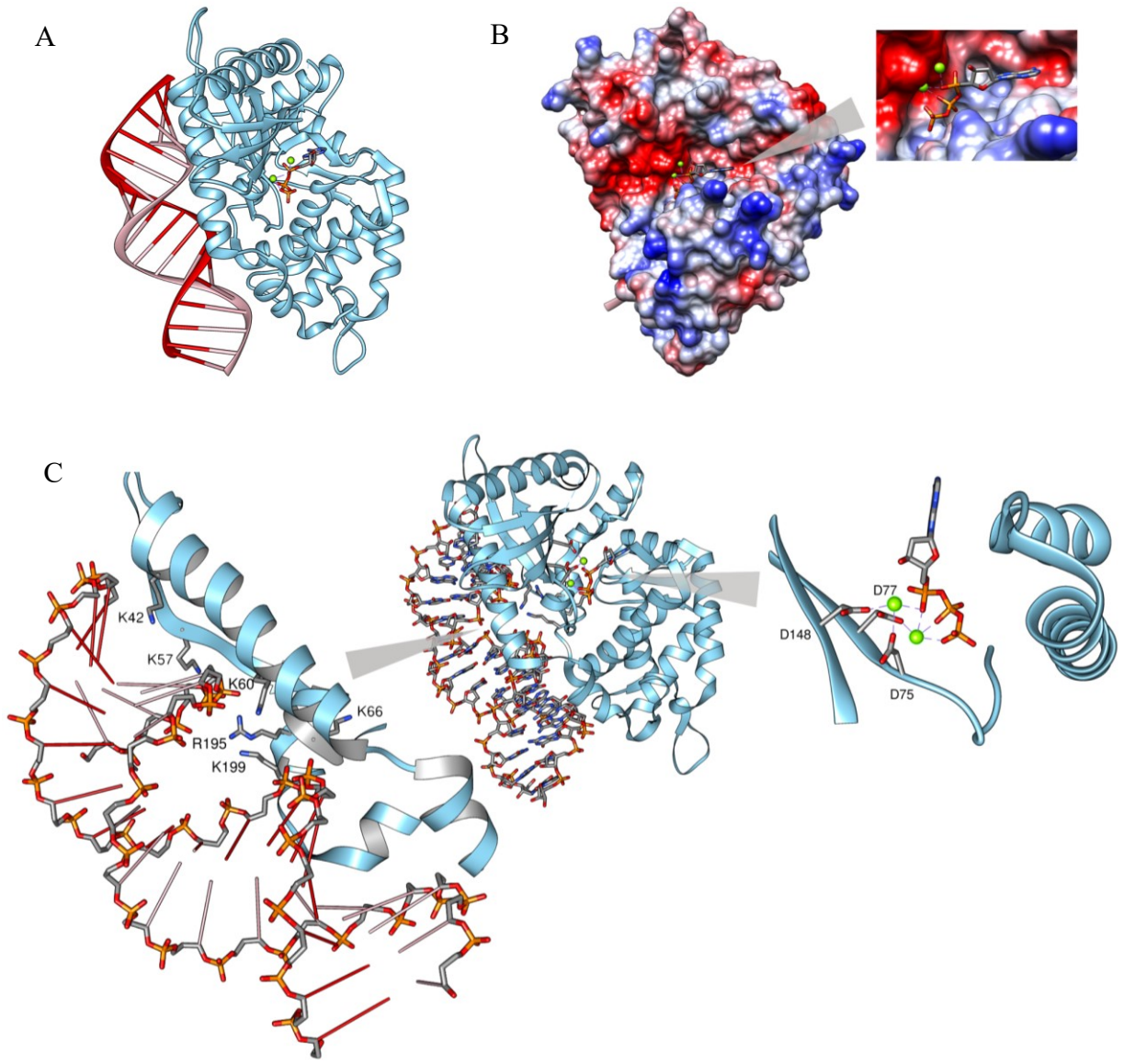

Figure 8. Crystal structure of human OAS1
Ribbon structure of OAS1 bound to dsRNA and ATP ligand (A). Electrostatic potential surface structure of OAS1 facing towards the negatively charged pocket of OAS1, which binds to ATP ligand (B). Residues needed for RNA binding (left) and residues forming part of the catalytic triad (right) in OAS1 (C). The crystal structure obtained from the RCSB protein data base (4ig8) where analyzed by USCF Chimera.

Alternative splicing of the *OAS1* gene can lead to the expression of several isoforms: P35, P42, P44a, P46, P48 and P52. Interestingly a SNP (rs10774671) found in OAS1 affects the expression of these isoforms (255). The SNP rs10774671 is positioned at the acceptor site of exon 6 and the nucleotides found at this position can vary between adenine or guanine (A or G allele

respectively). The genotype of this SNP can be determined by restriction fragment length polymorphism (RFLP) assays using AluI restriction enzyme (developed by Noguchi et al. 2012). Although 6 isoforms of OAS1 exists, P42 and P46 isoforms are most abundantly expressed in cells that are homozygous for the A or G allele respectively as compared to the other isoforms, suggesting that these isoforms are most crucial for mediating antiviral activity (254). However, analysis of the OAS1 SNP in patients and healthy cohorts has revealed that the genotype of the SNP is crucial for dictating antimicrobial and antiviral protection (246, 254, 256). Heterozygous expression of the G allele is sufficient to confer antiviral protection against to flaviviruses and is most likely attributed to the predominant expression of the P46 OAS1 isoform, similar to the phenotype observed in mice expressing full length Oas1b (Fig. 9). It is crucial to note that differences between OAS1 P42 and P46 are restricted to the C-terminal, which is very interesting considering that the antiviral phenotype of murine Oas1b is also mediated by differences at the C-terminus. This suggests that the C-termini of both human and mouse OAS1 are crucial for protection against invading pathogens through an RNase L independent mechanism that has yet to be described.

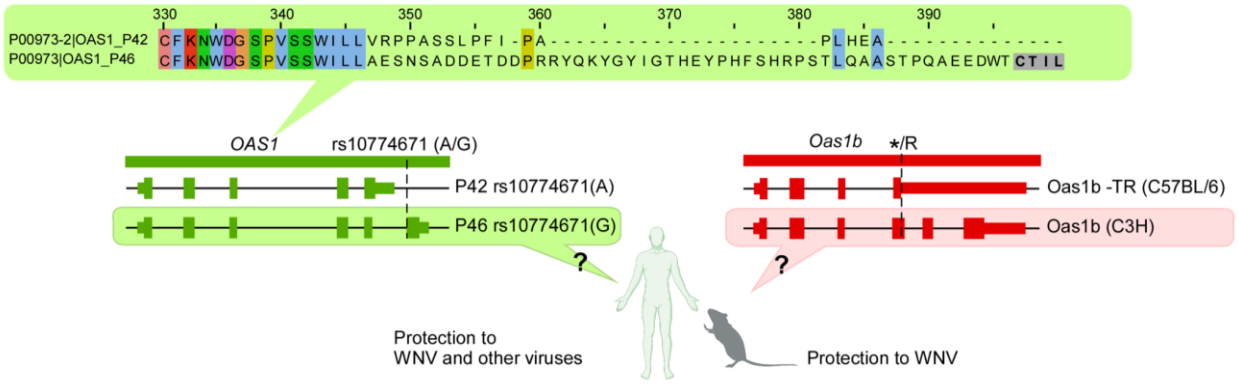

Figure 9. OAS1 SNP rs10774671 and Oas1b flavivirus associated alleles
Exon and intronic structure of human OAS1 p42 and p46 (left) and both truncated and full length Oas1b (right). The amino sequence alignment of the C-terminal region of OAS1 p42 and p46 is provided to highlight the differences of these two isoforms.

1.2.2.1 Antiviral role of OAS1

Early studies overexpressing both human and mouse OAS1 found that these proteins were capable of inhibiting viral replication of EMCV and it was thought that this antiviral activity was mediated through 2'-5' synthetase/RNase L activity (257, 258). However, Kristiansen et al. 2010 showed that extracellular porcine OAS1 was capable of inhibiting EMCV by a RNase L independent mechanism (245). Similarly, several studies have eluded to both RNase L dependent and independent mechanisms of antiviral activity against flavivirus infection (229, 244, 252, 253). Until now the mechanism of OAS1 antiviral activity is still not clear. However, the findings that OAS3 is mostly responsible for activation of RNase L and that Oas1b antiviral activity is strictly independent of RNase L, are sufficient evidence to hypothesize that human OAS1 is capable of restricting virus through an RNase L independent pathway. Additionally, genetic variation of the OAS1 SNP rs10774671 influences isoform expression and virus susceptibility (Fig. 9). This SNP in OAS1 has been shown to be crucial for the susceptibility of both Hepatitis B and C virus (HBV and HCV). Individuals homozygous for the A allele of rs10774671 are more susceptible to HBV infection, which can contribute to the development of the autoimmune disease Sjögren's syndrome. On the other hand, the presence of the G allele, which promotes OAS1 p46 expression is capable of inhibiting HBV replication (259). Interestingly, this same SNP in OAS1 was correlated to response to IFN therapy and disease progression of HCV. Individuals homozygous for the A allele were associated with non-responsive therapy as compared to better responses to therapy in individuals harboring at least one copy of the G allele (260). A similar trend has also been observed for WNV, in which individuals homozygous for the A allele were more susceptible to WNV infection as compared to individuals hetero- or homozygous for the G allele (243). These

correlative studies between the SNP rs10774671 and viral susceptibility suggest that OAS1 p46 is required for the antiviral activity of OAS1. Similarly, studies in murine Oas1b confirm that WNV antiviral activity is independent of RNase L.

1.2.2.2 Antibacterial role of OAS1

In response to bacterial infections host cells secrete IFN, however depending on the bacterium, the IFN response can restrict or enhance bacterial growth (102). Traditionally OAS family proteins have been shown to restrict virus, however several transcriptomic analysis have revealed that OASL is up-regulated in several cell types in response to several intracellular pathogens (261, 262). Both probacterial and antibacterial effects has been associated to OASL. STING dependent production of OASL was shown to promote survival of *Mycobacterium leprae* by inhibiting expression of antimicrobial peptides and autophagy, and knock-down of OASL promoted cGAS dependent autophagy and clearance of *M. leprae* (263). On the other hand, knock-down of OASL in the context of *M. tuberculosis* infection resulted in a decrease of pro-inflammatory molecules (IL-1β, TNFα and MCP-1) and increased replication of *M. tuberculosis* (262). In addition to OASL, OAS1 has been associated *M. tuberculosis* susceptibility. The same SNP in human OAS1, which is involved in virus susceptibility, rs10774671, also confers protection against *M. tuberculosis*. A case-control study genotyped whole blood, from TB infected patients and healthy cohorts, for the OAS1 rs10774671 SNP and found a correlation between the G allele and protection against *M. tuberculosis* (246). Although correlations between microbial protection and OAS family proteins have been established, the mechanisms are yet to be defined.

1.3 West Nile Virus

1.3.1 WNV Prevalence and Pathogenesis

WNV is a positive single stranded RNA virus belonging to the *Flaviviridae* family and is primarily transmitted through mosquitoes. It is one of the leading causes of mosquito borne illnesses in the continental United States (US) and can cause severe neurodegenerative disease in immunocompromised individuals. The enzootic cycle of WNV is maintained between mosquitos and birds, infected birds develop high titers of virus, which are transmitted from host to host through mosquito vectors (264). The disease can be transmitted to mammals through infected mosquitos; however, they are considered dead end hosts since they do not develop high levels of virus in their blood and are incapable of passing the virus on to uninfected mosquitos. Although transmission between mammals is highly unlikely, cases of WNV in the US remain prominent. From 1999-2018 the CDC has reported over 50,000 cases of WNV disease, 24,000 cases of WNV related neurodegenerative disease and 2300 deaths. Additionally, WNV has played a significant impact on the aviary ecosystem of the US causing mortality in over 300 bird species and massive population declines in at least 23 species (265, 266).

WNV was first isolated in Uganda in 1937 and remained endemic in African regions, Europe, Asia, Australia and the Middle East (265). It was first reported in the US in 1999 following an outbreak in NY, which quickly spread throughout the country. It reached its peak in 2003 with several of cases reported in 48 states and registered the largest number of neuroinvasive cases related to WNV (264, 267). As of 2004 the number of cases has relatively stabilized, with the exception of the 2012 outbreak, the largest outbreak in the US since 2003. The spread of WNV throughout the US can be tracked using the open-source tool nextstrain maintained by Grubaugh

Lab and James Hadfield (nextstrain.org/WNV/NA). Although the numbers of cases have stabilized in the US, there are several individuals at risk for WNV mediated disease and a cost-effective vaccine for WNV has yet to be licensed for use in humans. However several vaccines have been licensed for horses, another common dead end host of WNV (264). Prevalence of WNV is not exclusive to the US, throughout the years WNV spread through the Americas, however the severity of disease is not as high that could be related to cross-protection originating from infection with other mosquito-borne viruses (265, 268, 269). Outbreaks of WNV have been documented in birds, horses and humans in Europe and Eastern Mediterranean region as early as the 1950s (270, 271). Phylogenic analysis of WNV strains suggests that the 1999 NY strain originated from Israel and spread to the US (265, 270–272). Although WNV has transmitted globally, the level of concern is not as high as compared to more infectious and deadly viruses.

Most individuals infected with WNV remain asymptomatic, some develop common symptoms such as fever, aches or digestive problems. Few, such as the elderly, immunocompromised or people with chronic illness, can develop severe illness affecting the central nervous system, which can lead to encephalitis, meningitis and paralysis (273). Sejvar 2016, reviews the clinical manifestations of WNV in great detail (264). There are several genetic factors that influence WNV susceptibility, among these are polymorphisms in OAS1, IRF3 and MX1 and a homozygous gene deletion found in C-C motif chemokine receptor 5 (CCR5). Mice deficient in CCR5 exhibit reduced leukocyte trafficking to the central nervous system, increased viral burden and mortality in response to WNV infection. Further studies are needed to determine how polymorphisms in IRF3 and MX1 alter their protein expression and also investigate the mechanisms of OAS1 WNV antiviral defense (274). Due to the global emergence and spread of WNV and the lack of vaccines or effective antiviral therapies, it is important to identify crucial

components of the host immune response, required for clearing WNV, which could be used for therapy by potentiating the immune response against WNV.

1.3.2 Molecular Biology of WNV

WNV belongs to the *Flavivirus* genus, a group of enveloped positive senses single stranded RNA viruses. This genus includes: Zika (ZIKV), Dengue (DENV), Japanese encephalitis virus (JEV), Kunjin (KUNV) now considered a subtype of WNV and yellow fever virus among others. The WNV genome contains a type 1 cap structure (m7GpppAmp) at the 5' end and lacks a 3' poly A tail as seen in most flavivirus (275). At both the 5' and 3' ends of WNV RNA there are non-coding regions (NCR) required for folding of RNA into secondary stem loop structures, which are conserved among flavivirus and deletions in the stem loop sequence are detrimental in forming infectious particles (276).

The genome of WNV is translated into a single polyprotein, which is proteolytically cleaved into three structural proteins (capsid, membrane and envelope proteins) and seven non-structural proteins (NS1, NS2A, NS2B, NS3, NS4A, NS4B, and NS5). WNV membrane (M) and capsid (C) proteins are glycosylated, which allow them to interact with various glycosaminoglycans on the cell surface, followed by attachment to C-type lectin receptors and endocytosis (276, 277). Additionally, phosphatidylserine binding proteins belonging to the TIM family, cellular integrins and laminin-binding proteins have also been shown to facilitate WNV entry into host cells (278–280). Once engulfed, viral particles remain associated to endosomes, followed by fusion of viral and endosomal membranes, which releases nucleocapsids and virus RNA into the cytosol. The viral genome is translated into a single polyprotein and NS2B-NS3 serine proteases process the polyprotein into mature proteins (281). NS5 or viral RNA-dependent

RNA polymerase (RdRp) in conjunction with viral NSPs and host proteins initiates replication of negative sense RNA, which serve as templates for the replication of positive sense genome RNAs (275, 276, 282). Reorganization and assembly of synthesized genomes and translated proteins leads to association with rough ER membranes, where viral particles are packaged followed by release of infectious particles into the extracellular environment (276). In addition to their structural roles and functions in viral replication, several flaviviral proteins through pathogen-host evolutionary arm races, have developed the ability to antagonize host immune responses in order to promote virus survival (283). The mechanisms of flavivirus antagonism of host immune response is summarized in Fig. 10.

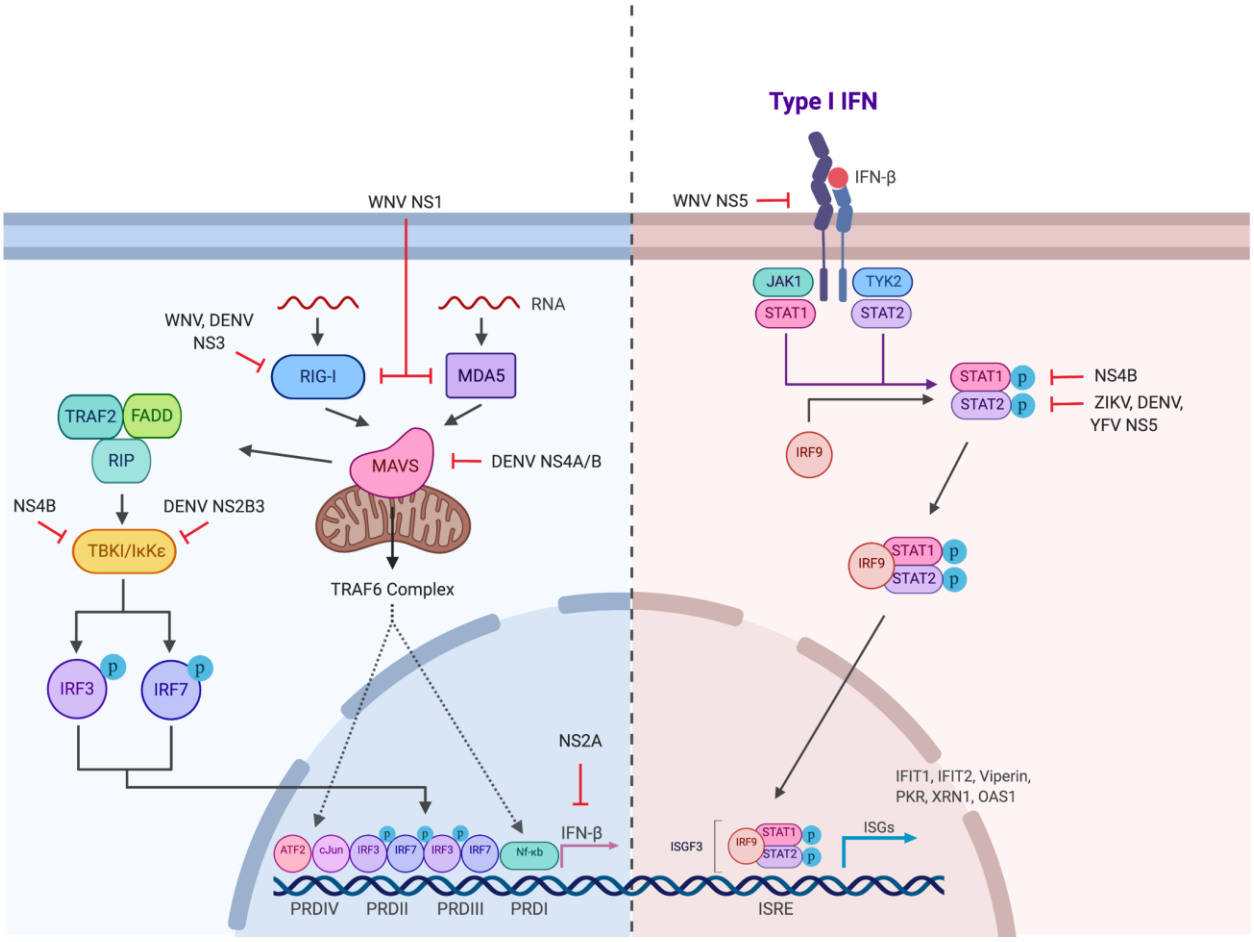

Virus Protein	Function	Reference
NS1	WNV NS1 binds to RLRs inhibiting IFN induction and promoting degradation of RIG-I and MDA5	(284)
NS2A	The majority of flaviviral NS2A proteins are potent inhibitors of IFNβ promoter driven transcription	(285)
NS2B3	DENV NS2B3 interacts with IkKε, masking its kinase domain, therefore inhibiting IRF3 phosphorylation and activation	(286)
NS3	WNV and DENV NS3 bind to 14-3-3e adaptor proteins required for translocation of RIG-I to mitochondrial surfaces	(287)
NS4A, NS4B	DENV NS4A and NS4B have been shown to bind to MAVS and disrupt interaction with RIG-I. DENV and WNV NS4B have been shown to block TBK1 phosphorylation and activation. The majority of flaviviral NS4B proteins have been shown to block activation and translocation of STAT1	(288–290)
NS5	WNV NS5 has been shown to decrease surface expression of IFNAR1 receptors. ZIKV, DENV and YFV NS5 have been shown to target and induce degradation of STAT2	(291–293)

Figure 10. Antagonism of host immune response by flavivirus
Several flaviviral non-structural proteins have been shown to antagonize RLR signaling and induction of IFNs (left) or antagonize IFN receptor signaling (right).

1.3.3 Host Antiviral Immune Response to WNV

In order to study pathogenesis and host immune responses to WNV several animal models have been developed, for example subcutaneous footpad injections in mice, which mimics mosquito delivered virus (274). WNV first replicates in skin keratinocytes and skin residents DCs, followed by viral replication in lymph nodes and spread to peripheral tissues and organs (294, 295). As mentioned above, WNV can cause neuroinvasive disease by infecting neuronal and myeloid cells within the CNS and it is believed that WNV crosses the blood brain barrier in order to establish infection (296, 297).

Control of WNV is dictated by innate antiviral responses that lead to the induction of IFN and expression of ISGs required for viral suppression, regulation of apoptosis and viral clearance and the establishment of adaptive immunity. WNV dsRNA intermediates are primarily recognized by RLRs, resulting in activation of MAVS and IRF3 leading to the induction of type I IFNs. IFN signaling leads to the induction of several ISGs known to restrict WNV such as IFITs, PKR, viperin, XRN1 and OAS1 (298). IFIT1 has been shown to inhibit virus lacking 2'-O-methylation, however several studies have shown that flavivirus, including WNV, exhibit 2'-O-methyltransferase activities that promote viral evasion of IFIT1 (299). On the other hand, cell type specific inhibition of WNV by IFIT2 has been documented in brain tissue of *Ifit2*-deficient mice (300). Similarly, deficiencies of PKR and Viperin or the presence of non-functional Oas1b, greatly enhance WNV susceptibility both *in-vitro* and *in-vivo* (243, 301, 302). Interestingly, recent studies have shown restriction of WNV by the cGAS-STING pathway. cGAS is a cytosolic sensor of DNA and the mechanism by which cGAS is activated during RNA virus infections is still unclear. However, deficiency of cGAS or STING in mice resulted in higher morbidity after infection with WNV suggesting novel functions of cGAS-STING immunity to restrict RNA viruses (303, 304). Infection with DENV has also been shown to activate cGAS pathway, and the importance of cGAS during infections is alluded by cGAS antagonisms by DENV NS2B (305–307). Currently it is proposed that cellular stress during flaviviral infection causes leakage of mitochondrial DNA into the cytosol, triggering cGAS activation and IFN induction (305, 308). Another component of innate immune responses to WNV include inflammasome signaling pathways that trigger IL-1β secretion and apoptosis. Deficiencies in NLRP3 inflammasome and IL-1β secretion show increased viral susceptibility and it is proposed that IL-1β promotes trafficking of innate and adaptive immune cells to sites of WNV infection (309, 310). However, IL-1β signaling has also

been implicated in neuropathology. Deficiencies of caspase 3 and 8 during WNV infection, increases survival and decreases CNS tissue injury in caspase deficient mice as compared to WT mice (311, 312).

It is clear that several innate immune mechanisms are required for clearing WNV infection, but similar to many biological processes a balance between restricting infection and maintaining cellular homeostasis is required for host survival. During infection, macrophages and DCs are crucial for the establishment of both innate and adaptive cellular immunity through the secretion of pro-inflammatory cytokine and cellular chemokines. The role of NK cells and neutrophils during WNV infections remains controversial. A small population of γδ CD3+ T cells are critical for eliciting protective immunity against WNV and deficiency of these cells is associated with enhanced viral susceptibility and spread to the CNS (274). However, adoptive transfer of IFNγ producing γδ T cells into TCRδ-deficient mice restored antiviral immunity to WNV (313). IFN signaling, in response to WNV, primes B cell and T cell immunity needed for viral clearance (314, 315). B cells are important in maintaining passive immunity against WNV. Studies have shown that serum from WNV infected mice, is capable of establishing protection against WNV in B cell and antibody deficient mice (μMT) or in B cell activating factor receptor (BAFFR) deficient mice (314, 316). Both CD4+ and CD8+ T cells are required for clearing WNV in the CNS, however recent studies suggest that CD4+ T cells help regulate B cell antibody responses and CD8 is required for viral clearance (317–319). Determining the mechanisms of WNV pathogenesis and antiviral immunity is critical for the development of targeted therapies and protection of susceptible individuals amongst the population. As with all viruses, WNV (and other flavivirus) have developed several mechanisms of antagonizing host immune responses (reviewed in Fig. 10) and understanding the roles of all ISGs, which have been developed through evolutionary arms

races, is critical. In this dissertation a novel mechanism of OAS1 WNV antiviral activity is described, which explains the RNase L independent protection to WNV provided by murine Oas1b and a functional equivalence to human OAS1.

1.4 Intracellular Bacterial Infections

Immune responses against bacteria begin with sensing PAMPs of bacterial origin by TLRs (Fig. 1), NLRs, AIM-like receptors (ALRs) and cytosolic sensors of both RNA and DNA (Fig. 2). However, intracellular bacteria can internalize within the host and avoid immune detection. In order to establish an effective infection, intracellular bacteria must first enter host cells through phagocytosis, receptor-mediated endocytosis in non-phagocytic cells or through bacterial secretion systems that promote actin polymerization and alter membrane integrity (320). Once within cells, bacteria thrive in pathogen-containing vacuoles where they evade detection, avoid triggering immune responses and can also reprogram both host and bacterial metabolism (321). When bacterial growth is saturated in a host cell, they can exit through lysis of existing host in order to spread to neighboring cells. Alternatively, some bacteria enter neighboring cells through direct cell to cell spread mediated through actin-based motility and formation of membrane protrusions (322). Although bacteria have developed sophisticated mechanisms of evading host immune responses, they are not full proof, and infection can trigger IFN production and expression of ISGs required for bacterial clearance.

IFN signaling is well established during virus infection, conferring antiviral immunity through the expression of ISGs and activation of immune cells needed to clear infection. However, the role of IFN during bacterial infections is more complex, in some cases providing protection

and in others is detrimental to host survival (7, 102). Beneficial roles of IFN during bacterial infection include enhancing tissue integrity, secretion of pro-inflammatory molecules, enhancing type II IFN signaling and cellular immunity and secretion of antibacterial peptides, which directly disrupt bacteria. On the other hand, infection with some intracellular bacteria, for example *L. monocytogenes* or *Francisella tularensis* exhibit detrimental effects of IFN signaling. Infection can trigger IFN production through cGAS-STING signaling, but induction of IFN in both cases is detrimental to the host and deficiencies in IFNAR1 or IRF3 confer protection to mice (102). IFN responses to *L. monocytogenes* have been associated with downregulation of IFNγ signaling and apoptosis of immune cells, which promotes dissemination and proliferation of bacteria (323, 324). Induction of IL-17 is required for neutrophil recruitment and clearance of bacterial pathogens. However, IFN signaling in response to *F. tularensis* has been shown to inhibit IL-17A in addition to promoting macrophage death, therefore conferring bacterial survival (7, 325). Although deficiency in IFNAR1 signaling confers protection against *L. monocytogenes* and *F. tularensis*, deficiency of AIM2 is detrimental to host survival. It is known that AIM2 activation and inflammasome signaling is a critical factor in clearing intracellular bacterial infections (124, 326–328). The IFN response against *M. tuberculosis* has shown both protective and detrimental roles during infections. Induction of IFNγ activates macrophages, which can directly inhibit *M. tuberculosis* through the IFNγ inducible GTPase Irgm1 (or LRG47) (329). Additionally, deficiencies in IFNγ receptor signaling enhance *M. tuberculosis* mediated disease (330–333).

Inflammasome activation in response to mycobacterial infections leads to the production of IL-1β, which is crucial for host defense against infection. Part of the detrimental roles of IFNs during *M. tuberculosis* infection include downregulation of IL-1β and other pro-inflammatory cytokines (334–336). Type I IFN leads to the expression of OAS1, and as previously discussed,

an SNP in OAS1 can confer protection to *M. tuberculosis* suggesting a protective role of type I IFNs as well. As the host IFN response to intracellular bacteria is quite complex, with both protective and detrimental roles to the host thus understanding these mechanisms can provide better insight for the development of therapies. Additionally, the use of intracellular models of bacterial infection can be beneficial for studying these mechanisms. In this dissertation, evidence is provided for a novel mechanism of OAS1 antibacterial immunity using *L. monocytogenes* and *F. novicida* as models of gram-positive and gram-negative intracellular infection.

1.4.1 Model Intracellular Bacteria

Several intracellular bacteria pose a significant risk for global public health, for example: *Mycobacterium tuberculosis* and *leprae*, which are associated to lung damage and leprosy respectively. The foodborne pathogen *L. monocytogenes*, *F. tularensis* known to cause pneumonic tularemia and *Salmonella*, which affects the intestinal tract, are further examples of intracellular bacteria that can cause harm. IFNγ is a key regulator of autophagy, immune cell function and ISGs needed to clear infection, in addition to inflammasome signaling and secretion of pro-inflammatory cytokines, which are also crucial to controlling infections (337–339). In order to study these signaling pathways, several models have been developed both *in-vitro* and *in-vivo*, which prove beneficial for modelling infections of highly pathogenic or fastidious microorganisms. For example, *M. tuberculosis* is a slow growing pathogen, which is endemic globally, and the World Health Organizations estimates 1.5 million tuberculosis associated deaths per year. The emergence of antibiotic resistance strains of *M. tuberculosis* and the lack of effective vaccines proves the necessity to further study signaling pathways that can contribute to host defense. Therefore, the use of non-virulent or attenuated strains of bacteria, which can easily be

cultured or worked on with minimal laboratory restrictions, are great tools for modelling bacterial infections and studying host immune responses to a broad spectrum of pathogens.

1.4.1.1 Listeria monocytogenes

L. monocytogenes is a foodborne gram-positive bacterial pathogen that can lead to listeriosis, characterized by fever, diarrhea and gastroenteritis. The CDC reports that older individuals, immunocompromised people and pregnant women, where infection can lead to miscarriage, are at a higher risk of disease. It is estimated that approximately 1,600 people suffer from listeriosis per year and approximately 260 die from the disease. Invasive listeriosis is characterized by spread beyond the intestinal tract, which can cause sepsis and meningoencephalitis the leading causes of death in high-risk individuals (340). Fortunately, listeriosis can be treated with a wide variety of antibiotics, which are effective in clearing infection, however the high morbidity of the disease and similarities in immune sensing and signaling to other intracellular pathogens is why there are several ongoing research studies to understand the host-pathogen interactions of listeriosis.

In response to *L. monocytogenes*, IFNγ is produced from innate immune cells, which activate macrophages for early control of infection and prime adaptive immune cells to clear bacteria. Therefore, infection with *Listeria* has been proven useful as a tool to study IFNγ responses to intracellular bacteria both *in-vitro* and *in-vivo*. For example, intraperitoneal infection of mice with the EDG strain (less virulent) of *L. monocytogenes* allows researchers to study IFNγ production by innate and adaptive immune cells, spread of bacteria to other organs and host survival to infection (341, 342). In fact *Listeria* has become a widely used model of host-

pathogen interactions and has provided insight into bacterial gene regulation, bacterial physiology, epigenetic modifications, interactions with gut microbiome and induction of innate and adaptive immunity (342–344). Studies relating to human infection of listeriosis are limited to epidemiological data, due to low incidence and long incubation periods. However, several animal models have been developed to effectively study gastrointestinal complications of disease, sepsis, neonatal infection and the cell biological and immunological responses to *Listeria.* Specifics of animals used in studies, infection routes, strains and protocols are summarized and reviewed in (341, 345–347).

1.4.1.2 Francisella novicida

Francisella is a genus of gram-negative bacteria, including *F. tularensis* which is associated to Tularemia a disease that varies in severity depending on how the bacteria enters the body. Disease can range from mild to life-threatening. Most cases include fever and ulcers at the site of infection and in more severe situations can lead to pneumonia, vomiting and diarrhea, splenomegaly and hepatomegaly. *F. tularensis* can enter the body through insect bites (mostly ticks), exposure to infected animals, contaminated food or inhaling airborne pathogen and the CDC reports hundreds of cases a year. Although infection with *F. tularensis* can be controlled with antibiotics, growing concerns over its high infectious rate and potential use of aerosols in bioterrorism has made it a focus for several research groups (348, 349).

Within the *Francisella* genus, *F. novicida* is genetically and biochemically similar to *F. tularensis* and is less pathogenic to humans, making it an ideal model for genetic manipulation and studying host-pathogen interactions to *Fransicella* (350). Several models have been adapted to study *Fransicella* in order to a gain insight on host immune responses and bacterial virulence

factors. Genetic screenings of *Drosophila melanogaster* infected with *F. novicida* have been used to study host-pathogen interactions and have identified several virulence factors such as transport proteins and DNA repair genes that help bacteria survive oxidative stress (351). Similarly, genetic screenings of *F. novicida* transposon mutations in mouse models lead to the identification of bacterial ATP synthase and thioredoxin, which when mutated increased host survival (352). Mice are highly susceptible to infection with *Fransicella* offering a unique model to study host-pathogen interactions (353). Mice can be infected through several biological routes, which mimic bacterial exposure to humans such as respiratory and gastrointestinal tracts, skin and conjunctiva, protocols associated with these infection routes are reviewed in (350, 353).

1.4.2 Host Defense to Intracellular Bacteria

Innate and adaptive cellular immunity, the induction of IFNs, expression of ISGs and inflammasome activation and signaling are all key hallmarks of controlling intracellular pathogen infections. Early responses to intracellular bacteria are attributed to the secretion of pro-inflammatory cytokines (IFNγ, IL-12 and TNFα) resulting in APC activation and enhanced oxidative burst and mice lacking these cytokines or respective receptors is associated with increased lethality (354, 355). Additionally, host cells can eliminate bacteria trapped in autophagosomes through autophagy, when these phagosomes fuse with lysosomes and digests the contents of the phagolysosome (356). In addition to maintaining cellular homeostasis and clearing pathogens, autophagy promotes MHC I and MHC II antigen presentation through presentation of antigens processed in the phagolysosome and enhances CD4+ and CD8+ T cell responses needed to clear infection (357).

Guanylate binding proteins (GBPs) are a family of IFNγ inducible proteins known to enhance immunity to intracellular pathogens by disrupting their membranes, promoting autophagy and enhancing inflammasome signaling (104, 206, 207). Antimicrobial activity to several intracellular pathogens by GBPs and immunity-related GTPases (IRGs), another family of IFNγ inducible GTPases, are reviewed in (358). Inflammasome activation in response to intracellular pathogens is essential for the production of IL-1β and IL-18, which are crucial for host defense. IL-18 regulates induction of IFNγ in NK and T cells, therefore enhancing the proliferation and cytotoxicity of NK and CD8+ T cells in addition to enhancing nitric oxide production in macrophages (359). Similarly, IL-1β enhances the induction of several chemokines and cytokine and leads to the recruitment of neutrophils to infections sites and stimulates the Th17 response (360). AIM2 inflammasome is crucial for the secretion of IL-1β and IL-18 in response to several intracellular bacteria, such as *L. monocytogenes*, *Fransicella* and *M. tuberculosis* (361, 362). GBPs are crucial for disrupting pathogen-containing vacuoles exposing bacterial ligands to AIM2 sensor, and recently the role of IRF1 driven expression of GBPs has been shown in *F. novicida* (124). Type I IFN signaling has been shown to be detrimental to host in response to several intracellular bacteria and some suggest that these detrimental effects may outweigh the benefits of AIM2 inflammasome signaling (102, 363). Additionally, mice lacking type I IFN signaling showed protection to *F. novicida*, however deficiencies in GBPs, IRF1 or AIM2 lead to increased susceptibility to infection (363). Therefore, it is likely that enhancing inflammasome signaling could prove beneficial in clearing intracellular bacterial infections. This dissertation describes a unique mechanism of OAS1 up-regulation of IRF1, which may be required for enhancing the transcription of GBPs to clear bacterial infections.

1.5 Rationale and Hypothesis

Studying the role of IFNs and ISGs during viral and bacterial infections is crucial for understanding the mechanisms of cellular immunity required to clear infection, providing insight into the development of antiviral or antimicrobial therapies. OAS proteins belong to an ancient family of NTase proteins described to activate RNase L and suppress global translation, including translation of viral mRNA. However, given the fact that OAS3 is sufficient and required for RNase L mediated antiviral activity and the existence of antiviral roles of non-catalytically active OAS proteins, it is clear that non-canonical mechanisms of host defense exist for OAS family proteins. In this dissertation, I report a novel mechanism of human and mouse OAS1 antiviral and antimicrobial activity, which is dependent on enhancing the translation of mRNAs related to innate immunity. OAS1 enhanced cGAS expression, leading to restriction of WNV mediated by type I IFNs. Similarly, IRF1 expression was enhanced by OAS1 and promoted antimicrobial activity ahainst *L. monocytogenes* and *F. novicida*, most likely mediated through the up-regulation of GBPs, inflammasome signaling and induction of IL-1β. Taken together, the findings in this dissertation clarify several previous findings related to RNase L independent restriction of WNV, provides evidence of OAS1 antimicrobial defense to intracellular bacteria, which could explain the mechanisms underlying restriction of *M. tuberculosis*, and overall increases our understanding for how OAS1 contributes to host immune responses during infection.

2.0 Materials and Methods

2.1 Materials

2.1.1 Cell Lines and Reagents

Table 2. Cell Lines

Cell Line	Description	Source
HEK293	Human embryonic kidney cells immortalized/ transformed by adenovirus transduction.	ATCC® (CRL-1573)
293T	HEK293 transformed with the SV40 Large T antigen.	Hornung Lab at Gene Center Munich
293FT	HEK293 transformed with the SV40 Large T antigen and used for lentiviral and retroviral packaging.	Invitrogen (CR700-07)
BJ-Tert	Foreskin fibroblast cells immortalized with hTERT.	ATCC BJ-5ta
BJ-Tert Ind. OAS1 P46	Doxycycline inducible cell line in WT background generated by transduction with OAS1 P46 lentivirus and selected with 1 µg/ml Puromycin.	Sarkar Lab
BJ-Tert Ind. Oas1b	Doxycycline inducible cell line in WT background generated by transduction with Oas1b lentivirus and selected with 1 µg/ml Puromycin.	Sarkar Lab
BJ-Tert OAS1-KO	OAS1-KO cell line generated by CRISPR/Cas9 editing.	Sarkar Lab
BJ-Tert OAS1-KO Ind. OAS1 P42	Doxycycline inducible cell line in OAS1-KO background generated by transduction with OAS1 P42 lentivirus and selected with 1 µg/ml Puromycin.	Sarkar Lab
BJ-Tert OAS1-KO Ind. OAS1 P46	Doxycycline inducible cell line in OAS1-KO background generated by transduction with OAS1 P46 lentivirus and selected with 1 µg/ml Puromycin.	Sarkar Lab

Table 2 continued

BJ-Tert OAS1-KO Ind. OAS1 P46 DADA	Doxycycline inducible cell line in OAS1-KO background generated by transduction with OAS1 P46 DADA lentivirus and selected with 1 μg/ml Puromycin.	Sarkar Lab
BJ-Tert cGAS-KO	cGAS-KO cell line generated by CRISPR/Cas9 editing	Sarkar Lab
BJ-Tert cGAS-KO Ind. OAS1 P46	Doxycycline inducible cell line in cGAS-KO background generated by transduction with OAS1 P46 lentivirus and selected with 1 μg/ml Puromycin.	Sarkar Lab
BJ-Tert cGAS-KO Ind. Oas1b	Doxycycline inducible cell line in cGAS-KO background generated by transduction with Oas1b lentivirus and selected with 1 μg/ml Puromycin.	Sarkar Lab
BJ-Tert IRF1-KO	IRF1-KO cell line generated by CRISPR/Cas9 editing.	Sarkar Lab
BJ-Tert IRF1-KO Ind. OAS1 P46	Doxycycline inducible cell line in IRF1-KO background generated by transduction with OAS1 P46 lentivirus and selected with 1 μg/ml Puromycin.	Sarkar Lab
BJ-Tert MAVS-KO	MAVS-KO cell line generated by CRISPR/Cas9 editing.	Sarkar Lab
BJ-Tert MAVS-KO Ind. OAS1 P46	Doxycycline inducible cell line in MAVS-KO background generated by transduction with OAS1 P46 lentivirus and selected with 1 μg/ml Puromycin.	Sarkar Lab
D1-4G2-4-15	B lymphocyte hybridoma cell line of mouse origin, which secretes 4G2 antibody in culture.	ATCC HB-112
Daudi	B lymphoblast cell line derived from a patient with Burkitt's lymphoma.	Change-Moore Lab
HeLa	Immortalized human adenocarcinoma cell line derived from cervical cancer tissue.	ATCC CCL-2
HeLa OAS1-KO	OAS1-KO cell line generated by CRISPR/Cas9 editing.	Sarkar Lab
HT1080	Immortalized human fibrosarcoma cell line derived from connective tissue.	ATCC CCL-121
HT1080 OAS1-KO	OAS1-KO cell line generated by CRISPR/Cas9 editing.	Sarkar Lab
HT1080 OAS1-KO Ind. OAS1 P42	Doxycycline inducible cell line in OAS1-KO background generated by transduction with OAS1 P42 lentivirus and selected with 1 μg/ml Puromycin.	Sarkar Lab
HT1080 OAS1-KO Ind. OAS1 P46	Doxycycline inducible cell line in OAS1-KO background generated by transduction with OAS1 P46 lentivirus and selected with 1 μg/ml Puromycin.	Sarkar Lab

Table 2 continued

HT1080 OAS1-KO Ind. OAS1 P46 DADA	Doxycycline inducible cell line in OAS1-KO background generated by transduction with OAS1 P46 DADA lentivirus and selected with 1 μg/ml Puromycin.	Sarkar Lab
HT1080 OAS1 RNase L-KO	RNase L-KO cell line generated by CRISPR/Cas9 editing.	Sarkar Lab
HT1080 OAS1/RNase L-DKO	RNase L-KO cell line on OAS1-KO background generated by CRISPR/Cas9 editing.	Sarkar Lab
HT1080 OAS1/RNase L-DKO Ind. OAS1 P46	Doxycycline inducible cell line in OAS1/RNase L-DKO background generated by transduction with OAS1 P46 lentivirus and selected with 1 μg/ml Puromycin.	Sarkar Lab
HT1080 OAS1/IFNAR1-DKO	IFNAR1-KO cell line on OAS1-KO background generated by CRISPR/Cas9 editing.	Sarkar Lab
HT1080 OAS1/IFNAR1-DKO Ind. OAS1 P46	Doxycycline inducible cell line in OAS1/IFNAR1-DKO background generated by transduction with OAS1 P46 lentivirus and selected with 1 μg/ml Puromycin.	Sarkar Lab
HT1080 OAS1-KO Ind. Oas1b K42E/K57E	Doxycycline inducible cell line in OAS1-KO background generated by transduction with Oas1b K42E/K57E lentivirus and selected with 1 μg/ml Puromycin.	Sarkar Lab
HT1080 OAS1-KO Ind. Oas1b K42E/K57E/K60E	Doxycycline inducible cell line in OAS1-KO background generated by transduction with Oas1b K42E/K57E/K60E lentivirus and selected with 1 μg/ml Puromycin.	Sarkar Lab
HT1080 OAS1-KO Ind. Oas1b K60E	Doxycycline inducible cell line in OAS1-KO background generated by transduction with Oas1b K60E lentivirus and selected with 1 μg/ml Puromycin.	Sarkar Lab
HT1080 OAS1-KO Ind. Oas1b K60E/K191E	Doxycycline inducible cell line in OAS1-KO background generated by transduction with Oas1b K60E/K191E lentivirus and selected with 1 μg/ml Puromycin.	Sarkar Lab
HT1080 OAS1-KO Ind. Oas1b K191E	Doxycycline inducible cell line in OAS1-KO background generated by transduction with Oas1b K191E lentivirus and selected with 1 μg/ml Puromycin.	Sarkar Lab
HT1080 OAS1-KO Ind. OAS1 P46 K60E	Doxycycline inducible cell line in OAS1-KO background generated by transduction with OAS1 P46 K60E lentivirus and selected with 1 μg/ml Puromycin.	Sarkar Lab

Table 2 continued

Mouse *Oas1b*$^{-/-}$ Fibroblasts	Mouse fibroblasts isolated from *Oas1b*$^{-/-}$ tails.	Sarkar Lab
Mouse *Oas1b*$^{+/+}$ Fibroblasts	Mouse fibroblasts isolated from *Oas1b*$^{+/+}$ tails.	Sarkar Lab
Mouse *Oas1b*$^{-/-}$ BMDM	Monocytes isolated from *Oas1b*$^{-/-}$ femur were differentiated into BMDMs by culturing in DMEM supplemented with L929 conditioning media.	Sarkar Lab
Mouse *Oas1b*$^{+/+}$ BMDM	Monocytes isolated from *Oas1b*$^{+/+}$ femur were differentiated into BMDMs by culturing in DMEM supplemented with L929 conditioning media.	Sarkar Lab
THP1	Human monocytic cell line derived from the peripheral blood of a patient with acute monocytic leukemia.	Hornung Lab at Gene Center Munich
THP1 OAS1-KO	OAS1-KO cell line generated by CRISPR/Cas9 editing.	Hornung Lab at Gene Center Munich
THP1 OAS1-KO Ind. OAS1 P42	Doxycycline inducible cell line in OAS1-KO background generated by transduction/spinoculation with OAS1 P42 lentivirus and selected with 1 µg/ml Puromycin.	Sarkar Lab
THP1 OAS1-KO Ind. OAS1 P46	Doxycycline inducible cell line in OAS1-KO background generated by transduction/spinoculation with OAS1 P46 lentivirus and selected with 1 µg/ml Puromycin.	Sarkar Lab
THP1 OAS1-KO Ind. OAS1 P46 DADA	Doxycycline inducible cell line in OAS1-KO background generated by transduction/spinoculation with OAS1 P46 DADA lentivirus and selected with 1 µg/ml Puromycin.	Sarkar Lab
THP1 OAS1-KO Ind. Oas1b K42E/K57E/K60E	Doxycycline inducible cell line in OAS1-KO background generated by transduction/spinoculation with Oas1b K42E/K57E/K60E lentivirus and selected with 1 µg/ml Puromycin.	Sarkar Lab
THP1 OAS1-KO Ind. Oas1b K60E	Doxycycline inducible cell line in OAS1-KO background generated by transduction/spinoculation with Oas1b K60E lentivirus and selected with 1 µg/ml Puromycin.	Sarkar Lab
THP1 OAS1-KO Ind. OAS1 P46 K60E	Doxycycline inducible cell line in OAS1-KO background generated by transduction/spinoculation with OAS1 P46 K60E lentivirus and selected with 1 µg/ml Puromycin.	Sarkar Lab

Table 2 continued

Vero	Interferon deficient Kidney epithelial cells isolated from African green monkey.	ATCC CCL-81

293T, 293FT, BJ-Tert, HeLa, HT1080, mouse fibroblast and Vero cells were cultured with DMEM (Fisher Scientific, Catalog number: MT10013CV) supplemented with 10% FBS (R&DSystems), 1% Pen-Strep (Fisher Scientific, Catalog number: BW17-602E) and 5µg/ml Plasmocin (Invivogen, Catalog number: ant-mpt) at 37ºC and 5% CO_2. D1-4G2-4-15, Daudi and THP1 cells were cultured with RPMI (Fisher Scientific, Catalog number: MT10040CV) supplemented with 10% FBS, 1% Pen-Strep and 5µg/ml Plasmocin at 37ºC and 5% CO_2. BMDMs were cultured with DMEM supplemented 10% FBS, 1% Pen-Strep, 5 µg/ml Plasmocin and 20% L929 conditioning media at 37ºC and 5% CO_2. For cell passage of adherent cells, cells were incubated with 0.05% Trypsin-EDTA (Fisher Scientific, Catalog number: 25-300-120) at 37ºC and 5% CO_2 and neutralized with corresponding culture media.

2.1.2 Plasmids

Table 3. Vectors and Plasmids

Plasmid	Description	Source
pENTR D-TOPO	Entry vector used for cloning desired gene sequences into destination vector by attR and attL driven recombination.	Invitrogen, Topo Cloning Kit, (K240020)
pcDNA-DEST47	Destination vector used for expressing protein of interest by transfection.	Invitrogen (12281010)
pLenti CMV Puro DEST (w118-1)	Destination vector used for expressing protein of interest by transfection.	Addgene (17452)
pLenti TRE-DEST-EFpuro-2A-rTA	Destination vector used for making doxycycline inducible cell lines expressing protein of interest.	Shuda Lab at the University of Pittsburgh
pCMV6-Entry	Cloning vector used for expressing protein of interest by transfection. Also used for cloning into pENTR D-TOPO and subsequently other destination vectors.	Origene
pCL Ampho	Retrovirus packaging vector.	Novus Biologicals (NBP2-29541)
psPAX2	Lentiviral envelope expressing plasmid used for lentiviral packaging.	Addgene (12260)
pMD2.G	VSV-G envelope expressing plasmid used for lentiviral packaging.	Addgene (12259)
OAS1 P42 in pENTR D-TOPO	Used to for TOPO Cloning of OAS1 P42 into destination vectors.	TOPO Cloning
OAS1 P42 in pcDNA-DEST47	Used for expression of OAS1 P42 by transfection.	LR reaction
OAS1 P42 in pLenti TRE-DEST-Efpuro-2A-rTA	Used for making cell lines with doxycycline inducible expression of OAS1 P42.	LR reaction
OAS1 P46 in pENTR D-TOPO	Used to for TOPO Cloning of OAS1 P46 into destination vectors.	TOPO Cloning
OAS1 P46 in pcDNA-DEST47	Used for expression of OAS1 P46 by transfection.	LR reaction
OAS1 P46 in pLenti TRE-DEST-Efpuro-2A-rTA	Used for making cell lines with doxycycline inducible expression of OAS1 P46.	LR reaction
OAS1 P46 DADA in pENTR D-TOPO	Used to for TOPO Cloning of OAS1 P46 DADA, catalytically inactive mutant, into destination vectors.	NEB site-directed mutagenesis

Table 3 continued

OAS1 P46 DADA in pcDNA-DEST47	Used for expression of OAS1 P46 DADA, catalytically inactive mutant, by transfection.	LR reaction
OAS1 P46 DADA in pLenti TRE-DEST-Efpuro-2A-rTA	Used for making cell lines with doxycycline inducible expression of OAS1 P46 DADA, catalytically inactive mutant.	LR reaction
OAS1 P46 K60E in pENTR D-TOPO	Used to for TOPO Cloning of OAS1 P46 K60E, RNA-binding mutant, into destination vectors.	NEB site-directed mutagenesis
OAS1 P46 K60E in pcDNA-DEST47	Used for expression of OAS1 P46 K60E, RNA-binding mutant, by transfection.	LR reaction
OAS1 P46 K60E in pLenti TRE-DEST-Efpuro-2A-rTA	Used for making cell lines with doxycycline inducible expression of OAS1 P46 K60E, RNA-binding mutant.	LR reaction
Oas1a in pCMV6	Used for expression of Oas1a by transfection.	Origene
Oas1b in pCMV6	Used for expression of Oas1b by transfection.	Origene
Oas1g in pCMV6	Used for expression of Oas1g by transfection.	Origene
Oas1h in pCMV6	Used for expression of Oas1h by transfection.	Origene
Oas1b in pENTR D-TOPO	Used to for TOPO Cloning of Oas1b into destination vectors.	TOPO Cloning
Oas1b in pLenti CMV Puro DEST	Used for expression of Oas1b by transfection.	LR reaction
Oas1b in pLenti TRE-DEST-Efpuro-2A-rTA	Used for making cell lines with doxycycline inducible expression of Oas1b.	LR reaction
Oas1b K42E/K57E pENTR D-TOPO	Used to for TOPO Cloning of Oas1b K42E/K57E, RNA-binding mutant, into destination vectors.	NEB site-directed mutagenesis
Oas1b K42E/K57E in pLenti CMV Puro DEST	Used for expression of Oas1b K42E/K57E, RNA-binding mutant, by transfection.	LR reaction
Oas1b K42E/K57E in pLenti TRE-DEST-Efpuro-2A-rTA	Used for making cell lines with doxycycline inducible expression of Oas1b K42E/K57E, RNA-binding mutant.	LR reaction
Oas1b K42E/K57E/K60E pENTR D-TOPO	Used to for TOPO Cloning of Oas1b K42E/K57E/K60E, RNA-binding mutant, into destination vectors.	NEB site-directed mutagenesis
Oas1b K42E/K57E/K60E in pLenti CMV Puro DEST	Used for expression of Oas1b K42E/K57E/K60E, RNA-binding mutant, by transfection.	LR reaction
Oas1b K42E/K57E/K60E in pLenti TRE-DEST-Efpuro-2A-rTA	Used for making cell lines with doxycycline inducible expression of Oas1b K42E/K57E/K60E, RNA-binding mutant.	LR reaction

Table 3 continued

Oas1b K60E pENTR D-TOPO	Used to for TOPO Cloning of Oas1b K60E, RNA-binding mutant, into destination vectors.	NEB site-directed mutagenesis
Oas1b K60E in pLenti CMV Puro DEST	Used for expression of Oas1b K60E, RNA-binding mutant, by transfection.	LR reaction
Oas1b K60E in pLenti TRE-DEST-Efpuro-2A-rTA	Used for making cell lines with doxycycline inducible expression of Oas1b K60E, RNA-binding mutant.	LR reaction
Oas1b K60E/K191E pENTR D-TOPO	Used to for TOPO Cloning of Oas1b K191E, RNA-binding mutant, into destination vectors.	NEB site-directed mutagenesis
Oas1b K60E/K191E in pLenti CMV Puro DEST	Used for expression of Oas1b K191E, RNA-binding mutant, by transfection.	LR reaction
Oas1b K60E/K191E in pLenti TRE-DEST-Efpuro-2A-rTA	Used for making cell lines with doxycycline inducible expression of Oas1b K191E, RNA-binding mutant.	LR reaction
Oas1b K191E pENTR D-TOPO	Used to for TOPO Cloning of Oas1b K60E/K191E, RNA-binding mutant, into destination vectors.	NEB site-directed mutagenesis
Oas1b K191E in pLenti CMV Puro DEST	Used for expression of Oas1b K60E/K191E, RNA-binding mutant, by transfection.	LR reaction
Oas1b K191E in pLenti TRE-DEST-Efpuro-2A-rTA	Used for making cell lines with doxycycline inducible expression of Oas1b K60E/K191E, RNA-binding mutant.	LR reaction

2.1.3 Virus and Bacterial Strains

Table 4. Virus

Virus	Description	Source
WNV-KUN	Less virulent WNV subtype (364). Used for all *in-vitro* infection assays.	Diamond Lab, grown and maintained in Sarkar Lab
WNV-NY	Strain responsible for the 1999 New York outbreak (365). Used for *in-vivo* experiments with Oas1b-KI mice.	Diamond Lab
POWV	Tickborne *Flavivirus* (366). Used for *in-vivo* experiments with Oas1b-KI mice.	Diamond Lab

Table 5. Bacteria

Bacteria	Description	Source
Francisella tularensis subsp. *Novicida,* Strain Utah 112	Intracellular gram-negative bacteria with rare disease occurrence in humans as compared to *Francisella tularensis* (366). However, mice are susceptible to *F. novicida* (367),therefore we used *F. novicida* as a model for our *in-vivo* experiments in Oas1b-KI mice.	BEI Resources (NR-13)
Listeria monocytogenes, Strain 10403s	Foodborne intracellular gram-positive bacteria extensively used as a model for characterizing bacterial and host factors for pathogenicity (368, 369). Used for *in-vivo* experiments with Oas1b-KI mice.	BEI Resources (NR-13223)
DH5α Competent *E. coli*	Used for bacterial transformation of pENTR D-TOPO and pcDNA plasmids.	Made in Sarkar Lab
NEB 5-alpha Competent *E. coli*	Used for bacterial transformation of plasmids altered by site-directed mutagenesis.	Purchased from NEB (C2988J)
STBL3 Competent *E. coli*	Used for bacterial transformation of lentiviral plasmids.	Made in Sarkar Lab
TOP10 Competent *E. coli*	Used for bacterial transformation of pENTR D-TOPO plasmids.	Included in TOPO Cloning Kit (K240020)

2.1.4 Restriction Digest and Molecular Cloning Enzymes

Table 6. Enzymes

Enzyme	Purpose	Company	Catalog Number
AluI	Genotyping of OAS1 A/G allele of rs10774671 SNP by RFLP assay.	NEB	R0137S
BamHI	Restriction digest of Oas1b and OAS1 plasmids.	NEB	R3136S
BspEI	Genotyping of Oas1b-KI mice.	NEB	R0540S
KpnI	Restriction digest of Oas1b and OAS1 plasmids.	NEB	R3142S
NotI	Restriction digest of Oas1b and OAS1 plasmids.	NEB	R3189S
DpnI	Digestion of methylated DNA.	NEB	R0176S
KLD Enzyme Mix	Kinase, Ligase and DpnI enzyme mix used in NEB site directed mutagenesis kit.	NEB	M0554S
LR Clonase II	Molecular cloning of target sequence from entry plasmid to destination plasmid by attR and attL driven recombination.	Fisher Scientific	11791020
OneTaq Hot Start Quick Load 2x Master Mix	DNA Polymerase with inert tracking dye. Used for most OAS1 and Oas1b genotyping assays.	NEB	M0489S
Q5 Hot-Start High-Fidelity 2x Master Mix	DNA Polymerase. Used for all non-genotyping PCR reactions.	NEB	M0494S
Topoisomerase I	Cloning of target sequence into pENTR/D-TOPO	ThermoFisher Scientific	Included in TOPO Cloning Kit (K240020)

All restriction enzymes were used with instructed buffers: 10X CutSmart Buffer (NEB, Catalog number: B7204S) or 10X NEBuffer 3.1 (NEB, Catalog number: B7203S). Topo cloning was performed with TOPO Cloning Kit (ThermoFisher Scientific, Catalog Number: K240020). Gateway cloning of desired sequence from pENTR/D-TOPO to destinations vectors was

performed with Gateway LR Clonase II Enzyme Mix (Fisher Scientific, Catalog number: 11791029). Site directed mutagenesis of desired sequence was performed using Q5 Site-Directed Mutagenesis Kit (NEB, Catalog number: E0554S).

2.1.5 Cytokines

Table 7. Cytokines

Cytokine	Working Concentration	Company	Catalog Number
hIFNα	1000-2000 U/ml	Prescription drug obtained from Kalinsky Lab	NDC 0085-0571-02
hIFNγ	200-500 U/ml	Miltenyl Biotec	130-096-873
mIFNγ	100 ng/ml	BioLegend	575306

2.1.6 Antibodies

Table 8. Antibodies

Target	Dilution	Company	Catalog Number
4G2	1:50 IF	Grown from D1-4G2-4-15 hybridoma cells from ATCC	ATCC HB-112
α-Tubulin	1:1000 WB	Cell Signaling Technologies	3873S
β-Actin	1:1000 WB	Santa Cruz Biotechnology	Sc-47778
Calnexin	1:1000 WB, 1:100 IF	Cell Signaling Technologies	2679S
Calnexin	1:200 IF	Novus Biologicals	NBP2-36571SS
cGAS	1:500 WB	Cell Signaling Technologies	15102S
cGAS (D-9)	1:500 WB, 1:50 IP	Santa Cruz	Sc-515777
FLAG	1:1000 WB, 1:200 IF	Cell Signaling Technologies	2368S
FLAG M2	1:1000 WB, 1:200 IF	Millipore Sigma	F1804

Table 8 continued

Goat anti-mouse IgG AF488	1:500-1000	ThermoFisher Scientific	A-11017
Goat anti-mouse IgG AF594	1:500-1000	ThermoFisher Scientific	A-32742
Goat anti-rabbit IgG AF488	1:500-1000	ThermoFisher Scientific	A-32731
Goat anti-rabbit IgG AF594	1:500-1000	Cell Signaling Technologies	8889S
Goat anti-rabbit IgG AF594	1:500-1000	ThermoFisher Scientific	A-11072
IFNAR1	1:500 WB	Abcam	Ab124764
IRF1	1:1000 WB, 1:50 IP	Cell Signaling Technologies	8478S
IRF1	1:1000 WB, 1:200 IF	Santa Cruz	Sc-514544
IRF1-PE	1:50 IF	Cell Signaling Technologies	12732S
MYC	1:1000 WB, 1:200 IF	OriGene	TA100010
J2	1:200 IF	Gift from Coyne Lab at the University of Pittsburgh	N/A
OAS1	1:250 WB, 1:50 IP, 1:100 IF	Cell Signaling Technologies	14498S
Rabbit mAb IgG Isotype Control-PE	1:50 IF	Cell Signaling Technologies	5742S
RNase L	1:1000 WB	Cell Signaling Technologies	27281S
Phosphor-Stat1 (Tyr701)	1:1000 WB	Cell Signaling Technologies	7649S
STAT3	1:200 WB	R&D Systems	1799
STAT5	1:1000 WB	Cell Signaling Technologies	25656S
EDD (UBR5)	1:1000 WB	Santa Cruz	Sc-515494
XRN1	1:1000 WB	Santa Cruz	Sc-165985

2.1.7 Transfection Reagents

Table 9. Transfection Reagents

Reagent	Company	Catalog Number
Lipofectamine 2000	ThermoFisher Scientific	11668027
Lipofectamine 3000	ThermoFisher Scientific	L3000008
Turbofect	ThermoFisher Scientific	R0531
X-tremeGene HP	Millipore Sigma	6366244001

2.1.8 CRISPR

Table 10. CRISPR guide RNAs and Plasmids

Plasmids	gRNA Target Sequence	Purpose
pLKO_OAS1_gRNA_SINGLE_BB	GATCAGTTAAATCGCCG	Generate OAS1-deficient cells
pLKO_RNaseL_gRNA_SINGLE_BB	GGGGGTTGTTATGATCCC	Generate RNase L-deficient cells
Retro_cGAS_DOUBLE_BB_CMV	AACTTTCCCGCCTTAGGCA	Generate cGAS-deficient cells
Retro_IFNAR1_DOUBLE_BB_CMV	CAGGAGCGATGAGTCTGTC	Generate IFNAR1-deficient cells
Retro_IRF1_DOUBLE_BB_CMV	GCCCAGCTCCGGAACAAAC	Generate IRF1-deficient cells
Retro_MAVS_DOUBLE_BB_CMV	ACTTCATTGCGGCACTGAG	Generate MAVS-deficient cells
pRZ_CAS9_mCherry	N/A	Co-expressed with SINGLE_BB plasmids

2.1.9 PCR Primers and Probes

Table 11. qPCR Primer Sequence

Gene	Primer / Probe Sequence	Source
cGAS (SYBR)	FWD 5'- TTCAAAACTGGCTTTCAGCA -'3 REV 3'- TAGCCGCCATGTTTCTTCTT -'5	Integrated DNA Technologies
cGAS (Taqman)	Primer + Probe Mix	Biorad (qHsaCEP0053484)
GAPDH (SYBR)	FWD 5'- TGCACCACCAACTGCTTAGC -'3 REV 3'- GGCATGGACTGTGGTCATGAG -'5	Integrated DNA Technologies
GAPDH (Taqman)	Primer + Probe Mix	Biorad (qHsaCEP0041396)
IRF1 (SYBR)	FWD 5'- AAAAGGAGCCAGATCCCAAGA -'3 REV 3'- CATCCGGTACACTCGCACAG -'5	Integrated DNA Technologies
IRF1 (Taqman)	Primer + Probe Mix	Biorad (qHsaCEP0051342)
STAT1 (SYBR)	FWD 5'- TCACTATAGTTGCGGAGAGT –'3 REV 3'- ATAGGGTCATGTTCGTAGGT –'5	Integrated DNA Technologies

2.2 Methods

2.2.1 Restriction Length Polymorphism Assay

Genotyping of all cell lines for OAS1 SNP rs10774671 was done by RFLP adapted from Noguchi et al. 2012 (370). Genomic DNA was isolated from 10^{5-6} cells using Wizard Genomic DNA Purification Kit (Promega, Catalog number: A1120). Genomic DNA (100 ng) was amplified by PCR using Q5 Hot-Start High-Fidelity 2x Master Mix and OAS1 specific primers containing the rs1077467 SNP (FWD: 5'-TCACAGTGTCTACCGTAAATGCTC-3' REV: 5'-AGAAAGTCAAGGCTGGAATTTCAT-3'). Samples were denatured at 95ºC for 30 seconds, followed by 45 cycles of amplification as follows: 98ºC for 15 seconds, 55ºC for 15 seconds, 68ºC for 30 seconds, and finally 68ºC for 5 minutes. First PCR reaction results in low yield of PCR product, therefore 2 µl of 1st PCR reaction was used as template for a second round of PCR amplification. 10 µl of product from the 2nd PCR reaction (1-2 µg DNA) was digested with 0.5 U/µl AluI overnight at 37ºC and analyzed by DNA electrophoresis on a 3% agarose gel.

2.2.2 Virus Stock and Purification

Stocks of WNV-KUN were obtained from Dr. Michael Diamond and were expanded and titered in Vero cells. Cells were cultured in Falcon Tissue Culture Treated 150cm^2 flasks (Fisher Scientific, Catalog number: 08-772-48) until 85% confluent and then split into three T150 cm^2 flasks containing 15ml 2% FBS DMEM. After 24 hours cells were infected with WNV-KUN at a MOI of 0.05 and incubated for 48 hours at 37ºC, CO_2. Supernatant was harvested and spun at 3500 rpm for 10 minutes at 4ºC. Cell free supernatant containing virus was then purified by

ultracentrifugation using a SW32 rotor on a Sorvall LYNX 4000 Ultracentrifuge. Ultra-tubes (Beckman Coulter, Catalog number: 344058) were prepared by adding 6ml cold 25% glycerol in TNE buffer (10 mM Tris-HCl pH 7.4, 150 mM NaCl and 1 mM EDTA at a final pH of 8) layered by virus-containing supernatant without exceeding 35 ml. Samples were spun at 30,000 rpm for 4 hours at 4ºC. After centrifugation, the top layer of TNE was removed leaving approximately 1 ml of TNE. Virus pellet was then re-suspended with 5 ml TNE and sonicated for 1 round of 20% power, 2 second pulses for a total of 30 seconds. Virus was aliquoted and stored at -80ºC and viral titer was quantified by FFU assay.

2.2.3 Florescent Foci Assay

For quantification of virus focus forming units, Vero cells were plated in 96-well plates with DMEM and infected when 80-90% confluent with serial dilutions (using DMEM containing no FBS) of virus supernatant for 2 hours with gentle shaking every 15 minutes at 37ºC, 5% CO_2. Following virus adsorption, virus supernatant was removed and fresh 2% FBS DMEM was added to sample wells. After 24 hours post infection, media was removed and wells were washed with PBS (Fisher Scientific, Catalog number: BW17512F12). Cells were fixed with a 1:1 ratio of Methanol:Acetone for 10 minutes at room temperature, followed by washing with PBS. Cells were then incubated with 1:50 4G2 antibody with gentle shaking for 1 hour at room temperature or overnight at 4ºC. Cells were washed and incubated with goat anti mouse AF488 secondary antibody in the dark with gentle shaking for 1 hour at room temperature, followed by washing with PBS and incubation with 1:200 DAPI containing PBS. FFUs were visualized and counted by fluorescent microscopy to calculate viral titers. The lowest virus concentration we were able to detect reliably in these virus growth measurements was 25 FFU/ml.

2.2.4 WNV Plaque Assay

For quantification of virus plaque forming units, Vero cells were plated in 6-well plates with DMEM and infected when 80-90% confluent with serial dilutions (using DMEM containing no FBS) of virus supernatant for 1 hour at 37ºC, 5% CO_2. After incubation, 2x MEM media, supplemented with 8% FBS, 2% Pen-strep, 2% HEPES (Fisher Scientific, Catalog number: 15-630-080) and 1% sodium bicarbonate, was combined 1:1 with 2% low melting point agarose (Invitrogen, Catalog number: 15517-022) and applied to samples in the 6-well plate until agarose solidified at room temperature. Cells were incubated for 72 hours at 37ºC, 5% CO_2. Cells were fixed with 10% paraformaldehyde for 45 minutes and stained with crystal violet. Plaques were visualized and counted to calculate viral titers. The lowest virus concentration we were able to detect reliably in our virus growth measurement was 20 PFU/ml.

2.2.5 *In-vivo* infection of mice with WNV and POWV

WT and Oas1b-KI mice were infected with WNV-NY and POWV by footpad injection and survival was monitored over a course of 3 weeks. Mice were infected with 100 PFU/ml WNV-NY and 100 FFU/ml POWV. Additionally, viral burden from serum, brain, spinal cord and spleen was measured by plaque assay after harvesting tissue or serum 2, 4 or 7 days post WNV-NY infection.

2.2.6 Bacterial stocks and culture

L. monocytogenes was grown in Brain Heart Infusion (BHI) broth with 200 rpm shaking at 37ºC or BHI-agar plates at 37ºC for individual colonies. Broth and agar were prepared from BHI powder (Millipore Sigma, Catalog number: 53286). *F. novicida* was grown in Mueller Hinton (MH) broth 200rpm shaking at 37ºC or MH-agar plates at 37ºC for individual colonies. Broth and agar were prepared from MH powder (Millipore Sigma, Catalog number: 70192).

2.2.7 Gentamicin Protection Assay

All *in-vitro* bacterial infections were analyzed by Gentamicin Protection Assays. *L. monocytogenes* was used as a model of gram-positive bacterial infection and *F. novicida* as a model of gram-negative bacterial infection. Prior to the day of infection, adherent cells were seeded at a cell number of 1.5×10^5 in 12-well plates and bacterial suspensions were prepared in 5 ml of culture medium and left to grow overnight with 200 rpm shaking at 37ºC. The following day, the optical density at 600 nm (OD_{600}) of bacterial cultures was measured to determine bacterial concentration. Bacterial cultures were diluted in infection medium, DMEM + 1% heat inactivated FBS, added directly to cells at indicated MOI, centrifuged at 2000 rpm for 5 minutes and incubated for 1 hour at 37ºC, 5% CO_2. After bacterial adsorption, wells were washed with DMEM containing 10% FBS and 50 μg/ml gentamycin, followed by incubation with fresh gentamycin-containing media at 37ºC, 5% CO_2. At 4 or 8 hours post incubation, cells were washed with PBS and lysed with 1% Triton X-100 (USBiological, Catalog number: 9002-93-1) diluted in PBS. Cell suspensions were collected, serial diluted in PBS, plated on appropriate agar plates and incubated for 18-20 hours for *Listeria* or 48 hours for *Francisella* at 37ºC, 5% CO_2. Lastly, bacterial colonies

were counted in order to calculate bacterial burden (CFU/ml). For infection of suspension cells, cells were grown at a cell density of 0.5-1 x 10^6 cells/ml, 1 x 10^6 cells were added to 2 ml of infection medium in 6-well plates at the intended MOI, centrifuged at 3500rpm for 5 minutes for attachment of bacteria to the cells and incubated for 1 hour at 37ºC, 5% CO_2. After bacterial adsorption, cells were collected in tubes, spun at 1500rpm for 5 minutes, washed with gentamycin containing media, re-suspended in gentamycin containing media and incubated for 4 or 8 hours at 37ºC, 5% CO_2. At desired time points post incubation, cells were collected in microcentrifuge tubes, spun down at 5000rpm for 5 minutes, washed once in PBS and lysed with 1% Triton X-100 diluted in PBS. Cell suspensions were collected, serial diluted in PBS, plated on appropriate agar plates and incubated as described previously. Lastly, bacterial colonies were counted in order to calculate intracellular bacteria and expressed as CFU/ml.

2.2.8 In-vivo infection of mice with L. monocytogenes and F. novicida

WT and Oas1b-KI mice were infected with *L. monocytogenes* intraperitoneally or *F. novicida* by subcutaneous injection. Mice were infected with 1 x 10^5 CFU/ml *L. monocytogenes* and 1 x 10^4 CFU/ml *F. novicida*. Survivability and body weight were monitored for 10 or 13 days respectively.

2.2.9 Immunoblot

For all WB analysis, protein concentration of WCL (prepared with standard lysis buffer: 0.1% sodium deoxycholate, 1% Triton X-100, 20 mM HEPES pH 7.4, 150 mM NaCl, 1.5 mM $MgCl_2$, 2 mM EGTA, 2 mM DTT, 10 mM NaF, 12.5 mM β-glycerophosphate, 1 mM Na_3VO_4, 1 mM PMSF and protease inhibitor [Millapore Sigma, Catalog number: 5892970001]) was measured by Bradford Assay (Bio-Rad, Catalog number: 500-0006). Samples were prepared with equal amounts of protein extract and resolved on 10% or 12% SDS-polyacrylamide gels by SDS-PAGE. Proteins were then transferred to Polyvinylidene difluoride (PVDF) membranes (Fisher Scientific, Catalog number: IPVH00010). Protein membranes were blocked with 5% dry milk (Bio-rad, Catalog number: 170-6404) made in Tris-buffered saline with 1X Tween 20 (TBST) (Santa Cruz, Catalog number: sc-362311) for 1 hour at room temperature with gentle shaking. Afterwards, membranes were incubated with primary antibody diluted in 5% dry milk and 0.02% sodium azide (Millapore Sigma, Catalog number: S2002) in TBST overnight with gentle shaking at 4ºC. Antibody concentrations for desired proteins are listed in Table 8. Membranes were then washed three times with 1X TBST and incubated with horseradish peroxidase-conjugated anti-mouse or anti rabbit immunoglobulin G (IgG) (Rockland, Catalog numbers: 610-1302 and 6111-103-122 respectively) diluted 1:10,000 in 5% dry milk in TBST. After 1hour secondary body incubation, membranes were washed three times with 1X TBST and developed by chemiluminescence using Clarity or Clarity Max ECL Western Blotting Substrates (Bio-rad, Catalog numbers: 1705061 and 1705062 respectively).

2.2.10 Immunofluorescence

In order to determine subcellular localization of target proteins, cells were treated with IFN, expressed by transfection or inducibly expressed with doxycycline and analyzed by fluorescent confocal microscopy. Prior to treatment, cells were seeded overnight in 4-well chamber slides (ThermoFisher Scientific, Catalog number: 154526PK). After treatment or transfection, cells were fixed with 4% paraformaldehyde (Electron Microscopy Sciences, Catalog number: 15710) diluted in PBS for 15 minutes at room temperature, rinsed 3 times with PBS and incubated in 100% methanol for 10 minutes at -20ºC. After methanol permeabilization, cells were rinsed once in PBS and blocked with blocking buffer (5% FBS and 1% BSA in 1X PBS) for 1 hour at room temperature. After blocking, cells were incubated with primary antibody diluted 1:100-200 in antibody dilution buffer (1% BSA and 0.3% Triton X-100 in 1X PBS) overnight shaking at 4ºC. Cells were rinsed 3 times with PBS and incubated with filtered fluorochrome-conjugates secondary antibodies (Listed in Table 8) diluted 1:500 in antibody dilution buffer for 1-2 hours in the dark at room temperature. Cells were rinsed 3 times with PBS and mounted with Vectashield mounting medium with DAPI (Vector Laboratories, Catalog number: H-1500). Glass clover slips were placed over chamber slides and sealed with nail polish. Samples were then analyzed by confocal microscopy.

2.2.11 Molecular Cloning, Bacterial Transformation and Plasmid Preparation

2.2.11.1 TOPO Cloning

For insertion of desired PCR product into pENTR/D-TOPO vectors, primers were designed as instructed by TOPO Cloning Kit instructions. Forward orientations primers contained a 5' CACC overhang sequence to allow directional cloning of PCR product into the TOPO vector. PCR was performed with Q5 Hot-Start High-Fidelity 2x Master Mix under the following PCR cycle conditions: denaturation at 95ºC for 2 minutes, followed by 30 cycles of: 95ºC for 15 seconds, 60-65ºC for 30 seconds, 72ºC for 45 seconds, and finally 72ºC for 10 minutes. Approximately 2-5 µl of PCR product was analyzed by DNA electrophoresis on a 1% agarose gel to verify successful amplification and purity of product, PCR Clean-up was performed if needed using QIAquick PCR Purification Kit (QIAGEN, Catalog number: 28104). PCR product was then digested with DpnI at a final concentration of 1 U/µl for 1 hour at 37ºC, followed by heat inactivation for 20 minutes at 80ºC. Next, the TOPO reaction was performed by combining DpnI digested product with TOPO vector as described in the TOPO Cloning Kit for 1 hour or overnight at room temperature. TOP10 cells were then transformed with the TOPO reaction and plated on 50 µg/ml Kanamycin LB agar plates for selection. Individual bacterial colonies were screened by colony PCR using the same PCR cycle parameters for the original product and DNA gel electrophoresis with 1% agarose gel. Colonies with successful incorporation of product into TOPO vector were expanded and plasmid DNA was isolated by Mini Prep (Qiagen, Catalog number: 27106).

2.2.11.2 Site Directed Mutagenesis

Site directed mutagenesis was performed using NEB Site Directed Mutagenesis Kit. Primers used for nucleotide substitutions were designed using NEB's web-based tool NEBase Changer. PCR was performed with Q5 Hot-Start High-Fidelity 2x Master Mix under the following PCR cycle conditions: denaturation at 98ºC for 30 seconds, followed by 25 cycles of: 98ºC for 10 seconds, 62-69ºC for 20 seconds, 72ºC for 1 minute, and finally 72ºC for 2 minutes. Approximately 5µl of PCR product was analyzed by DNA electrophoresis on a 1% agarose gel to verify successful amplification and purity of product. 1 µl of PCR product was incubated with KLD enzyme mixture for 5 minutes at room temperature, KLD reaction mixture was transformed in NEB 5-alpha Competent *E. coli* and plated on LB agar plates containing appropriate antibiotics for selection. Individual colonies were picked and grown in antibiotic containing 2X LB broth overnight followed by isolation of plasmid DNA by Mini Prep. Plasmid DNA was then analyzed by restriction digestion by incubating DNA-enzyme mixture for 2 hours at 37ºC followed by DNA electrophoresis on a 1% agarose gel. Finally, approximately 500-800 ng of DNA was sent to GENEWIZ for sequencing using GENWIZ universal primers M13-40FOR (5'-GTTTTCCCAGTCACGAC-3') and T7 (5'-TAATACGACTCACTATAGGG-3'). Sequence and chromatogram were aligned to the original plasmid sequence in order to verify successful nucleotide substitution by mutagenesis.

2.2.11.3 LR Cloning

Cloning of pENTR/D-TOPO entry vectors into desired destinations vectors was done by gateway cloning using LR Clonase II. 50-100 ng of entry vector was combined with 150 ng of destination vector and incubated with Tris-EDTA buffer and LR Clonase II overnight at room temperature. LR reaction was terminated by addition of Proteinase K (Fisher Scientific, Catalog number: BP1700-100) for 10 minutes at 37ºC. LR reaction mixture was transformed in DH5α or STBL3 Competent *E. coli* and plated on 50 μg/ml ampicillin LB agar plates for selection. Individuals colonies were picked and grown in ampicillin containing 2X LB broth overnight followed by isolation of plasmid DNA by Mini Prep. Plasmid DNA was then analyzed by restriction digestion by incubating DNA-enzyme mixture for 2 hours at 37ºC followed by DNA electrophoresis on a 1% agarose gel. To obtain higher yields of plasmid DNA, bacterial broth from positive clones was cultured overnight in 100 ml ampicillin containing 2X LB broth followed by plasmid Midi Prep (Qiagen, Catalog number: 12143).

2.2.11.4 Bacterial Transformation

All plasmid DNA was transformed into appropriate competent bacteria by adding 5-10 μl (after cloning reactions) or 1-2 μl (for expanding purified plasmid) to 50 μl of competent bacteria followed by incubation for 30 minutes on ice. Bacterial cells were then heat-shocked for 30-45 seconds at 42ºC. Heat-shocked cells were chilled on ice for 5 minutes and 450 μl of 2X LB or SOC medium was added to the mixture. Bacterial cultures were incubated for 1 hour with shaking at 37ºC and spread on LB agar plates containing Kanamycin or Ampicillin for selection

(designated by antibiotic resistant gene expression in plasmid). Bacterial plates were incubated overnight at 37ºC.

2.2.11.5 Plasmid Mini and Midi Prep

For isolation of plasmid DNA, bacterial cultures were processed by QIAPrep Spin Miniprep Kit or QIAGEN Plasmid Midi Kit (QIAGEN, Catalog numbers: 27106 and 12143 respectively). Plasmid DNA was then analyzed by restriction digestion by incubating DNA-enzyme mixture for 2 hours at 37ºC followed by DNA electrophoresis on a 1% agarose gel to ensure successful isolation of intended plasmid DNA. Expression of proteins pertaining to genes of interest in plasmid sequence was validated by transfection of cells with plasmid DNA using Turbofect or X-tremeGene HP followed by WB analysis.

2.2.12 Production of High Titer lentivirus and Transduction

All lentivirus and retrovirus were made in high titer for the purpose of transducing cells. Prior to transfection with viral plasmids, 2 x 10^6 293FT cells were seeded in 10 cm^2 tissue culture dishes (Fisher Scientific, Catalog number: 08-772-4F) and were grown overnight. Lentiviral transfection mix was assembled with 5 μg lentiviral plasmid, 3.75 μg psPAX2 and 1.25 μg pMD2.G in 500 μl Opti-MEM (Fisher Scientific, Catalog number: 31-985-070) and retroviral transfection mix was assembled with 5 μg retroviral plasmid and 5 μg pCL Ampho in 500 μl Opti-MEM. 30 μl Lipofectamine 2000 was diluted in 500 μl Opti-MEM and incubated for 5 minutes. Afterwards the DNA and Lipofectamine 2000 solutions were combined and incubated for 20 minutes at room temperature. Transfection mix was then applied dropwise to 293FT cells with 7

ml DMEM and incubated for 6 hours at 37ºC, 5% CO_2. After 6 hours, media was replaced with fresh DMEM and incubated for 72 hours at 37ºC, 5% CO_2 for lentivirus and 32ºC, 5% CO_2 for retrovirus. At 72 hours post transfection, virus containing supernatant was filtered through 0.45μm filters, aliquoted and kept at -80ºC.

For transducing adherent cells, cells were seeded the day before infection in 10 cm^2 dishes or 6-well plates. 1ml virus was added to the cells in a total volume of 5 ml or 2 ml (10 cm^2 or 6well plate) with 6 μg/ml polybrene (Millipore Sigma, Catalog number: TR-1003) and incubated for 24 hours at 37ºC, 5% CO_2. The following day media was replaced with fresh media (DMEM or RPMI) and cells were incubated for an additional 72 hours at 37ºC, 5% CO_2. After incubation, media was replaced with fresh media containing specific antibiotics (designated by eukaryotic antibiotic resistance genes) and incubated for 72-96 hours at 37ºC, 5% CO_2 if using Puromycin (InvivoGen, Catalog number: ant-pr-1) or 1-2 weeks at 37ºC, 5% CO_2 if using Geneticin (G418) (InvivoGen, Catalog number: ant-gn-1). After selection, cells were validated for expression of desired protein by WB analysis.

For transducing suspension cells, cells were infected with virus by spinoculation. In a 12-well plate 2 x 10^5 cells were infected with 1 ml virus in a total volume of 2 ml with 8 μg/ml polybrene. Cells were spun at 2500 rpm for 1 hour, cells were re-suspended in the same medium and transferred to 15 ml conical tubes (Fisher Scientific, Catalog number: 14-959-70C). Cells were spun at 1500 rpm for 5 minutes, supernatant was discarded, cells were re-suspended in media at a cell density of 50,000 cells/ml in 4 ml volume and transferred to a 6-well plate. Cells were incubated for 72 hours at 37ºC, 5% CO_2. After incubation, cells were spun at 1500 rpm for 5 minutes, supernatant discarded and cells were re-suspended in 4 ml of antibiotic selection media

for 72-96 hours at 37ºC, 5% CO_2, if using puromycin or 1-2 weeks at 37ºC, 5% CO_2, if using Neomycin. After selection cells were validated for expression of desired protein by WB analysis.

2.2.13 Generation of Knockout Cell Lines

All KO cell lines generated in Sarkar Lab (Table 2) were done by transfection using Lipofectamine 2000, Lipofectamine 3000 or X-tremeGene HP of single (SBB) or double backbone (DBB) CRISPR/Cas9 plasmids, with co-transfection of Cas9 for SBB plasmids expressing GFP. Alternatively, transduction of CRISPR plasmids was performed if cell lines are difficult to transfect, for example BJ-Tert cells. After 24 hours of transfection or 48-72 hours of transduction, cells were observed by fluorescent microscope in order to determine transfection or transduction efficiency. Cells were then sorted for GFP and mCherry double positive cells (for SBB plasmids) or mCherry positive cells (for DBB plasmids). Following clonal selection, cells were expanded and analyzed by WB for deficiency of the protein of interest.

2.2.14 Generation and Characterization of Doxycycline Inducible Cell Lines

All doxycycline inducible cell lines generated in Sarkar Lab (Table 2) were made by transduction of lentivirus. First Gateway cloning of pENTR vectors listed in Table 3 into pLenti TRE-DEST-EFpuro-2A-rTA destination vector was performed and plasmids were then packaged into lentivirus and transduced into target cells. After antibiotic selection, cells were treated with increasing concentrations of doxycycline (ranging from 0-5 μg/ml of doxycycline) for 24-48 hours and analyzed by WB for inducible expression of desired proteins. 24 hours of doxycycline

treatment is sufficient for expression of proteins, however optimal expression is achieved at 48 hours.

2.2.15 Genotyping of Oas1b-KI Mouse Model

A mouse model expressing full length Oas1b was obtained by restoring Oas1b by CRISPR homology driven repair, replacing the stop codon responsible for truncated Oas1b with an Arginine residue (X253R). Additionally, a new BspEI restriction site was inserted to allow genotyping of Oas1b-KI mice. To genotype these mice, tail snips were collected from mice and digested overnight at 55ºC with a tissue lysis mixture consisting of 120 µl 0.5 M EDTA, pH 8.0, 500 µl Nuclei Lysis Solution (from Wizard Genomic DNA Purification Kit) and 40 mg/ml of Proteinase K. Next samples were treated with 10 mg/ml RNase and incubated for 15 minutes at 37ºC. Samples were cooled to room temperatures and protein precipitation solution was added and DNA isolation continued as instructed in Wizard Genomic DNA Purification Kit. Concentration of genomic DNA was quantified by NanoDrop and 50-100 ng of DNA was amplified by PCR using OneTaq Hot Start Quick Load 2x Master Mix and Oas1b specific primers (FWD: 5'-TGACTGGGTGTGACAGTGTG-3', REV: 5'-AGGGCTGTAGGACCTCATGT-3'). PCR cycle conditions were as following: denaturation at 95ºC for 30 seconds, followed by 45 cycles of: 58ºC for 15 seconds, 55ºC for 15 seconds, 68ºC for 30 seconds, and finally 68ºC for 5 minutes. PCR product was digested with 250 U/ml BspEI overnight at 37ºC and 20µl of digested PCR product was analyzed by DNA electrophoresis on a 2% agarose gel. DNA from WT mice resulted in a 500 bp undigested product and DNA from Oas1b-KI mice resulted in a 250 bp product after digestion.

2.2.16 Isolation of Mouse Fibroblasts and Bone Marrow Derived Macrophages

2.2.16.1 Isolation of Mouse Fibroblasts from tails

To isolate fibroblasts from mouse tails, mice were sacrificed, and tails were collected after dissection. Tails were sliced into smaller pieces in PBS using a razor blade under sterile conditions and collected in a 15 ml conical tube containing 1 ml of 1:1 PBS and Pen-Strep. 1 ml of collagenase (ThermoFisher Scientific, Catalog number: 17104019) was added to samples at a final concentration of 1000 U/ml and incubated for 30 minutes with repeated shaking at 37ºC. Cells were spun at 1200 rpm for 5 minutes; pellets were washed with 1.5 ml Hank's Balanced Salt Solution (HBBS) (Millipore Sigma, Catalog number: 55021C) and again spun at 1200 rpm for 5 minutes. Cell pellets were incubated with 2-3 ml 0.05% Trypsin-EDTA for 20 minutes with repeated shaking at 37ºC. DMEM containing 20% FBS was added to mixture prior to a final spin at 1200 rpm for 5 minutes. Cells were re-suspended in DMEM containing 20% FBS, transferred to 10 cm^2 plates and incubated at 37ºC, 5% CO_2. After cells became confluent tail pieces were removed and cells were split for freezing and continued culture.

2.2.16.2 Isolation and differentiation of BMDMs from femur

To obtain BMDMs from mice, mice were sacrificed, dissected and monocytes were isolated from femurs. Cells were differentiated in DMEM with 20% L929 conditioning media. Excess tissue was removed from collected femurs and cells inside were flushed out with DMEM using a 25-gauge needle. Cells were collected in a 15 ml conical tube and spun down at 500 rpm for 1 minute, to remove tissue debris, and supernatant was transferred to a new 15 ml conical tube

and spun at 1000 rpm for 10 minutes. Cell were resuspended in DMEM containing 20% conditioning media, transferred to 10 or 60 cm^2 tissue culture plates and incubated at 37ºC, 5% CO_2 with changing of media every 2 days. After 7 days of culture, cells differentiated into macrophages and were frozen or used for experiments.

2.2.17 ELISA

To measure apical secretion of IFNβ from mouse BMDMs, cell supernatants were collected from cells transfected with poly (dA:dT) or p(I):p(C) and cells infected with Herpes Simplex Virus (HSV) or Sendai Virus (SeV). Samples were frozen at -80ºC until analyzed. IFNβ ELISA was adapted from Banerjee et al. 2018 (371). 96-well plates were first coated with rat anti-mouse IFNβ capture antibody (Santa Cruz, Catalog number: sc-57201) diluted 1:500 in coating buffer (0.1 M Sodium Carbonate pH 9.5) followed by overnight incubation at 4ºC. Wells were washed 3 times with wash buffer (0.05% Tween-20 in PBS), blocked with assay diluent (10% FBS in PBS) for 1 hour at room temperature and washed an additional 3 times with wash buffer prior to the addition of ELISA standards and samples to the plate. Standard and samples were incubated overnight at 4ºC, washed 5 times with wash buffer, and incubated with rabbit anti-mouse IFNβ detection antibody (R&D Systems, Catalog number: 32400-1) diluted 1:2000 in assay diluent for 3 hours at room temperature. Wells were washed 5 times with wash buffer and incubated with goat anti-rabbit HRP-linked secondary antibody (CST, Catalog number: 7074) diluted 1:2000 in assay diluent for 2 hours at room temperature. Wells were washed 7 times with wash buffer and incubated with Tetramethylbenzidine chromogenic substrate (BD Biosciences, Catalog number: 555214) in the dark for 15 minutes at room temperature. Chromogenic reaction

was terminated by the addition of Stop Solution 2N Sulfuric Acid (Millipore Sigma, Catalog number: 258105) and the absorbance at 450 nm of samples was read within 30 minutes of stopping the reaction.

2.2.18 RNA extraction and RT-qPCR

Total RNA from cells was extracted using Macherey-Nagel Nucleospin RNA Kit (Fisher Scientific, Catalog number: NC9581114), according to manufacturer's instructions, or with TRIzol reagent (ThermoFisher Scientific, Catalog number: 15596018). For RNA isolation using TRIzol, cell pellets were re-suspended with 0.5 ml TRIzol followed by addition of Chloroform (Fisher Scientific, Catalog number: AC423555000) and vigorous mixing by vortex. Samples were centrifuged at 12000 rpm for 5 minutes and the upper aquatic phase was transferred to microcentrifuges tubes containing 250 µl isopropanol for 10 minutes at room temperature, followed by RNA precipitation by centrifugation at 12000 rpm for 5 minutes. Samples were washed with 75% ethanol and centrifuged at 12000 rpm to remove excess salts. Supernatant was removed, RNA pellets were air-dried for 10-20 minutes and re-suspended in RNase-free H_2O. RNA concentration was measured by NanoDrop and 0.5-1 µg RNA was used for synthesis of complementary DNA (cDNA) using iScript cDNA Synthesis Kit (Bio-Rad, Catalog number: 1708891). cDNA was diluted 1:2 in water and gene expression was evaluated by RT-qPCR using SsoFast EvaGreen Supermix (Bio-Rad, Catalog number: 172-5200) or Sso Advanced Advanced Universal Probes Supermix (Bio-Rad, Catalog number: 172-5281) for Taqman probed-based qPCR. Primers used for amplification of target genes are listed on Table 11.

2.2.19 RNA sequencing

2 x 10^6 WT and OAS1-KO THP1 cells in T75cm^2 flasks were treated with 500 U/ml IFNγ for or 0, 1, 2, 4 and 8 hours, harvested and RNA sequencing was performed (Health Sciences Sequencing Core at the UPMC Children's Hospital of Pittsburgh). RNA was extracted using RNeasy Plus Mini kit (Qiagen, Catalog number: 74134) following manufacturer's instructions. Total RNA input was enriched for mRNA and fragmented. Random primers initiated first strand and second strand cDNA synthesis. Adenylation of 3'ends was followed by adapter ligation and library amplification with indexing. Sequencing was performed on an Illumina NextSeq 500. RNAseq FASTQ data were processed and mapped to the human reference genome (hg19) using CLC Genomics Workbench 11 (Qiagen). The mean RPKM values, with a cutoff of WT RPKM > 1, from the RNaseq data from two biological replicates was used to calculate the ratio of WT to OAS1-KO RPKM values. Heatmaps of RPKM ratios ranging from 0.55 to 1.75 were generated using pheatmap package in R studio (rstudio.com).

2.2.20 SILAC Analysis

WT and OAS1-KO THP1 cells were cultured at a cell density of 2-5 x 10^5 cells/ml for 8 generations in media containing heavy (^{13}C-6 ^{15}N-2 L-Lysine 2HCl and ^{13}C-6^{15}N-4 L-Arginine HCl) or light (L-Lysine 2HCl and L-Arginine HCl) isotope containing amino acids respectively. Cells were treated with 500 U/ml IFNγ for 0, 4 and 8 hours, harvested and SILAC analysis performed (MS Bioworks). Cell lysates were analyzed for incorporation efficiency (99.6%), followed by fractionation on SDS-PAGE, trypsin digestion and LC/MS/MS analysis. The mass spectrometer was operated in data-dependent mode, with MS and MS/MS performed in the

Orbitrap at 70,000 FWHM and 17,500 FWHM resolution, respectively. Data was processed and analyzed in MaxQuant software 1.6.0.16 (www.maxquant.org). Peptides with and FDR of 0.01 and Q-value (posterior error probability) of ≤ 0.05 were normalized and filtered by removing all proteins with less than 2 unique peptides throughout all the readings, with the exception of those proteins with 1 unique peptide across multiple reads. The average peptide ratios for 0, 4 and 8 hours were calculated from two experiments and the ratio values were transformed to $\log_2$ values. Further filtering was performed to remove proteins with no significant $\log_2$ (ratio) fold change [0.99 > $\log_2$ (peptide ratio) > -0.99]. Next the RPKM values of the corresponding proteins was imported from our RNAseq data into the same worksheet. Proteins with RPKM values < 1 in WT samples or RPKM WT/OAS1-KO ratios not within 0.55-1.75 were removed from the dataset. From this final list of proteins, the top 10 post transcriptionally upregulated proteins in WT from each timepoint were used to generate heatmaps of $\log_2$ (peptide ratio) and RPKM ratios ranging from 0.55 to 1.75 using pheatmap package in R studio (Chapter 3). From this list of post transcriptionally regulated proteins, a few bacterial infection related cellular proteins were detected and RPKM values were represented in heatmaps (Chapter 4). To identify IFNγ-inducible genes transcriptionally regulated by OAS1, the dataset was filtered to create a list of proteins up-regulated 2 fold at 4 and 8 hours post treatment. Next the $\log_2$ fold change of WT to OAS1-KO RPKM ratio was calculated and genes up-regulated [$\log_2$ (RPKM ratio) ≥ 1] or down-regulated (RPKM ratio) ≤ -1) in WT cells were compiled into a list (Appendix B.2, Table 14). Additionally, functional annotation of several gene lists was performed using The Database for Annotation, Visualization and Integrated Discovery (DAVID) bioinformatics tool (372, 373).

2.2.21 Ribosome Profiling

Ribosome profiling was performed on THP1 WT and OAS1-KO cells after 0 or 4 hours of 500 U/ml IFNγ treatment, followed by incubation with 100 μg/ml cycloheximide in PBS for 5 minutes at 37ºC, 5% CO_2. Cells were washed twice in PBS and harvested with polysome lysis buffer (50 mM Tris-HCL pH 7.5, 100 mM KCL, 12 mM $MgCl_2$, 1% NP-40, 1 mM DTT, 1X HALT protease inhibitor, 100 μg/ml cycloheximide). Lysate was cleared by centrifugation at 8000 g for 10 minutes at 4ºC, supernatants were layered on 10-50% sucrose gradient and spun at 230,000 g for 2.5 hours at 4ºC. Gradients were fractionated while monitoring absorbance at 254 nm. Total RNA was isolated from fractions using Direct-zol 96 RNA Kit (Zymo Research, Catalog number: R2054), according to manufacturer's instructions. RNA was used for synthesis of cDNA using iScript cDNA Synthesis Kit and gene expression was evaluated by RT-qPCR using Sso Advanced Advanced Universal Probes Supermix. Expression of cGAS and IRF1 mRNA in polysome fractions was carried out using TaqMan primers and probes listed on Table 11.

2.2.22 Radiation pulse-chase of nascent protein synthesis

Nascent protein synthesis was analyzed in THP1 WT and OAS1-KO cells by radiolabeling with ^{35}S-labeled amino acids (EasyTag EXPRESS ^{35}S Protein Labeling Mix, Perkin-Elmer, Catalog number: NEG772014MC), protein immunoprecipitation and SDS-PAGE. For analysis of IRF1 protein levels, 10 million cells per time point were grown at a cell density of 2-5 x 10^5 cells/ml and treated with 500 U/ml IFNγ for 2 hours. Cells were harvested by centrifugation at 1600 rpm for 3 minutes, re-suspended in 30 ml starvation media (RPMI without methionine, cystine or L-glutamine, Millipore Sigma, Catalog number: R7513) containing 4 mM L-glutamine

and 500 U/ml IFNγ for 10 minutes at room temperature followed by centrifugation at 1600 rpm for 3 minutes and re-suspension with 12 ml starve media containing 0.08 mCi/ml ^{35}S labelling mix. Cells were labeled for 30 minutes at room temperature and radiolabeled pulse samples were collected at different time points. The remaining cells were spun at 1600 rpm for 3 minutes, re-suspended in 15 ml chase media: standard RPMI media without FBS, 1% Pen-Strep, 5mM L-methionine (Millipore Sigma, Catalog number: M5308), 5 mM L-cystine (Millipore Sigma, Catalog number: C6852), 10 mM HEPES and chase samples were collected at different time points. Samples were kept on ice, centrifuged at 13000 rpm for 1 minute and lysed with lysis buffer containing 1% Triton X-100. For analysis of cGAS protein levels, 6 million cells per time point were grown at a cell density of 2-5 x 10^5 cells/ml. Cells were harvested by centrifugation at 1600rpm for 3 minutes, re-suspended in 20 ml starvation media containing 4 mM L-glutamine for 10 minutes at room temperature followed by centrifugation at 1600 rpm for 3 minutes and re-suspension with 12 ml starvation media containing 0.08 mCi/ml ^{35}S labelling mix. Cells were labeled for 30 minutes at room temperature and radiolabeled pulse samples were collected at different time points. The remaining cells were spun at 1600 rpm for 3 minutes, re-suspended in 6ml chase media and chase samples were collected at different time points. Samples were kept on ice, centrifuged at 13000 rpm for 1 minute and lysed with lysis buffer containing 1% Triton X-100. All samples were then immunoprecipitated with IRF1 or cGAS antibody by incubation with 1:50 antibody for 1 hour with rotation at 4ºC followed by incubation with Protein A/G Agarose Beads (Santa Cruz, Catalog number: sc-2003) overnight with rotation at 4ºC. Samples were spun down at 2000 rpm for 30 seconds, washed 3 times with IP buffer (standard lysis buffer without proteinase inhibitor) and after a final PBS wash, re-suspended in 1X sample buffer (Bio-Rad, Catalog number: 1610747). Pulse-chase and total protein samples were separated on 12% SDS-

polyacrylamide gels by SDS-PAGE, gels were dried for 45 minutes at 70ºC using a gel dryer and gels were placed in a phosphorimager plate for 3-5 days until analyzed by phosphorimaging using a Typhoon Biomolecular Imager. Gel images were analyzed using ImageQuant.

2.2.23 RNA Immunoprecipitation

Protein-RNA interactions of OAS1 was analyzed by RNA IP (RIP) after formaldehyde crosslinking, followed by RNA extraction and RT-qPCR analysis. Cells were harvested after treatment with or without 500 U/ml IFNγ for 2-4 hours. Cells were spun down at 1500 rpm for 10 minutes, washed twice in PBS and re-suspended in a 1:1 mix of PBS and 1% formaldehyde. Cell suspension was incubated for 10 minutes at room temperature followed by addition of cold 1M glycine (Bio-Rad, Catalog number: 56-40-6) and incubation for 10 minutes at room temperature. Cells were centrifuged at 1500 rpm for 10 minutes and cell pellets were flash frozen in liquid nitrogen and stored at -80ºC until analyzed. Samples were re-suspended in buffer B (0.5% NP-40, 0.25% sodium deoxycholate, 0.1% SDS, 10 mM EDTA, 50 mM Tris-HCL pH 8, 1X protease inhibitor, 40 U/ml RNase inhibitor) and incubated for 30 minutes with rotation at 4ºC. Samples were spun down and lysate was sonicated for 15 cycles of 30 seconds on and 30 seconds off. Sonicated lysate was centrifuged at 10000 rpm for 3 minutes and supernatant was pre-cleared by the addition of pre-washed Protein A/G agarose beads. RIP buffer (0.5% NP-40, 1.2 mM EDTA, 16.7 mM Tris-HCL pH 8, 167 mM NaCl, 1X protease inhibitor, 40 U/ml RNase inhibitor) was added to bead + lysate mixture and incubated for 45-60 minutes with rotation at 4ºC. After pre-clearing, samples were centrifuged at 10000 rpm for 3 minutes, supernatant was transferred to new microcentrifuge tubes and brought to 1 ml volume with RIP buffer. Samples were divided in three parts: 100 µl for input, 450 µl for IP with IgG isotype control and 450 µl for IP with OAS1/FLAG

antibody. IP was performed by adding 1 µg antibody and RNase inhibitor to the samples followed by incubation overnight with rotation at 4ºC. Samples were centrifuged at 10000 rpm for 3 minutes, supernatant was added to Protein A/G agarose beads and incubated for 2 hours with rotation at 4ºC. Again, samples were centrifuged at 10000 rpm for 3 minutes, supernatant was discarded, and beads were washed with 300 µl RIP buffer. Similar to RIP buffer washes, beads were washed with 300 µl High Salt Buffer (0.1% SDS, 1% Triton X-100, 2 mM EDTA, 20 mM Tris-HCL pH 8 and 500 mM NaCl) and then washed with TE buffer (1 mM EDTA and 10 mM Tris-HCL pH 8). After final washes, supernatant was discarded, and RNA was eluted from beads by incubation with 100µl Elution buffer (5 mM Tris-HCL pH 8, 150 mM NaCl, 1 mM $MgCl_2$, 1% SDS, 40 U/ml RNase inhibitor and 20 µg Proteinase K) for 5 minutes at 55ºC. Samples were spun down, elution was collected in a new microcentrifuge tube, RNA elution of beads was repeated once more with 200 µl Elution buffer without proteinase K for 25 minutes at 55ºC. Eluted samples from IgG and OAS1 IP were de-crosslinked with 12 µl 5 M NaCl and input sample was de-crosslinked with 4 µl 5 M NaCl followed by incubation for 2 hours at 65ºC. RNA was then isolated from samples using Macherey-Nagel Nucleospin RNA Kit, according to manufacturer's instructions. cDNA was synthesized from isolated RNA using iScript cDNA Synthesis Kit. Expression of mRNA associated to the protein of interest was evaluated by RT-qPCR using SsoFast EvaGreen Supermix and primers specific to target mRNA (listed on Table 11).

2.2.24 Statistics

For *in-vitro* experiments, statistical significance was calculated as indicated in the Figure Legends and represented as * $p < 0.05$, ** $p < 0.002$, *** $p < 0.001$ and **** $p < 0.0001$ using GraphPad PRISM 8.0. For all *in-vivo* survival experiments, statistical significance was calculated using a Mantel-Cox test.

3.0 OAS1 enhances cGAS protein synthesis and restricts WNV replication

3.1 Introduction

WNV remains widespread throughout the globe and has become the leading cause of mosquito-borne disease in the United States since it was first detected in New York in 1999 (268). Although approximately 80% of individuals infected with WNV remain asymptomatic, neuroinvasive disease can develop in older or immunocompromised individuals resulting in death (264). WNV neuroinvasive disease is established once WNV gains access to the CNS by crossing the blood-brain barrier and replicating efficiently in neurons and myeloid cells. Unfortunately, cost-effective vaccines against WNV have yet to be developed for human use, sparking a need to study the pathogenesis of WNV and host immunity in order to identify individuals susceptible to WNV infection and therapies to clear infection. Early cell-intrinsic immunity and induction of type I IFN is needed for control of WNV followed by adaptive humoral and T cells responses needed to clear infection (274). However, WNV among other flavivirus have developed several mechanisms of antagonizing IFN induction and signaling to establish persistent infection in the host (Fig. 10). Therefore, it is crucial to understand the mechanisms of host immunity in response to WNV to identify IFN inducible proteins needed to clear infection. A SNP located at the C-terminal of human OAS1 (rs10774671) has been associated to WNV antiviral resistance and influences the expression of OAS1 isoforms (243, 254). In mice, WNV resistance has been mapped to enzymatically inactive Oas1b (228). Laboratory strains mice susceptible to WNV have been shown to contain an early stop codon at exon 4 of Oas1b resulting in a truncation of Oas1b, whereas resistant mice express full length Oas1b. Additionally, recent studies have confirmed that

RNase L activity is not required for Oas1b mediated resistance to WNV and In humans OAS3 has been shown to primarily activate RNase L, with little contribution of OAS1 and OAS2 (17, 253). OASL, another enzymatically inactive OAS protein, has been shown to confer antiviral resistance by potentiating RIG-I signaling, making it clear that non-catalytic antiviral activities exist for OAS family proteins (238).

In this chapter we investigate the role of human and mouse OAS1 during WNV infection and clarify the mechanisms by which these proteins restrict WNV replication. The G allele of OAS1 SNP rs10774671 was shown to be protective to WNV through expression of OAS1 P46 and antiviral protection was independent of OAS1 enzymatic activity and activation of RNase L. We demonstrate that OAS1 post transcriptionally increases protein levels of several basal and IFNγ inducible proteins by binding to their mRNA and enhancing protein synthesis. Among these proteins, cGAS was shown to mediate OAS1 and Oas1b antiviral activity to WNV through type I IFN signaling. Lastly, an RNA binding residue of OAS1 and Oas1b was identified as a critical factor of WNV antiviral activity and impaired post transcriptional regulation of IRF1 and cGAS protein. Overall these studies identify a new mechanism of OAS1 and Oas1b antiviral activity to WNV and confirm that non-canonical roles exist for OAS family members.

3.2 Results

OAS1 SNP rs10774671 influences isoform splicing and antiviral activity against WNV, but the mechanisms of WNV antiviral activity by OAS1 are not well understood. This SNP is located at the 3' end of human *OAS1* and isoform expression is dependent on the expression of the G/A allele at this site (Fig. 11 A). Homozygous expression of the A allele incorporates an additional Alu I digestion site allowing for genotyping of human cell lines by RFLP assay. Therefore, we genotyped several commonly used human cell lines and found that 293T and HeLa cells have homozygous A/A; THP1, HT1080 and BJ-Tert have heterozygous G/A; and Daudi has homozygous G/G genotypes (Fig. 11 B). Expression of OAS1 after IFNα treatment was determined in order to validate the expression of OAS1 P42 and P46 isoforms corresponded to the genotype of the A/G allele (Fig. 11 C). As expected, HeLa cells (A/A) expressed P42 as compared to THP1, HT1080 and BJ-Tert cells (G/A), which all expressed P46 primarily after IFN treatment.

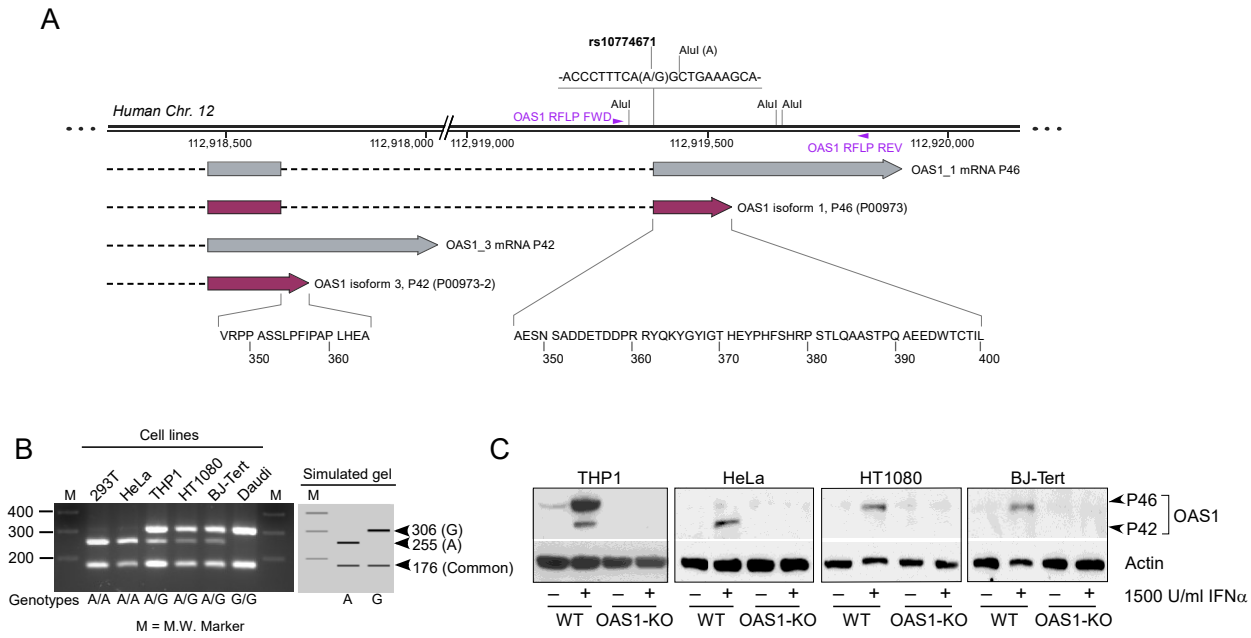

Figure 11. Human OAS1 SNP rs10774671 genotyping and isoform expression
Schematic of OAS1 rs10774671 SNP and RFLP Assay design. Presence of the A allele leads to an additional AluI digestion site allowing for differentiating A genotypes from G genotypes (A). Human cell lines were genotyped for the A or G allele of OAS1 SNP rs10774671 by RFLP Assay using AluI restriction enzyme (B). WT and OAS1-KO THP1, HeLa, HT1080 and BJ-Tert cells were treated with 1500 U/ml of IFNα overnight and expression of OAS1 was examined by immunoblotting of whole cell lysates (C).

Given that WNV resistance has been linked to expression of the G allele in OAS1 (243), we assessed the isoform-specific functions of OAS1 by creating multiple OAS1-deficient (OAS1-KO) cell lines either in homozygous A/A (HeLa) or heterozygous G/A (THP1, HT1080 and BJ-Tert) background using CRISPR/Cas9 gene editing (Fig. 11 C) and infected these cells WNV Kunjin strain (WNV-KUN) (Fig. 12 A-C). Heterozygous G/A cell lines (HT1080 and BJ-Tert), expressed P46 and were capable of restricting WNV-KUN replication, which was impaired in OAS1-deficient cells (Fig. 11 C, Fig. 12 B-C) as compared to homozygous A/A HeLa cells, which did not restrict WNV-KUN. (Fig. 12 A). This suggests that the antiviral activity of OAS1 against WNV-KUN is associated with the expression of OAS1 P46 isoform.

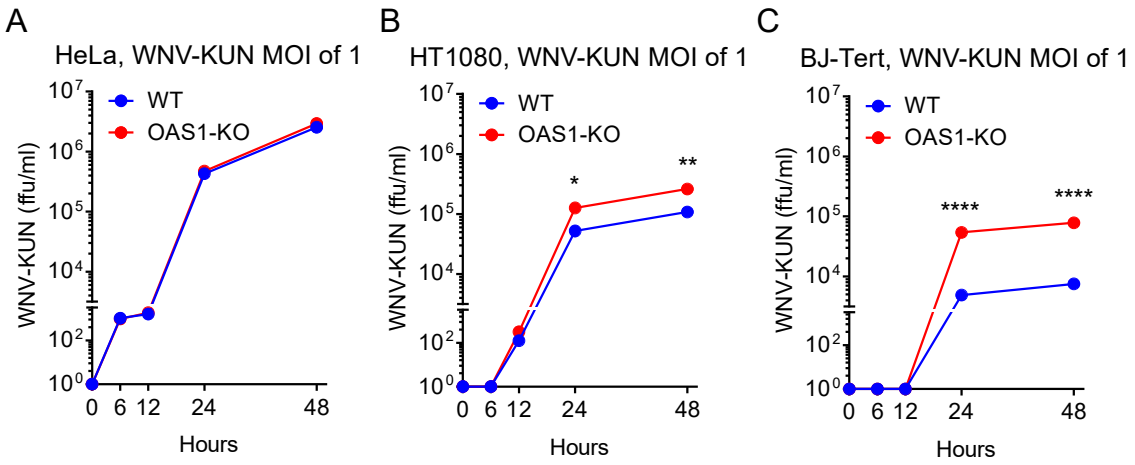

Figure 12. Cell lines with G allele and OAS1 P46 expression inhibit WNV infection
WT and OAS1-KO HeLa (A), HT1080 (B) and BJ-Tert (C) cells were infected with WNV-KUN at a MOI of 1. Culture supernatants collected at indicated time points post infection were quantified for infectious virus particles by florescent foci assay (FFU assay) on Vero cells. For each timepoint, supernatants from two independent infections were used to infect Vero cells in duplicates, mean and SEM of the calculated FFU/ml were plotted. Statistical significance of OAS1-KO cells compared to WT cells was assessed using a two-way ANOVA with Sidak's multiple comparison test.

We validated our previous finding by inducibly expressing P42 and P46 in OAS1-KO HT1080 cells (Fig. 13 A), followed by infection with WNV-KUN. Doxycycline (Dox) inducible expression of OAS1 P46, but not P42, was capable of inhibiting WNV-KUN growth (Fig. 13 B-C), indicating that the protective role of OAS1 to WNV infection results from the rs10774671 G genotype and expression of the P46 isoform.

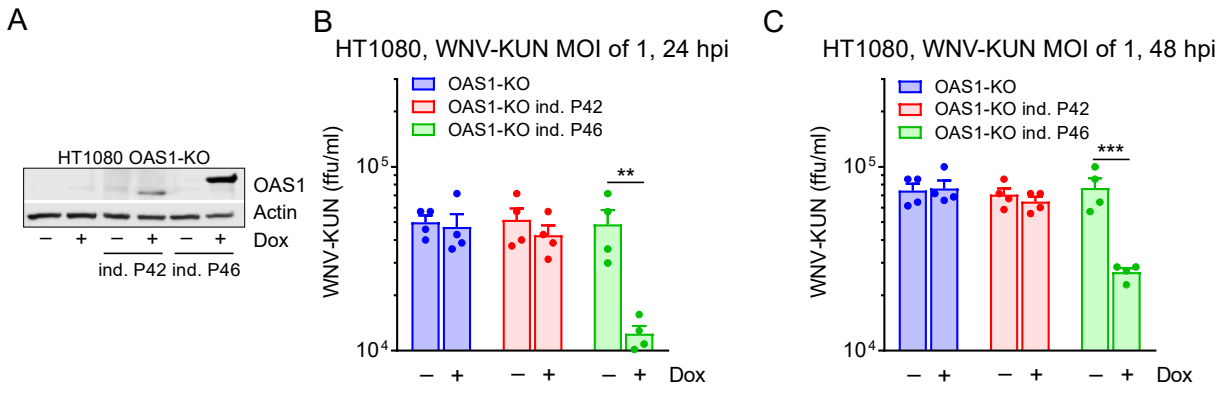

Figure 13. Inducible expression of OAS1 P46 inhibits WNV infection
HT1080 OAS1-KO, OAS1-KO inducible OAS1 P42 and OAS1 P46 were pre-treated with 2.5 and 1 µg/ml Doxycycline (Dox) respectively for 24 h and then infected with WNV-KUN at a MOI of 1. Cell lysates were prepared 24 h post Dox treatment and analyzed by immunoblotting with OAS1 and Actin antibody (A). Culture supernatants were collected 24 and 48 h post infection and infectious particles were quantified by FFU assay on Vero cells as described previously. Mean and SEM were calculated from two dilutions of duplicate samples. Significance of Dox treated cells compared to untreated cells was assessed using a two-way ANOVA with Sidak's multiple comparison test.

We next examined whether the NTase activity of OAS1 was necessary for the antiviral activity of P46. Previous studies had identified critical Asp residues, composing a catalytic triad in the active site of OAS enzymes. These Asp residues are needed for NTase activity and mutations of these residues abolish catalytic function (235, 236). We inducibly expressed an enzymatically inactive mutant of P46 D75A/D77A (DADA) in HT1080 (Fig. 14 A). Both WT and P46 DADA mutant restricted WNV replication to the same degree (Fig. 14 B-C) and these results were validated in BJ-Tert cells by inducibly expressing P42, P46 and P46 DADA (Fig. 14 D). Similarly, WT P46 and P46 DADA mutant inhibited viral growth (Fig. 14 E-F), confirming that enzyme activity is not required for the antiviral activity of P46.

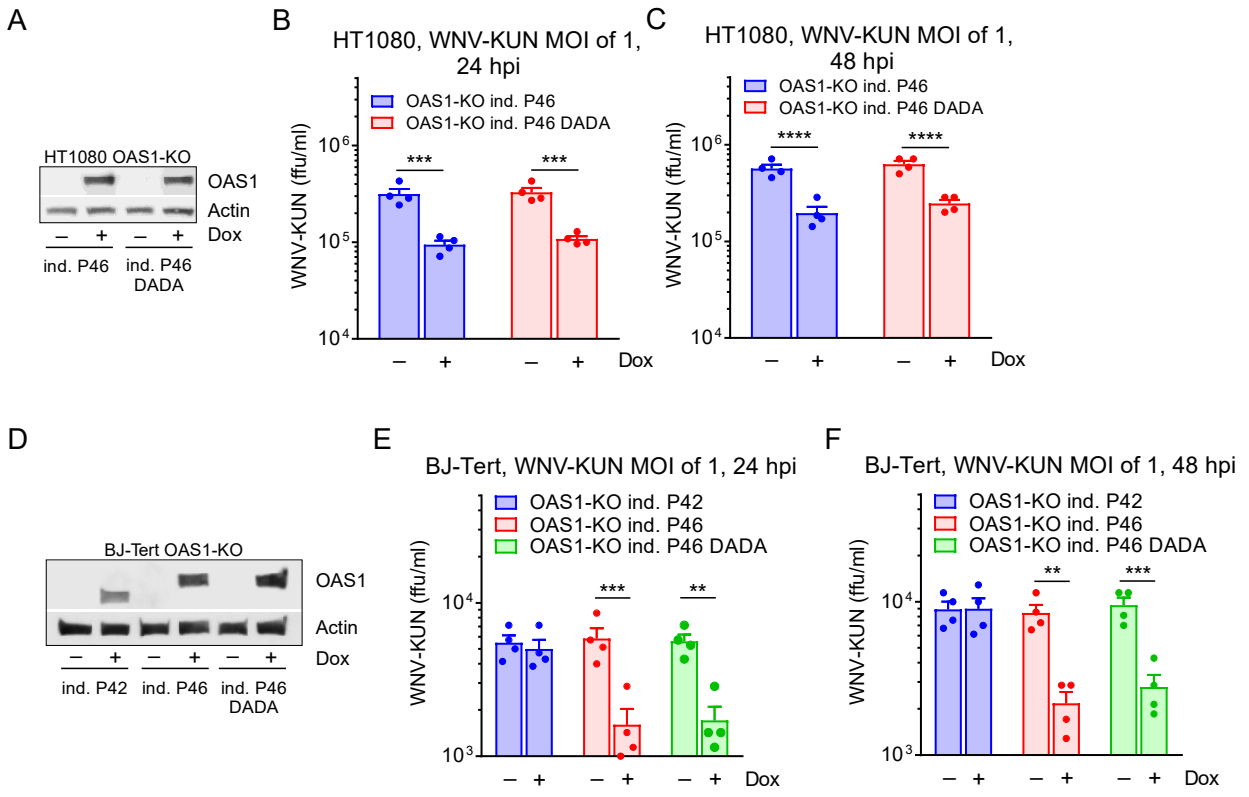

Figure 14. OAS1 antiviral activity against WNV is independent of its NTase activity
HT1080 OAS1-KO cells expressing inducible OAS1 P46 and OAS1 P46 D75A/D77A (DADA) mutant were pre-treated with 1µg/ml Dox for 24 h and infected with WNV-KUN at a MOI of 1. Cell lysates were prepared 24 h post Dox treatment and analyzed by immunoblotting with OAS1 and Actin antibody (A). Culture supernatants were collected at indicated time points followed by FFU assay on Vero cells as described before (B-C). BJ-Tert OAS1-KO inducibly expressing OAS1 P42, OAS1 P46 and OAS1 P46 D75A/D77A (DADA) were pre-treated with 5, 2 and 5 µg/ml Dox respectively for 24 h and then infected with WNV-KUN at a MOI of 1. Cell lysates were collected 24 h post Dox treatment and analyzed by immunoblotting with OAS1 and Actin antibody (D). Culture supernatants were collected 24 and 48 h post infection and infectious particles were quantified by FFU assay on Vero cells (E-F). Mean and SEM values were determined as in Fig. 13. Statistical significance of Dox treated cells compared to untreated cells was assessed using a two-way ANOVA with Sidak's multiple comparison test.

The NTase activity OAS proteins, responsible for the production of 2'-5' oligoadenylates, is required for activation of RNase L and suppression of global RNA translation, including viral RNA (162, 374). Given that P46 restricted WNV independent of NTase activity, we hypothesized that RNase L was not required for OAS1 P46-specific WNV antiviral activity. Therefore, we generated RNase L-deficient (RNase L-KO), and OAS1/RNase L-double deficient (OAS1/RNase L-DKO) HT1080 cells, in which we inducibly expressed P46 (Fig. 15 A). These cells were infected

with WNV-KUN. As expected, WT and RNase L-KO cells inhibited viral growth as compared to OAS1-KO cells and inducible expression of P46 in OAS1/RNase L-DKO cells had reduced virus production in a manner equivalent to its ectopic expression in WT and RNase L-KO cells (Fig. 15 B-C). Together this data confirms that OAS1 P46 inhibits WNV replication through a novel mechanism independent of NTase activity and RNase L activation.

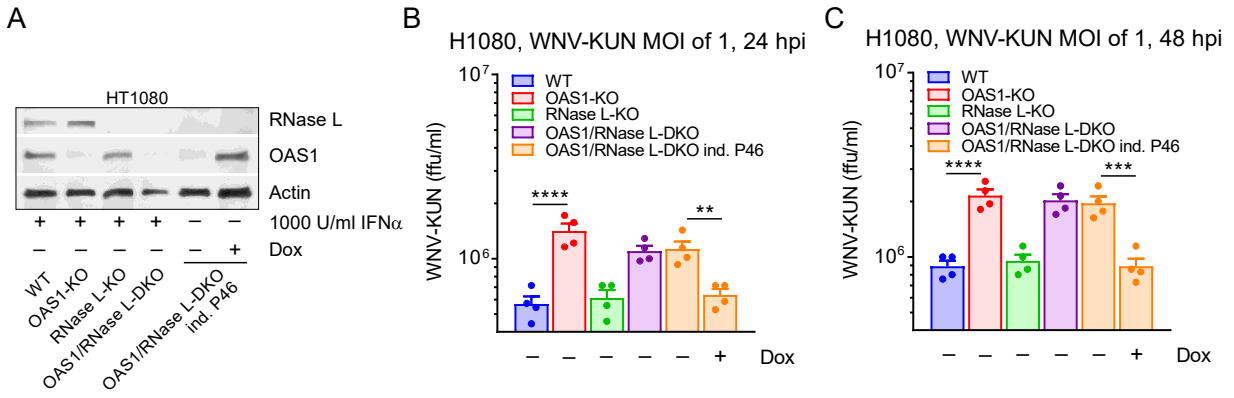

Figure 15. OAS1 antiviral activity against WNV is independent of RNase L activation
Expression of OAS1 and RNaseL was validated by treating the indicated cells overnight with 1000 U/ml of IFNα. Inducible expression of OAS1 was validated by treating OAS1/RNaseL-DKO inducible OAS1 P46 cells with 1 µg/ml Dox for 24 h. Cell lysates were analyzed by immunoblotting with RNaseL, OAS1 and Actin antibody (A). HT1080 WT, OAS1-KO, RNaseL-KO, OAS1/RNaseL-DKO and OAS1/RNaseL-DKO inducible OAS1 P46 (pre-treated with 1µg/ml Dox for 24 h) were infected with WNV-KUN at a MOI of 1. Culture supernatants for each cell line were collected 24 and 48 h post infection and infectious particles were quantified by FFU assay on Vero cells as. Mean and SEM were plotted as described previously and the statistical significance of all groups was assessed using a one-way ANOVA with Turkey's multiple comparison test.

To define the mechanistic bases of OAS1 antiviral activity, we characterized type I and type II IFN signaling in THP1 and BJ-Tert OAS1-deficient cells. The levels of IFIT1 and IFIT3 protein was comparable between WT and OAS1-deficient cells (Fig. 16 A-C), concluding that OAS1 does not affect IFNα signaling. On the contrary, a significant loss of IRF1 protein was observed after treatment of THP1 and BJ-Tert OAS1-deficient cells with IFNγ as compared to WT

cells (Fig. 16 D). Additionally, IRF1 protein levels were unaffected in RNase L-deficient THP1 cells indicating that the phenotypic loss of IRF1 is independent of RNase L activation (Fig. 16 E).

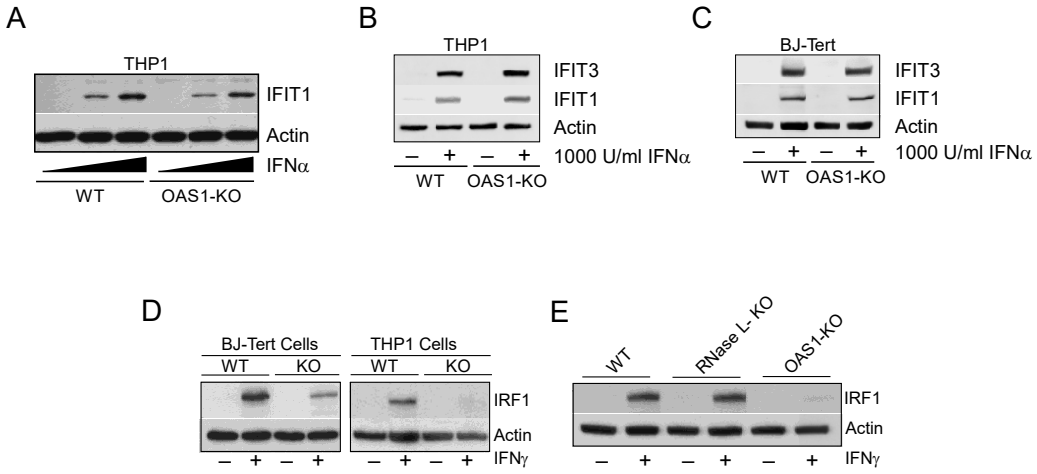

Figure 16. Type I and Type II IFN signaling in OAS1-deficient cells
WT and OAS1-KO THP1 cells were treated overnight with 100 and 1000 U/ml IFNα. Cell lysates were collected after treatment and analyzed by immunoblotting with IFIT1 and Actin antibody (A). WT and OAS1-KO THP1 and BJ-Tert cells were treated overnight with 1000 U/ml IFNα. Cell lysates were collected after treatment and analyzed by immunoblotting with IFIT1, IFIT3 and Actin antibody (B-C). WT and OAS1-KO BJ-Tert and THP1 cells were treated with 500 U/ml of IFNγ for 4 h (D). WT, RNAse L-KO and OAS1-KO THP1cells were treated with 500 U/ml of IFNγ for 4 h. Cell lysates were prepared after treatment and analyzed by immunoblotting with IRF1 and Actin antibody (E).

To explore the defects in type II IFN signaling observed in OAS1-KO cells, we examined STAT1 phosphorylation and IRF1 mRNA induction in WT and OAS1-KO THP1 cells following IFNγ treatment. The lack of OAS1 did not affect IFNγ mediated STAT1 phosphorylation at Tyr701 (Fig. 17 A) or STAT1 and IRF1 mRNA induction (Fig. 17 B-C), suggesting that IRF1 is regulated by OAS1 post transcriptionally.

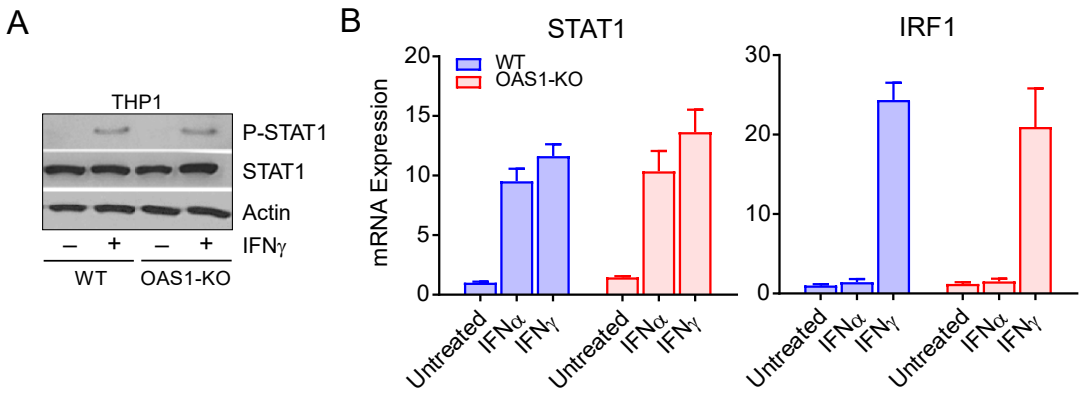

Figure 17. Deficiency in type II IFN signaling is downstream of transcription and STAT1 activation
THP1 WT and OAS1-KO cells were treated overnight with 1000 U/ml IFNα or 1000 U/ml IFNγ for 4 h. Cell lysates were analyzed by immunoblotting with STAT1, phospho-STAT1, IRF1 and Actin antibody (A). As indicated, THP1 WT and OAS1-KO cells were treated overnight with 1000 U/ml IFNα or 500 U/ml IFNγ for 4 h. Total RNA was extracted from cells and STAT1 and IRF1 mRNA were quantified by RT-qPCR. Mean and SEM were calculated for each treatment from three replicates.

In order to determine the effect of OAS1 loss on cellular physiology and IFNγ response we simultaneously characterized the proteasome and transcriptome of OAS1-deficient THP1 Cells. WT and OAS1-KO THP1 cells were treated with IFNγ and analyzed by RNA sequencing (RNAseq) and Stable Isotope Labeling by/with Amino acids in Cell culture (SILAC). WT cells were grown in the presence of heavy isotope labeled amino acids and analyzed for incorporation efficiency (99.6%). OAS1-KO cells were grown in the presence of light isotope labeled amino acids. Cells were treated with IFNγ for different durations and analyzed by liquid chromatography-tandem mass spectroscopy analysis. Similarly, treated cells were analyzed in parallel by RNAseq. Because our findings showed that OAS1 post transcriptionally regulated IRF1, we focused our analysis on proteins with altered levels without significant differences in corresponding mRNA levels. This strategy limits the detection of proteins for which levels were altered due to changes in transcription resulting from up-regulation of upstream transcription factors, for example IRF1. We then filtered the data set with FDR ($p < 0.01$) and determined the ratio of peptide intensities between WT and OAS1-KO cells at each time point and sorted from highest to lowest fold change

(detailed in Methods, Section 2.2.21). Similar ratio of RPKM (Reads Per Kilobase of transcript, per Million mapped reads) values of the corresponding genes below 1.7-fold indicated whether the mRNA for the same gene was not altered. We detected total 87 proteins (Appendix B, Table 12) that were post transcriptionally reduced more than 2-fold in OAS1-KO cells at any time point and Fig. 18 A highlights the top 30 proteins affected by the loss OAS1. Several proteins were up-regulated in WT cells at the basal level (0 h), including cGAS, compared to OAS1-KO cells and there were no significant differences in corresponding mRNA levels (Fig. 18A). Similarly, several IFNγ inducible proteins with known antiviral activity such as IRF1, UBR5 (375), XRN1 (376), TAP2 (377) and several STAT proteins were reduced in OAS1-KO cells without significant reduction of corresponding mRNAs (Fig. 17A). Few proteins were up-regulated in OAS1-KO cells (Appendix B, Table 13), however none were associated with known cellular antiviral response pathways. We validated these findings by immunoblotting of select proteins in THP1, BJ-Tert and HT1080 WT and OAS1-KO cells (Fig. 18 B).

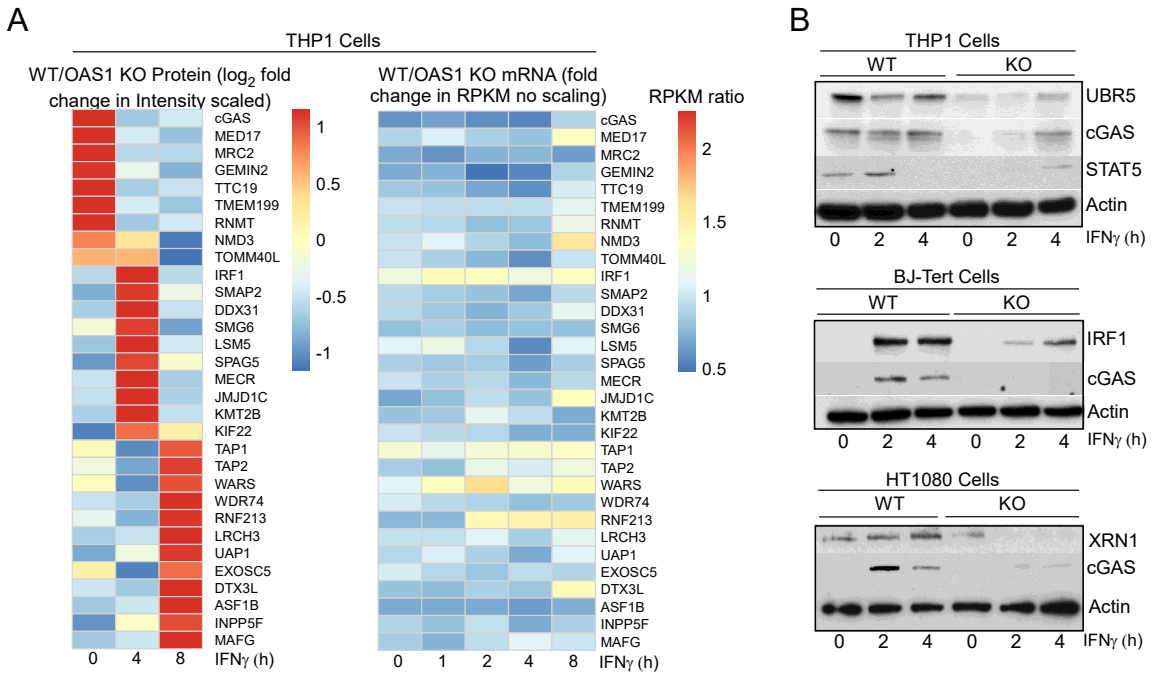

Figure 18. OAS1 deficiency leads to a loss of steady state protein levels
THP1 WT and OAS1 KO cells were cultured for 8 generations in media containing heavy isotope amino acids (^{13}C-6 ^{15}N-2 L-Lysine, and ^{13}C-6 ^{15}N-4 L-Arginine) and light isotope amino acids (L-Lysine and L-Arginine) respectively. Cells were then treated with 500 U/ml IFNγ for 0,4 and 8 h for SILAC analysis. In parallel, cells grown in regular media were treated with 500 U/ml IFNγ for 0, 1, 2, 4 and 8 h and analyzed by RNAseq analysis. Following filtering (STAR Methods) of the SILAC data peptide ratios were scaled for each protein and represented by heatmap. Corresponding mRNA RPKM values were plotted in the heatmap as fold change without scaling (A). WT and OAS1-KO THP1, BJ-Tert and HT1080 cells were treated with 500 U/ml of IFNγ for 0, 2 and 4 h. Cell lysates were analyzed by immunoblotting with indicated antibodies (B).

Next we confirmed that OAS1 P46 was responsible for post transcriptional regulation of target proteins by measuring protein levels of cGAS and IRF1 after inducible expression of WT P46 and P46 DADA mutant in OAS1-deficient THP1 cells. Expression of both WT P46 and P46 DADA were capable of rescuing cGAS protein expression (Fig. 19 A) and similarly rescued IRF1 and STAT3 protein levels in IFNγ treated cells (Fig. 19 B). Additionally, P42 was not capable of restoring IRF1 or STAT3 (Fig. 19 B) indicating that P46 is responsible for regulating levels of specific proteins at a post transcriptional level.

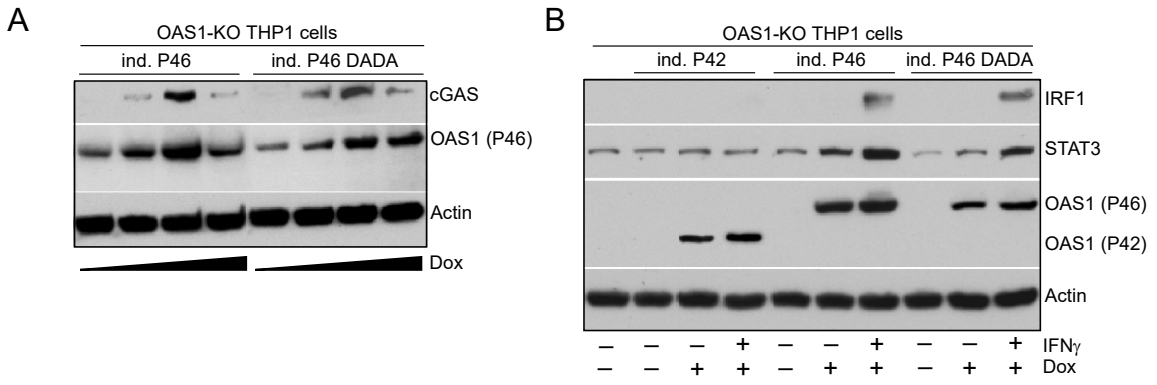

Figure 19. Inducible expression of OAS1 P46 rescues cGAS, IRF1 and STAT3 protein levels
THP1 OAS1-KO inducible OAS1 P46 and P46 DADA cells were treated with 0.5, 1, 2.5 and 5 μg/ml Dox. Cell lysates were analyzed by immunoblotting with cGAS, OAS1 and Actin antibody (A). THP1 OAS1-KO inducible OAS1 P42, P46 and P46 DADA cells were treated with 2.5, 1 and 1 μg/ml Dox respectively for 48 h followed by treatment with 1000 U/ml IFNγ for 4 h. Cell lysates were prepared after treatment and analyzed by immunoblotting with IRF1, STAT3, OAS1 and Actin antibody (B).

Our findings that OAS1 P46 regulates the expression of cGAS and IRF1 at a protein level without affecting steady state levels of their mRNA, suggesting that P46 regulates the translation of target mRNA. To further understand the mechanism, we measured protein synthesis in THP1 WT and OAS1-KO cells. First, we performed polysome profiling on these cells, a powerful tool used to monitor subsets of actively translating mRNAs in a cell, by sucrose gradient separation of polysomes associated to mRNA (378). Polysome profiling of WT and OAS1-KO THP1 cells with or without IFNγ treatment showed that the peak of IFNγ induced IRF1 mRNA was shifted towards the monosome fractions in the OAS1-KO cells compared to the WT cells (Fig. 20). Similarly, the polysome-associated fraction of cGAS mRNA was reduced in OAS1-KO cells (Fig. 20). Association with polysomes is an indicator of active translation of bound mRNA, therefore notable shifts of IRF1 and cGAS mRNA towards the monosome fractions in OAS1-KO cells suggests that OAS1 augments translation of these mRNAs.

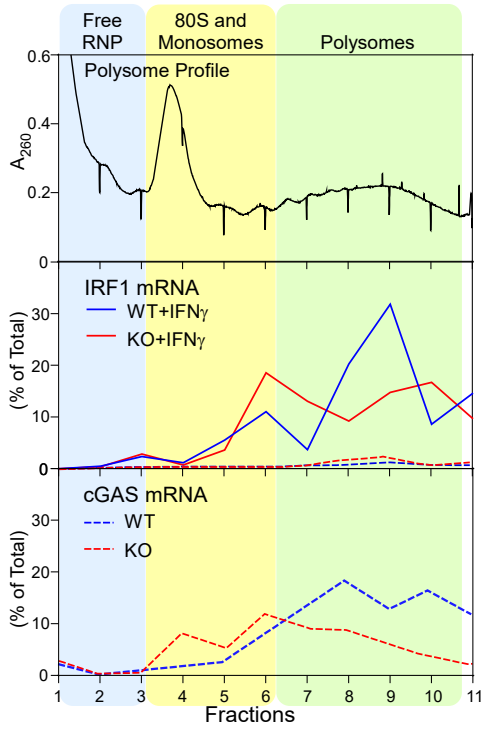

Figure 20. OAS1 shits target mRNA to polyribosome fractions
Polysome profiling was performed on THP1 WT and OAS1-KO cells after 0 or 4 h of 500 U/ml IFNγ treatment. Following translational arrest with 100 µg/ml cycloheximide cell lysates were fractionated on a 10-50% sucrose gradient at 230,000g for 2.5 h. Total RNA from each fraction were isolated followed by RT-qPCR analysis for cGAS and IRF1 mRNA.

To validate the results from our polysome profiling, we measured the rate of protein synthesis and decay using pulse-chase ^{35}S labeling followed by immunoprecipitation (IP) of IRF1 and cGAS. There were no apparent differences in the levels of total protein synthesis (Fig. 21 A, first two lanes), however IRF1 and cGAS accumulation was reduced in OAS1-KO cells (Fig. 21 A, IP lanes). In order to determine the rate of IRF1 and cGAS translation and protein decay, ^{35}S labeled IRF1 and cGAS band intensities were fitted with linear regression during the pulse period or by fitting the band intensities with a single-phase exponential decay equation and quantifying the half-life of the exponential decay during the chase period (Fig. 21 B). Analysis revealed that the rate of translation (determined by the slope of the linear regression) was reduced by 6- and 3-fold for IRF1 and cGAS respectively, in OAS1-KO cells. However, the half lives of IRF1 between

WT (16.4 min) and OAS1-KO (12.1 min) cells were quite similar and cGAS band intensity did not diminish during this period (Fig. 21 B). Together the results of polysome profiling and pulse-chase experiments indicate that OAS1 does not regulate the decay of these proteins, but instead enhances their synthesis.

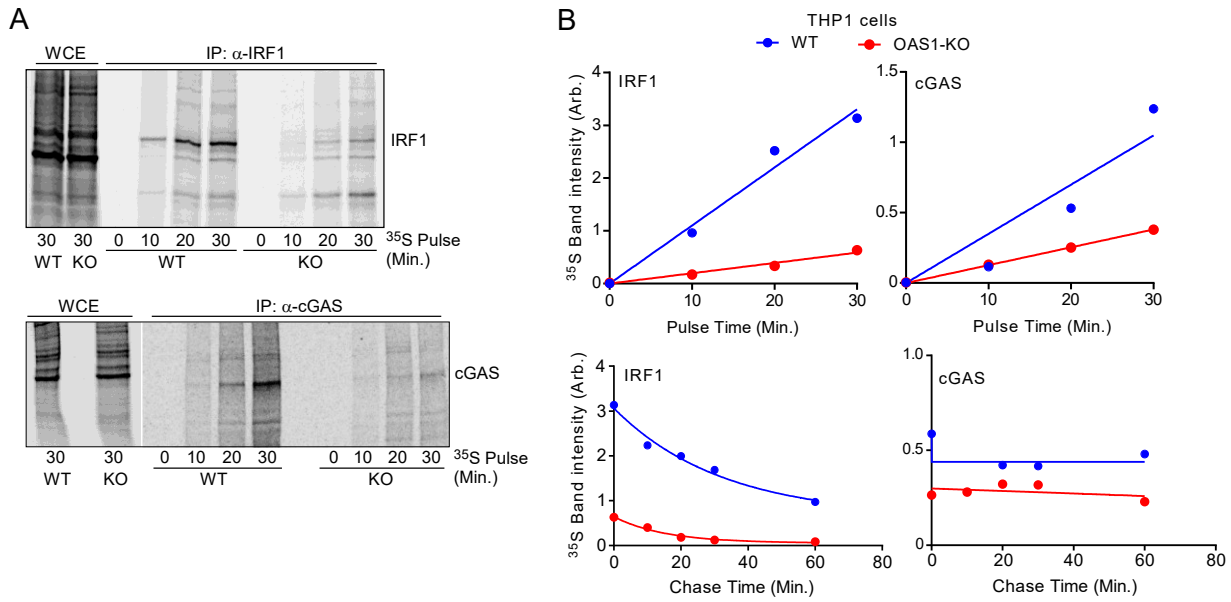

Figure 21. Effect of OAS on IRF1 and cGAS protein synthesis and decay
WT and OAS1-KO THP1 cells were pulse labelled with ^{35}S-L-methionine and ^{35}S-L-cysteine mixture for 30 min, followed by chase with cold amino acids for 60 min. Cell lysates were immunoprecipitated with IRF1 or cGAS antibodies and analyzed by SDS-PAGE and autoradiography with a Typhoon imager (A). IRF1 and cGAS band intensities were quantified, plotted and fitted with a linear regression for protein synthesis or fitted with a single exponential decay equation to measure protein degradation (B). Representative figures from at least twice repeated experiments are shown.

Having established that P46 enhances the translation of IRF1 and cGAS mRNA, we sought to determine the molecular mechanism of OAS1 translational regulation by OAS1 using RNA-immunoprecipitation (RIP) experiments. During RIP analysis, cells are subjugated to formaldehyde treatment to generate protein-RNA cross-links between proximal molecules followed by immunoprecipitation of proteins of interest. Reverse cross-linking of the IPed protein and RNA complexes allows recovery of the associated RNA that is and quantified by RT-qPCR

(379). In order to determine if OAS1 directly bound to IRF1 and cGAS mRNA, we performed RIP analysis on IFNγ treated HT1080 OAS1-deficient cells inducibly expressing P42 and P46. Only P46 induced by Dox showed enrichment of cGAS mRNA as compared to P42, which did not show any association with cGAS mRNA. Additionally, the control GAPDH mRNA was not enriched in P46 expressing cells (Fig. 22 A). Similarly, IRF1 mRNA was enriched in cells expressing P46 after IFNγ induction, but not in cells expressing P42 (Fig. 22 B). These results indicate that human P46 associates with specific mRNA to enhance their translation.

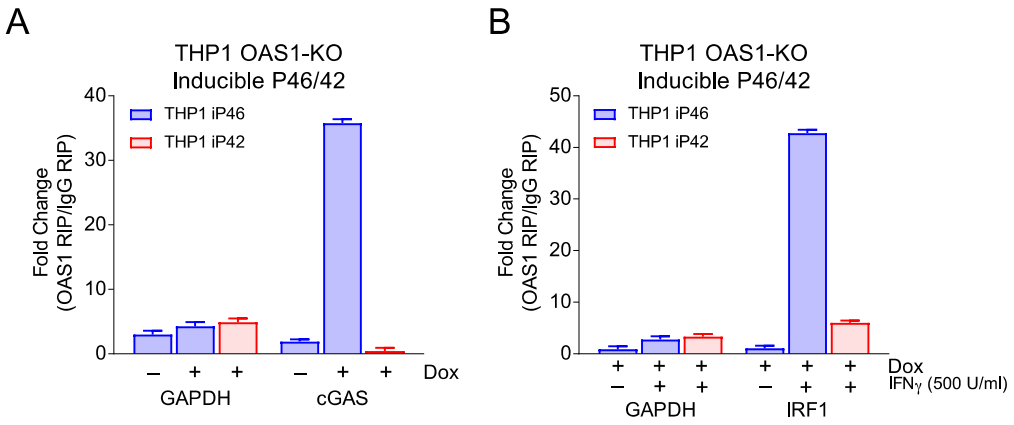

Figure 22. OAS1 P46 binds directly to target mRNA
THP1 OAS1-KO expressing inducible OAS1 P42 and P46 cells were treated with 1.5μg/ml Dox for 48 h. Formaldehyde crosslinked cell lysates were prepared followed by RNA-immunoprecipitation (RIP) with OAS1 and control IgG antibody. GAPDH and cGAS mRNA was quantified in input and RIP samples by RT-qPCR. Percent enrichment of specific mRNA were calculated with respect to the input mRNA. Mean and SEM of the fold enrichment values with respect to the control IgG were plotted from three replicates.

Given that OAS1 P46 restricts WNV and regulates the translation of several antiviral proteins, we hypothesize that OAS1 antiviral activity was mediated downstream through a specific protein or pathway regulated by P46. As both cGAS and IRF1 have been shown to restrict WNV (380, 381), we used cGAS-KO and IRF1-KO BJ-tert cells to inducibly express P46 and examine the antiviral activity of these cells to WNV. Additionally, we included WT, OAS1-KO and MAVS-KO BJ-Tert cells as controls. All cell lines were verified for the loss of expression of the target

protein and inducible expression of P46 in each cell line (Fig. 23 A) followed by infection with WNV-KUN in the absence or presence of doxycycline. Viral titers in individuals cell lines without inducible expression of P46 showed the expected patterns of enhanced virus replication in IRF1, MAVS and OAS1-KO cells confirming their antiviral roles. However, expression of P46 restricted viral growth in all cell lines except cGAS-KO cells (Fig. 23 B) establishing a requirement for cGAS to mediate downstream antiviral effects of P46. The antiviral activity of cGAS to WNV was confirmed by ectopically expressing FLAG-tagged cGAS and measuring WNV replication (Fig. 23 C-D).

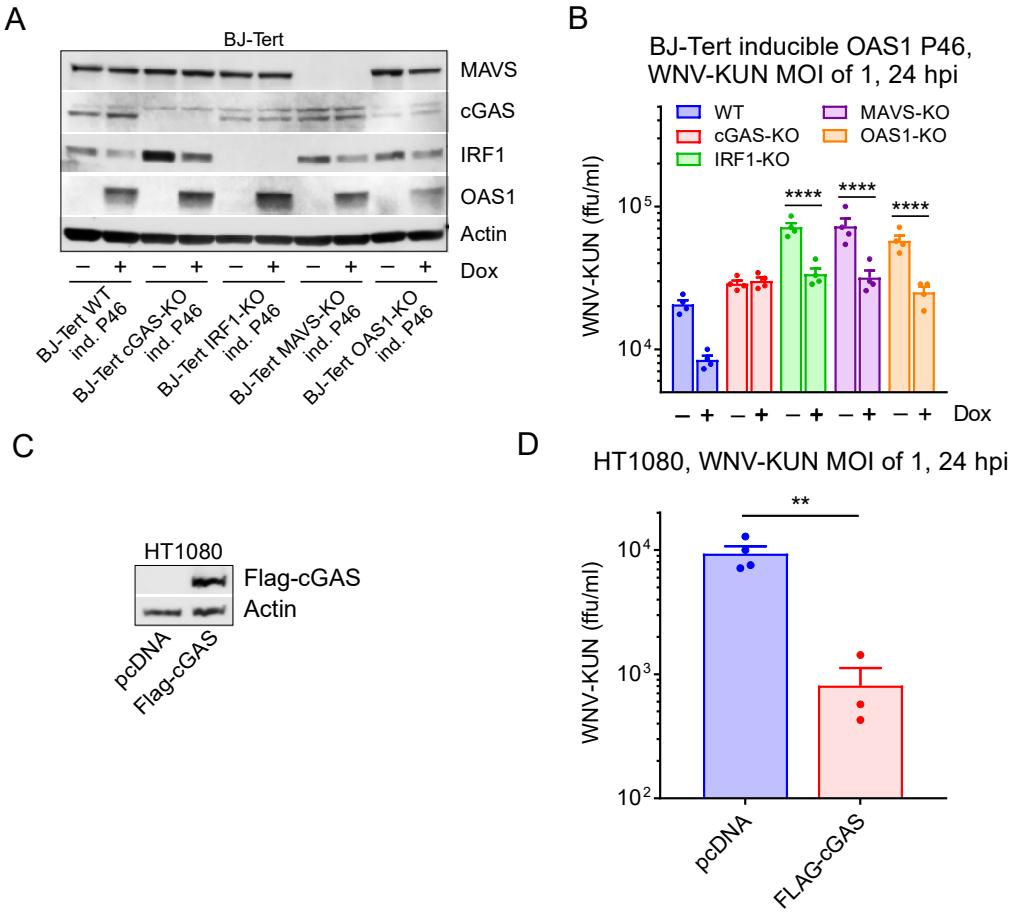

Figure 23. OAS1 antiviral activity is mediated through cGAS
BJ-Tert WT, cGAS-KO, IRF1-KO, MAVS-KO and OAS1-KO cells with inducible P46 expression were pre-treated with 2µg/ml Dox for 24 h and then infected with WNV-KUN at a MOI of 1. Cell lysates collected 24 h post Dox treatment, were analyzed by immunoblotting with cGAS, IRF1, MAVS, OAS1 and Actin antibody (A). Culture supernatants from each KO cell line were collected 24 h post infection and infectious particles were quantified by FFU assay on Vero cells (B). Mean and SEM were plotted from as before followed by statistical analysis using a two-way ANOVA with Sidak's multiple comparison test. HT1080 cells were transfected with pcDNA-Flag-cGAS overnight, followed by infection with WNV-KUN at a MOI of 1. Cell lysates were prepared from transfected samples and analyzed by immunoblotting with Flag and Actin antibody (C). Culture supernatants were collected 24 h post infection and virus particles were quantified by FFU assay on Vero cells as before (D). Statistical significance of cGAS transfected cells compared to pcDNA transfected cells was assessed using an Unpaired t test.

cGAS senses cytosolic DNA resulting in the production of the second messenger cGAMP and subsequent activation of STING in order to induce transcriptional activation of type I IFNs and ISGs needed to restrict viral growth (382). However, cGAS has also been implicated in restricting RNA virus infection and it is thought that cGAS is activated due to leakage of mitochondrial DNA during virus infection (308, 383). Our findings that cGAS is required for the

antiviral activity of OAS1 to WNV suggests that intact IFN signaling is needed to inhibit virus. We examined this hypothesis using IFN-receptor-deficient (IFNAR-KO) cells. We infected OAS1/IFNAR1-DKO BJ-Tert cells with or without inducible expression of P46 (Fig. 24 A). OAS1/IFNAR1-DKO cells were incapable of repressing WNV-KUN replication, as compared to WT cells, and inducible expression of P46 did not inhibit virus (Fig. 24 B-C), suggesting that downstream IFN signaling presumably through cGAS is required for the antiviral activity of P46.

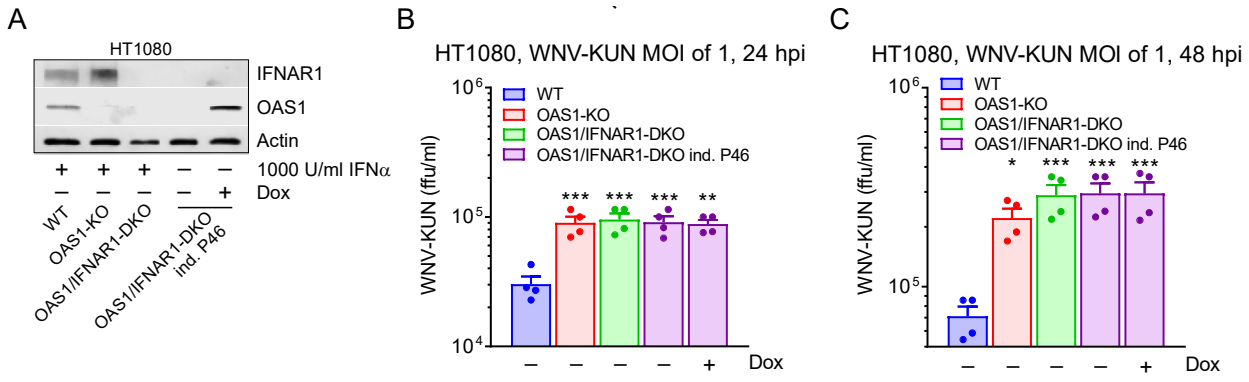

Figure 24. OAS1 antiviral activity requires cGAS mediated IFN signaling
Expression of OAS1 and IFNAR1 was validated by treating HT1080 WT, OAS1-KO and OAS1/IFNAR1-DKO with 1000 U/ml of IFNα overnight. Inducible expression of OAS1 was validated by treating OAS1/IFNAR1-DKO inducible OAS1 P46 cells with 2µg/ml Dox for 24 h. Cell lysates were analyzed by immunoblot with IFNAR1, OAS1 and Actin antibody (A). HT1080 WT, OAS1-KO, OAS1/IFNAR1-DKO and OAS1/IFNAR1-DKO inducible OAS1 P46 (pre-treated with 2µg/ml Dox for 24 h) were infected with WNV-KUN at a MOI of 1. Culture supernatants were collected 24 and 48 h post infection and infectious particles were quantified by FFU assay on Vero cells (B-C). Mean and SEM values were plotted as described before. Statistical significance of KO cells compared to WT cells was assessed using a one-way ANOVA with Dunnett's multiple comparison test.

Having established that OAS1 antiviral activity against WNV is mediated through cGAS and IFN signaling, we proceeded to characterize murine Oas1 proteins in order to identify the functional equivalent to human OAS1. There are 8 *Oas1* genes (Fig. 5) of which only *Oas1a* and *Oas1g* exhibit NTase activity. *Oas1b* is the only variant linked to restricting WNV lacking NTase activity and this protection has been shown to be independent of RNase L activation (228, 253, 384). In order to determine the antiviral activity of several enzymatically active ($NTase^{+}$) and

inactive (NTase$^-$) *Oas1* genes, we used our human HT1080 OAS1/RNase L-DKO cell system and tested WNV growth in these cells. As expected, expression of *Oas1b* (NTase$^-$) robustly inhibited viral replication, as compared to *Oas1g* (NTase$^+$), which inhibited virus to a small degree, and *Oas1a* (NTase$^+$), which had no effect on viral growth (Fig. 25. A-B). Poor expression of *Oas1h* (NTase$^-$) cDNA precluded us from determining the effects of *Oas1h* on viral growth (Fig. 25 A). This data validates that *Oas1b* WNV antiviral activity is NTase and RNase L independent.

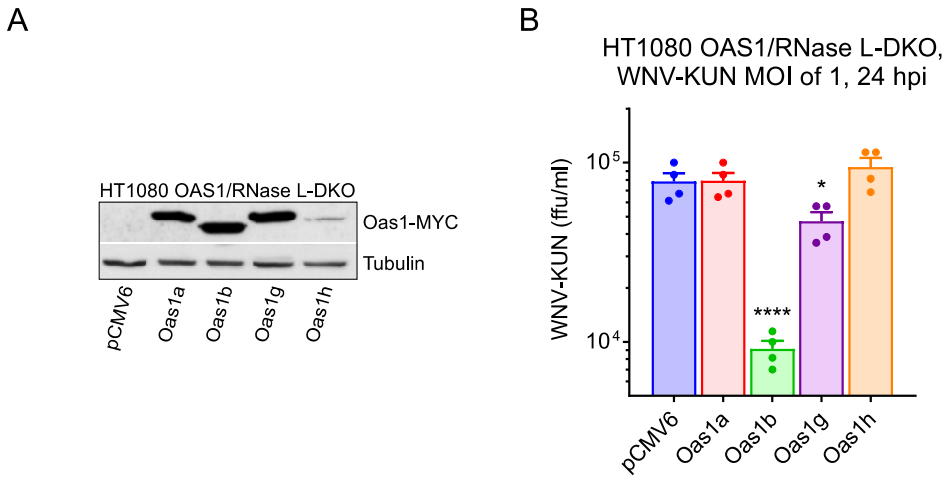

Figure 25. Mouse Oas1b restricts WNV replication in-vitro
HT1080 OAS1/RNaseL-DKO cells were transfected with pCMV6-Oas1-Flag-MYC constructs carrying various Oas1 isoforms (Oas1a, Oas1b, Oas1g, Oas1h) overnight, followed by infection with WNV-KUN at a MOI of 1. Cell lysates were prepared from transfected samples and analyzed by immunoblotting with MYC and Tubulin antibody (A). Supernatants from transfected cells were collected 24 h post infection and infectious particles were quantified by FFU assay on Vero cells (B). Vero cells were infected in duplicate and mean FFU and SEM was calculated from two dilutions corresponding to each replicate. Statistical significance of Oas1b transfected cells compared to pCMV6 transfected cells was assessed using a one-way ANOVA with Dunnett's multiple comparison test.

To determine if the antiviral activity of Oas1b protein is related to cGAS signaling, we inducibly expressed Oas1b in WT and cGAS-KO BJ-Tert cells (Fig. 26 A) and infected these cells with WNV-KUN. As seen with human OAS1, inducible expression of Oas1b was incapable of restricting virus in the absence of cGAS protein (Fig. 26 B), indicating that Oas1b mediated antiviral activity requires cGAS and IFN signaling to confer protection. These results suggest that

murine Oas1b is functionally equivalent to human OAS1 and clarify the mechanism of Oas1b WNV antiviral reported in previous studies.

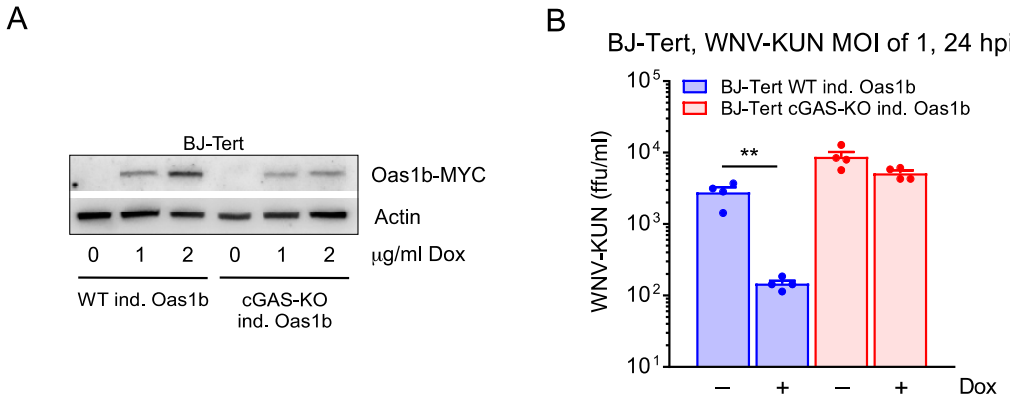

Figure 26. Murine cGAS is required for Oas1b mediated WNV antiviral activity
BJ-Tert WT and cGAS-KO cells with inducible Oas1b expression were treated with 0, 1 and 2 µg/ml Dox for 24 h followed by immunoblotting with MYC and Actin antibody (A). Similarly treated cells with 1µg/ml Dox for 24 h were infected with WNV-KUN as indicated followed by FFU assay on Vero cells (B). Mean and SEM were calculated as before. Statistical significance of Dox treated cells compared to untreated cells was assessed using an Unpaired t test.

To establish if cGAS mediated antiviral activity of Oas1b was mechanistically similar to human OAS1, we performed RIP analysis on OAS1-deficient HT1080 cells inducibly expressing Oas1b. Previous studies have identified several residues within the positively charged surface of OAS1 (Fig. 8) as essential for binding dsRNA and have been confirmed by mutagenesis (236, 385). We used cells expressing two Oas1b RNA binding mutants (K42E/K57E/K60E and K60E) (Fig. 27 A) in our RIP analysis in order to determine if mutations of these residues impaired mRNA association with Oas1b. We first established the specificity of Oas1b in our RIP experiments by inducibly expressing FLAG tagged Oas1b and showed that only Dox treated samples were enriched in cGAS mRNA after anti-FLAG IP compared to IgG control, whereas control GAPDH mRNA was not enriched (Fig. 27 B). We then proceeded to characterize our RNA binding mutants and showed that enrichment of cGAS mRNA observed in WT Oas1b was lost in both mutants

(Fig. 27 C). These results suggest that similar to human OAS1, Oas1b enhances protein synthesis of cGAS by directly binding its mRNA and the K60 residue is critical for this interaction. We validated these results in OAS1-deficient THP1 cells inducibly expressing WT Oas1b and Oas1b K60E (Fig. 27 D). We showed significant enrichment of cGAS and IRF1 mRNA, but not control GAPDH mRNA, confirming that Oas1b also targets IRF1 mRNA (Fig. 27 E). Similarly, enrichment of cGAS mRNA was lost in THP1 OAS1-KO cells inducibly expressing Oas1b K60E as compared to WT Oas1b (Fig. 27 F). Overall this data indicates that murine Oas1b, similar to human OAS1, associates to specific mRNAs, including IRF1 and cGAS, in order to enhance their translation. Together this data suggests that Oas1b is mechanistically similar to human OAS1 in terms of regulating protein synthesis and antiviral activity.

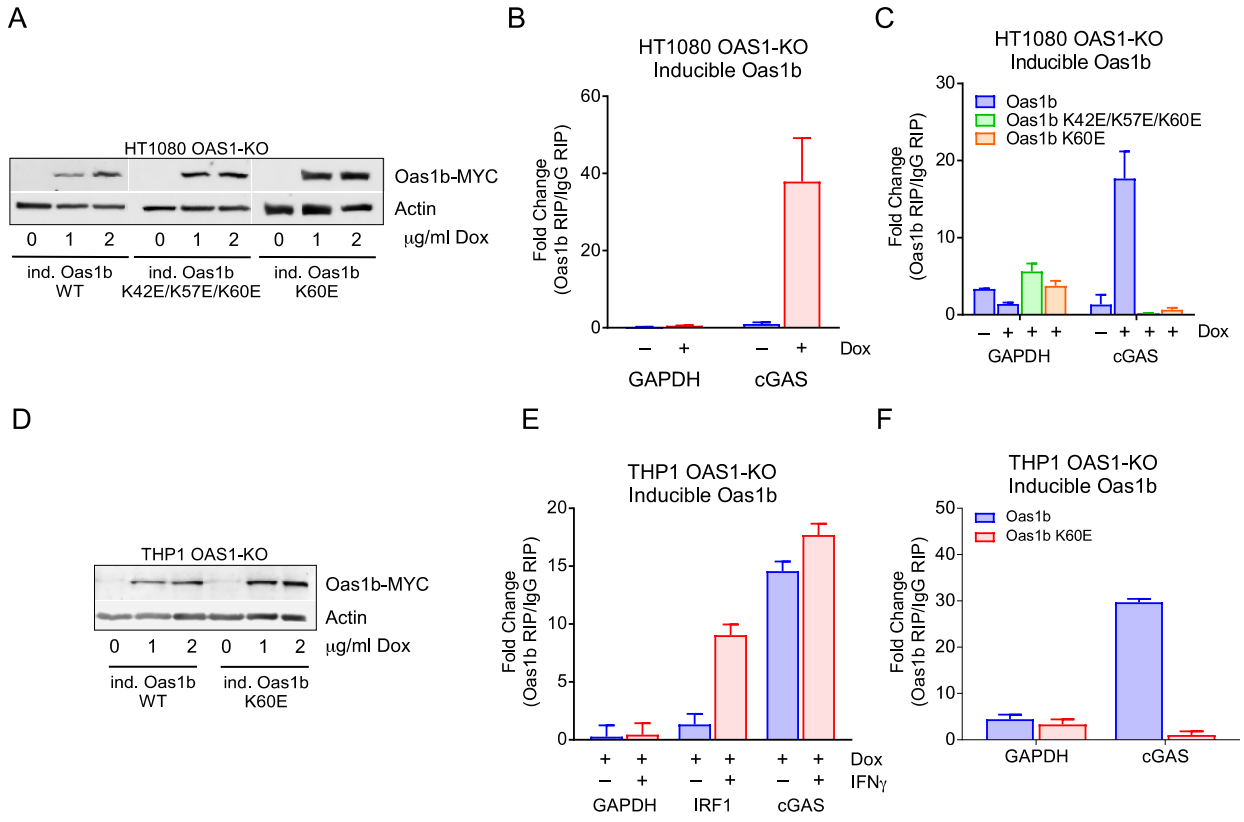

Figure 27. Murine Oas1b binds directly to target mRNA
HT1080 OAS1-KO inducible Oas1b, Oas1b K42E/K57E/K60E and Oas1b K60E cells were characterized by 0, 1 and 2 µg/ml Dox treatment for 48 h. THP1 OAS1-KO cells with inducible Oas1b and Oas1b K60E expression were treated with 0, 1 and 2 µg/ml Dox for 48 h. Cell lysates were prepared post treatment and analyzed by immunoblotting with OAS1 and Actin antibody (A, D). HT1080 OAS1-KO inducible Oas1b cells were treated with 1.5 µg/ml Dox for 48 h and cell lysates were subjected to RNA-immunoprecipitation with FLAG antibody and control IgG antibody, followed by quantitation of GAPDH and cGAS mRNA by RT-qPCR (B-C). THP1 OAS1-KO inducible Oas1b cells were treated with 1.5µg/ml Dox for 48 h followed by treatment with 500 U/ml IFNγ for 4 h. Formaldehyde crosslinked cell lysates were prepared followed by RNA-immunoprecipitation (RIP) with FLAG and control IgG antibody. GAPDH, IRF1 and cGAS mRNA was quantified in input and RIP samples by RT-qPCR (E-F) Percent enrichment of specific mRNA were calculated with respect to the input mRNA. Mean and SEM were calculated from three technical replicates (B-C, E-F).

We have shown that a specific residue in Oas1b (K60) is needed for binding to IRF1 and cGAS mRNA, to enhance protein synthesis and confer antiviral protection. To establish the necessity of K60 of OAS1/Oas1b for WNV antiviral activity, we ectopically expressed several Oas1b mutants targeting consensus RNA binding residues in HT1080 OAS1-KO cells followed by infections with WNV-KUN (Fig. 28 A). Analysis of viral titers revealed that the K60E mutant

abolished the antiviral activity of Oas1b (Fig. 28 B). Similarly, the same K60 mutation in human P46 resulted in a loss of antiviral activity against WNV (Fig. 28 C-F). This data indicates that K60 of both P46 and Oas1b is essential for regulating the translation of cGAS mRNA needed confer antiviral protection against WNV, establishing the functional equivalence between human and murine OAS1.

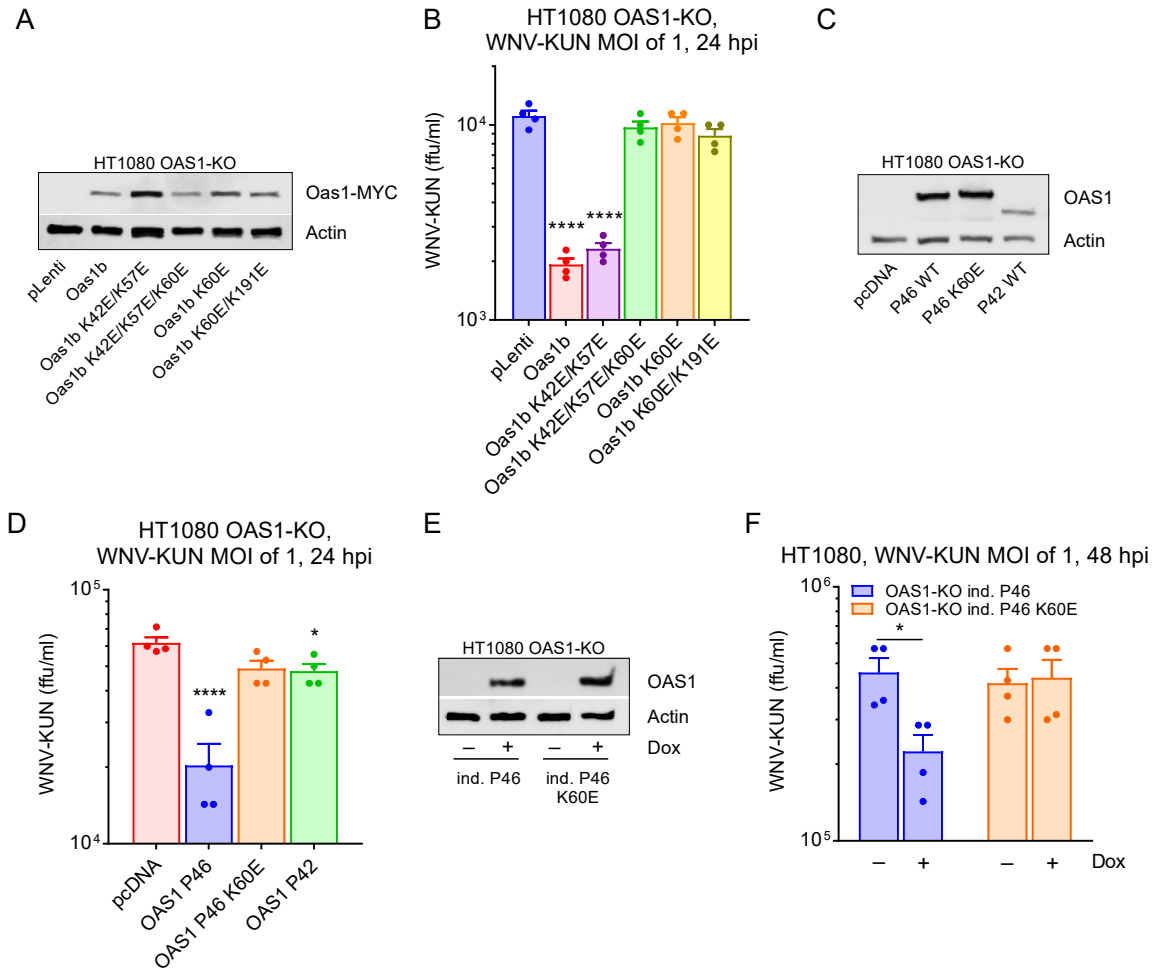

Figure 28. Oas1b and OAS1 K60 residue is essential for WNV antiviral activity
HT1080 OAS1-KO cells were transfected overnight with different pLenti-Oas1-Flag-MYC Oas1b WT and RNA binding mutants (Oas1b, Oas1b K42E, Oas1b K42E/K57E/K60E, Oas1b K60E, Oas1b K60E/K191E) or different pcDNA3-OAS1 isoforms (OAS1 P46, OAS1 P46 K60E, OAS1 P42)for 24 h, followed by WNV-KUN infection at 1 MOI. Cell lysates were prepared from transfected samples and analyzed by immunoblotting with MYC and Actin antibody (A) or OAS1 and Actin antibody (C). Cell supernatants were collected 24 h post infection and infectious particles were quantified by FFU assay on Vero cells (B, D). Mean and SEM were calculated from two dilutions of duplicate samples. Statistical significance of Oas1b transfected cells compared to pLenti transfected cells and OAS1 transfected cells compared to pcDNA transfected cells was assessed using a one-way ANOVA with Dunnett's multiple comparison test. HT1080 OAS1-KO inducible OAS1 P46 and OAS1 P46 K60E were pre-treated with 2 µg/ml Dox for 24 h and infected with WNV-KUN at a MOI of 1. Cell lysates were prepared 24 h post Dox treatment and analyzed by immunoblotting with OAS1 and Actin antibody (E). Supernatants were collected 24 h post infection and infectious particles were quantified by FFU assay on Vero cells (F). Mean and SEM were calculated as in panel B and D. Statistical significance of Dox treated cells compared to untreated cells was calculated using a two-way ANOVA with Sidak's multiple comparison test.

Although we have shown that OAS1 enhances the synthesis of several proteins by binding to their respective mRNA, the mechanism by which translation is enhanced by OAS1 remains unknown. It is known that translation of mRNA is compartmentalized between cytosolic and ER-bound ribosomes and previous ribosome profiling suggested that ER-associated ribosomes play an important role in global mRNA translation (386). The C-terminal domain of OAS1 P46, but not P42, harbors a conserved CAAX motif, important for prenylation and membrane association (387–389). Additionally, a transmembrane domain at the C terminus of Oas1b (a.a. 354-371) has been shown to anchor Oas1b to the ER and is important for WNV antiviral activity (384). Notably this transmembrane domain is missing in truncated Oas1b, found in laboratory strain mice (Fig.6), suggesting that the localization of Oas1b mediates its antiviral activity. To determine if OAS1 similar to Oas1b is localize to the ER, we used fluorescent confocal microscopy to determine the cellular localization of inducibly expressed OAS1 P42 and P46 in addition to ectopically expressed Oas1b and Oas1g. We first determined the specificity of our assay by immunofluorescent staining of IFNα treated HT1080 WT and OAS1-KO cells using OAS1 specific antibody followed by visualization using confocal microscopy. OAS1 signal was detected in WT cells but not in OAS1-KO cells and OAS1 seemed to localize around the nucleus (Fig. 29 A, left panel). In order to determine the isoform specific localization of human OAS1, we inducible expressed P46 and P42 in OAS1-deficient HT1080 cells and stained these cells with OAS1 and Calnexin (ER marker) antibodies. Additionally, we ectopically expressed FLAG-tagged Oas1b and Oas1g in HT1080 OAS1-KO cells and analyzed these cells with FLAG and Calnexin antibodies. We found that OAS1 P46 and Oas1b co-localize to the ER, P42 and Oas1g were diffused throughout the cells (Fig. 29), suggesting that like Oas1b, P46 localization to the ER is needed for antiviral activity. Our previous characterization of OAS1 post transcriptional regulation in combination with our

localization results, suggests that OAS1 and Oas1b localization might be important for enhancing protein synthesis and restricting virus. We hypothesize that OAS1 binds to and directs mRNA to the ER for association with polyribosomes and effective translation, although we have yet to define how the localization of OAS1 impacts mRNA translation. This hypothesis will be explored in future studies.

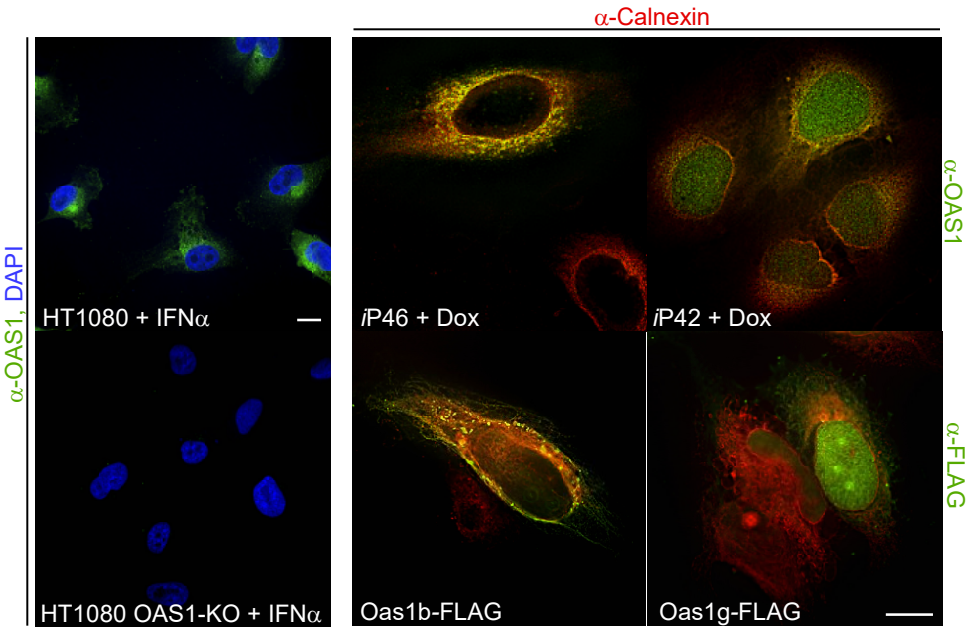

Figure 29. Subcellular localization of human and mouse OAS1
Validation of α-OAS1 antibody staining of endogenous OAS1 in IFNα treated HT1080 cells. WT and OAS1-KO HT1080 cells were treated with IFNα followed by immunofluorescence (IF) staining with anti-OAS1 antibody (left column). HT1080 OAS1-KO P46 and P42 cells were inducibly expressed with Dox followed by anti-OAS1 (green) and anti-Calnexin (ER, red) staining (Top). HT1080 OAS1-KO cells were transfected with FLAG-tagged Oas1b and Oas1g followed by anti-FLAG (green) and anti-Calnexin (ER, red) staining. Imaging was done using an Olympus confocal microscope. Scale bars = 10 μm.

Lastly, to define the *in-vivo* role of Oas1b to WNV, we generated mice expressing full length Oas1b. Several strains of laboratory mice, including C57BL/6 and BALB/c mice, carry a premature stop codon at the C-terminal *Oas1b* coding region resulting in truncation of Oas1b protein and WNV sensitivity (228, 251). Using CRISPR/Cas9-based gene editing, we created an Oas1b-knockin (Oas1b-KI) mouse restoring the full-length *Oas1b* expression in C57BL/6J

background (Fig. 30. A-C). The premature stop codon was replaced with Arg, which allowed full length expression of Oas1b (Fig. 30 A, highlighted in red), in addition to several nucleotide substitutions giving rise to a BspE I restriction site, which facilitated genotyping of mice (Fig. 30 C).

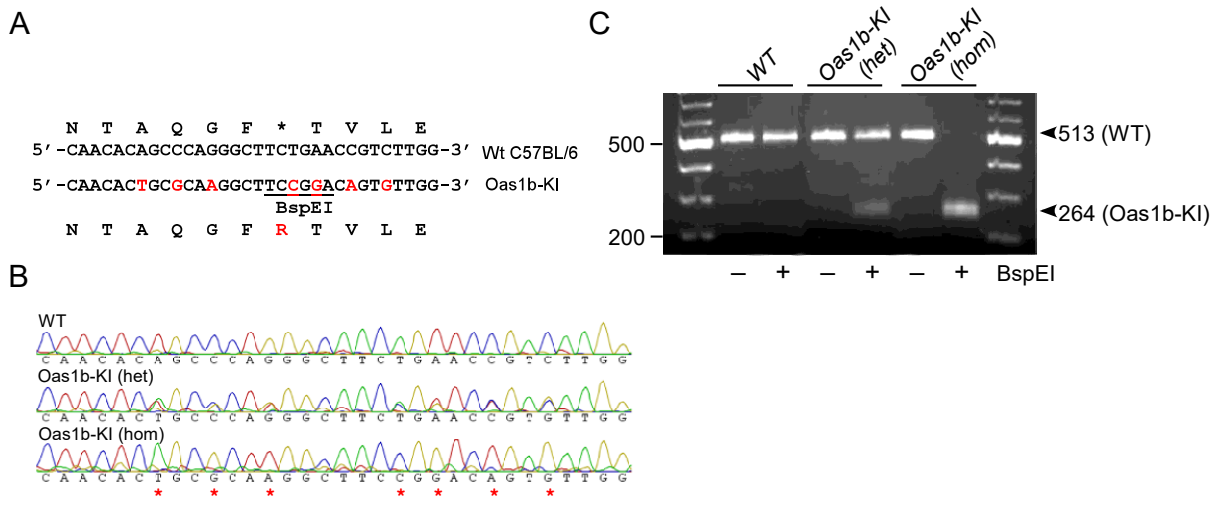

Figure 30. Oas1b-KI Mouse Model
Oas1b-KI mouse model generated by CRISPR/Cas9 homology directed repair. Sequence of the WT C56BL/6J mice and Oas1b-KI mice showing the targeted nucleotides (highlighted in red) in the Oas1b locus (A). Representative sanger sequencing traces (B) and sample genotyping (C) with BspEI from WT, Oas1b-KI heterozygous and homozygous mice.

Primary fibroblasts were obtained from WT and Oas1b-KI mice and infected with WNV-KUN. Fibroblasts from Oas1b-KI mice showed resistance to WNV growth as compared to cells from WT mice (Fig. 31 A). Previously we showed that inducible expression of Oas1b in BJ-Tert OAS1-KO cells conferred cGAS mediated antiviral activity to WNV (Fig. 26 B). Therefore, to confirm the effect of Oas1b on cGAS function, we examined primary BMDMs derived from WT and Oas1b-KI mice. Basal expression levels of cGAS were higher in BMDMs derived from Oas1b-KI mice as compared to WT BMDMs (Fig. 31 B, inset). Additionally, treatment of the BMDMs with DNA (poly(dA:dT)) or DNA virus (Herpes simplex virus, HSV) but not RNA (poly(I:C)) or RNA virus (Sendai virus, SeV) resulted in increased IFNβ induction (Fig. 31 B). These results

demonstrate that like human OAS1, Oas1b enhances synthesis of cGAS protein, which restricts WNV replication in a type I IFN dependent manner.

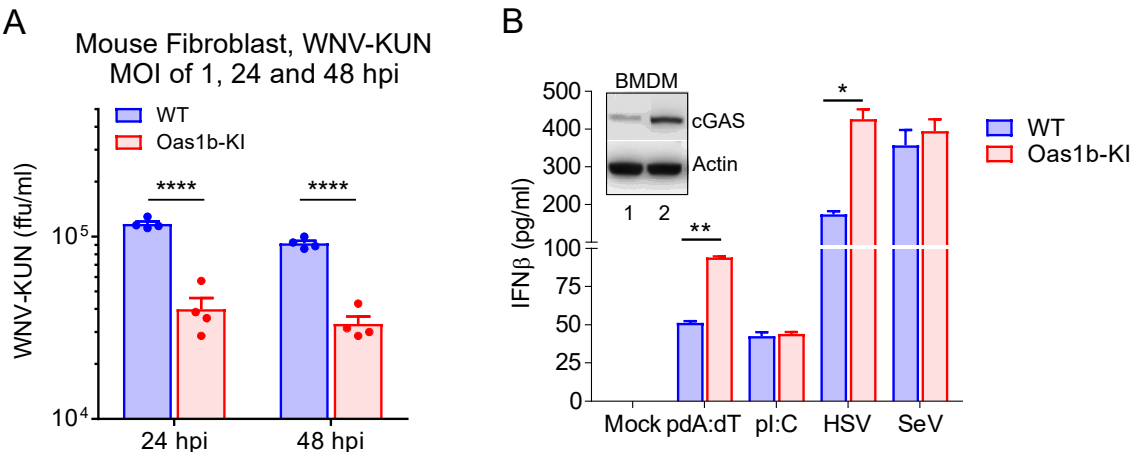

Figure 31. Oas1b Primary Fibroblasts and BMDMs confer protection to WNV
Primary fibroblasts from WT and Oas1b-KI mice were infected with WNV-KUN at a MOI of 1. 24 h post infection virus particles were quantified by FFU assay on Vero cells. Mean and SEM were calculated from two dilutions of duplicate infections on Vero cells. Statistical significance of Oas1b-KI cells compared to WT cells was assessed using a two-way ANOVA with Sidak's multiple comparison test (A). Bone Marrow Derived Macrophages (BMDMs) from WT and Oas1b-KI mice were transfected with poly dA:dT or p(I):p(C) (pI:C)(0.5 µg/ml for both) or infected with Herpes Simplex Virus (10 MOI) or Sendai Virus (80HAU/ml). Culture supernatants were analyzed for IFNβ production by ELISA (B). Statistical significance of Oas1b-KI cells compared to WT cells was assessed using multiple unpaired t test per condition. Inset: Cell lysates from WT (1) and Oas1b-KI (2) were collected and analyzed by immunoblotting with cGAS and Actin antibody.

Using a subcutaneous infection model with WNV (New York 1999 strain, WNV-NY) and Powassan virus (POWV), another neurotropic tick-transmitted flavivirus, we assessed the *in-vivo* role of Oas1b. Oas1b-KI mice infected with WNV-NY, were completely protected from lethality (Fig. 32 A) and analysis of viral burden in different organs of these mice revealed markedly reduced virus infection in the Oas1b-KI mice compared to WT mice (Fig. 32 B). Similarly, Oas1b-KI mice were completely resistant to lethal infection with POWV as compared to WT mice (Fig. 32 C). Taken together, these results confirm that mouse Oas1b confers resistance to flavivirus infection *in-vitro* and *in-vivo* in a RNase L independent manner.

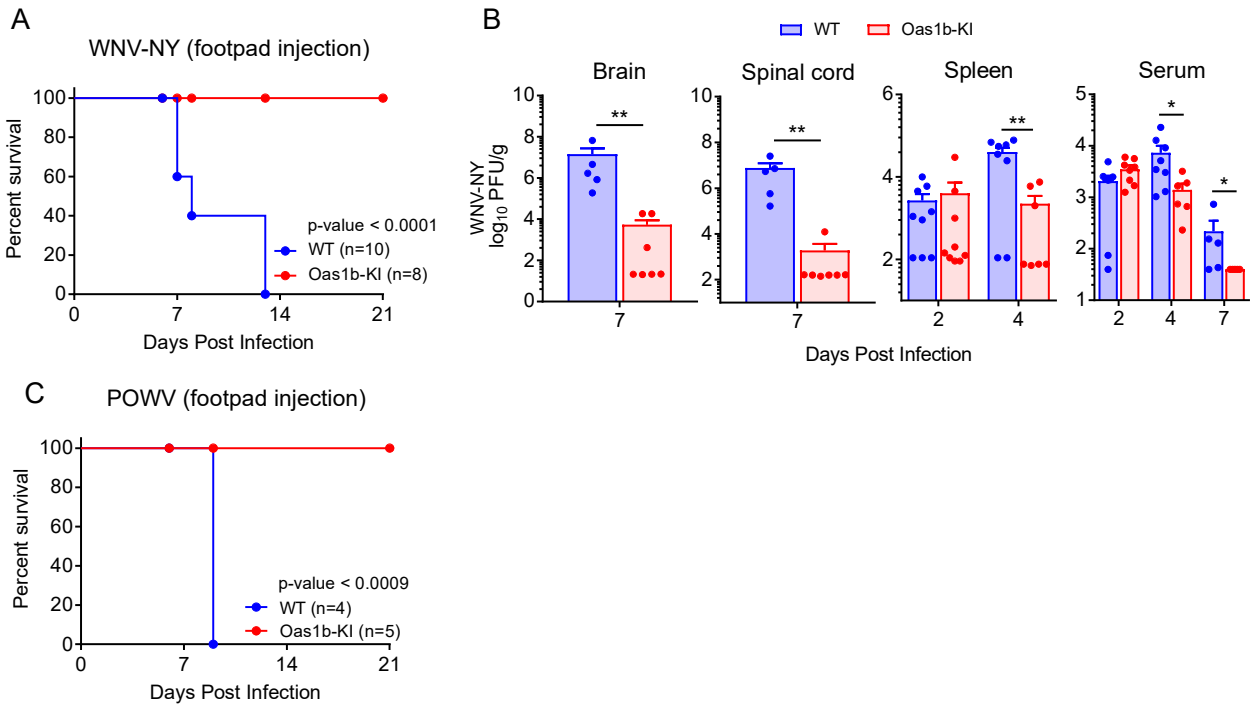

Figure 32. Oas1b confers protection to WNV and Powassan virus in-vivo
Survival and virus burden in tissue of WT and Oas1b-KI mice infected with WNV-NY (100 PFU/ml) by footpad infection. Mouse survival was measured for 21 days (A). Statistical significance of Oas1b-KI survival compared to WT mice was assessed using a Mantel-Cox test. WNV-NY virus burden in the brains, spinal cords, spleens and serum of WT and Oas1b-KI mice was determined by plaque assay of samples from mice at days 2, 4 and 7 post infection (B). Mean and SEM of viral loads from tissue were plotted and statistical significance of Oas1b-KI compared to WT mouse tissue titers was assessed using a Mann-Whitney test. Survival of WT and Oas1b-KI C57BL/6 mice infected with POWV (100 FFU) by footpad injection. Mouse survival was measured for 21 days. Statistical significance of Oas1b-KI survival compared to WT mice was assed using a Mantel-Cox test (C).

3.3 Discussion

WNV remains endemic around the world and is the leading cause of mosquito-borne disease in the USA. Although infection with WNV may not present serious disease progression in healthy individuals, it can cause neuroinvasive disease in the elderly and immunocompromised. Among the flavivirus family, several have been associated with severe disease progression, for example hemorrhagic dengue fever and congenital birth defects by ZIKV infection (390, 391). Structural and non-structural proteins are conserved among flavivirus, therefore understanding the host immune response against these viruses is crucial for the development of therapies and vaccines. Flavivirus RNA is detected by cytosolic sensors, leading to the induction of IFN and ISGs. However, flavivirus have developed several mechanisms of antagonizing IFN induction and signaling in order to efficiently replicate in host cells (284, 284, 287, 291–293, 392–394). Among these mechanisms of IFN antagonism, reports of degradation of cGAS by DENV NS2B, suggests that cGAS may play a role during flaviviral infection (306). Although flavivirus are RNA virus, it has been shown that virus infection can lead to cellular stress and mitochondrial damage allowing leakage of mitochondrial into the DNA and activation of cGAS-STING pathways (298, 304–306, 308). These studies suggest that cGAS plays an important role during flaviviral infection and in this chapter, we confirmed that the WNV antiviral activity of OAS1 is mediated through cGAS protein.

A SNP in human OAS1 has been shown to influence isoform expression and confer protection against WNV (243), which lead us to investigate the isoform specific function of OAS1 to WNV. We showed that cells carrying the G haplotype, responsible for expression of OAS1 P46, conferred protection against WNV. Inducible expression of OAS1 P46, but not P42, restricted WNV replication confirming that the G haplotype and P46 is protective to WNV. Given that the

antiviral activity of enzymatically inactive Oas1b is independent of RNase L and other studies have shown that OAS3 is required and sufficient for RNase L activation (17, 253), we investigated if the catalytic activity of OAS1 was necessary for inhibiting WNV. Using a catalytically inactive mutant of P46, we demonstrated that the enzyme activity of OAS1 was not necessary for restricting WNV. Similarly, using viral growth assays in RNAse L-deficient cells we confirmed that RNAse L is not required for OAS1 antiviral activity against WNV. In order to determine the mechanism by which OAS1 restricts WNV, we performed proteomic and transcriptome analysis on OAS1-deficient cells. These analyses revealed that OAS1 post transcriptionally regulated basal expression and IFNγ mediated induction of several antiviral genes. Using polysome profiling, we determined that OAS1 shifted target mRNAs towards polysome fractions and analysis of nascent protein synthesis by radiolabeling revealed enhanced synthesis of cGAS and IRF1 protein. RIP analysis revealed that OAS1 P46 associated with mRNA suggesting that this association of P46 isoform with target mRNA is needed for enhancing the translation of these mRNAs. Taken together these results suggest that P46 regulates the translation of several proteins that may be needed for antiviral defense against WNV. Through inducible expression of OAS1 in cells deficient in several antiviral genes, we showed that cGAS and downstream IFN signaling was primarily responsible for the antiviral activity of OAS1. Similarly, Oas1b antiviral activity was shown to require cGAS expression.

Several studies have described critical residues in the positively charged region of OAS1 needed for RNA binding, however these were done in the context of dsRNA binding required to trigger OAS1 2'-5' enzymatic activity and RNase L activation (236, 237, 385). In this study we show that K60 residue, conserved in mouse and human (Appendix A, Fig. 43), is essential for binding target mRNA in order enhance protein synthesis and confer antiviral protection. Although

we have established that OAS1 associates with mRNA and enhances their translation, the mechanism by which this occurs is not completely understood. Subcellular localization of human and mouse OAS1 revealed that these proteins localize in the ER and it is possible that OAS1 binds to and directs mRNA to ER-associated polyribosomes in order to mediate their translation (386, 395). However, this hypothesis is yet to be tested and will be addressed in the future. In our final experiments, we show that full length Oas1b restored protection against WNV, as described before (251) and BMDMs derived from Oas1b-KI mice revealed that cGAS protein levels and IFN signaling were enhanced as compared to WT mice. Together these results indicate that Oas1b is functionally equivalent to human OAS1 and enhances cGAS synthesis to confer antiviral protection through IFN signaling. This study provides a non-canonical mechanism of OAS1 antiviral activity and clarifies the mechanism by which Oas1b restricts WNV. Additional studies have shown that the G haplotype and expression of P46 is protective against HCV and DENV (229, 260), suggesting that OAS1 may provide protection to a broad range of viral pathogens through the translational regulation of host antiviral mRNAs.

4.0 OAS1 mediates intracellular bacterial infection

4.1 Introduction

Several bacterial ligands are recognized through TLRs and intracellular receptors that lead to IFN induction and activation of inflammatory pathways. However, the roles of IFNs during bacterial infections remains challenging to interpret. Type I IFN signaling may be beneficial or detrimental to the host, dependent on the bacterial species (7, 102). Type II IFN signaling is crucial for mediating immunity towards intracellular pathogens and deficiencies in IFNγ signaling leads to enhanced susceptibility to several bacteria, including mycobacteria and *L. monocytogenes* (341). IFNγ enhances MHC I and II processing, induces secretion of chemokines and other inflammatory molecules, promotes immune cell differentiation and enhances the antibacterial functions of several innate and adaptive immune cells, which altogether is required for bacterial clearance (103, 333, 396, 397). IFNs also regulate the expression of several ISGs, however their role in bacterial pathogenesis remains unclear. OAS family proteins are ISGs, first described to promote antiviral protection through activation of RNase L and suppression of translation. However, the characterization of OASL and Oas1b enzyme independent mechanisms of antiviral activity (238, 253), in addition to the results presented in this dissertation for human OAS1, reveal that non-canonical roles exist for OAS family members. In chapter 3 we showed that OAS1 enhanced protein synthesis of several basal and IFNγ inducible proteins. Among these proteins, cGAS was responsible for conferring antiviral protection to WNV independent of RNase L activation. Additionally, the levels of several antimicrobial related proteins were elevated, including IRF1, suggesting potential antibacterial roles of OAS1. To my knowledge, mechanisms of antibacterial

activity for OAS proteins have not been described, however the same SNP in OAS1 that confers resistance to WNV has been associated with protection against *M. tuberculosis* (246). We used *L. monocytogenes* and *F. novicida* (herein referred to as Lm and Fn respectively) to model intracellular infections both *in-vitro* and *in-vivo* as tools for studying host responses to bacterial infection (341, 345, 347, 351, 353, 398).

In this chapter, we explore the role of OAS1 during bacterial infections. Similar to the antiviral role of OAS1, protection against Lm and Fn is related to the expression of OAS1 isoform P46 and is independent of enzyme activity. OAS1 post transcriptionally regulates IRF1 and we show that P46 antibacterial activity is mediated through IRF1. Proteomic and transcriptome analysis revealed that the transcription of several IFNγ-regulated genes was down-regulated in OAS1-deficient cells. OAS1 enhances the synthesis of several proteins without directly altering mRNA levels. Therefore, it is likely that these OAS1 regulated transcripts are dependent on transcription factors post-transcriptionally regulated by OAS1. Among these transcription factors, IRF1 is known to regulate the expression of several IFNγ-inducible genes and it is likely that IRF1 regulated proteins contribute to bacterial defense. Lastly, we demonstrate that Oas1b can confer protection to Lm and Fn *in-vitro* and *in-vivo* establishing OAS1 as a critical component of host antibacterial activity to these pathogens.

4.2 Results

Previously I described a novel mechanism of OAS1 antiviral activity against WNV, which was dependent on the expression of P46 isoform. P46 was capable of binding target mRNAs and enhanced the synthesis of basal and IFNγ-inducible proteins. Given that the same SNP, which promotes P46 expression, also confers protection to *M. tuberculosis*, we hypothesized that OAS1 might contribute to antibacterial defense through the same translational mechanism described before. First, to determine the susceptibility of OAS1-deficient cells to intracellular bacterial infections, we used the gram-positive bacteria Lm as a model. We infected THP1 and BJ-Tert WT and OAS1-KO cells with Lm at different MOI and analyzed intracellular bacterial growth by Gentamicin protection assay (Fig. 33 A-D). At 8 h post infection, bacterial burden was significantly higher in both THP1 and BJ-Tert OAS1-deficient cells (Fig. 33 A-B and C-D respectively), suggesting that OAS1 is protective against *Listeria*.

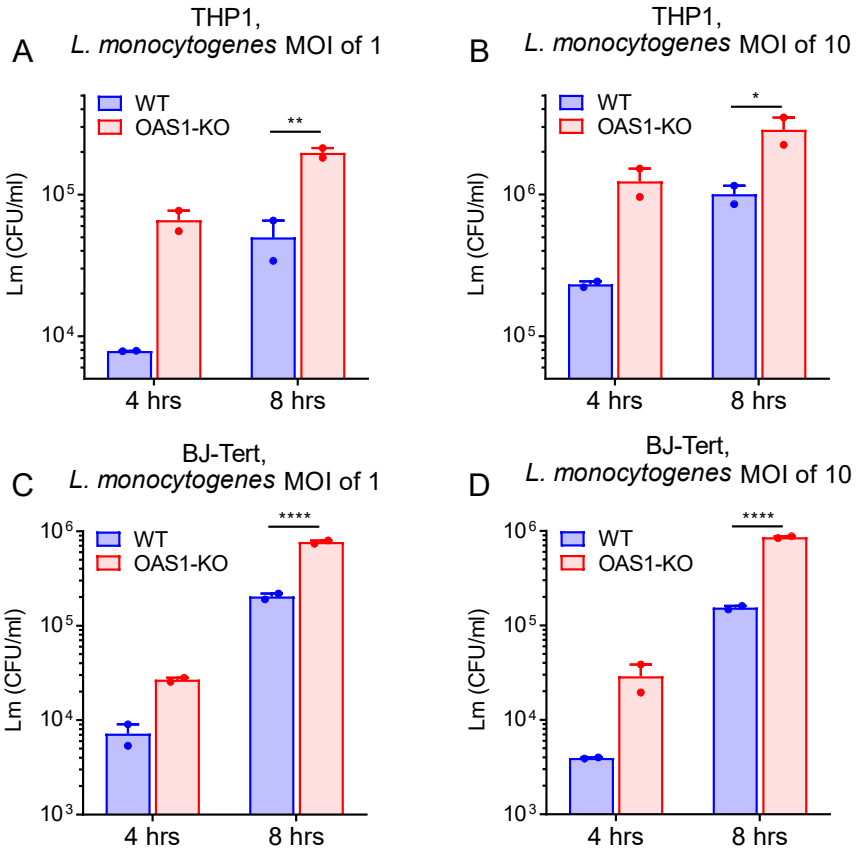

Figure 33. OAS1 confers protection against L. monocytogenes
WT and OAS1-deficient THP1 (A-B) and BJ-Tert (C-D) cells were infected with Lm at a MOI of 1 and 10. Following bacterial adsorption for 1 h, cells were incubated in medium containing 50 µg/ml Gentamycin for 4 or 8 h. Cells were collected, lysed and plated on BHI-agar plates. After 18-20 h, CFU/ml were determined. Data points represent duplicate averages taken from two biological replicates. Statistical significance of OAS1-KO cells to WT was determined with two-way ANOVA with Sidak's multiple comparison test.

To validate the antibacterial activity of OAS1, we inducibly expressed P42, P46 and P46 DADA in THP1 OAS1-KO cells, followed by infections with Lm. Dox inducible expression of OAS1 P46, but not P42, was capable of restricting intracellular bacterial growth (Fig. 34 A-B). Additionally, expression of the enzymatically inactive mutant P46 DADA was able to suppress bacterial growth similar to P46 (Fig. 34 A-B). Together these results indicate that P46, expressed through the rs10774671 G allele, provides protection against *Listeria,* which is independent on NTase activity.

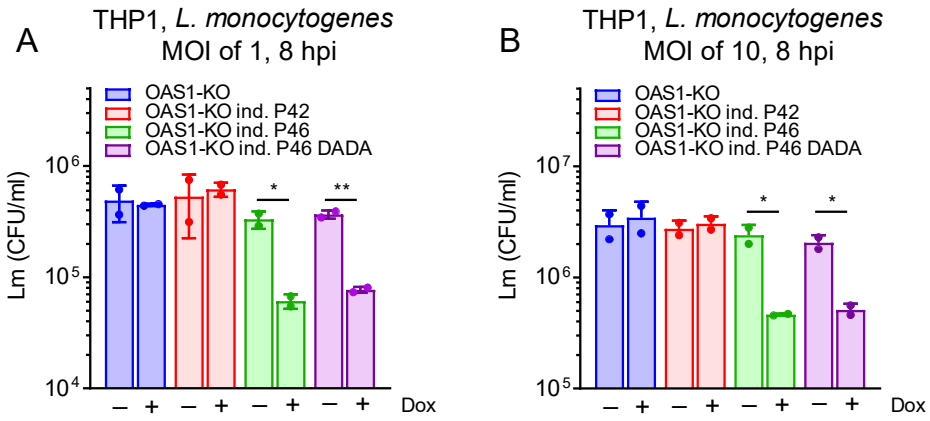

Figure 34. OAS1 P46 and P46 DADA inhibit L. monocytogenes growth
THP1 OAS1-KO, OAS1-KO inducible P42 and P46 were pre-treated with 2 µg/ml Dox for 48 h, followed by infection with Lm at a MOI of 1 and 10. After adsorption, cells were grown in 50 µg/ml Gentamycin containing media for 8 h. Cells were lysed and plated on BHI-agar plates. After 18-20 h, CFU/ml were determined. Duplicate averages taken from two biological replicates were plotted and statistical significance between Dox-treated and untreated cells was assessed using Multiple t tests (A-B).

To study the antibacterial role of OAS1 in another model organism, we infected THP1 and BJ-Tert OAS1-KO cells with the gram-negative bacterium Fn. Similar to infection with listeria, bacterial load was higher in OAS1-KO cells at 8 h post infection (Fig. 35 A-D). These findings confirm that OAS1 confers protection against several intracellular pathogens through expression of OAS1 P46. This suggests that protection against *M. tuberculosis* through the G genotype is most likely mediated through P46 as well.

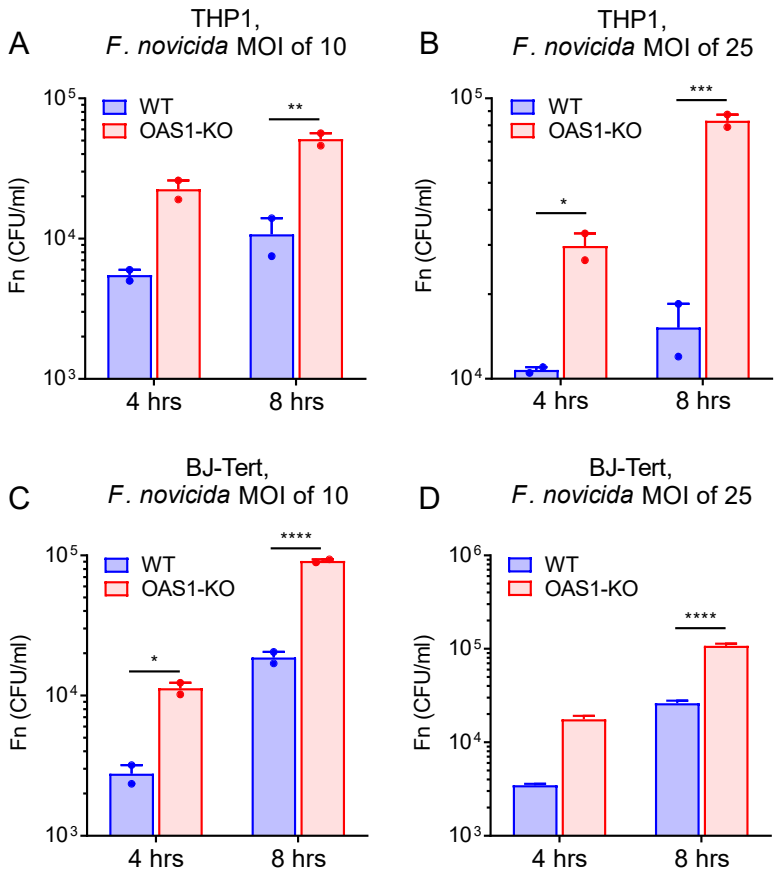

Figure 35. OAS1 confers protection against F. novicida
WT and OAS1-KO THP1 (A-B) and BJ-Tert (C-D) cells were infected with Fn at a MOI of 10 and 25. After adsorption, cells were incubated in medium containing 50 µg/ml Gentamycin for 4 or 8 h. Cells were collected, lysed and plated on MH-agar plates. After 18-20 h, CFU/ml were determined, and statistical significance was assessed as in Fig. 32.

Previously we have shown Type I IFN signaling was not affected in OAS1-deficient cells, however Type II IFN signaling and expression of IRF1 was impaired in OAS1-KO cells (Fig. 16). IFNγ induction is critical for restricting the replication of several intracellular pathogens and deficiencies in IFNγ signaling lead to increased susceptibility to bacterial infections (333, 399). Therefore, to characterize the mechanism by which OAS1 inhibits bacterial growth, we filtered our proteomic and transcriptomic data (described in Chapter 3 and Appendix B) to include IFNγ-regulated proteins that were post transcriptionally regulated by OAS1. This analysis revealed a few IFNγ inducible proteins down-regulated in OAS1-KO cells with potential antibacterial

properties, including IRF1 (124, 400), ankyrin repeat domain 17 (ANKRD17) (401) (Fig. 36 A), gamma-interferon-inducible lysosome thiol reductase (IFI30) (402) and tryptophanyl-tRNA synthetase (WARS) (403). The expression of IRF1 was validated in both BJ-Tert and WT cells after IFNγ treatment. Similar to our proteomic data, IRF1 was down regulated in cells deficient in OAS1 (Fig. 36 B). Additionally, infection with Lm induced a dose dependent increase in IRF1 protein levels (Fig. 36 C). This suggests that in response to bacterial infection, OAS1 enhances the synthesis of IRF1 protein required for controlling bacterial growth.

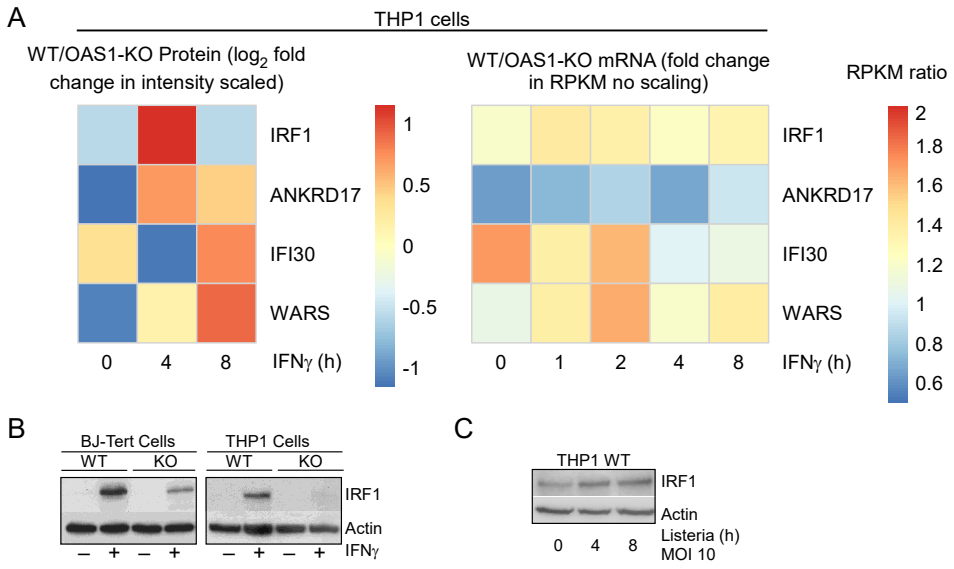

Figure 36. OAS1 regulates levels of several antibacterial proteins

THP1 WT and OAS1 KO cells were cultured for 8 generations in media containing heavy isotope amino acids (^{13}C-6 ^{15}N-2 L-Lysine, and ^{13}C-6 ^{15}N-4 L-Arginine) and light isotope amino acids (L-Lysine and L-Arginine) respectively. Cells were then treated with 500 U/ml IFNγ for 0, 4 and 8 h for SILAC analysis. In parallel, cells grown in regular media were treated with 500 U/ml IFNγ for 0, 1, 2, 4 and 8 h and analyzed by RNAseq analysis. Following filtering of the SILAC data (Section 2.2.21), peptide ratios were scaled for each protein and represented by heatmap. Corresponding mRNA RPKM values were plotted in the heatmap as fold change without scaling (A). WT and OAS1-KO BJ-Tert and THP1 cells were treated with 500 U/ml IFNγ 4 h and cell lysates were analyzed by immunoblotting with IRF1 and Actin antibody (B). WT THP1 cells were infected with Lm at a MOI of 10 for 0, 4 and 8 h followed by immunoblotting with IRF1 and Actin antibody.

To test the hypothesis that OAS1 antibacterial activity is mediated through IRF1 protein, we first confirmed the requirement of IRF1 in regulating bacterial infection. We infected BJ-Tert WT, OAS1-KO and IRF1-KO cells with Lm and determined the bacterial burden in these cells. As seen before, OAS1-KO cells were more susceptible to infection and IRF1-KO cells showed a significantly higher bacterial load as compared to WT cells (Fig. 37 A). Next, we assessed whether IRF1 was essential for OAS1 mediated antibacterial protection by inducibly expressing OAS1 P46 in WT and IRF1-deficient cells, followed by infection with Lm and Fn. Inducible expression of P46 was capable of restricting bacterial growth in WT cells, but not in the absence of IRF1 (Fig. 37 B-C). These results establish the requirement for IRF1 to mediate the downstream antibacterial effects of P46.

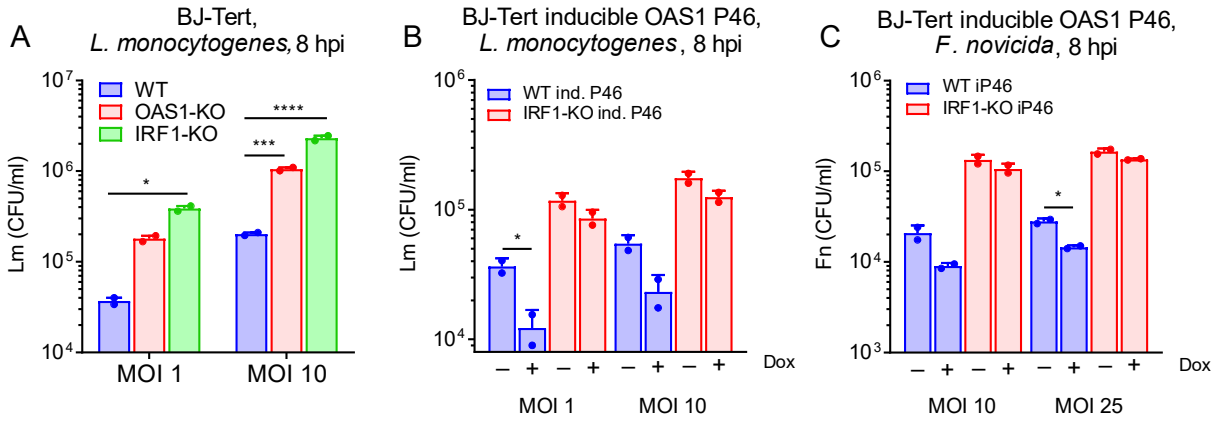

Figure 37. IRF1 is required for OAS1 mediated antibacterial activity
BJ-Tert WT, OAS1-KO and IRF1-KO cells were infected with Lm at a MOI of 1 and 10 (A). BJ-Tert OAS1-KO and IRF1-KO inducible P46 were pre-treated with 2 µg/ml Dox for 48 h, followed by infection with Lm at a MOI of 1 and 10 (B) or Fn at a MOI of 10 and 25 (C). Following bacterial adsorption, cells were incubated in 50 µg/ml Gentamycin containing media for 8 h. Cells infected with Lm were lysed and plated on BHI-agar plates for 18-20 h (B). Cells infected with Fn were lysed and plated on MH-agar plates for 48 h. CFU/ml were determined as described before and data points represent duplicate averages taken from two biological replicates. Statistical significance between WT, OAS1-KO and IRF1-KO cells was determined with two-way ANOVA with Sidak's multiple comparison test (A). Statistical significance between Dox-treated and untreated cells was assessed two-way ANOVA with Tukey's multiple comparison test (B-C).

IRF1 is a transcription factor known to regulate the expression of several genes following IFNγ treatment to inhibit infection through these ISGs. Additionally, IRF1 can enhance T cell differentiation needed to clear infection and IRF1-deficient mice show impaired Th1 responses to *Listeria* (404). During *Francisella* infection, IRF1 has been shown to promote the expression of GBPs needed for disrupting bacteria-containing vacuoles exposing bacterial DNA to AIM2 and promoting inflammasome activation (124, 363). These previous studies suggest a critical role of IRF1 in regulating intracellular bacterial infections through GBPs and inflammasome signaling. To establish if IRF1 regulated proteins were downregulated in OAS1-KO cells, we filtered our SILAC and RNAseq data sets to represent genes that were transcriptionally regulated after IFNγ treatment. The heatmaps in Fig. 38 represent genes in which mRNA was down-regulated in OAS1-KO cells as compared to WT, resulting in a decrease in protein expression. The RPKM and peptide intensity values of several genes known to enhance immunity were decreased in OAS1-deficient THP1 cells (Fig. 38). Several GBP proteins were shown to be enhanced by OAS, which is likely dependent on IRF1 signaling. Together these results suggest that OAS1 antibacterial activity is mediated through downstream signaling of IRF1.

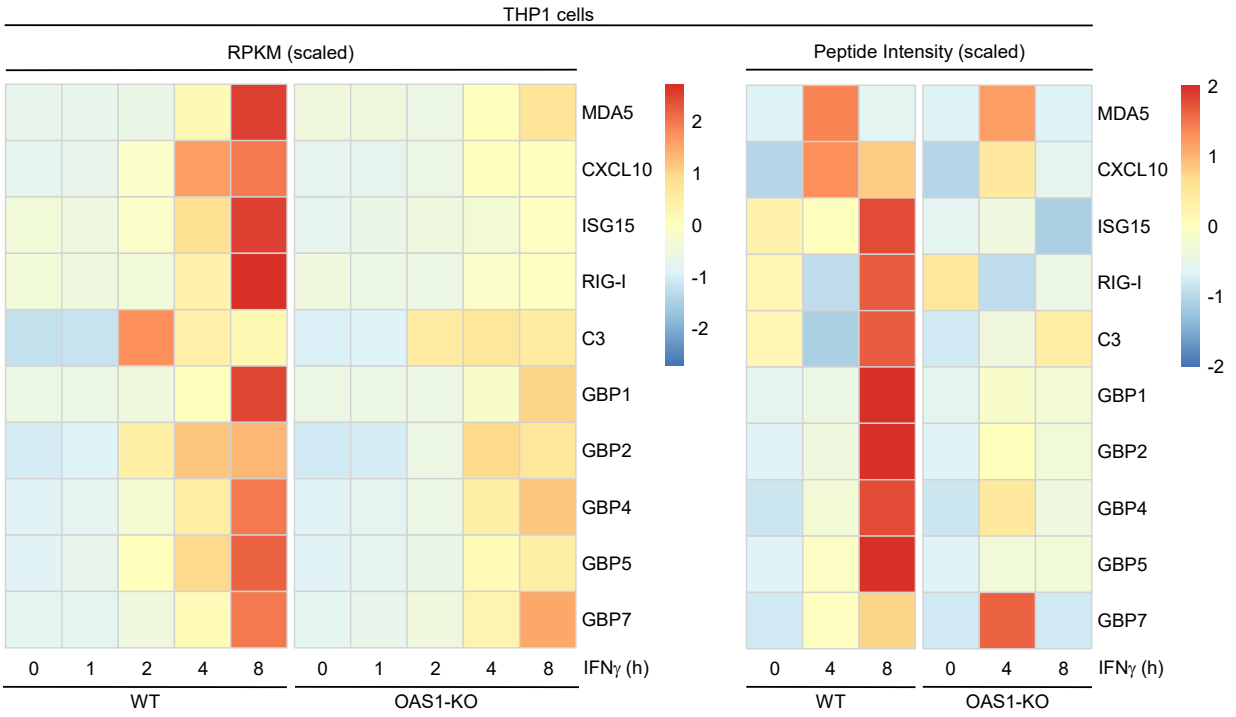

Figure 38. OAS1 upregulates transcription of several IFNγ-induced genes and protein levels
THP1 WT and OAS1-KO cells were analyzed by SILAC and RNAseq as described in Fig. 4. Following filtering of SILAC data for transcriptionally regulated genes (Section 2.2.21), RPKM and peptide intensity values were scaled and represented by heatmaps.

In Chapter 3 of this dissertation, we established murine Oas1b as the functional equivalent to human OAS1. Oas1b was capable of binding cGAS and IRF1 mRNA and conferred protection to WNV and POWV through cGAS induction of type I IFNs. To determine if mouse Oas1b plays a role during bacterial infections, we infected BMDMs collected from WT and Oas1b-KI mice with *Listeria*. BMDMs from Oas1b-KI mice showed a significant reduction in bacterial burden at both 4 and 8 h (Fig. 39 A-B), confirming that Oas1b is capable of restricting bacterial growth. These findings suggest that both human OAS1 and Oas1b have dual roles in restricting both virus and bacterial growth through a common mechanism dependent on enhancing the translation of several immune related proteins needed to clear infection.

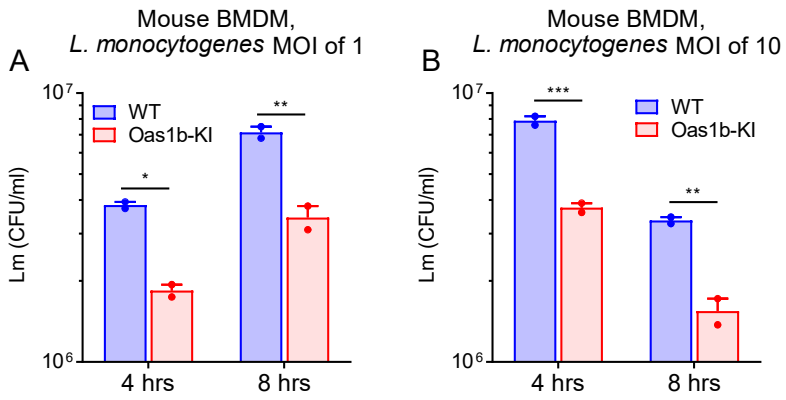

Figure 39. Oas1b confers antibacterial protection to L. monocytogenes
BMDMs from WT and Oas1b-KI mice were infected with Lm at a MOI of 1 and 10. Following adsorption, cells were incubated in media containing 50 µg/ml Gentamycin. After 4 and 8 h post infections cells were collected, lysed and plated on BHI-agar plates. CFU/ml were calculated 18-20 h after plating. Duplicate averages taken from two biological replicates were plotted. Statistical significance between WT and Oas1b-KI BMDMs was determined with two-way ANOVA with Sidak's multiple comparison test.

Finally, we assessed the *in-vivo* role of OAS1 by measuring the survival of WT and Oas1b-KI mice following infection with Lm or Fn. Mice were infected intraperitoneally with Lm or subcutaneously with Fn and survival was measured for 10 and 13 days respectively. All WT mice succumbed to infection with Lm, however most Oas1b-KI survived infection (Fig. 40 A). Similarly, WT mice presented a heavy loss of body weight after infection with Fn as compared to Oas1b-KI mice (Fig. 40 B). Consequently, all the WT mice died after infection, whereas 90% of Oas1b-KI mice survived. Our results confirm that Oas1b confers a protective phenotype to both *Listeria* and *Francisella*. Together the results presented in this chapter suggest that OAS1 and Oas1b, in addition to their antiviral role, are protective against intracellular bacteria.

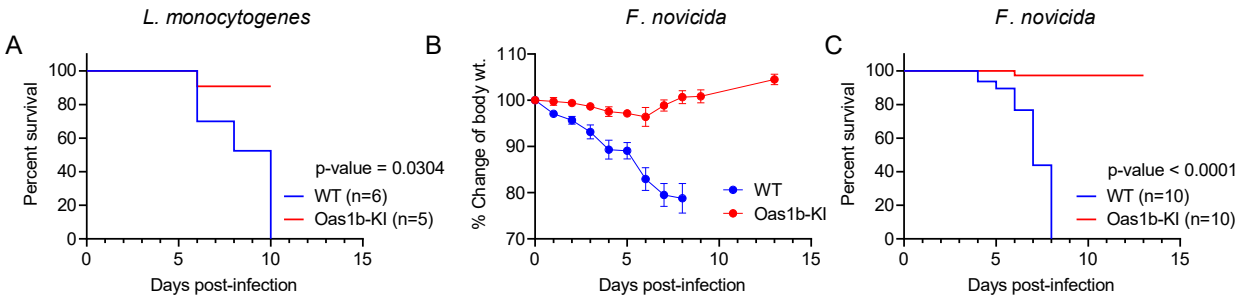

Figure 40. Oas1b confers protection to mice against *L. monocytogenes* and *F. novicida in-vivo*
Oas1b-KI and WT mice were infected with 1 x 10^5 CFU/ml *L. monocytogenes* intraperitoneally and survival was measured for 10 days (A). A separate group of mice was infected with 1 x 10^4 CFU/ml *F. novicida* subcutaneously and survival was measured for 13 days (B). Statistical significance of Oas1b-KI survival compared to WT mice was assessed using a Mantel-Cox test.

4.3 Discussion

OAS are family of ancient proteins first described to inhibit viral replication through the synthesis of 2'-5' oligoadenylates and activation of RNase L. These proteins have no known antibacterial functions, however some studies have associated OAS proteins with progression of *M. tuberculosis* (246, 261–263, 405). The G genotype of the SNP rs10774671 in OAS1 has been associated with resistance to *M. tuberculosis* (246). In this chapter, we explored the antibacterial role of OAS1 using Lm and Fn as models of intracellular bacterial infection. Several of these microorganisms have been associated with disease progression. *M. tuberculosis* in particular, remains the leading cause of death worldwide from a single infectious agent (406). *Listeria* is a foodborne pathogen and is one of the leading causes of hospitalization due to foodborne illness (345). Although listeriosis is rare, it can cause severe disease to developing fetus in pregnant women leading to miscarriage. It can also lead to sepsis or infection of the brain in older or immunocompromised individuals. *F. tularensis* can cause tularemia, a disease which ranges from mild to life-threatening, and needs to be handled under biosafety level 3 (BSL-3) conditions, making it a challenging pathogen to study. *F. novicida* U112 (Fn U112) is an attenuated strain of *Francisella* with a high genetic identity to *F. tularensis*. Additionally, Fn U112 is easily genetically manipulated, can infect macrophages *in-vitro* and mice infected with this strain exhibit illness, making it an excellent model to study the pathogenesis of *F. tularensis* (353, 407). The immune response to intracellular bacteria is quite complicated. IFNs have been shown to be both beneficial and detrimental during infection (7, 102, 324, 333). Therefore, understanding the mechanisms behind bacterial host-pathogen interactions is important in defining critical components of host immunity required for antibacterial defense.

Previously, we described how OAS1 confers antiviral protection through enhancing the protein synthesis of cGAS. In this chapter, we show that the antibacterial activity of OAS1 is mediated through another OAS1 regulated protein, IRF1. We first measured the bacterial burden in OAS1-deficient cells infected with Lm and Fn. We confirmed that in the absence of OAS1, bacterial growth was significantly increased, suggesting that OAS1 is protective during bacterial infection. Since the G allele of the SNP rs10774671 was related to susceptibility to *M. tuberculosis,* we believed that the antibacterial activity of OAS1 was mediated through P46 isoform. Inducible expression of P42 did not inhibit bacterial growth, however expression of P46 and NTase-deficient P46 DADA significantly reduced bacterial burden. This confirmed that the isoform-specific antibacterial activity of P46 was independent of catalytic activity and RNase L activation. To determine the specific proteins or pathways required for OAS1 mediated antibacterial protection we re-evaluated our proteomic and transcriptome data. Our data revealed that some antibacterial related proteins were post transcriptionally regulated by OAS1, in addition to IRF1. These proteins included ANKRD17, IFI30 and WARS. ANKRD17 functions as a binding partner of NLRs, required for pathogen sensing and induction of inflammatory pathways (408), and deficiency in ANKRD17 resulted in decreases cytokine secretion during *Shigella flexneri* infection (401). IFI30 is a thiol reductase expressed in the lysosomes of antigen-presenting cells and is crucial for MHC antigen processing and presentation (402, 409). WARS (or WRS) is secreted rapidly during infection and primes innate immune responses by binding myeloid differentiation factor 2 (MD2) on macrophages inducing phagocytosis and chemokine production (403, 410). The antibacterial role of IRF1 has been well established, promoting immune cell differentiation and activation of inflammasome pathways (121, 124, 404). This led us to investigate the role of IRF1 during *Listeria* and *Francisella* infection. As expected, IRF1-deficient cells were more susceptible to infection,

similar to OAS1-deficient cells. To determine if OAS1 antibacterial activity was mediated through IRF1, we inducibly expressed P46 in WT and IRF1-KO cells and found that the antibacterial activity of OAS1 was abolished in the absence of IRF1.

Since IRF1 is known to regulate the expression of a variety of IFNγ-inducible genes (125, 411), we filtered our SILAC and RNAseq data to represent the RPKM and peptide intensity of genes that were transcriptionally downregulated in the absence of OAS1. We found several IFNγ inducible genes, with known antibacterial functions, that were downregulated in OAS1-deficient cells resulting in a loss of protein. Among these, we found RIG-I and MDA5 transcription was elevated by OAS1, which are well established sensors of viral RNAs and have also been shown to elicit IFN signaling in response to bacterial ligands (412–416). ISG15 was up-regulated in WT cells, a well-established antiviral ISG that has also been shown to restrict *Listeria* and is associated with *M. tuberculosis* disease severity (175, 200, 417, 418). C3 complement protein was also up-regulated in our analysis, which is crucial for restricting several intracellular pathogens through activation of complement pathways, including *Listeria* and *M. tuberculosis* (419–422). Additionally, the pro-inflammatory chemokine CXCL10 was up-regulated in WT cells, which is known to promote chemotaxis, cell growth and apoptosis during infection (423). CXCL10 has been shown to restrict Lm growth and CXCL10 is highly induced during infection with *M. tuberculosis* and has been proposed as a biomarker of active tuberculosis (424–426). Lastly, the transcription of several GBPs was up-regulated in WT type cells compared to OAS1-KO cells. This family of GTPases is known to promote antimicrobial defense through disruption of pathogen containing vacuoles or direct disruption of bacterial membranes to release antigens into the cytosol and induce activation of inflammasome pathways (104, 205, 207, 427). Inflammasome signaling leads to the processing of pro-inflammatory cytokines such as IL-1β and IL-18 crucial for clearing

bacteria (334, 359, 428). Altogether, our proteomic and RNAseq analysis revealed that several antibacterial genes are transcriptionally enhanced in the presence of OAS1. OAS1 has not been described to bind DNA, suggesting that the transcriptional regulation of these genes is mediated by transcription factors regulated by OAS1. IRF1 is known to drive the expression of GBPs and promotes inflammation activation, suggesting that the antibacterial activity of OAS1 could be mediated downstream of the IRF1 signaling pathway (124, 363, 427).

Finally, we explored the *in-vitro* and *in-vivo* role of Oas1b during bacterial infections. BMDMs collected from Oas1b-KI infected with Lm showed a decreased bacterial burden as compared to WT cells. Additionally, Oas1b-KI mice infected with Lm and Fn exhibited increased survival as opposed to WT mice, establishing that murine Oas1b confers the same antibacterial activity as human OAS1. The results presented in this chapter establish that OAS1 and Oas1b are capable of restricting intracellular bacterial growth. This inhibition of bacterial replication is most likely mediated through IRF1, which is post transcriptionally regulated by OAS1. Additionally, we hypothesize that downstream signaling of IRF1, leading to the transcription of ISG15, GBPs and other IFNγ-inducible proteins (429–431), is required for the antibacterial phenotype of OAS1. This hypothesis is yet to be confirmed. The role of OAS family proteins during bacterial infections is currently being investigated in our laboratory.

5.0 Conclusions and Future Perspectives

OAS family proteins were discovered over 40 years ago, and were first described to synthesize 2'-5' oligoadenylates required for RNAse L activation and suppression of virus replication (211, 213, 217). Several residues in the negatively charged active site of OAS were shown to be crucial for NTase activity, required for OAS antiviral activity (235, 236). However, the discovery of enzyme independent mechanisms of antiviral activity in Oas1b and OASL have made it clear that there are alternative mechanisms of OAS mediated antiviral immunity (13, 228, 230, 237, 253). Furthermore, among human NTase^{+} OAS proteins, OAS3 was sufficient and necessary for the activation of RNase L with no contribution from OAS1 and OAS2 (17). Additional studies have shown that OAS3 engages longer dsRNA, requires lower concentrations of RNA to become active as compared to OAS1, and synthesizes longer 2'-5' oligoadenylates, which may be required for efficient activation of RNase L (432, 433). Overexpression of OAS1 and OAS2 have been associated with lower viral titers of several flavivirus (229, 434, 435), suggesting potential RNase L independent roles of enzymatically active OAS proteins. In this study, we investigate NTase independent antiviral and antibacterial roles of OAS1.

An SNP (rs10774671) located at the C-terminal domain of OAS1, has been shown to influence isoform expression and susceptibility to WNV (243, 389). We confirmed that cells containing the G haplotype of the rs10774671 SNP, were resistant to WNV replication. Inducible expression of OAS1 isoform P46, but not P42, was necessary for restricting viral replication. Furthermore, inducible expression of the NTase-deficient mutant D75A/D77A (DADA) was also capable of restricting WNV to the same extent as P46, suggesting that OAS1 enzyme activity is not required for antiviral activity to WNV. Similarly, inducible expression of P46 in OAS1/RNase

L-double deficient cells restricted viral growth, confirming that OAS1 restricts WNV through a novel mechanism independent of RNase L activation. We next performed proteomic and transcriptome analysis to determine which proteins or pathways may be required for mediating the antiviral of OAS1. We found that OAS1 regulated the expression of several basal and IFNγ-inducible proteins. Our dataset confirmed that 105 proteins were post-transcriptionally regulated by OAS1 (Appendix B, Table 12-13), meaning that protein levels were enhanced or decreased without significant changes in mRNA expression. This led us to hypothesize that OAS1 regulated the translation of target mRNAs. Through polysome profiling and radiolabeling of nascent protein synthesis we revealed that OAS1 enhanced the synthesis of cGAS and IRF1 protein. Additionally, through RIP analysis we showed that OAS1 and Oas1b directly bound to cGAS and IRF1 mRNA. K60 residue found on the positively charged face of OAS1, conserved between human OAS1 and mouse Oas1b (Appendix A), was shown to be essential for binding mRNA and conferring antiviral resistance to WNV. We next sought to identify which well-known cellular antiviral proteins may be required for the WNV antiviral activity of OAS1, by inducible expressing P46 in OAS1-, IRF1-, cGAS- and MAVS-deficient cells lines. We observed that P46 antiviral activity was abolished in cGAS-KO cells, suggesting that inhibition of WNV by OAS1 was mediated through cGAS. Similarly, inducible expression of Oas1b in cGAS-KO cells was not capable of restricting virus, establishing a functional equivalence between human OAS1 and mouse Oas1b. We also demonstrated that the antiviral activity of OAS1 was abolished in IFNAR1-KO cells, therefore indicating that cGAS must restrict WNV through the induction of Type I IFNs. Furthermore, mouse cGAS protein levels were increased in BMDMs isolated from Oas1b-KI mice (expressing full length Oas1b) as compared to WT (expressing truncated Oas1b), which consequently enhanced type I IFN signaling in response to DNA stimuli or HSV infection. *In-vivo* data using

our Oas1b-KI mouse model revealed less viral load and enhanced survival in response to WNV infection as compared to WT mice, confirming that Oas1b is protective to WNV as reported previously (248, 251, 253). Together our results clarify the mechanism of OAS1 antiviral activity to WNV. We establish that OAS1 P46 and Oas1b enhance the synthesis of cGAS protein, which through IFN signaling suppresses WNV replication.

Having established the role of OAS1 during WNV infection, we next explored the potential antibacterial role of OAS1. The functions of OAS family proteins have mostly been confined to suppressing virus replication. However, some studies have correlated OAS1 and OASL with suppression of *M. tuberculosis* (246, 261–263). Similarly, the same SNP in OAS1, which confers resistance to WNV has also been associated to restriction of *M. tuberculosis* (246), suggesting that OAS1 P46 may confer protection to intracellular bacterial infection through a similar mechanism. To explore this hypothesis, we used *in-vitro* and *in-vivo* models of *L. monocytogenes* (Lm) and *F. novicida* (Fn) infection to investigate the antibacterial activity of OAS1 and Oas1b. We first showed that OAS1-deficient cells were more susceptible to infection with both Lm and Fn, confirming that OAS1 confers protection to intracellular bacteria. Similarly, inducible expression P46 and P46 DADA mutant, but not P42, restricted Lm, confirming that the antibacterial activity of OAS1 is conferred through isoform P46 and is independent of RNase L activation. Having previously established that OAS1 enhanced the synthesis of several proteins and cGAS was needed for OAS1 antiviral activity, we screened our dataset for antibacterial proteins regulated by OAS1. This strategy allowed us to identify IRF1 as an essential protein required to mediate the antibacterial activity of OAS1, since inducible expression of P46 in IRF1-deficient cells resulted in a complete loss of antibacterial activity. Our transcriptome and proteomic analysis had also identified 145 genes that were transcriptionally regulated by OAS1, resulting in enhanced protein

levels after IFNγ treatment (Appendix B, Table 14). OAS1 has not been described to bind DNA, therefore it is unlikely that OAS1 is directly enhancing the transcription of these genes. Given that several transcription factors were post-transcriptionally regulated by OAS1 (Appendix B, Fig. 44), it is likely that these transcription factors are responsible for enhancing the transcription of OAS1 regulated genes. Among these proteins were GBPs, known to be regulated by IRF1 and promote inflammasome signaling. Given that GBPs and inflammasome signaling have been shown to restrict intracellular bacteria (104, 204–207, 356, 363, 427), we hypothesize that IRF1 mediated antibacterial activity of OAS1 requires the expression of GBPs in order to promote inflammasome signaling. Lastly, we established the *in-vivo* phenotype of OAS1 antibacterial activity by infecting WT and Oas1b-KI mice with Lm and Fn. Survival experiments revealed that all WT mice succumbed to infection as compared to Oas1b-KI, which showed a significant increase in survival. Together these results establish the antibacterial phenotype of OAS1 and Oas1b, mediated through IRF1, which regulates the expression of several IFNγ-inducible genes required for controlling intracellular bacterial infections.

We have established that OAS1 confers protection to both virus and bacterial infections by regulating the protein levels of cGAS and IRF1 needed to restrict virus and bacterial growth respectively. We showed that OAS1 and Oas1b directly bound to cGAS and IRF1 mRNA and established that this binding is mediated through K60 residue in both human and mouse. OAS1 has previously been described to bind ssRNA and microRNA (miRNA) in order to promote OAS1 enzyme activity (436–438). However, we show that OAS1 binds cellular mRNA and influences their translation independently of NTase activity. Regulation of translation by OAS family proteins has been reported before. Oasl1 has been shown to suppress the translation of IRF7 mRNA by binding to the 5' untranslated region (UTR) of IRF7 (439), and our study provides another example

of translational modulation by OAS proteins. Given that the location of K60 residue in OAS1 and Oas1b is not towards the C-terminal region of these proteins (Appendix A, Fig. 43), it alone does not describe the isoform specific functions of human OAS1 or clarify the antiviral phenotypes between full length or truncated mouse Oas1b. Previous studies have identified a CaaX motif in OAS1 P46, not found in P42, that is required for prenylation and membrane association (440, 441). Similarly, a transmembrane domain in Oas1b, not present in truncated Oas1b, has been shown to anchor Oas1b to the ER (384). Therefore, we investigated the subcellular localization of OAS1 P42/46 and Oas1b/g and confirmed that both OAS1 and Oas1b localized to the ER. There are several ribosomes associated to the ER surface, and through polysome profiling have been shown to serve a global role in mRNA translation (386, 395). It is likely that OAS1/Oas1b binds to and traffics mRNA to the ER where they are effectively translated by ER membrane-bound ribosomes. Previous studies have shown that under stress RNase L reprograms mRNA translation by promoting global suppression of host mRNA (442). However, several immune related mRNAs are able to escape RNase L mediated decay, allowing for enhanced translation of these specific mRNAs, including IFNs (374, 442, 443). Therefore, another possibility is that OAS1 localizes to the ER and sequesters mRNA, providing protection to RNase L mediated degradation and allowing for the synthesis of antiviral or antibacterial proteins. Although we have not yet identified sequence motifs within these mRNAs that could be targeted by OAS1, our transcriptome and proteomic analysis serve as a starting point to identify these structural elements and clarify the mechanism by which OAS1 enhances mRNA translation.

The mechanisms of OAS1 mediated antiviral and antibacterial activity described in this study provide explanations for the WNV and *M. tuberculosis* resistant phenotypes observed in the G allele of OAS1 SNP rs10774671. We have confirmed that cells with the G genotype primarily

express P46 and this isoform is responsible for enhancing the translation of target mRNAs, resulting in protection to WNV, Lm and Fn. Additionally, we have shown that OAS1 regulates the transcription of several antiviral genes, for examples IFIT proteins (Appendix B), suggesting that in addition to its role in restricting flavivirus, it could promote a broad protection to several groups of virus. Therefore, studying this SNP in OAS1 could prove useful as a biomarker for both viral and bacterial susceptibility. Although less common, the OAS1 rs10774671 SNP has also been linked to several autoimmune disease, including: Multiple Sclerosis (MS), Sjögren's Syndrome and Type I Diabetes (259, 444–446). This autoimmune response results from homozygous expression of the G allele, which may overexert the immune response leading to cellular and tissue damage. Given that both cGAS and IRF1 have been associated with the development of autoimmune responses (447, 448), it is possible that autoimmunity related to homozygous expression of OAS1 P46 or Oas1b is mediated by these proteins. We have conducted preliminary studies of autoimmune development by applying a model of experimental autoimmune encephalomyelitis (EAE) in our Oas1b-KI mice (used to model human MS). In this model, EAE is induced by activating self-reactive CD4+ T cells against myelin antigen, which migrate to the CNS and initiate inflammatory responses resulting in paralysis and death (449–451). Our preliminary experiments revealed higher EAE scores in Oas1b-KI mice as compared to WT mice (Fig. 41), suggesting that Oas1b-KI mice are more susceptible to autoimmune disease. Therefore, it is possible that P46 and Oas1b, in addition to providing host protection to infection, may predispose the host to autoimmunity. This may explain why the majority of Eastern populations are heterozygous for the G allele of OAS1 rs10774671, originating from evolution and selective pressure. Together these results prove that non-canonical mechanisms exist for OAS family proteins that are required for controlling viral and bacterial infections.

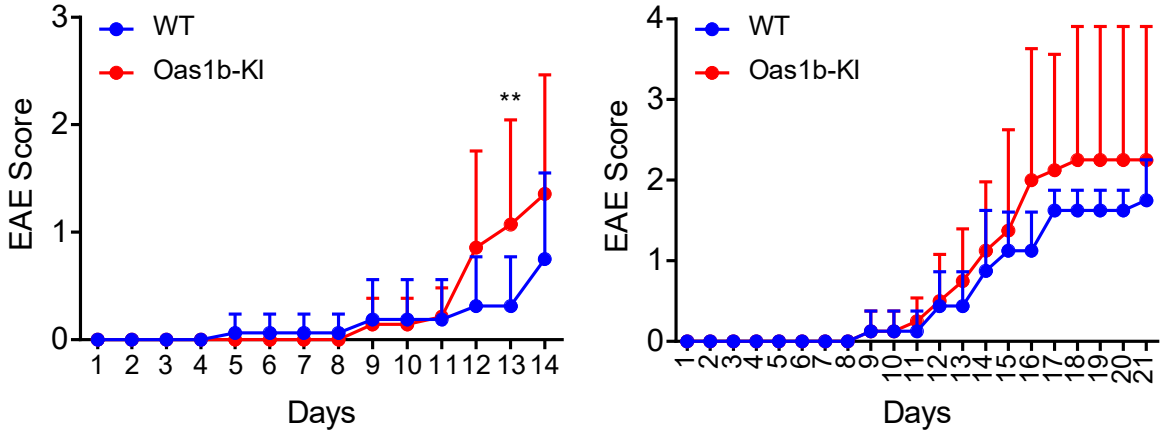

Figure 41. Heterozygous expression of Oas1b predisposes mice to autoimmunity
Autoimmunity of WT and Oas1b-KI mice was assessed by an EAE model adapted from McGeachy et al. 2009 (451). Mice were immunized subcutaneously in the flanks with myelin antigen in emulsified complete Freund's adjuvant (CFA). Additionally, pertussis toxin was administered intraperitoneally on the day of immunization and 2 days post immunization. We observed clinical signs of paralysis in two independent experiments (14 and 21 days each). The EAE scored were reported for each day and represent the following: 1 = limp tail, 2 = impaired motor function, 3 = partial paralysis of hind limbs, 4 = complete paralysis of hind limbs, 5 = fore limb weakness with hind limb paralysis, 6 = dead or moribund.

In conclusion, our studies propose a novel mechanism of OAS1 antiviral activity to WNV and antibacterial activity to Lm and Fn, which is independent on NTase activity and RNase L activation (Fig. 42). During viral and bacterial infections type I and II IFNs are induced, leading to the expression of several ISGs. Among these ISGs, OAS1 confers host protection by enhancing the synthesis of several proteins. OAS1 localizes to the ER and directly binds to mRNAs to enhance their translation, promoting the synthesis of several basal and IFNγ-inducible proteins including cGAS and IRF1. cGAS is known to be activated by endogenous DNA originating from mitochondria under cellular stress, which is triggered by virus infection (382). Once active, cGAS induces type I IFN signaling required to clear infection in an autocrine and paracrine manner. During infection, OAS1 enhances the synthesis of several transcription factors, including IRF1. We believe that these transcription factors mediate the transcriptional regulation of several innate immune genes upregulated by OAS1. Among these genes are several GBPs, which are known to

confer antibacterial protection by disrupting bacteria containing vacuoles or directly affecting the integrity of bacterial membranes. This leads to the activation of inflammasome pathways needed to secrete inflammatory cytokines responsible for clearing infection. However, the direct impact of GBPs and inflammasome signaling in OAS1 mediated antibacterial immunity has yet to be determined and is being explored in ongoing research projects in our lab. Additionally, several antiviral proteins are transcriptionally regulated by OAS1, including RLRs, IFIT proteins and ISG15 (Appendix B). This suggests that OAS1 may potentiate immune signaling to several intracellular pathogens providing a broad spectrum of host immunity. Overall, our studies highlight the importance in understanding the mechanisms by which OAS family proteins restrict intracellular pathogens, providing a basis for the development of targeted therapies to improve host immunity.

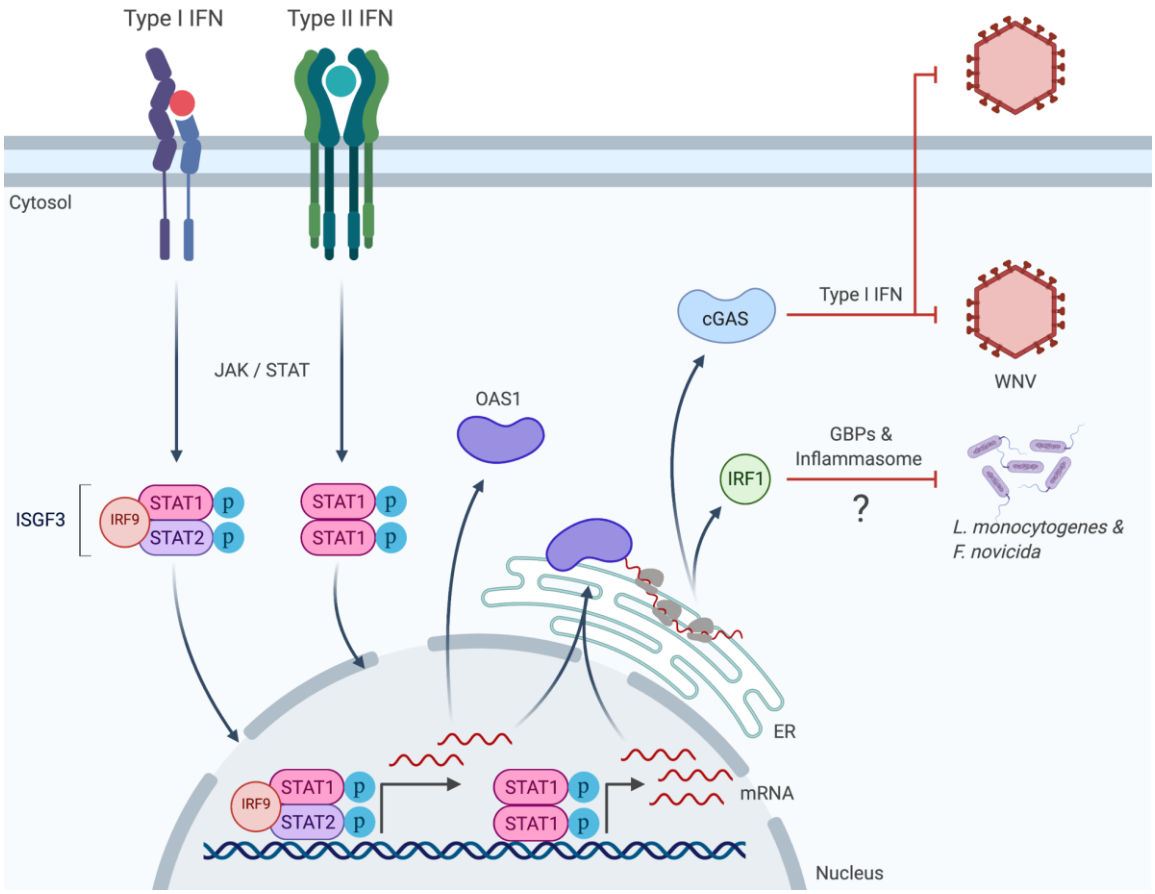

Figure 42. Model of non-canonical antiviral and antibacterial activity of OAS1
During intracellular infection IFN are induced, which act in an autocrine and paracrine manner to induce immune protection. Type I IFN leads to the expression of OAS1 that then localizes to the ER. OAS1 binds basal and IFNγ-inducible mRNAs, facilitates association with polyribosomes found on the ER surface and enhances translation of these mRNAs. cGAS and IRF1 levels are enhanced through this mechanism, which are required for antiviral and antibacterial activity respectively.

Appendix A

OAS1 sequence alignment

A.1 Background and Alignment

As previously described in Fig. 5, there are several OAS1 isoforms expressed by the *OAS1* gene and different murine Oas1 protein expressed from different genes in the same locus. The expression of OAS1 isoforms has been linked to the SNP rs10774671 at the acceptor site of exon 6 of *OAS1* (Fig. 9) (255, 260). Additionally, the presence of the G allele leads to the expression of P46 isoform and confers protection to WNV and *M. tuberculosis* (243, 246). Genotyping of susceptible individuals found a correlation between the A allele and P42 expression (referred to as p41/4 in the alignment, Fig. 43), suggesting that P46 is the protective factor against these pathogens. In this dissertation we confirmed that expression of P46 enhanced the translation of several target mRNAs, including cGAS and IRF1. cGAS was shown to be necessary for antiviral activity against WNV and IRF1 was shown to be required for antibacterial activity against *L. monocytogenes* (Lm) and *F. novicida* (Fn). Alignment between different OAS1 isoforms revealed that P42 and P46 differ only in the C-terminal (Fig. 43), therefore the protective factor is outside of the catalytic domain of these proteins and must be related to the C-terminal of P46. The sequence of P46 reveals a CAAX motif, not found in P42, required for prenylation, which confers a high affinity for the ER (441). Additionally, truncation of Oas1b at the C-terminal has been associated with susceptibility to WNV, as compared to mice expressing full length Oas1b, which promotes

RNase L independent antiviral activity to WNV (228, 251, 253). Amino acids 354-371 found at the C-terminus of Oas1b are within a transmembrane domain shown to anchor Oas1b to the ER (Fig. 43) (384). Our experiments have shown that OAS1 and Oas1b both localize to the ER, suggesting that these sequences found at their C-terminal domains are necessary for localization and function.

Previous studies had identified critical residues within a catalytic triad for OAS proteins needed for synthesis of 2'-5' oligoadenylates (235, 236). A catalytic mutant made in porcine OAS1 (DADA) abolishes catalytic function, and through sequence alignment we identified these residues, D75A and D77A, in human OAS1 highlighted with black arrows (Fig. 42). We performed NEB mutagenesis to create this mutant in order to determine the necessity for catalytic activity for OAS1 antiviral and antibacterial immunity. We showed that P46 DADA was capable of inhibiting both WNV-KUN and Lm, confirming that the NTase activity of OAS1 is not needed for these phenotypes. Similarly, several amino acid residues of OAS proteins are essential for binding dsRNA and NTase activity (237, 385). We showed that a critical residue of OAS1 (K60), which is conserved in mouse Oas1b (Fig. 43), was required for binding mRNA and promoting their translation and antiviral activity against WNV. We first created several RNA binding mutants in Oas1b using NEB mutagenesis and the residues targeted for mutagenesis are highlighted with black arrows (K42E, K57E, K60E and K191E) in Fig. 43. Mutagenesis of K60 was sufficient to abolish RNA binding and promote susceptibility to WNV. Since the K60 residue is conserved between human OAS1 and mouse Oas1b, we created the K60E mutant in human OAS1 and showed that RNA binding was not apparent and resulted in higher viral titers. This data confirmed that translational enhancement of mRNAs by OAS1 is dependent on direct RNA binding, and consequently antiviral and antibacterial activity.

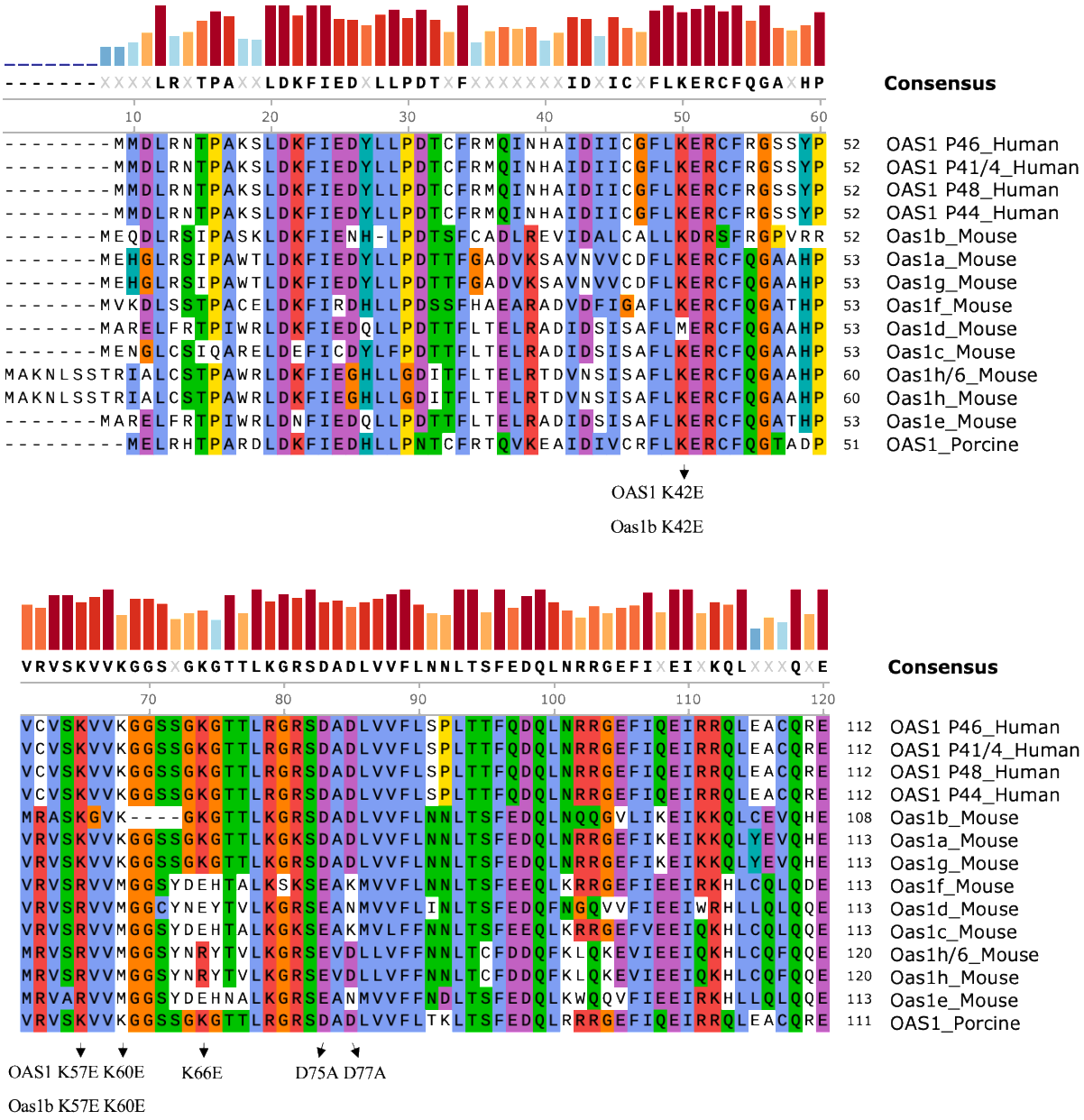
Consensus
OAS1 P46_Human
OAS1 P41/4_Human
OAS1 P48_Human
OAS1 P44_Human
Oas1b_Mouse
Oas1a_Mouse
Oas1g_Mouse
Oas1f_Mouse
Oas1d_Mouse
Oas1c_Mouse
Oas1h/6_Mouse
Oas1h_Mouse
Oas1e_Mouse
OAS1_Porcine
OAS1 K42E
Oas1b K42E
Consensus
OAS1 P46_Human
OAS1 P41/4_Human
OAS1 P48_Human
OAS1 P44_Human
Oas1b_Mouse
Oas1a_Mouse
Oas1g_Mouse
Oas1f_Mouse
Oas1d_Mouse
Oas1c_Mouse
Oas1h/6_Mouse
Oas1h_Mouse
Oas1e_Mouse
OAS1_Porcine
OAS1 K57E K60E
Oas1b K57E K60E
K66E
D75A D77A

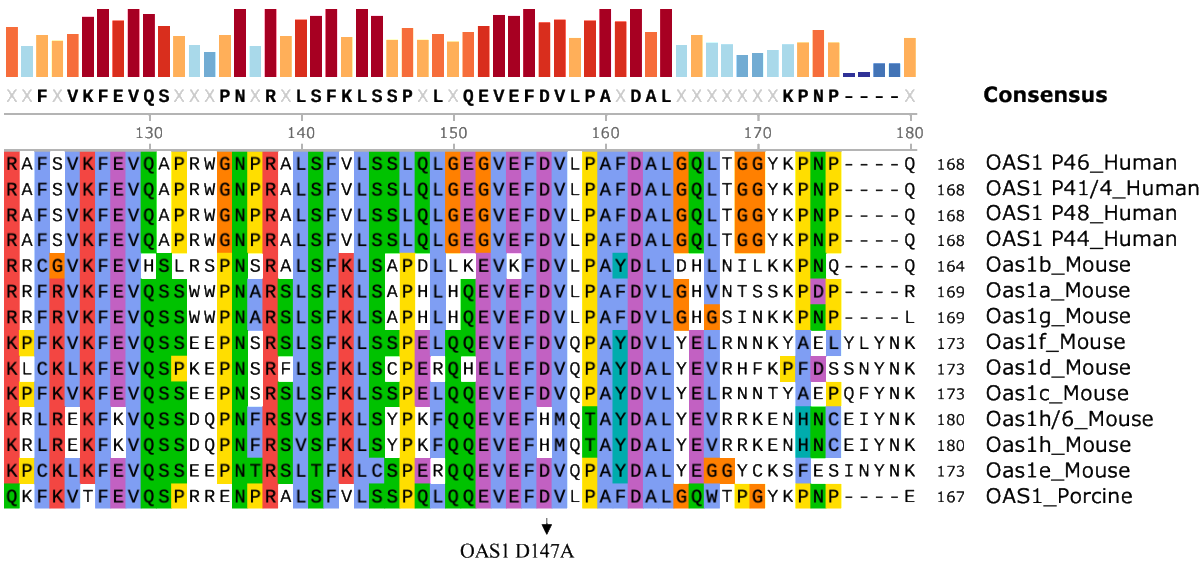
Consensus
OAS1 P46_Human
OAS1 P41/4_Human
OAS1 P48_Human
OAS1 P44_Human
Oas1b_Mouse
Oas1a_Mouse
Oas1g_Mouse
Oas1f_Mouse
Oas1d_Mouse
Oas1c_Mouse
Oas1h/6_Mouse
Oas1h_Mouse
Oas1e_Mouse
OAS1_Porcine
OAS1 D147A

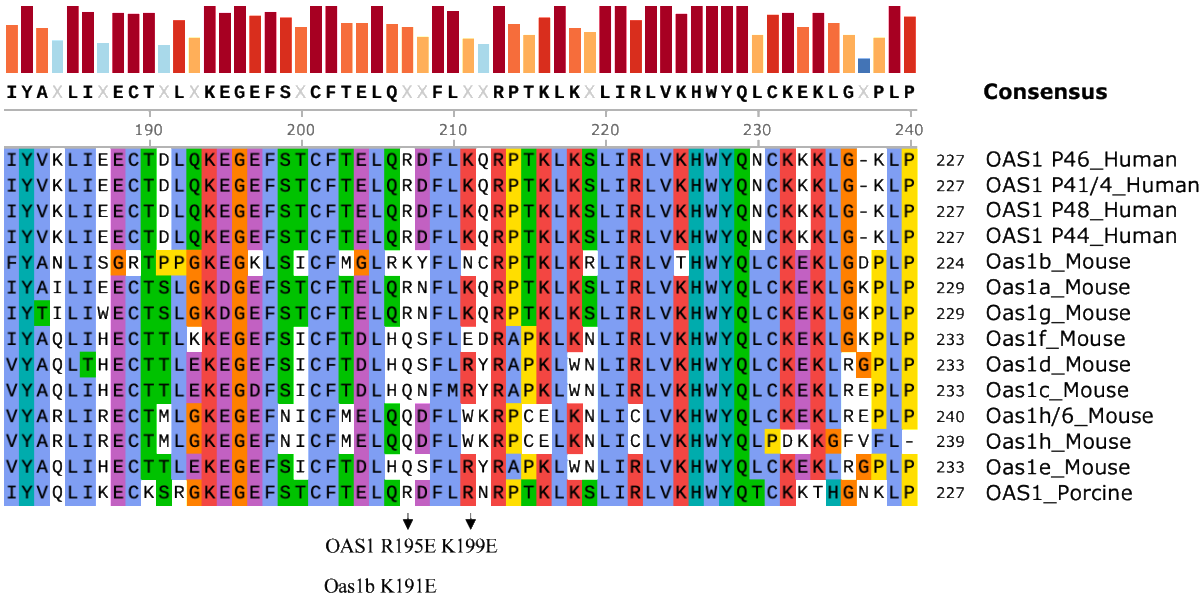
Consensus
OAS1 P46_Human
OAS1 P41/4_Human
OAS1 P48_Human
OAS1 P44_Human
Oas1b_Mouse
Oas1a_Mouse
Oas1g_Mouse
Oas1f_Mouse
Oas1d_Mouse
Oas1c_Mouse
Oas1h/6_Mouse
Oas1h_Mouse
Oas1e_Mouse
OAS1_Porcine
OAS1 R195E K199E
Oas1b K191E

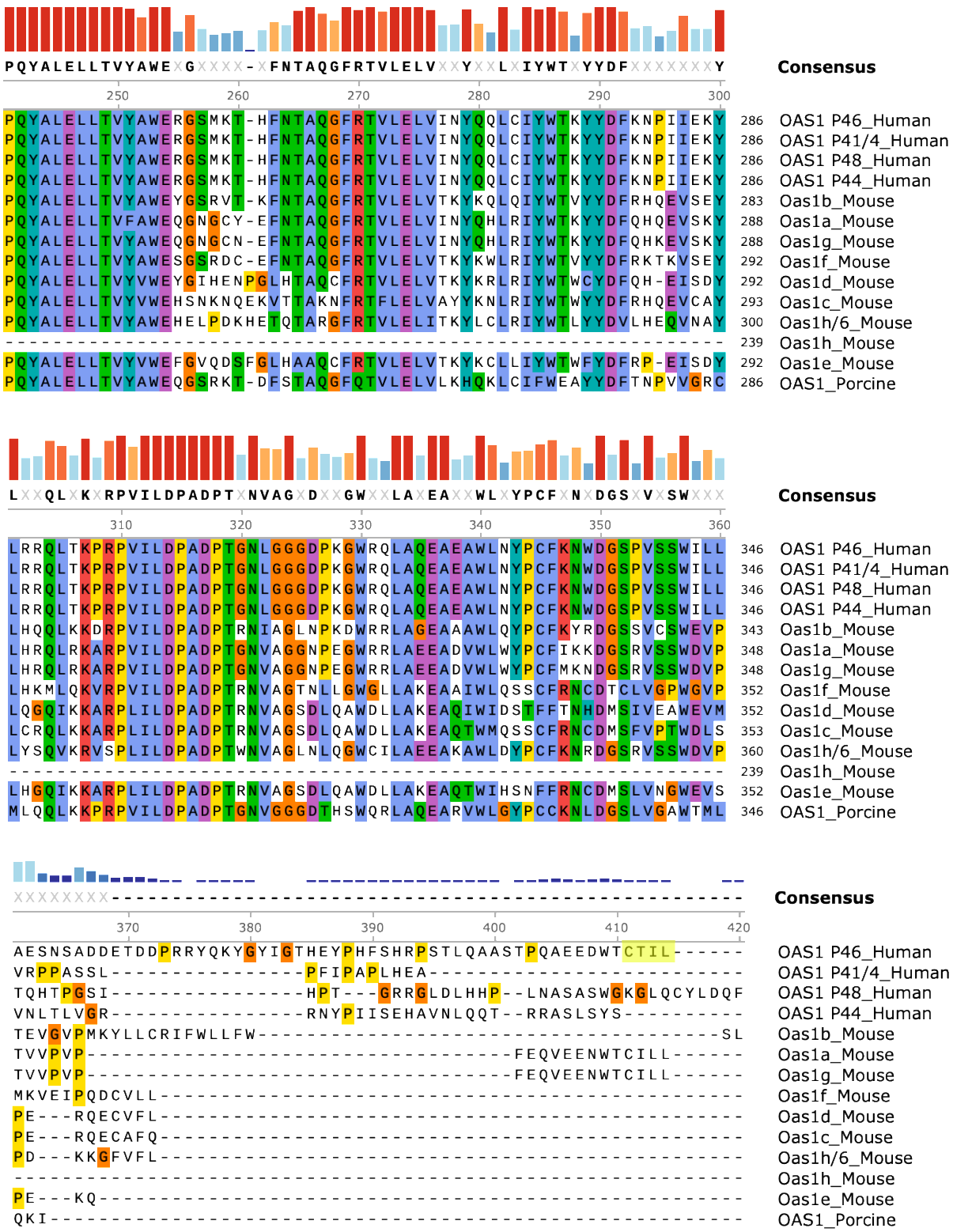
Consensus
250
260
270
280
290
300
286 OAS1 P46_Human
286 OAS1 P41/4_Human
286 OAS1 P48_Human
286 OAS1 P44_Human
283 Oas1b_Mouse
288 Oas1a_Mouse
288 Oas1g_Mouse
292 Oas1f_Mouse
292 Oas1d_Mouse
293 Oas1c_Mouse
300 Oas1h/6_Mouse
239 Oas1h_Mouse
292 Oas1e_Mouse
286 OAS1_Porcine
Consensus
310
320
330
340
350
360
346 OAS1 P46_Human
346 OAS1 P41/4_Human
346 OAS1 P48_Human
346 OAS1 P44_Human
343 Oas1b_Mouse
348 Oas1a_Mouse
348 Oas1g_Mouse
352 Oas1f_Mouse
352 Oas1d_Mouse
353 Oas1c_Mouse
360 Oas1h/6_Mouse
239 Oas1h_Mouse
352 Oas1e_Mouse
346 OAS1_Porcine
Consensus
370
380
390
400
410
420
OAS1 P46_Human
OAS1 P41/4_Human
OAS1 P48_Human
OAS1 P44_Human
Oas1b_Mouse
Oas1a_Mouse
Oas1g_Mouse
Oas1f_Mouse
Oas1d_Mouse
Oas1c_Mouse
Oas1h/6_Mouse
Oas1h_Mouse
Oas1e_Mouse
OAS1_Porcine

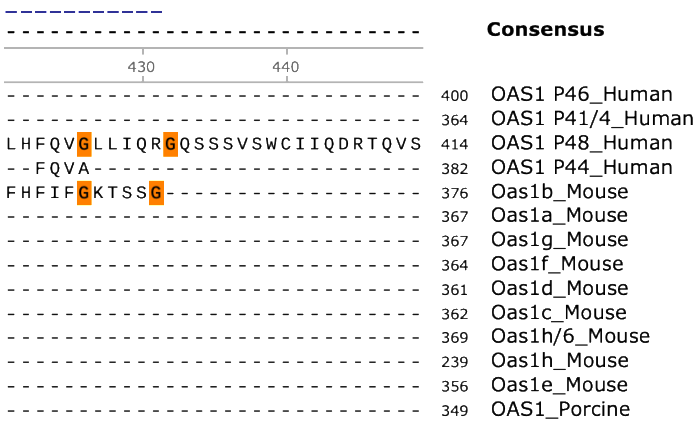

Figure 43. OAS1 sequence alignment

The amino acids sequences of human OAS1 isoforms, mouse Oas1 genes and porcine OAS1 were aligned using Clustal Omega (452). Consensus sequence represents the most frequent amino acids with a consensus threshold of 50%. Sequence conservation for each column is represented by colored bars above the consensus sequence. Low sequence conservation is indicated by smaller blue bars as compared to higher conserved residues represented by larger yellow and red colored bars. Amino acids in each column were marked based on properties and conservation (Blue = hydrophobic, Cyan = aromatic, Purple = negative, Green = polar, Red = positive, Orange = glycine, Yellow = proline). CTIL CaaX motif of OAS1 P46 is highlighted in light yellow.

Appendix B

OAS1 regulates the protein levels of several basal and IFNγ-inducible proteins

B.1 Introduction

The role of OAS proteins was first attributed to antiviral defense through the synthesis of 2'-5' oligoadenylates and RNase L activation. However, this does not explain the antiviral phenotype observed in murine Oas1b to WNV, which is independent of enzyme activity (253). Furthermore, OASL exhibits enzyme independent antiviral activity through enhancing RIG-I signaling pathways (13, 239), and OAS3 has been shown to be required and sufficient for RNase L activation (17). Together these studies suggest that non-canonical roles may exists for other OAS family members. In this dissertation we demonstrate that OAS1 can provide antiviral and antibacterial activity through isoform P46. To determine the mechanisms by which P46 conferred protection, we evaluated the proteomic and transcriptome of OAS1-deficient THP1 cells compared to WT cells. These analyses identified several proteins that were post transcriptionally regulated by OAS1. cGAS and IRF1 protein levels were enhanced and through polysome profiling, radiolabeling of nascent protein synthesis and RIP analysis, we revealed that OAS1 directly bound cGAS and IRF1 mRNA in order to promote translation of these two mRNA. Overall P46 enhanced the protein synthesis of several basal and IFNγ-inducible proteins, including cGAS and IRF1, which were shown to mediate antiviral and antibacterial activity respectively. In chapter 3 we highlighted the top 30 most post transcriptionally down-regulated proteins in OAS1-deficient cells

and in this section, we list all 87 proteins down-regulated and all 18 proteins up-regulated in the absence of OAS1. Additionally, we identified 145 genes that were transcriptionally regulated by OAS1, many with potential antiviral and antimicrobial activity.

B.2 Results and Discussion

SILAC and RNAseq analysis was carried out as described in Methods 2.2.21-22. To determine the antiviral and antibacterial mechanisms of OAS1, we screened our proteomic and RNAseq analyses to identify proteins or pathways that may be required for these activities. Our data set was divided in two groups: proteins post transcriptionally regulated by OAS1 (Table 12-13), and proteins transcriptionally regulated by OAS1 (Table 14). In this dissertation we found that OAS1 directly enhanced translation of target mRNAs, which explains why several proteins levels were downregulated in OAS1-deficient cells without significant changes in mRNA expression as compared to WT cells (Table 12). The levels of a few proteins were significantly decreased in OAS1-KO cells as compared to WT cells (Table 13), however there have not been any major antiviral functions associated to these proteins.

Table 12. Proteins post transcriptionally upregulated by OAS1

WT/OAS1-KO	Log_2 (Peptide Intensity Ratio) after IFNγ treatment			RPKM Ratio after IFNγ treatment				
Gene	**0 h**	**4 h**	**8 h**	**0 h**	**1 h**	**2 h**	**4 h**	**8 h**
cGAS	3.58	-0.68	-0.13	0.60	0.66	0.59	0.56	0.90
MED17	3.16	0.51	0.00	0.90	1.05	0.88	0.82	1.36
MP68	3.04	0.48	0.44	0.71	0.62	0.74	0.75	0.64
GEMIN2	2.86	0.44	-0.45	0.69	0.74	0.48	0.56	0.89
TTC19	2.60	0.00	0.22	0.84	0.81	0.68	0.60	1.04
SMAP2	2.48	2.67	2.54	0.93	0.87	0.82	0.68	0.94
TMEM199	2.48	-0.05	-0.48	0.98	0.95	0.95	0.95	1.10
TOMM40L	2.42	2.42	0.35	0.99	0.88	0.75	0.59	0.99
RNMT	1.70	-0.18	0.05	0.95	0.92	0.79	0.83	1.16
NMD3	1.68	1.25	0.00	0.98	1.09	0.89	0.78	1.60
WDR4	1.62	0.52	0.00	0.95	0.84	0.75	1.06	0.89
RSRC2	1.54	-0.58	0.22	0.68	0.89	1.03	0.57	0.84
TRAM1	1.54	-0.46	0.00	0.74	0.77	0.64	0.71	1.40
FUCA1	1.53	0.00	0.00	0.74	0.78	0.72	0.54	0.82
JMJD1C	0.43	6.54	0.06	0.69	0.80	0.95	0.80	1.37
KMT2B	-0.22	3.63	0.00	0.80	0.85	1.12	0.95	0.70
KIF22	0.01	2.90	1.88	0.99	0.93	0.92	0.73	0.72
SMAP2	2.48	2.67	2.54	0.93	0.87	0.82	0.68	0.94
INPP5F	-0.26	2.62	5.97	0.90	0.81	0.97	0.70	0.88
DNAJB1	2.17	2.60	2.69	0.81	0.96	0.92	0.72	0.86
TOMM40L	2.42	2.42	0.35	0.99	0.88	0.75	0.59	0.99
LSM5	0.06	2.26	0.36	1.07	1.18	0.92	0.57	1.07
SMG6	0.82	2.12	0.00	0.79	0.85	0.78	0.82	0.79
SPAG5	0.01	2.08	0.90	0.88	0.85	0.87	0.64	0.86
MECR	0.17	2.05	0.00	0.98	0.89	0.93	0.76	0.94
DDX31	1.14	2.03	1.22	0.93	0.85	0.73	0.84	1.12
ETFDH	0.17	1.96	0.76	0.98	0.96	0.91	0.80	1.18
CENPE	0.54	1.84	0.93	0.72	0.83	0.94	0.61	1.07
SLC37A4	0.19	1.79	-0.11	0.59	0.58	0.64	0.52	0.52
ARHGAP9	-0.38	1.78	-0.65	1.01	0.82	0.74	0.63	0.62
MARS	1.14	1.74	1.27	1.04	1.05	1.12	0.88	0.94
DPP9	0.21	1.74	1.40	1.13	1.11	1.15	1.32	1.16
NBAS	-0.16	1.69	0.28	1.04	0.86	0.74	0.79	1.17
AGPAT3	-0.23	1.65	0.43	0.83	0.75	0.83	0.82	0.91
DDX27	1.20	1.63	1.39	0.92	0.84	0.86	0.71	0.92
DHRS9	0.91	1.63	0.00	0.91	0.97	0.92	0.74	0.96
CEP250	0.00	1.62	-7.55	0.74	0.67	0.90	0.71	0.88
FASTKD2	1.40	1.61	0.99	0.82	0.91	0.86	0.74	1.42
PCCA	0.00	1.60	-0.22	0.86	0.84	0.79	0.67	1.00
TMEM230	0.00	1.58	0.76	0.96	1.00	0.91	0.68	1.11

Table 12 continued

GCHFR	0.00	1.56	1.36	1.44	1.26	1.20	1.54	1.21
UBR5	-0.52	1.55	-0.34	0.72	0.77	0.85	0.65	1.04
CCZ1;CCZ1B	0.09	1.51	0.55	0.88	0.98	0.98	0.57	0.86
STAT5A	0.01	1.22	0.44	0.88	0.83	0.62	0.57	0.66
STAT5B	0.01	1.22	0.44	0.83	0.79	0.70	0.64	0.75
INPP5F	-0.26	2.62	5.97	0.90	0.81	0.97	0.70	0.88
MAFG	-0.73	-0.26	3.61	0.85	0.74	0.94	1.09	1.01
UAP1	0.09	1.05	2.97	0.91	1.05	0.88	0.71	1.07
DNAJB1	2.17	2.60	2.69	0.81	0.96	0.92	0.72	0.86
LRCH3	0.14	0.36	2.60	0.98	0.97	1.07	0.86	1.11
SMAP2	2.48	2.67	2.54	0.93	0.87	0.82	0.68	0.94
WDR74	0.46	0.25	2.37	1.04	0.93	0.90	0.79	0.84
TAP2	0.71	-0.14	2.26	0.86	0.80	1.17	1.04	1.20
TAP1	0.95	-0.54	2.23	1.25	1.13	1.25	1.29	1.32
RNF213	0.24	-0.48	2.23	0.75	0.76	1.44	1.47	1.51
ASF1B	-0.23	0.00	1.93	0.70	0.70	0.70	0.66	0.72
WARS	0.53	-0.91	1.91	1.08	1.38	1.65	1.19	1.40
KIF22	0.01	2.90	1.88	0.99	0.93	0.92	0.73	0.72
DTX3L	0.00	-0.23	1.87	0.81	0.78	0.88	0.82	1.39
EXOSC5	1.08	-0.36	1.86	1.03	0.92	0.83	0.96	0.90
TRAFD1	0.00	0.01	1.84	0.88	0.86	1.10	1.21	1.28
PARP14	0.14	-0.71	1.81	0.71	0.73	1.14	0.95	1.48
MED14	0.54	0.70	1.80	0.74	0.82	0.83	0.68	1.10
IFI30	1.32	-0.28	1.76	1.71	1.38	1.62	1.02	1.10
MAD2L2	0.44	0.00	1.75	1.70	1.54	1.50	1.35	1.24
PLEKHO2	-0.08	-0.17	1.74	0.98	0.91	0.90	0.96	1.37
DIEXF	0.18	1.11	1.73	1.03	1.14	1.03	0.90	1.37
XRN1	0.63	0.00	1.72	0.67	0.88	1.07	0.83	1.66
WDR70	1.07	0.09	1.71	1.18	1.11	1.09	1.00	1.51
PCBD2	1.07	1.27	1.69	1.63	1.50	1.52	1.23	1.68
PCTP	0.21	0.37	1.68	0.76	0.81	0.59	0.67	0.99
LGALS3BP	0.00	-1.77	1.67	1.30	0.86	1.22	0.82	0.88
SP110	0.00	-1.52	1.67	1.15	1.17	0.97	0.78	1.39
ANKRD17	0.74	0.26	1.65	0.64	0.73	0.85	0.67	0.94
SLC27A2	1.01	1.05	1.65	1.32	1.38	1.21	0.82	1.22
FARS2	1.26	0.90	1.58	1.67	1.59	1.28	1.34	1.65
STAT1	0.29	-0.85	1.57	0.67	0.77	0.79	0.76	1.40
NUB1	-0.02	-0.06	1.56	0.81	0.76	0.91	0.90	1.20
ZNFX1	0.00	0.25	1.54	0.71	0.83	1.19	0.85	1.12
DIMT1	1.04	1.20	1.54	1.59	1.54	1.14	0.72	1.23
LRRC8C	0.52	0.91	1.52	1.17	1.21	1.16	0.91	1.69
MRPS36	1.08	1.27	1.52	0.93	0.88	0.94	0.79	0.98
ISCU	1.20	0.84	1.51	1.03	1.08	0.94	0.81	1.19

Table 12 continued

FTL	0.82	1.09	1.51	1.47	1.30	1.49	1.14	1.39
IRF1	0.00	0.46	0.00	1.20	1.41	1.36	1.22	1.34
STAT2	-0.03	-0.64	1.41	1.06	0.92	1.02	0.93	1.35
STAT3	0.16	-0.02	0.91	0.73	0.79	0.99	0.87	1.10

Table 13. Proteins post transcriptionally downregulated by OAS1

WT/OAS1-KO	**Log_2 (Peptide Intensity Ratio) after IFNγ treatment**			**RPKM Ratio after IFNγ treatment**				
Gene	**0 h**	**4 h**	**8 h**	**0 h**	**1 h**	**2 h**	**4 h**	**8 h**
CTSG	-1.73	-1.67	-2.24	0.64	0.63	0.69	0.58	0.58
ICAM3	-1.80	-2.10	-1.92	0.77	0.69	0.67	0.65	0.58
NO66	-1.89	0.14	0.24	0.94	0.98	0.81	0.78	0.90
CKAP4	-1.94	-1.37	-1.73	0.70	0.60	0.45	0.49	0.73
KIF20A	-2.08	1.23	0.95	0.93	1.00	1.06	0.82	1.20
GOLGA4	-2.57	-0.14	0.00	0.69	0.76	0.78	0.65	1.09
JUP	-4.78	-5.07	-4.41	1.38	1.19	1.33	1.37	1.40
SP110	0.00	-1.52	1.67	1.15	1.17	0.97	0.78	1.39
EXO5	-0.23	-1.71	0.00	0.79	0.80	0.85	0.75	0.91
LGALS3BP	0.00	-1.77	1.67	1.30	0.86	1.22	0.82	0.88
UBE2L6	0.00	-2.01	0.16	0.87	0.70	0.69	0.60	0.79
FAR2	-0.16	-2.27	-0.40	0.80	0.83	0.75	0.60	0.99
NFIX	-1.13	-8.18	-8.00	0.92	0.83	0.80	0.82	0.79
AZU1	-1.44	-1.20	-2.07	1.15	0.94	1.02	1.05	0.68
NME4	-0.88	-0.10	-2.65	1.05	0.96	1.14	0.77	0.63
AKAP2	-0.05	-0.19	-2.10	1.02	1.04	0.93	0.95	1.44
PPP6R2	0.00	0.23	-4.48	0.99	0.86	0.97	0.98	0.91
RNASE2	-1.32	-1.43	-1.49	0.93	0.91	1.10	0.58	0.76

Among these proteins, we identified cGAS as a critical component of OAS1 and Oas1b mediated antiviral activity to WNV (Chapter 3). Additionally, the antiviral activity of OAS1 was abolished in IFNAR1-deficient cells and IFNβ signaling was enhanced in Oas1b-KI BMDMs, suggesting that cGAS mediated antiviral activity required downstream type I IFN signaling. Similarly, IRF1 protein levels were enhanced by OAS1 and IRF1 was essential for mediating OAS1 antibacterial activity against *L. monocytogenes* and *F. novicida* (Chapter 4). Beyond these

immune phenotypes described, other proteins affected by the loss of OAS1 may modulate other cellular processes. Functional annotation analysis was performed on gene lists generated from our datasets (Fig. 44), using DAVID bioinformatics tools (Methods 2.22.2) (372, 373). Among these proteins post transcriptionally regulated by OAS1, we identified several DNA and RNA binding proteins in addition to several proteins known to regulate gene transcription. Many of these are involved in regulating innate immune signaling leading to a global suppression of virus and bacterial replication, including cGAS, IRF1, and STAT proteins. Others are important in transcription, maturation of mRNA and translation, for example the transcription factor MAFG (453), RNA guanine-7 methyltransferase (RNMT) (454) and mediators of RNA polymerase II transcription complex subunit 14 and 17 (MED14 and MED17) (455, 456).

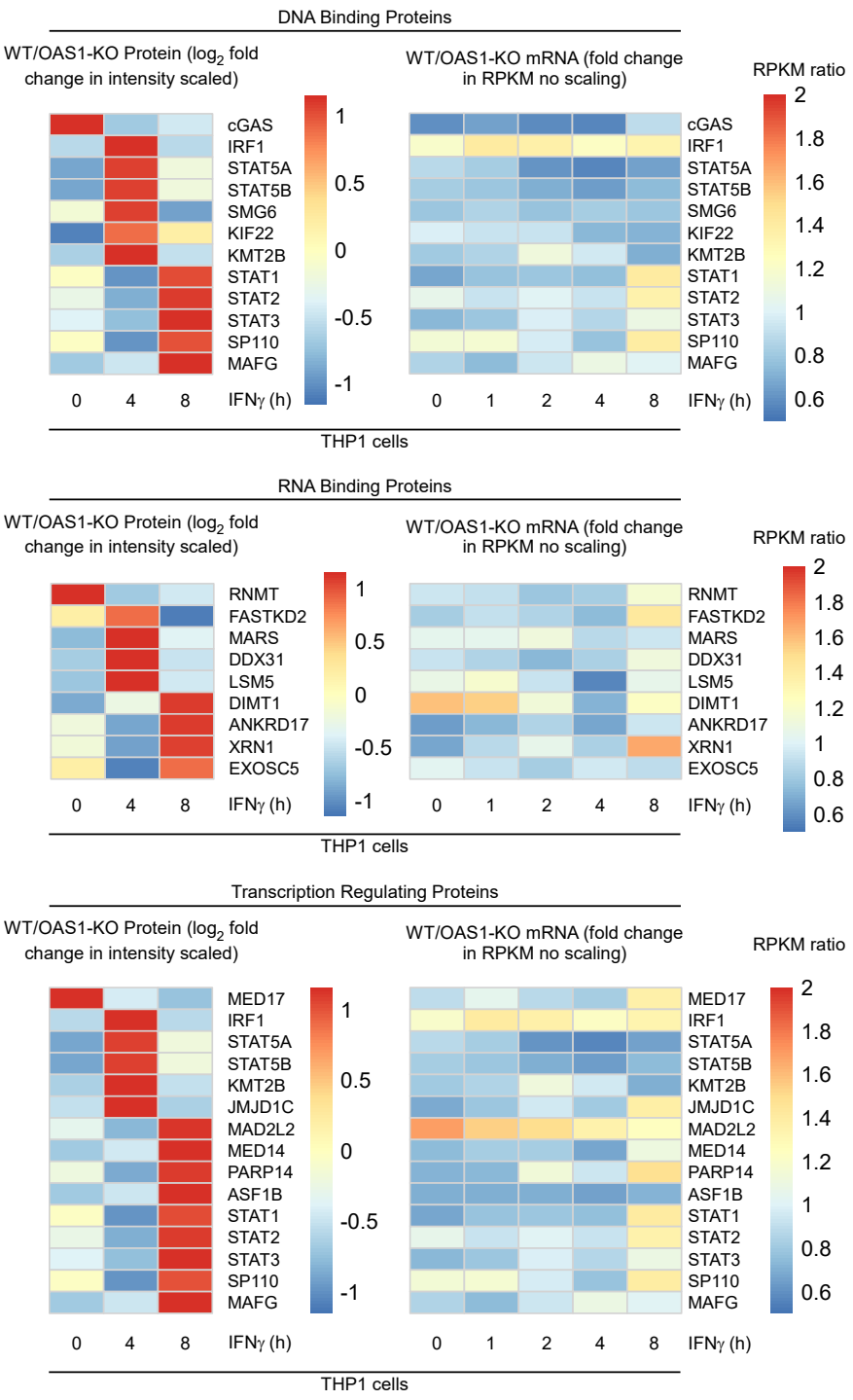

Figure 44. Potential roles for proteins post transcriptionally regulated by OAS1
The list of genes from Table 12 were uploaded and submitted to the online DAVID bioinformatics tool. Function annotation analysis was performed to predict major biological functions associated to genes post transcriptionally regulated by OAS1. The data is represented as heatmaps using Z-scored scaled log_2 fold change of WT to OAS1-KO peptide intensity ratio and unscaled RPKM WT to OAS1-KO ratio.

OAS1 also enhanced the levels of several proteins that were related to increased mRNA transcription. However, OAS1 has not been described to bind DNA, therefore it is unlikely that OAS1 directly affected the transcription of these genes. It is more probable that several transcription factors post transcriptionally by OAS1, identified in Fig. 44, are responsible for regulating the transcription of these target genes. For example, IRF1 is known to regulate the expression of several IFNγ-inducible genes, and in Chapter 4 we described that the antibacterial activity of OAS1 is mediated through this transcription factor. Therefore, it is likely that OAS1 provides antibacterial protection through the expression of these IFNγ–inducible genes. To identify genes transcriptionally up/downregulated in the absence of OAS1, we filtered our dataset for proteins induced at 4 and 8 h of IFNγ treatment with significant changes in their RPKM values (Methods 2.2.22). We identified a total of 145 genes transcriptionally regulated by OAS1 and these are listed in Table 14.

Table 14. Proteins transcriptionally regulated by OAS1

WT/OAS1-KO	Log_2 (Peptide Intensity Ratio) after IFNγ treatment			RPKM Ratio after IFNγ treatment				
Gene	**0 h**	**4 h**	**8 h**	**0 h**	**1 h**	**2 h**	**4 h**	**8 h**
IFIT1	0.0	0.0	3.6	1.02	0.30	0.71	0.97	2.18
GCH1	0.0	0.0	3.4	-0.39	-0.26	0.57	0.63	1.14
AKR1C2	4.2	4.0	3.3	6.40	6.09	6.62	5.84	7.36
AKR1C1	4.2	4.0	3.3	2.07	2.72	2.70	2.94	2.20
GBP7	0.0	-1.3	3.2	0.00	-2.79	0.00	-0.23	0.31
IFIT2	0.0	0.0	3.1	-0.18	0.13	1.30	0.39	1.12
GBP1	0.0	-1.5	3.0	0.00	1.22	1.86	0.53	0.92
OAS2	0.0	0.0	2.9	0.09	0.09	0.06	0.30	1.60
CXCL10	0.0	1.3	2.9	-1.66	1.39	1.63	1.65	1.76
GBP5	0.0	-0.6	2.8	1.94	1.34	1.96	0.91	1.25
GBP4	0.0	-1.4	2.7	-0.39	0.39	1.02	0.02	0.49
ISG15	1.0	0.6	2.6	0.77	0.44	0.42	1.26	1.72
APOL2	0.0	-0.7	2.6	0.28	0.19	1.29	0.54	0.30
GBP2	0.0	-1.0	2.6	1.27	1.19	1.59	0.14	0.49
HMOX1	0.0	0.6	2.6	0.55	1.82	3.19	2.55	1.83
PPP1R27	3.9	2.6	2.6	4.51	4.25	4.56	4.49	3.96
NCF1	1.6	0.2	2.5	1.79	1.50	1.69	1.79	1.47
NCF1C	1.6	0.2	2.5	1.67	1.19	1.27	1.54	1.22
NCF1B	1.6	0.2	2.5	1.05	0.98	1.41	1.24	1.10
IFIH1	0.0	-0.5	2.5	-0.84	-0.61	-0.35	-0.05	1.04
IFIT3	0.0	-1.8	2.2	0.13	-0.04	0.90	0.27	1.31
NLN	1.2	2.2	2.2	0.69	0.86	0.78	0.56	1.34
FTH1	-0.5	0.9	2.1	1.15	0.99	1.04	0.89	1.40
PPWD1	1.0	2.2	2.0	0.81	0.93	1.18	0.36	0.96
NQO1	1.7	1.9	1.9	0.76	0.65	0.67	0.53	1.22
CD36	1.2	1.6	1.9	1.61	1.74	1.56	1.51	2.72
NDUFAF2	1.5	0.0	1.8	1.16	1.41	1.33	0.41	1.23
APOC2	1.5	1.7	1.8	1.56	1.51	1.81	0.85	0.82
TAF13	0.7	0.0	1.8	0.24	0.17	-0.10	0.11	1.13
S100A10	1.2	1.4	1.7	1.19	1.04	1.21	0.36	0.62
PCK2	1.7	1.0	1.7	1.06	0.93	0.78	0.65	0.45
ACOT13	1.7	1.7	1.7	0.88	0.94	1.16	0.22	0.65
NXN	2.4	2.1	1.7	2.26	2.08	2.01	1.82	2.47
GTF2H2	1.0	1.4	1.6	1.42	1.17	1.15	0.68	1.75
NCAM1	1.7	2.0	1.6	1.50	1.53	1.69	1.25	1.65
ASS1	1.3	1.5	1.6	1.83	1.76	1.69	1.49	1.36
DDX58	0.0	0.0	1.6	0.09	0.32	0.53	0.64	2.17
THBD	0.0	0.9	1.6	1.29	1.01	-0.10	0.32	1.50
SAMD9	0.2	0.0	1.6	-0.78	-0.50	0.03	-0.26	1.08
SNX18	1.4	1.6	1.6	0.48	0.90	1.07	0.42	1.69

Table 14 continued

NUP153	1.3	1.6	1.6	0.27	0.32	0.54	0.45	1.20
VIM	1.8	1.8	1.6	0.99	1.12	1.16	0.79	1.18
EEF1E1	1.4	1.6	1.5	1.01	1.17	0.85	0.54	1.20
LGALS3	1.4	0.5	1.5	1.29	1.24	1.15	0.67	1.10
C3	0.0	0.0	1.5	-1.69	-1.16	0.54	-0.38	-0.35
SKIV2L2	1.0	1.4	1.4	0.79	0.86	0.64	0.43	1.29
DHX29	1.5	1.3	1.4	0.11	0.29	0.27	0.32	1.19
PHGDH	1.4	1.4	1.4	1.23	1.13	0.80	0.72	0.59
IPO11	1.2	1.2	1.4	0.76	0.63	0.43	0.37	1.30
EMB	0.0	0.0	1.3	0.49	0.68	0.80	0.32	1.29
DPYSL2	1.2	1.4	1.3	1.32	1.20	0.75	0.51	0.39
MCCC2	1.2	1.2	1.3	0.61	0.68	0.69	0.38	1.07
RIPK1	0.0	0.9	1.3	0.66	0.58	0.78	0.74	1.24
CLCC1	0.7	1.2	1.3	1.20	1.01	1.37	0.44	1.03
MAPK10	0.8	0.6	1.3	-1.11	0.00	-1.00	-3.36	-1.43
PLD3	1.2	1.1	1.3	1.07	0.90	1.05	1.21	0.98
TNFAIP8	1.2	0.6	1.2	1.10	1.41	1.17	1.24	1.52
SLC16A1	1.0	0.9	1.2	0.46	0.62	0.37	0.35	1.07
AK6	1.4	1.3	1.2	0.77	0.99	0.76	0.19	1.12
ENO3	0.9	0.7	1.2	-0.43	-0.38	-0.18	-0.57	-1.20
GNL3L	0.1	0.5	1.1	-0.84	-1.24	-0.16	0.37	-0.20
DDAH2	0.8	0.9	1.1	1.29	1.06	1.11	0.86	0.35
SRFBP1	0.9	0.4	1.1	-0.42	-0.29	-0.11	0.09	1.13
HSD11B1	0.0	0.0	1.1	-0.96	-1.00	-0.96	-0.39	0.37
LARP4	0.0	0.0	1.1	-0.83	-0.79	-1.01	-0.84	0.33
CBS	1.2	1.2	1.1	0.84	0.91	0.74	0.46	1.21
CRELD2	-1.0	-0.6	1.1	-0.93	-1.16	-1.21	-1.00	-0.97
PGD	1.2	1.0	1.1	0.97	0.90	0.91	0.95	1.13
RASA1	0.8	0.8	1.1	0.47	0.48	0.33	0.30	1.32
PHIP	0.3	0.3	1.0	-1.00	-0.63	-0.38	-0.83	0.05
PIK3R1	0.8	1.1	0.9	0.34	0.48	0.38	0.55	1.29
CHI3L1	1.0	1.1	0.8	1.86	1.64	1.83	1.71	1.83
GLRX	0.9	1.0	0.7	0.81	0.66	0.59	0.09	1.11
CWC27	0.8	1.4	0.6	0.92	0.95	0.69	0.37	1.10
MSRA	1.2	0.4	0.6	-0.50	-0.12	0.43	-1.21	-1.17
MYO5C	0.6	1.1	0.5	-0.74	-1.74	-2.17	-3.00	-1.00
ABCB10	0.2	0.8	0.5	-0.82	-0.75	-1.09	-0.74	0.19
CTNNA2	0.5	2.5	0.5	0.00	0.45	-0.81	-0.58	-1.12
MT-ND2	1.2	0.8	0.4	-0.50	-0.12	0.43	-1.21	-1.17
MRPS30	0.4	1.2	0.4	1.37	1.33	1.35	0.67	1.61
GK	0.7	1.1	0.3	0.33	0.39	0.57	0.30	1.02
MTO1	-1.1	0.5	0.3	-0.90	-0.75	-0.52	-1.06	-0.30
PIK3C2A	0.8	0.7	0.3	-1.02	-0.72	-0.43	-0.66	0.38

Table 14 continued

DNAJA4	-0.9	-1.3	0.2	-1.25	-0.97	-0.93	-1.40	-1.14
STAM	-1.1	0.1	0.0	-0.88	-0.75	-0.84	-1.05	-0.39
ATP2A3	-1.2	0.0	0.0	-0.67	-0.87	-0.85	-1.01	-1.52
STXBP5L	-1.5	0.0	0.0	-1.39	-1.44	-1.22	-1.47	-0.79
PRAM1	-2.0	0.0	0.0	-1.43	-1.74	-1.67	-1.94	-1.91
RAP1GAP2	-2.8	-1.2	0.0	-1.93	-2.20	-2.00	-2.40	-1.86
CLGN	-0.3	-1.3	0.0	-1.69	-1.56	-1.40	-1.92	-1.33
PM20D2	-1.6	-1.5	0.0	-1.64	-1.47	-1.47	-1.72	-0.70
DYNC2H1	-0.5	-3.6	0.0	-1.14	-1.25	-1.17	-1.30	-0.40
IGHA1	-3.5	-4.6	0.0	0.00	2.50	1.58	0.32	0.00
ARL6IP5	-1.1	0.0	-0.4	-0.51	-0.33	-0.58	-1.01	-0.03
UNC13D	-1.1	0.0	-0.4	-1.10	-1.30	-1.48	-1.36	-1.42
GEMIN2	2.9	0.4	-0.4	-0.53	-0.44	-1.06	-0.85	-0.16
LMO7	-0.7	-1.2	-0.5	-0.95	-0.64	-0.65	-1.36	-0.89
BMI1	-0.4	-1.6	-0.5	-1.55	-1.31	-1.30	-1.47	-0.21
NCF2	-0.8	-1.1	-0.7	-1.00	-0.91	-0.93	-1.24	-0.63
APP	-0.8	-1.4	-0.7	-1.07	-0.98	-1.14	-0.93	-0.27
EI24	-0.9	-1.0	-0.7	-0.80	-0.81	-0.93	-1.24	-0.73
CDK2AP1	-1.4	-1.2	-0.8	-0.58	-0.34	-0.60	-1.06	-0.39
SH2B2	-1.7	-1.3	-0.8	-0.76	-1.03	-0.87	-1.00	-0.77
SPATS2L	-1.2	-1.8	-0.9	-1.43	-1.50	-1.46	-1.50	-0.55
DCPS	-1.1	-1.1	-0.9	-1.10	-1.27	-1.26	-1.36	-1.11
SLC22A18	-1.0	0.0	-1.0	-0.21	-0.57	-0.50	-0.73	-1.04
NUDT19	0.0	-1.7	-1.0	-0.37	-0.45	-0.78	-1.18	-0.46
H1F0	-1.1	-1.2	-1.0	-0.66	-0.97	-1.19	-1.34	-0.96
PGM1	-0.9	-1.0	-1.0	-0.40	-0.63	-1.16	-0.92	-0.74
CTSZ	-1.3	-1.1	-1.0	-1.05	-1.05	-0.77	-0.80	-0.79
LY75	-1.3	-0.9	-1.1	-1.01	-0.99	-1.12	-0.79	-0.05
HK1	-1.1	-1.2	-1.1	-0.65	-0.77	-0.97	-1.24	-0.97
AIF1	-0.8	-1.2	-1.1	-0.41	-0.55	-0.74	-1.40	-0.66
CDK19	-0.9	0.0	-1.1	-0.66	-0.58	-0.96	-1.11	-0.53
ECHDC1	-1.0	-0.9	-1.1	-0.63	-0.59	-0.81	-1.00	-0.11
NLRX1	-1.2	-1.3	-1.1	-0.98	-1.17	-1.38	-1.26	-1.21
PDLIM1	-0.9	-1.0	-1.1	-0.35	-0.43	-0.43	-1.05	-0.65
HSP90AB4P	0.0	-0.2	-1.2	-0.32	0.81	2.58	-1.32	0.58
MYEF2	-1.4	-0.7	-1.2	-1.01	-0.82	-0.93	-1.41	-0.76
PITRM1	-1.2	-1.0	-1.2	-0.88	-0.91	-0.93	-1.12	-0.70
SYNJ2BP	-1.3	-0.8	-1.2	-1.07	-1.08	-0.98	-1.35	-0.29
MYO18A	-1.1	-1.0	-1.2	-0.80	-0.98	-0.81	-1.10	-1.54
RAB32	-1.3	-1.3	-1.2	-0.82	-0.97	-1.85	-1.49	-0.95
FLI1	-1.5	-1.0	-1.2	-0.75	-0.71	-1.03	-1.49	-0.67
TCEAL3	-1.4	-1.1	-1.3	-0.42	-0.61	-0.69	-1.11	-0.75
GCA	-1.5	-1.3	-1.3	-1.40	-1.13	-1.77	-1.68	-0.61

Table 14 continued

HIST2H2AA3	-0.4	-0.3	-1.3	0.83	0.57	0.84	1.91	0.83
PLD4	-1.1	-1.2	-1.4	-1.18	-1.48	-1.24	-1.06	-1.17
MARCKS	-1.7	-1.4	-1.5	-1.93	-1.67	-1.85	-0.91	0.26
IFT27	-0.9	-0.7	-1.7	-0.66	-0.68	-0.72	-1.23	-0.97
HINT3	-1.4	0.0	-1.7	-0.92	-0.70	-1.12	-0.94	-0.07
CKAP4	-1.9	-1.4	-1.7	-0.52	-0.73	-1.16	-1.02	-0.46
NRGN	-1.6	-1.3	-1.7	-0.68	-1.11	-0.80	-1.32	-1.62
ST14	-1.6	-0.9	-1.8	-1.57	-1.79	-1.77	-1.55	-1.79
LARP4B	-0.8	-1.1	-1.9	-0.90	-0.83	-0.79	-1.01	-0.61
CLEC11A	-1.3	-0.9	-2.0	-0.68	-1.23	-1.20	-0.81	-1.31
S100A8	-2.2	-2.4	-2.1	-1.02	-1.05	-1.20	-2.06	-1.27
S100A9	-2.4	-2.6	-2.3	-1.57	-1.80	-2.01	-1.95	-1.44
C7orf55	-0.1	-0.1	-2.4	-0.02	-0.32	-0.62	-0.74	-1.09
BIK	-2.1	-1.6	-2.8	-0.97	-1.30	-1.41	-1.75	-1.53
NR2E3	-3.6	-3.6	-3.7	-0.58	0.00	2.34	0.00	0.00
TGM3	-1.7	-4.0	-4.4	-2.25	0.00	0.58	-1.22	-2.64
GSDMA	-3.4	-2.2	-6.1	-1.93	-2.58	-2.58	-2.00	-0.87
NFIA	-1.1	-8.2	-8.0	-0.74	-1.58	-1.42	-1.58	-0.81
NFIB	-1.1	-8.2	-8.0	0.00	-1.59	-2.25	0.00	0.02

To investigate the biological functions of genes up-regulated by OAS1, functional annotation analysis was performed using DAVID bioinformatics tools (Methods 2.22.2) (Fig. 45). As expected, we found several genes that were involved in innate immune signaling pathways. For example, RLRs, C3 complement protein and IFIT 1-3. The role of IFIT proteins in antiviral immunity has been well established (166, 167, 300, 457), suggesting that OAS1 may provide broad antiviral protection through the activation of transcription factors and expression of several ISGs. Additionally, several GBP proteins were up-regulated, which are regulated by IRF1 and confer antibacterial activity through inflammasome activation (Chapter 4, Fig. 39) (124, 205, 430).

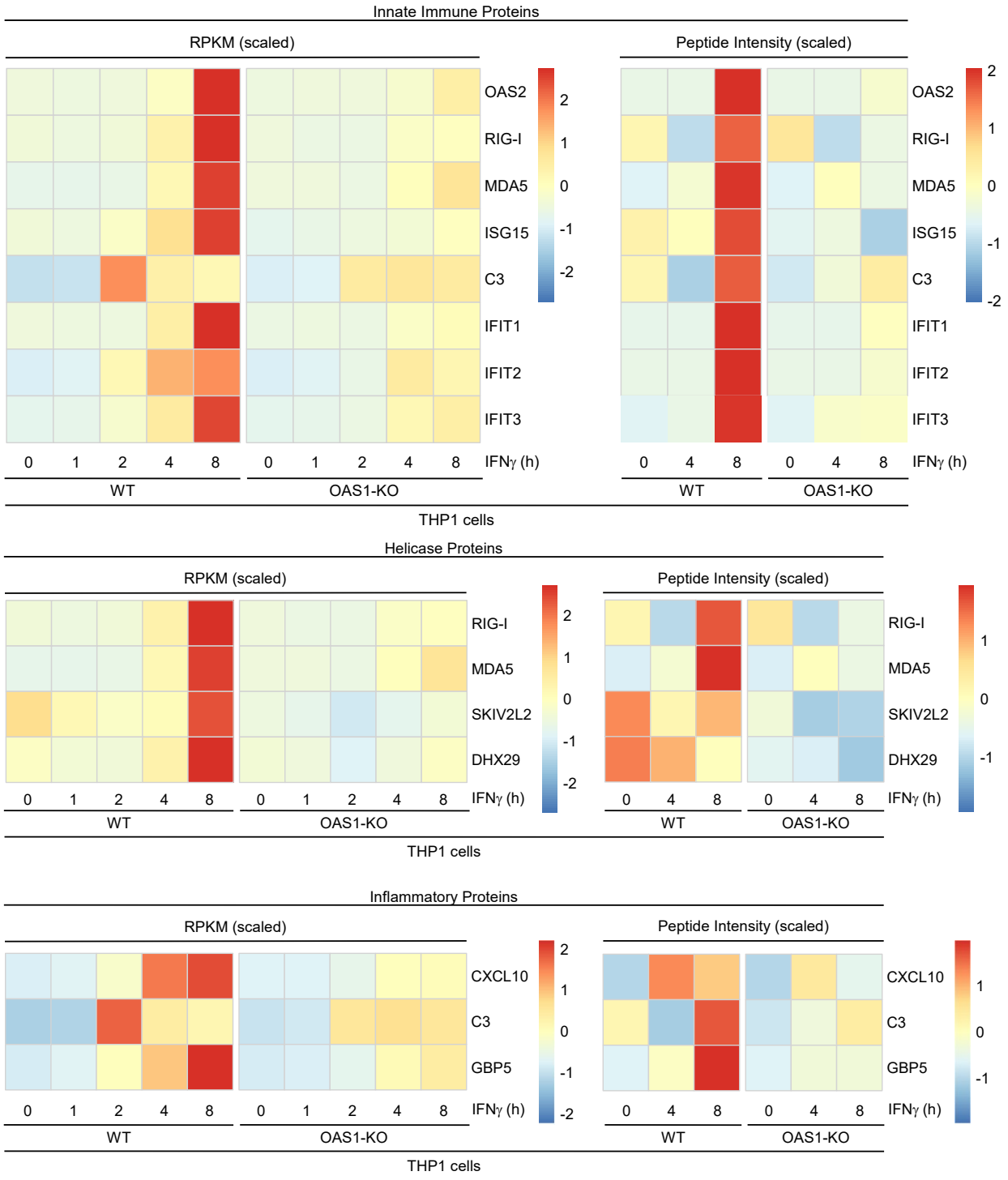

Figure 45. Potential roles for proteins transcriptionally regulated by OAS1
The list of genes from Table 14 were uploaded and submitted to the online DAVID bioinformatics tool. Function annotation analysis was performed to predict major biological functions associated to genes transcriptionally regulated by OAS1. The data is represented as heatmaps using Z-scored scaled RPKM and peptide intensity values of WT and OAS1-KO cells.

All together our proteomic and transcriptome analysis revealed that OAS1 enhanced the levels of several basal and IFNγ-inducible proteins by directly enhancing mRNA translation or regulating gene transcription through transcription factors. These proteins have broad functions, including regulating transcription, inflammation, antiviral defense and antimicrobial immunity. As we have done with cGAS and IRF1, this dataset serves a starting point to study the relationship between OAS1 and several other proteins described here, which are beyond the scope of my dissertation.

Bibliography

1. Doherty, M., and M. J. Robertson. 2004. Some early Trends in Immunology. *Trends Immunol.* 25: 623–631.

2. Sattler, S. 2017. The role of the immune system beyond the fight against infection. In *Advances in Experimental Medicine and Biology* vol. 1003. Springer New York LLC. 3–14.

3. Janeway, C. A. 2013. Pillars article: approaching the asymptote? Evolution and revolution in immunology. Cold spring harb symp quant biol. 1989. 54: 1-13. *J. Immunol.* 191: 4475–87.

4. Amarante-Mendes, G. P., S. Adjemian, L. M. Branco, L. C. Zanetti, R. Weinlich, and K. R. Bortoluci. 2018. Pattern recognition receptors and the host cell death molecular machinery. *Front. Immunol.* 9: 2379.

5. Beutler, B. 2004. Innate immunity: an overview. *Mol. Immunol.* 40: 845–859.

6. Albiger, B., S. Dahlberg, B. Henriques-Normark, and S. Normark. 2007. Role of the innate immune system in host defence against bacterial infections: focus on the Toll-like receptors. *J. Intern. Med.* 261: 511–528.

7. Kovarik, P., V. Castiglia, M. Ivin, and F. Ebner. 2016. Type I interferons in bacterial infections: A balancing act. *Front. Immunol.* 7: 1–8.

8. Hoffmann, H.-H., W. M. Schneider, and C. M. Rice. 2015. Interferons and viruses: an evolutionary arms race of molecular interactions. *Trends Immunol.* 36: 124–138.

9. Yan, N., and Z. J. Chen. 2012. Intrinsic antiviral immunity. *Nat. Immunol.* 13: 214–222.

10. Banerjee, S., A. Chakrabarti, B. K. Jha, S. R. Weiss, and R. H. Silverman. 2014. Cell-Type-Specific Effects of RNase L on Viral Induction of Beta Interferon. *MBio* 5.

11. Kristiansen, H., H. H. Gad, S. Eskildsen-Larsen, P. Despres, and R. Hartmann. 2011. The Oligoadenylate Synthetase Family: An Ancient Protein Family with Multiple Antiviral Activities. *J. Interf. Cytokine Res.* 31: 41–47.

12. Leisching, G., V. Cole, A. T. Ali, and B. Baker. 2019. OAS1, OAS2 and OAS3 restrict intracellular M. tb replication and enhance cytokine secretion. *Int. J. Infect. Dis.* 80: S77–S84.

13. Zhu, J., Y. Zhang, A. Ghosh, R. A. Cuevas, A. Forero, J. Dhar, M. S. Ibsen, J. L. Schmid-Burgk, T. Schmidt, M. K. Ganapathiraju, T. Fujita, R. Hartmann, S. Barik, V. Hornung, C. B. Coyne, and S. N. Sarkar. 2014. Antiviral Activity of Human OASL Protein Is Mediated by Enhancing Signaling of the RIG-I RNA Sensor. *Immunity* 40: 936–948.

14. Eskildsen, S., R. Hartmann, N. O. Kjeldgaard, and J. Justesen. 2002. Gene structure of the murine 2′-5′-oligoadenylate synthetase family. *Cell. Mol. Life Sci.* 59: 1212–1222.

15. Diamond, M. S., and M. Gale. 2012. Cell-intrinsic innate immune control of West Nile virus infection. *Trends Immunol.* 33: 522–530.

16. Mashimo, T., M. Lucas, D. Simon-Chazottes, M. P. Frenkiel, X. Montagutelli, P. E. Ceccaldi, V. Deubel, J. L. Guénet, and P. Desprès. 2002. A nonsense mutation in the gene encoding 2′-5′-oligoadenylate synthetase/L1 isoform is associated with West Nile virus susceptibility in laboratory mice. *Proc. Natl. Acad. Sci. U. S. A.* 99: 11311–11316.

17. Li, Y., S. Banerjee, Y. Wang, S. A. Goldstein, B. Dong, C. Gaughan, R. H. Silverman, and S. R. Weiss. 2016. Activation of RNase L is dependent on OAS3 expression during infection with diverse human viruses. *Proc. Natl. Acad. Sci.* 113: 2241–2246.

18. Gasteiger, G., A. D'osualdo, D. A. Schubert, A. Weber, E. M. Bruscia, and D. Hartl. 2017. Cellular Innate Immunity: An Old Game with New Players. *J. Innate Immun.* 9: 111–125.

19. Luo, Y., and S. G. Zheng. 2016. Hall of fame among pro-inflammatory cytokines: Interleukin-6 gene and its transcriptional regulation mechanisms. *Front. Immunol.* 7: 604.

20. Sokol, C. L., and A. D. Luster. 2015. The chemokine system in innate immunity. *Cold Spring Harb. Perspect. Biol.* 7: 1–20.

21. Dunkelberger, J. R., and W. C. Song. 2010. Complement and its role in innate and adaptive immune responses. *Cell Res.* 20: 34–50.

22. Mahlapuu, M., J. Håkansson, L. Ringstad, and C. Björn. 2016. Antimicrobial peptides: An emerging category of therapeutic agents. *Front. Cell. Infect. Microbiol.* 6.

23. Lemaitre, B., E. Nicolas, L. Michaut, J. M. Reichhart, and J. A. Hoffmann. 1996. The dorsoventral regulatory gene cassette spatzle/Toll/Cactus controls the potent antifungal response in Drosophila adults. *Cell* 86: 973–983.

24. Poltorak, A., X. He, I. Smirnova, M. Y. Liu, C. Van Huffel, X. Du, D. Birdwell, E. Alejos, M. Silva, C. Galanos, M. Freudenberg, P. Ricciardi-Castagnoli, B. Layton, and B. Beutler. 1998. Defective LPS signaling in C3H/HeJ and C57BL/10ScCr mice: Mutations in Tlr4 gene. *Science (80-.).* 282: 2085–2088.

25. Kawasaki, T., and T. Kawai. 2014. Toll-like receptor signaling pathways. *Front. Immunol.* 5: 461.

26. Bell, J. K., G. E. D. Mullen, C. A. Leifer, A. Mazzoni, D. R. Davies, and D. M. Segal. 2003. Leucine-rich repeats and pathogen recognition in Toll-like receptors. *Trends Immunol.* 24: 528–533.

27. Zheng, C., J. Chen, F. Chu, J. Zhu, and T. Jin. 2020. Inflammatory Role of TLR-MyD88 Signaling in Multiple Sclerosis. *Front. Mol. Neurosci.* 12.

28. Takeda, K., and S. Akira. 2004. TLR signaling pathways. *Semin. Immunol.* 16: 3–9.

29. Zhang, Q., M. J. Lenardo, and D. Baltimore. 2017. Leading Edge Review 30 Years of NF-kB: A Blossoming of Relevance to Human Pathobiology. .

30. Deng, L., C. Wang, E. Spencer, L. Yang, A. Braun, J. You, C. Slaughter, C. Pickart, and Z. J. Chen. 2000. Activation of the Iκb kinase complex by TRAF6 requires a dimeric ubiquitin-conjugating enzyme complex and a unique polyubiquitin chain. *Cell* 103: 351–361.

31. Zheng, C., Q. Yin, and H. Wu. 2010. Structural studies of NF-κB signaling. *Nat. Publ. Gr.* 21: 183–195.

32. Zhao, J., L. Zhang, X. Mu, C. Doebelin, W. Nguyen, C. Wallace, D. P. Reay, S. J. McGowan, L. Corbo, P. R. Clemens, G. M. Wilson, S. C. Watkins, L. A. Solt, M. D. Cameron, J. Huard, L. J. Niedernhofer, T. M. Kamenecka, and P. D. Robbins. 2018. Development of novel NEMO-binding domain mimetics for inhibiting IKK/NF-κB activation. *PLOS Biol.* 16: e2004663.

33. Hinz, M., and C. Scheidereit. 2014. The IκB kinase complex in <scp>NF</scp> -κB regulation and beyond. *EMBO Rep.* 15: 46–61.

34. Baud, V., and M. Karin. 2009. Is NF-κB a good target for cancer therapy? Hopes and pitfalls. *Nat. Rev. Drug Discov.* 8: 33–40.

35. Zhao, M., J. Joy, W. Zhou, S. De, W. H. Wood, K. G. Becker, H. Ji, and R. Sen. 2018. Transcriptional outcomes and kinetic patterning of gene expression in response to NF-κB activation. *PLOS Biol.* 16: e2006347.

36. Karin, M., Z.-G. Liu, and E. Zandi. 1997. AP-1 function and regulation. *Curr. Opin. Cell Biol.* 9: 940–246.

37. Mason, N. J., J. Fiore, † Takashi Kobayashi, K. S. Masek, Y. Choi, and C. A. Hunter. 2004. TRAF6-Dependent Mitogen-Activated Protein Kinase Activation Differentially Regulates the Production of Interleukin-12 by Macrophages in Response to Toxoplasma gondii. *Infect. Immun.* 72: 5662–5667.

38. Shi, J. H., and S. C. Sun. 2018. Tumor necrosis factor receptor-associated factor regulation of nuclear factor κB and mitogen-activated protein kinase pathways. *Front. Immunol.* 9: 1849.

39. Hasselblatt, P., M. Rath, V. Komnenovic, K. Zatloukal, and E. F. Wagner. 2007. Hepatocyte survival in acute hepatitis is due to c-Jun/AP-1-dependent expression of inducible nitric oxide synthase. *Proc. Natl. Acad. Sci. U. S. A.* 104: 17105–17110.

40. Eferl, R., M. Sibilia, F. Hilberg, A. Fuchsbichler, I. Kufferath, B. Guertl, R. Zenz, E. F. Wagner, and K. Zatloukal. 1999. Functions of c-Jun in liver and heart development. *J. Cell Biol.* 145: 1049–1061.

41. Yamamoto, M., S. Sato, H. Hemmi, K. Hoshino, T. Kaisho, H. Sanjo, O. Takeuchi, M.

Sugiyama, M. Okabe, K. Takeda, and S. Akira. 2003. Role of adaptor TRIF in the MyD88-independent toll-like receptor signaling pathway. *Science (80-.).* 301: 640–643.

42. Kawai, T., O. Takeuchi, T. Fujita, J. Inoue, P. F. Mühlradt, S. Sato, K. Hoshino, and S. Akira. 2001. Lipopolysaccharide Stimulates the MyD88-Independent Pathway and Results in Activation of IFN-Regulatory Factor 3 and the Expression of a Subset of Lipopolysaccharide-Inducible Genes. *J. Immunol.* 167: 5887–5894.

43. Li, F., Y. Li, H. Liang, T. Xu, Y. Kong, M. Huang, J. Xiao, X. Chen, H. Xia, Y. Wu, Z. Zhou, X. Guo, C. Hu, C. Yang, X. Cheng, C. Chen, and X. Qi. 2018. HECTD3 mediates TRAF3 polyubiquitination and type I interferon induction during bacterial infection. *J. Clin. Invest.* 128: 4148–4162.

44. Lin, W. W., B. S. Hostager, and G. A. Bishop. 2015. TRAF3, ubiquitination, and B-lymphocyte regulation. *Immunol. Rev.* 266: 46–55.

45. Häcker, H., P. H. Tseng, and M. Karin. 2011. Expanding TRAF function: TRAF3 as a tri-faced immune regulator. *Nat. Rev. Immunol.* 11: 457–468.

46. Häcker, H., and M. Karin. *Regulation and Function of IKK and IKK-Related Kinases*,.

47. Platnich, J. M., and D. A. Muruve. 2019. NOD-like receptors and inflammasomes: A review of their canonical and non-canonical signaling pathways. .

48. Broz, P., and V. M. Dixit. 2016. Inflammasomes: Mechanism of assembly, regulation and signalling. *Nat. Rev. Immunol.* 16: 407–420.

49. Lamkanfi, M., and V. M. Dixit. 2014. Mechanisms and functions of inflammasomes. *Cell* 157: 1013–1022.

50. Loo, Y. M., and M. Gale. 2011. Immune Signaling by RIG-I-like Receptors. *Immunity* 34: 680–692.

51. Chow, K. T., M. Gale, and Y.-M. Loo. 2018. RIG-I and Other RNA Sensors in Antiviral Immunity. .

52. Yoneyama, M., M. Kikuchi, K. Matsumoto, T. Imaizumi, M. Miyagishi, K. Taira, E. Foy, Y.-M. Loo, M. Gale, S. Akira, S. Yonehara, A. Kato, and T. Fujita. 2005. Shared and Unique Functions of the DExD/H-Box Helicases RIG-I, MDA5, and LGP2 in Antiviral Innate Immunity. *J. Immunol.* 175: 2851–2858.

53. Satoh, T., H. Kato, Y. Kumagai, M. Yoneyama, S. Sato, K. Matsushita, T. Tsujimura, T. Fujita, S. Akira, and O. Takeuchi. 2010. LGP2 is a positive regulator of RIG-I- and MDA5-mediated antiviral responses. *Proc. Natl. Acad. Sci. U. S. A.* 107: 1512–1517.

54. Yoneyama, M., M. Kikuchi, T. Natsukawa, N. Shinobu, T. Imaizumi, M. Miyagishi, K. Taira, S. Akira, and T. Fujita. 2004. The RNA helicase RIG-I has an essential function in double-stranded RNA-induced innate antiviral responses. *Nat. Immunol.* 5: 730–737.

55. Kolakofsky, D., E. Kowalinski, and S. Cusack. 2012. A structure-based model of RIG-I activation. *RNA* 18: 2118–2127.

56. Schmidt, A., T. Schwerd, W. Hamm, J. C. Hellmuth, S. Cui, M. Wenzel, F. S. Hoffmann, M. C. Michallet, R. Besch, K. P. Hopfner, S. Endres, and S. Rothenfusser. 2009. 5′-triphosphate RNA requires base-paired structures to activate antiviral signaling via RIG-I. *Proc. Natl. Acad. Sci. U. S. A.* 106: 12067–12072.

57. Goubau, D., M. Schlee, S. Deddouche, A. J. Pruijssers, T. Zillinger, M. Goldeck, C. Schuberth, A. G. Van Der Veen, T. Fujimura, J. Rehwinkel, J. A. Iskarpatyoti, W. Barchet, J. Ludwig, T. S. Dermody, G. Hartmann, and C. Reis E Sousa. 2014. Antiviral immunity via RIG-I-mediated recognition of RNA bearing 59-diphosphates. *Nature* 514: 372–375.

58. Schuberth-Wagner, C., J. Ludwig, A. K. Bruder, A. M. Herzner, T. Zillinger, M. Goldeck, T. Schmidt, J. L. Schmid-Burgk, R. Kerber, S. Wolter, J. P. Stümpel, A. Roth, E. Bartok, C. Drosten, C. Coch, V. Hornung, W. Barchet, B. M. Kümmerer, G. Hartmann, and M. Schlee. 2015. A Conserved Histidine in the RNA Sensor RIG-I Controls Immune Tolerance to N1-2'O-Methylated Self RNA. *Immunity* 43: 41–51.

59. Rehwinkel, J., and M. U. Gack. 2020. RIG-I-like receptors: their regulation and roles in RNA sensing. *Nat. Rev. Immunol.* 1–15.

60. Cadena, C., S. Ahmad, A. Xavier, J. Willemsen, S. Park, J. W. Park, S. W. Oh, T. Fujita, F. Hou, M. Binder, and S. Hur. 2019. Ubiquitin-Dependent and -Independent Roles of E3 Ligase RIPLET in Innate Immunity. *Cell* 177: 1187-1200.e16.

61. Kawai, T., K. Takahashi, S. Sato, C. Coban, H. Kumar, H. Kato, K. J. Ishii, O. Takeuchi, and S. Akira. 2005. IPS-1, an adaptor triggering RIG-I- and Mda5-mediated type I interferon induction. *Nat. Immunol.* 6: 981–988.

62. Jiang, X., L. N. Kinch, C. A. Brautigam, X. Chen, F. Du, N. V. Grishin, and Z. J. Chen. 2012. Ubiquitin-Induced Oligomerization of the RNA Sensors RIG-I and MDA5 Activates Antiviral Innate Immune Response. *Immunity* 36: 959–973.

63. Berke, I. C., and Y. Modis. 2012. MDA5 cooperatively forms dimers and ATP-sensitive filaments upon binding double-stranded RNA. *EMBO J.* 31: 1714–1726.

64. Wu, B., A. Peisley, C. Richards, H. Yao, X. Zeng, C. Lin, F. Chu, T. Walz, and S. Hur. 2013. Structural Basis for dsRNA Recognition, Filament Formation, and Antiviral Signal Activation by MDA5. *Cell* 152: 276–289.

65. Brisse, M., and H. Ly. 2019. Comparative structure and function analysis of the RIG-I-like receptors: RIG-I and MDA5. *Front. Immunol.* 10: 1586.

66. Sen, G. C., and S. N. Sarkar. 2005. Hitching RIG to action. *Nat. Immunol.* 6: 1074–1076.

67. Seth, R. B., L. Sun, C. K. Ea, and Z. J. Chen. 2005. Identification and characterization

of MAVS, a mitochondrial antiviral signaling protein that activates NF-κB and IRF3. *Cell* 122: 669–682.

68. Zhang, P., A. Reichardt, H. Liang, R. Aliyari, D. Cheng, Y. Wang, F. Xu, G. Cheng, and Y. Liu. 2012. Single amino acid substitutions confer the antiviral activity of the TRAF3 adaptor protein onto TRAF5. *Sci. Signal.* 5: ra81–ra81.

69. Shi, Z., Z. Zhang, Z. Zhang, Y. Wang, C. Li, X. Wang, F. He, L. Sun, S. Jiao, W. Shi, and Z. Zhou. 2015. Structural insights into mitochondrial antiviral signaling protein (MAVS)-Tumor necrosis factor receptor-associated factor 6 (TRAF6) signaling. *J. Biol. Chem.* 290: 26811–26820.

70. Vazquez, C., and S. M. Horner. 2015. MAVS Coordination of Antiviral Innate Immunity. *J. Virol.* 89: 6974–6977.

71. Hou, F., L. Sun, H. Zheng, B. Skaug, Q. X. Jiang, and Z. J. Chen. 2011. MAVS forms functional prion-like aggregates to activate and propagate antiviral innate immune response. *Cell* 146: 448–461.

72. Refolo, G., T. Vescovo, M. Piacentini, G. M. Fimia, and F. Ciccosanti. 2020. Mitochondrial Interactome: A Focus on Antiviral Signaling Pathways. *Front. Cell Dev. Biol.* 8: 8.

73. Stetson, D. B., and R. Medzhitov. 2006. Recognition of cytosolic DNA activates an IRF3-dependent innate immune response. *Immunity* 24: 93–103.

74. Ishikawa, H., and G. N. Barber. 2008. STING is an endoplasmic reticulum adaptor that facilitates innate immune signalling. *Nature* 455: 674–678.

75. Ishikawa, H., Z. Ma, and G. N. Barber. 2009. STING regulates intracellular DNA-mediated, type I interferon-dependent innate immunity. *Nature* 461: 788–792.

76. Wu, J., L. Sun, X. Chen, F. Du, H. Shi, C. Chen, and Z. J. Chen. 2013. Cyclic GMP-AMP is an endogenous second messenger in innate immune signaling by cytosolic DNA. *Science (80-.).* 339: 826–830.

77. Burdette, D. L., K. M. Monroe, K. Sotelo-Troha, J. S. Iwig, B. Eckert, M. Hyodo, Y. Hayakawa, and R. E. Vance. 2011. STING is a direct innate immune sensor of cyclic di-GMP. *Nature* 478: 515–518.

78. Ablasser, A., M. Goldeck, T. Cavlar, T. Deimling, G. Witte, I. Röhl, K. P. Hopfner, J. Ludwig, and V. Hornung. 2013. CGAS produces a 2′-5′-linked cyclic dinucleotide second messenger that activates STING. *Nature* 498: 380–384.

79. Civril, F., T. Deimling, C. C. De Oliveira Mann, A. Ablasser, M. Moldt, G. Witte, V. Hornung, and K. P. Hopfner. 2013. Structural mechanism of cytosolic DNA sensing by cGAS. *Nature* 498: 332–337.

80. Li, X., C. Shu, G. Yi, C. T. Chaton, C. L. Shelton, J. Diao, X. Zuo, C. C. Kao, A. B.

Herr, and P. Li. 2013. Cyclic GMP-AMP Synthase Is Activated by Double-Stranded DNA-Induced Oligomerization. *Immunity* 39: 1019–1031.

81. Zhou, W., A. T. Whiteley, C. C. de Oliveira Mann, B. R. Morehouse, R. P. Nowak, E. S. Fischer, N. S. Gray, J. J. Mekalanos, and P. J. Kranzusch. 2018. Structure of the Human cGAS–DNA Complex Reveals Enhanced Control of Immune Surveillance. *Cell* 174: 300-311.e11.

82. Motwani, M., S. Pesiridis, and K. A. Fitzgerald. 2019. DNA sensing by the cGAS–STING pathway in health and disease. *Nat. Rev. Genet.* 20: 657–674.

83. Shang, G., C. Zhang, Z. J. Chen, X.-C. Bai, and X. Zhang. Cryo-EM structures of STING reveal its mechanism of activation by cyclic GMP-AMP. *Nature* .

84. Tanaka, Y., and Z. J. Chen. 2012. STING specifies IRF3 phosphorylation by TBK1 in the cytosolic DNA signaling pathway. *Sci. Signal.* 5: ra20.

85. Zhao, B., F. Du, P. Xu, C. Shu, B. Sankaran, S. L. Bell, M. Liu, Y. Lei, X. Gao, X. Fu, F. Zhu, Y. Liu, A. Laganowsky, X. Zheng, J. Y. Ji, A. P. West, R. O. Watson, and P. Li. 2019. A conserved PLPLRT/SD motif of STING mediates the recruitment and activation of TBK1. *Nature* 569: 718–722.

86. Dunphy, G., M. Flannery, J. F. Almine, M. M. Nevels, and A. G. Bowie. 2018. Non-canonical Activation of the DNA Sensing Adaptor STING by ATM and IFI16 Mediates NF-κB Signaling after Nuclear DNA Damage. .

87. Fang, R., C. Wang, Q. Jiang, M. Lv, P. Gao, X. Yu, P. Mu, R. Zhang, S. Bi, J.-M. Feng, and Z. Jiang. 2017. NEMO–IKKβ Are Essential for IRF3 and NF-κB Activation in the cGAS–STING Pathway. *J. Immunol.* 199: 3222–3233.

88. 1957. Virus interference. I. The interferon. *Proc. R. Soc. London. Ser. B - Biol. Sci.* 147: 258–267.

89. Stein, S., C. Kenny, and H. J. Friesen. 1980. NH2-terminal amino acid sequence of human fibroblast interferon. *Proc. Natl. Acad. Sci. U. S. A.* 77: 5716–5719.

90. Rubinstein, M., W. P. Levy, J. A. Moschera, C. Y. Lai, R. D. Hershberg, R. T. Bartlett, and S. Pestka. 1981. Human leukocyte interferon: Isolation and characterization of several molecular forms. *Arch. Biochem. Biophys.* 210: 307–318.

91. Rubinstein, M., S. Rubinstein, P. C. Familletti, R. S. Miller, A. A. Waldman, and S. Pestka. 1979. Human leukocyte interferon: Production, purification to homogeneity, and initial characterization. *Proc. Natl. Acad. Sci. U. S. A.* 76: 640–644.

92. Pestka, S., J. A. Langer, K. C. Zoon, and C. E. Samuel. 1987. Interferons and their Actions. *Annu. Rev. Biochem.* 56: 727–777.

93. Pestka, S., C. D. Krause, and M. R. Walter. 2004. Interferons, interferon-like cytokines, and their receptors. *Immunol. Rev.* 202: 8–32.

94. Castro, F., A. P. Cardoso, R. M. Gonçalves, K. Serre, and M. J. Oliveira. 2018. Interferon-gamma at the crossroads of tumor immune surveillance or evasion. *Front. Immunol.* 9: 847.

95. Wack, A., E. Terczyńska-Dyla, and R. Hartmann. 2015. Guarding the frontiers: The biology of type III interferons. *Nat. Immunol.* 16: 802–809.

96. Pestka, S., C. D. Krause, M. R. Walter, and S. Petska. *Interferons, interferon-like cytokines, and their receptors*,.

97. Schneider, W. M., M. D. Chevillotte, and C. M. Rice. 2014. Interferon-Stimulated Genes: A Complex Web of Host Defenses. *Annu. Rev. Immunol.* 32: 513–545.

98. Steen, H. C., and A. M. Gamero. 2013. STAT2 phosphorylation and signaling. *JAK-STAT* 2: e25790.

99. Lazear, H. M., J. W. Schoggins, and M. S. Diamond. 2019. Immunity Review Shared and Distinct Functions of Type I and Type III Interferons. .

100. Li, S. F., M. J. Gong, F. R. Zhao, J. J. Shao, Y. L. Xie, Y. G. Zhang, and H. Y. Chang. 2018. Type i interferons: Distinct biological activities and current applications for viral infection. *Cell. Physiol. Biochem.* 51: 2377–2396.

101. Divangahi, M., J. Zhu, A. Lamarre, A. A. Ashkar, and A. J. Lee. 2018. The Dual Nature of Type I and Type II Interferons. *Cit. Lee AJ Ashkar AA* 9: 2061.

102. Boxx, G. M., and G. Cheng. 2016. The Roles of Type i Interferon in Bacterial Infection. *Cell Host Microbe* 19: 760–769.

103. Shtrichman, R., and C. E. Samuel. 2001. The role of gamma interferon in antimicrobial immunity. *Curr. Opin. Microbiol.* 4: 251–259.

104. Tretina, K., E. S. Park, A. Maminska, and J. D. MacMicking. 2019. Interferon-induced guanylate-binding proteins: Guardians of host defense in health and disease. *J. Exp. Med.* 216: 482–500.

105. Assani, K., M. F. Tazi, A. O. Amer, and B. T. Kopp. 2014. IFN-γ Stimulates Autophagy-Mediated Clearance of Burkholderia cenocepacia in Human Cystic Fibrosis Macrophages. *PLoS One* 9: e96681.

106. Bhat, P., G. Leggatt, N. Waterhouse, and I. H. Frazer. 2017. Interferon-γ derived from cytotoxic lymphocytes directly enhances their motility and cytotoxicity. *Cell Death Dis.* 8: e2836.

107. Odendall, C., A. A. Voak, and J. C. Kagan. 2017. Type III IFNs Are Commonly Induced by Bacteria-Sensing TLRs and Reinforce Epithelial Barriers during Infection. *J. Immunol.* 199: 3270–3279.

108. Zhou, J., Y. Wang, Q. Chang, P. Ma, Y. Hu, and X. Cao. 2018. Type III Interferons

in Viral Infection and Antiviral Immunity. *Cell. Physiol. Biochem.* 51: 173–185.

109. Yamamoto, M., T. Kato, C. Hotta, A. Nishiyama, D. Kurotaki, M. Yoshinari, M. Takami, M. Ichino, M. Nakazawa, T. Matsuyama, R. Kamijo, S. Kitagawa, K. Ozato, and T. Tamura. 2011. Shared and Distinct Functions of the Transcription Factors IRF4 and IRF8 in Myeloid Cell Development. *PLoS One* 6: e25812.

110. Kröger, A. 2017. IRFs as competing pioneers in T-cell differentiation. *Cell. Mol. Immunol.* 14: 649–651.

111. Lien, C., C. M. Fang, D. Huso, F. Livak, R. Lu, and P. M. Pitha. 2010. Critical role of IRF-5 in regulation of B-cell differentiation. *Proc. Natl. Acad. Sci. U. S. A.* 107: 4664–4668.

112. Gabriele, L., and K. Ozato. 2007. The role of the interferon regulatory factor (IRF) family in dendritic cell development and function. *Cytokine Growth Factor Rev.* 18: 503–510.

113. Yanai, H., H. Negishi, and T. Taniguchi. 2012. The IRF family of transcription factors inception, impact and implications in oncogenesis. *Oncoimmunology* 1: 1376–1386.

114. Tamura, T., H. Yanai, D. Savitsky, and T. Taniguchi. 2008. The IRF Family Transcription Factors in Immunity and Oncogenesis. *Annu. Rev. Immunol.* 26: 535–584.

115. Mogensen, T. H. 2019. IRF and STAT transcription factors - From basic biology to roles in infection, protective immunity, and primary immunodeficiencies. *Front. Immunol.* 10: 3047.

116. Taniguchi, T., K. Ogasawara, A. Takaoka, and N. Tanaka. 2001. IRF F AMILY OF T RANSCRIPTION F ACTORS AS R EGULATORS OF H OST D EFENSE. *Annu. Rev. Immunol.* 19: 623–655.

117. Paun, A., and P. M. Pitha. 2007. The IRF family, revisited. *Biochimie* 89: 744–753.

118. Honda, K., A. Takaoka, and T. Taniguchi. 2006. Review Type I Inteferon Gene Induction by the Interferon Regulatory Factor Family of Transcription Factors. *Immunity* 25: 349–360.

119. Lohoff, M., and T. W. Mak. 2005. Roles of interferon-regulatory factors in T-helper-cell differentiation. *Nat. Rev. Immunol.* 5: 125–135.

120. Kröger, A., M. Köster, K. Schroeder, H. Hauser, and P. P. Mueller. 2002. Review: Activities of IRF-1. *J. Interf. Cytokine Res.* 22: 5–14.

121. Giang, S., and A. La Cava. 2017. IRF1 and BATF: Key drivers of type 1 regulatory T-cell differentiation. *Cell. Mol. Immunol.* 14: 652–654.

122. Lohoff, M., and T. W. Mak. 2005. Roles of interferon-regulatory factors in T-helper-cell differentiation. *Nat. Rev. Immunol.* 5: 125–135.

123. Langlais, D., L. B. Barreiro, and P. Gros. 2016. The macrophage IRF8/IRF1 regulome is required for protection against infections and is associated with chronic inflammation. *J. Exp. Med.* 213: 585–603.

124. Man, S. M., R. Karki, R. K. S. Malireddi, G. Neale, P. Vogel, M. Yamamoto, M. Lamkanfi, and T.-D. Kanneganti. 2015. The transcription factor IRF1 and guanylate-binding proteins target activation of the AIM2 inflammasome by Francisella infection. *Nat. Immunol.* 16: 467–475.

125. Kuriakose, T., M. Zheng, G. Neale, and T.-D. Kanneganti. 2018. IRF1 Is a Transcriptional Regulator of ZBP1 Promoting NLRP3 Inflammasome Activation and Cell Death during Influenza Virus Infection. *J. Immunol.* 200: 1489–1495.

126. Ohsugi, T., K. Yamaguchi, C. Zhu, T. Ikenoue, K. Takane, M. Shinozaki, G. Tsurita, H. Yano, and Y. Furukawa. 2019. Anti-apoptotic effect by the suppression of IRF1 as a downstream of Wnt/β-catenin signaling in colorectal cancer cells. *Oncogene* 38: 6051–6064.

127. Antonczyk, A., B. Krist, M. Sajek, A. Michalska, A. Piaszyk-Borychowska, M. Plens-Galaska, J. Wesoly, and H. A. R. Bluyssen. 2019. Direct inhibition of IRF-dependent transcriptional regulatory mechanisms associated with disease. *Front. Immunol.* 10: 1176.

128. Honda, K., T. Mizutani, and T. Taniguchi. 2004. Negative regulation of IFN-α/β signaling by IFN regulatory factor 2 for homeostatic development of dendritic cells. *Proc. Natl. Acad. Sci. U. S. A.* 101: 2416–2421.

129. Honey, K. 2004. IRF2 directs cell distinction. *Nat. Rev. Immunol.* 4: 322–322.

130. Kriegsman, B. A., P. Vangala, B. J. Chen, P. Meraner, A. L. Brass, M. Garber, and K. L. Rock. 2019. Frequent Loss of IRF2 in Cancers Leads to Immune Evasion through Decreased MHC Class I Antigen Presentation and Increased PD-L1 Expression. *J. Immunol.* 203: 1999–2010.

131. Hiscott, J. 2007. Triggering the innate antiviral response through IRF-3 activation. *J. Biol. Chem.* 282: 15325–15329.

132. Lazear, H. M., A. Lancaster, C. Wilkins, M. S. Suthar, A. Huang, S. C. Vick, L. Clepper, L. Thackray, M. M. Brassil, H. W. Virgin, J. Nikolich-Zugich, A. V. Moses, M. Gale, K. Früh, and M. S. Diamond. 2013. IRF-3, IRF-5, and IRF-7 Coordinately Regulate the Type I IFN Response in Myeloid Dendritic Cells Downstream of MAVS Signaling. *PLoS Pathog.* 9.

133. Negishi, H., Y. Ohba, H. Yanai, A. Takaoka, K. Honma, K. Yui, T. Matsuyama, T. Taniguchi, and K. Honda. 2005. Negative regulation of Toll-like-receptor signaling by IRF-4. *Proc. Natl. Acad. Sci. U. S. A.* 102: 15989–15994.

134. Hagman, J. 2017. Critical Functions of IRF4 in B and T Lymphocytes. *J. Immunol.* 199: 3715–3716.

135. Shaffer, A. L., N. C. Tolga Emre, P. B. Romesser, and L. M. Staudt. 2009. IRF4: Immunity. Malignancy! Therapy? *Clin. Cancer Res.* 15: 2954–2961.

136. Wang, X., J. Guo, Y. Wang, Y. Xiao, L. Wang, and S. Hua. 2018. Expression levels of interferon regulatory factor 5 (Irf5) and related inflammatory cytokines associated with severity, prognosis, and causative pathogen in patients with community-acquired pneumonia. *Med. Sci. Monit.* 24: 3620–3630.

137. Almuttaqi, H., and I. A. Udalova. 2019. Advances and challenges in targeting IRF5, a key regulator of inflammation. *FEBS J.* 286: 1624–1637.

138. Yanai, H., H. M. Chen, T. Inuzuka, S. Kondo, T. W. Mak, A. Takaoka, K. Honda, and T. Taniguchi. 2007. Role of IFN regulatory factor 5 transcription factor in antiviral immunity and tumor suppression. *Proc. Natl. Acad. Sci. U. S. A.* 104: 3402–3407.

139. Kousa, Y. A., E. Fuller, and B. C. Schutte. 2018. IRF6 and AP2A Interaction Regulates Epidermal Development. *J. Invest. Dermatol.* 138: 2578–2588.

140. De La Garza, G., J. R. Schleiffarth, M. Dunnwald, A. Mankad, J. L. Weirather, G. Bonde, S. Butcher, T. A. Mansour, Y. A. Kousa, C. F. Fukazawa, D. W. Houston, J. R. Manak, B. C. Schutte, D. S. Wagner, and R. A. Cornell. 2013. Interferon regulatory factor 6 promotes differentiation of the periderm by activating expression of grainyhead-like 3. *J. Invest. Dermatol.* 133: 68–77.

141. Ingraham, C. R., A. Kinoshita, S. Kondo, B. Yang, S. Sajan, K. J. Trout, M. I. Malik, M. Dunnwald, S. L. Goudy, M. Lovett, J. C. Murray, and B. C. Schutte. 2006. Abnormal skin, limb and craniofacial morphogenesis in mice deficient for interferon regulatory factor 6 (Irf6). *Nat. Genet.* 38: 1335–1340.

142. Li, D., P. Cheng, J. Wang, X. Qiu, X. Zhang, L. Xu, Y. Liu, and S. Qin. 2019. IRF6 Is Directly Regulated by ZEB1 and ELF3, and Predicts a Favorable Prognosis in Gastric Cancer. *Front. Oncol.* 9: 220.

143. Ning, S., J. S. Pagano, and G. N. Barber. 2011. IRF7: Activation, regulation, modification and function. *Genes Immun.* 12: 399–414.

144. Yang, Z., W. Chen, W. Zhu, H. Meng, J. Chen, and J. Zhang. 2017. Overexpression of interferon regulatory factor 7 (IRF7) reduces bone metastasis of prostate cancer cells in mice. *Oncol. Res.* 25: 511–522.

145. Tailor, P., T. Tamura, H. J. Kong, T. Kubota, M. Kubota, P. Borghi, L. Gabriele, and K. Ozato. 2007. The Feedback Phase of Type I Interferon Induction in Dendritic Cells Requires Interferon Regulatory Factor 8. *Immunity* 27: 228–239.

146. Lee, W., H. S. Kim, S. Y. Baek, and G. R. Lee. 2016. Transcription factor IRF8 controls Th1-like regulatory T-cell function. *Cell. Mol. Immunol.* 13: 785–794.

147. Wang, H., M. Yan, J. Sun, S. Jain, R. Yoshimi, S. M. Abolfath, K. Ozato, W. G. Coleman, A. P. Ng, D. Metcalf, L. DiRago, S. L. Nutt, and H. C. Morse. 2014. A Reporter Mouse Reveals Lineage-Specific and Heterogeneous Expression of IRF8 during Lymphoid and Myeloid Cell Differentiation. *J. Immunol.* 193: 1766–1777.

148. Yang, D., M. Thangaraju, D. D. Browning, Z. Dong, B. Korchin, D. C. Lev, V. Ganapathy, and K. Liu. 2007. IFN Regulatory Factor 8 Mediates Apoptosis in Nonhemopoietic Tumor Cells via Regulation of Fas Expression. *J. Immunol.* 179: 4775–4782.

149. Rengachari, S., S. Groiss, J. M. Devos, E. Caron, N. Grandvaux, and D. Panne. 2018. Structural basis of STAT2 recognition by IRF9 reveals molecular insights into ISGF3 function. *Proc. Natl. Acad. Sci. U. S. A.* 115: E601–E609.

150. Platanitis, E., D. Demiroz, A. Schneller, K. Fischer, C. Capelle, M. Hartl, T. Gossenreiter, M. Müller, M. Novatchkova, and T. Decker. 2019. A molecular switch from STAT2-IRF9 to ISGF3 underlies interferon-induced gene transcription. *Nat. Commun.* 10: 1–17.

151. Minton, K. 2003. Apoptosis: A deadly combination. *Nat. Rev. Cancer* 3: 634.

152. Tian, W. L., R. Guo, F. Wang, Z. X. Jiang, P. Tang, Y. M. Huang, and L. Sun. 2018. The IRF9-SIRT1-P53 axis is involved in the growth of human acute myeloid leukemia. *Exp. Cell Res.* 365: 185–193.

153. Larner, A. C., G. Jonak, Y. S. Cheng, B. Korant, E. Knight, and J. E. Darnell. 1984. Transcriptional induction of two genes in human cells by β interferon. *Proc. Natl. Acad. Sci. U. S. A.* 81: 6733–6737.

154. Knight, E., and B. D. Korant. 1979. Fibroblast interferon induces synthesis of four proteins in human fibroblast cells. *Proc. Natl. Acad. Sci. U. S. A.* 76: 1824–1827.

155. Schoggins, J. W. 2019. Interferon-Stimulated Genes: What Do They All Do? *Annu. Rev. Virol.* 14.

156. Der, S. D., A. Zhou, B. R. G. Williams, and R. H. Silverman. 1998. Identification of genes differentially regulated by interferon α, β, or γ using oligonucleotide arrays. *Proc. Natl. Acad. Sci. U. S. A.* 95: 15623–15628.

157. Schneider, W. M., M. D. Chevillotte, and C. M. Rice. 2014. Interferon-Stimulated Genes: A Complex Web of Host Defenses. *Annu. Rev. Immunol.* 32: 513–545.

158. Schoggins, J. W., and C. M. Rice. 2011. Interferon-stimulated genes and their antiviral effector functions. *Curr. Opin. Virol.* 1: 519–525.

159. Li, Y., H. L. Wilson, and E. Kiss-Toth. 2017. Regulating STING in health and disease. *J. Inflamm. (United Kingdom)* 14.

160. Borden, E. C., G. C. Sen, G. Uze, R. H. Silverman, R. M. Ransohoff, G. R. Foster, and G. R. Stark. 2007. Interferons at age 50: Past, current and future impact on biomedicine. *Nat. Rev. Drug Discov.* 6: 975–990.

161. Sarkar, S. N., and G. C. Sen. 2004. Novel functions of proteins encoded by viral stress-inducible genes. *Pharmacol. Ther.* 103: 245–259.

162. Silverman, R. H. 2007. Viral Encounters with 2′,5′-Oligoadenylate Synthetase and RNase L during the Interferon Antiviral Response. *J. Virol.* 81: 12720–12729.

163. Chakrabarti, A., B. K. Jha, and R. H. Silverman. 2011. New insights into the role of RNase L in innate immunity. *J. Interf. Cytokine Res.* 31: 49–57.

164. García, M. A., J. Gil, I. Ventoso, S. Guerra, E. Domingo, C. Rivas, and M. Esteban. 2006. Impact of Protein Kinase PKR in Cell Biology: from Antiviral to Antiproliferative Action. *Microbiol. Mol. Biol. Rev.* 70: 1032–1060.

165. Medrano, L. M., J. Berenguer, M. A. Jiménez-Sousa, T. Aldámiz-Echevarria, F. Tejerina, C. Diez, L. Vigón, A. Fernández-Rodríguez, and S. Resino. 2017. ADAR1 polymorphisms are related to severity of liver fibrosis in HIV/HCV-coinfected patients. *Sci. Rep.* 7: 1–12.

166. Diamond, M. S., and M. Farzan. 2013. The broad-spectrum antiviral functions of IFIT and IFITM proteins. *Nat. Rev. Immunol.* 13: 46–57.

167. Liu, X.-Y., W. Chen, B. Wei, Y.-F. Shan, and C. Wang. 2011. IFN-Induced TPR Protein IFIT3 Potentiates Antiviral Signaling by Bridging MAVS and TBK1. *J. Immunol.* 187: 2559–2568.

168. Kane, M., S. S. Yadav, J. Bitzegeio, S. B. Kutluay, T. Zang, S. J. Wilson, J. W. Schoggins, C. M. Rice, M. Yamashita, T. Hatziioannou, and P. D. Bieniasz. 2013. MX2 is an interferon-induced inhibitor of HIV-1 infection. *Nature* 502: 563–566.

169. Verhelst, J., E. Parthoens, B. Schepens, W. Fiers, and X. Saelens. 2012. Interferon-Inducible Protein Mx1 Inhibits Influenza Virus by Interfering with Functional Viral Ribonucleoprotein Complex Assembly. *J. Virol.* 86: 13445–13455.

170. Haller, O., P. Staeheli, M. Schwemmle, and G. Kochs. 2015. Mx GTPases: Dynamin-like antiviral machines of innate immunity. *Trends Microbiol.* 23: 154–163.

171. Gizzi, A. S., T. L. Grove, J. J. Arnold, J. Jose, R. K. Jangra, S. J. Garforth, Q. Du, S. M. Cahill, N. G. Dulyaninova, J. D. Love, K. Chandran, A. R. Bresnick, C. E. Cameron, and S. C. Almo. 2018. A naturally occurring antiviral ribonucleotide encoded by the human genome. *Nature* 558: 610–614.

172. Seo, J. Y., R. Yaneva, and P. Cresswell. 2011. Viperin: A multifunctional, interferon-inducible protein that regulates virus replication. *Cell Host Microbe* 10: 534–539.

173. Luo, X., X. Wang, Y. Gao, J. Zhu, S. Liu, G. Gao, and P. Gao. 2020. Molecular Mechanism of RNA Recognition by Zinc-Finger Antiviral Protein. *Cell Rep.* 30: 46-52.e4.

174. Lenschow, D. J., C. Lai, N. Frias-Staheli, N. V. Giannakopoulos, A. Lutz, T. Wolff, A. Osiak, B. Levine, R. E. Schmidt, A. García-Sastre, D. A. Leib, A. Pekosz, K. P. Knobeloch, I. Horak, and H. W. Virgin IV. 2007. IFN-stimulated gene 15 functions as a critical antiviral molecule against influenza, herpes, and Sindbis viruses. *Proc. Natl. Acad. Sci. U. S. A.* 104: 1371–

1376.

175. Perng, Y. C., and D. J. Lenschow. 2018. ISG15 in antiviral immunity and beyond. *Nat. Rev. Microbiol.* 16: 423–439.

176. Swaim, C. D., A. F. Scott, L. A. Canadeo, J. M. Huibregtse Correspondence, and J. M. Huibregtse. 2017. Extracellular ISG15 Signals Cytokine Secretion through the LFA-1 Integrin Receptor Article Extracellular ISG15 Signals Cytokine Secretion through the LFA-1 Integrin Receptor. *Mol. Cell* 68: 581-589.e6.

177. Ebert, E. C., and B. Jabri. 2008. Massive interleukin-12-induced interferon-γ production by interleukin-15-stimulated lamina propria lymphocytes followed by down-regulation of the interleukin-12 receptor. *Immunology* 124: 453–460.

178. Ye, J., J. R. Ortaldo, K. Conlon, R. Winkler-Pickett, and H. A. Young. 1995. Cellular and molecular mechanisms of IFN-γ production induced by IL-2 and IL-12 in a human NK cell line. *J. Leukoc. Biol.* 58: 225–233.

179. Okamura, H., S. I. Kashiwamura, H. Tsutsui, T. Yoshimoto, and K. Nakanishi. 1998. Regulation of interferon-γ production by IL-12 and IL-18. *Curr. Opin. Immunol.* 10: 259–264.

180. Grohmann, U., M. L. Belladonna, C. Vacca, R. Bianchi, F. Fallarino, C. Orabona, M. C. Fioretti, and P. Puccetti. 2001. Positive Regulatory Role of IL-12 in Macrophages and Modulation by IFN-γ. *J. Immunol.* 167: 221–227.

181. Jiang, H., and S. Dhib-Jalbut. 1998. Differential induction of IL-12 by IFN-β and IFN-γ in human macrophages. *J. Interf. Cytokine Res.* 18: 697–703.

182. Kuo, P. T., Z. Zeng, N. Salim, S. Mattarollo, J. W. Wells, and G. R. Leggatt. 2018. The role of CXCR3 and its chemokine ligands in skin disease and cancer. *Front. Med.* 5: 271.

183. Singh, U. P., S. Singh, N. Iqbal, C. T. Weaver, J. R. McGhee, and J. W. Lillard. 2003. IFN-γ-Inducible Chemokines Enhance Adaptive Immunity and Colitis. *J. Interf. Cytokine Res.* 23: 591–600.

184. Steimle, V., C. A. Siegrist, A. Mottet, B. Lisowska-Grospierre, and B. Mach. 1994. Regulation of MHC class II expression by interferon-γ mediated by the transactivator gene CIITA. *Science (80-.).* 265: 106–109.

185. Morrison, B. J., J. C. Steel, and J. C. Morris. 2018. Reduction of MHC-I expression limits T-lymphocyte-mediated killing of Cancer-initiating cells. *BMC Cancer* 18: 469.

186. Drukker, M., G. Katz, A. Urbach, M. Schuldiner, G. Markel, J. Itskovitz-Eldor, B. Reubinoff, O. Mandelboim, and N. Benvenisty. 2002. Characterization of the expression of MHC proteins in human embryonic stem cells. *Proc. Natl. Acad. Sci. U. S. A.* 99: 9864–9869.

187. Gessani, S., L. Conti, M. Del Cornò, and F. Belardelli. 2014. Type I interferons as regulators of human antigen presenting cell functions. *Toxins (Basel).* 6: 1696–1723.

188. Doyle, T., O. Moncorgé, B. Bonaventure, D. Pollpeter, M. Lussignol, M. Tauziet, L. Apolonia, M. T. Catanese, C. Goujon, and M. H. Malim. 2018. The interferon-inducible isoform of NCOA7 inhibits endosome-mediated viral entry. *Nat. Microbiol.* 3: 1369–1376.

189. Narayana, S. K., K. J. Helbig, E. M. McCartney, N. S. Eyre, R. A. Bull, A. Eltahla, A. R. Lloyd, and M. R. Beard. 2015. The interferon-induced transmembrane proteins, IFITM1, IFITM2, and IFITM3 inhibit hepatitis C virus entry. *J. Biol. Chem.* 290: 25946–25959.

190. Lascano, J., P. D. Uchil, W. Mothes, and J. Luban. 2016. TRIM5 Retroviral Restriction Activity Correlates with the Ability To Induce Innate Immune Signaling. *J. Virol.* 90: 308–316.

191. Lukic, Z., S. Hausmann, S. Sebastian, J. Rucci, J. Sastri, S. L. Robia, J. Luban, and E. M. Campbell. 2011. TRIM5α associates with proteasomal subunits in cells while in complex with HIV-1 virions. *Retrovirology* 8: 93.

192. Grütter, M. G., and J. Luban. 2012. TRIM5 structure, HIV-1 capsid recognition, and innate immune signaling. *Curr. Opin. Virol.* 2: 142–150.

193. Harris, R. S., and J. P. Dudley. 2015. APOBECs and virus restriction. *Virology* 479–480: 131–145.

194. le Tortorec, A., S. Willey, and S. J. D. Neil. 2011. Antiviral inhibition of enveloped virus release by Tetherin/BST-2: Action and counteraction. *Viruses* 3: 520–540.

195. Wilson, S. J., J. W. Schoggins, T. Zang, S. B. Kutluay, N. Jouvenet, M. A. Alim, J. Bitzegeio, C. M. Rice, and P. D. Bieniasz. 2012. Inhibition of HIV-1 particle assembly by 2′,3′-cyclic- nucleotide 3′-Phosphodiesterase. *Cell Host Microbe* 12: 585–597.

196. Gariano, G. R., V. Dell'Oste, M. Bronzini, D. Gatti, A. Luganini, M. de Andrea, G. Gribaudo, M. Gariglio, and S. Landolfo. 2012. The intracellular DNA sensor IFI16 gene acts as restriction factor for human Cytomegalovirus replication. *PLoS Pathog.* 8.

197. Johnson, K. E., V. Bottero, S. Flaherty, S. Dutta, V. V. Singh, and B. Chandran. 2014. IFI16 Restricts HSV-1 Replication by Accumulating on the HSV-1 Genome, Repressing HSV-1 Gene Expression, and Directly or Indirectly Modulating Histone Modifications. *PLoS Pathog.* 10: e1004503.

198. Unterholzner, L., S. E. Keating, M. Baran, K. A. Horan, S. B. Jensen, S. Sharma, C. M. Sirois, T. Jin, E. Latz, T. S. Xiao, K. A. Fitzgerald, S. R. Paludan, and A. G. Bowie. 2010. IFI16 is an innate immune sensor for intracellular DNA. *Nat. Immunol.* 11: 997–1004.

199. Yoshimura, A., T. Naka, and M. Kubo. 2007. SOCS proteins, cytokine signalling and immune regulation. *Nat. Rev. Immunol.* 7: 454–465.

200. Radoshevich, L., F. Impens, D. Ribet, J. J. Quereda, T. N. Tham, M. A. Nahori, H. Bierne, O. Dussurget, J. Pizarro-Cerdá, K. P. Knobeloch, and P. Cossart. 2015. ISG15 counteracts Listeria monocytogenes infection. *Elife* 4.

201. Helbig, K. J., M. Y. Teh, K. M. Crosse, E. A. Monson, M. Smith, E. N. Tran, A. J. Standish, R. Morona, and M. R. Beard. 2019. The interferon stimulated gene viperin, restricts Shigella. flexneri in vitro. *Sci. Rep.* 9: 1–12.

202. Casson, C. N., J. Yu, V. M. Reyes, F. O. Taschuk, A. Yadav, A. M. Copenhaver, H. T. Nguyen, R. G. Collman, and S. Shin. 2015. Human caspase-4 mediates noncanonical inflammasome activation against gram-negative bacterial pathogens. *Proc. Natl. Acad. Sci. U. S. A.* 112: 6688–6693.

203. Sollberger, G., G. E. Strittmatter, M. Kistowska, L. E. French, and H.-D. Beer. 2012. Caspase-4 Is Required for Activation of Inflammasomes. *J. Immunol.* 188: 1992–2000.

204. Kim, B.-H. H., J. D. Chee, C. J. Bradfield, E.-S. S. Park, P. Kumar, and J. D. MacMicking. 2016. Interferon-induced guanylate-binding proteins in inflammasome activation and host defense. *Nat. Immunol.* 17: 481–489.

205. Kim, B. H., A. R. Shenoy, P. Kumar, R. Das, S. Tiwari, and J. D. MacMicking. 2011. A family of IFN-γ-inducible 65-kD GTPases protects against bacterial infection. *Science (80-.).* 332: 717–721.

206. Al-Zeer, M. A., H. M. Al-Younes, D. Lauster, M. A. Lubad, and T. F. Meyer. 2013. Autophagy restricts Chlamydia trachomatis growth in human macrophages via IFNG-inducible guanylate binding proteins. *Autophagy* 9: 50–62.

207. Praefcke, G. J. K. 2018. Regulation of innate immune functions by guanylate-binding proteins. *Int. J. Med. Microbiol.* 308: 237–245.

208. Roberts, W. K., M. J. Clemens, and I. M. Kerr. 1976. Interferon induced inhibition of protein synthesis in L cell extracts: An ATP dependent step in the activation of an inhibitor by double stranded RNA. *Proc. Natl. Acad. Sci. U. S. A.* 73: 3136–3140.

209. Kerr, I. M., R. E. Brown, and A. G. Hovanessian. 1977. Nature of inhibitor of cell-free protein synthesis formed in response to interferon and double-stranded RNA. *Nature* 268: 540–542.

210. Hovanessian, A. G., R. E. Brown, and I. M. Kerr. 1977. Synthesis of low molecular weight inhibitor of protein synthesis with enzyme from interferon-treated cells. *Nature* 268: 537–540.

211. Kerr, I. M., and R. E. Brown. 1978. *pppA2'p5'A2'p5'A: An inhibitor of protein synthesis synthesized with an enzyme fraction from interferon-treated cells (cell-free systems/double-stranded RNA/low molecular weight inhibitor/oligomeric series/protein kinase)*,.

212. HOVANESSIAN, A. G., and I. M. KERR. 1979. The (2′-5′)Oligoadenylate (pppA2′-5′A2′-5′A) Synthetase and Protein Kinase(s) from Interferon-Treated Cells. *Eur. J. Biochem.* 93: 515–526.

213. Hovanessian, A. G., J. Wood, E. Meurs, and L. Montagnier. 1979. Increased nuclease

activity in cells treated with pppA2’p5’A2’p5’A. *Proc. Natl. Acad. Sci. U. S. A.* 76: 3261–3265.

214. Williams, B. R. G., R. R. Golgher, and I. M. Kerr. 1979. Activation of a nuclease by pppA2′p5′ A2′p5′ A in intact cells. *FEBS Lett.* 105: 47–52.

215. Zhou, A., B. A. Hassel, and R. H. Silverman. 1993. *Expression Cloning of 2-5A-Dependent RNAase: A Uniquely Regulated Mediator of Interferon Action*,.

216. Dong, B., and R. H. Silverman. 1995. 2-5A-dependent RNase molecules dimerize during activation by 2-5A. *J. Biol. Chem.* 270: 4133–4137.

217. Cole, J. L., S. S. Carroll, and L. C. Kuo. 1996. Stoichiometry of 2′,5′-oligoadenylate-induced dimerization of ribonuclease L: A sedimentation equilibrium study. *J. Biol. Chem.* 271: 3979–3981.

218. Laurent, G. S., O. Yoshie, G. Floyd-Smith, H. Samanta, P. B. Sehgal, and P. Lengyel. 1983. Interferon action: Two (2′-5′) (A)n synthetases specified by distinct mRNAs in Ehrlich ascites tumor cells treated with interferon. *Cell* 33: 95–102.

219. Kaiyu Yangs, Himadri Samanta, Joseph Dougherty, Bettadapura Jayaram, Robert Broeze, A., and Peter Lengyel. 1981. Interferons, double-stranded RNA, and RNA degradation. Isolation and characterization of homogeneous human (2’-5’)(a)n synthetase. *J. Biol. Chem.* 256: 9324–9328.

220. Joseph P. Dougherty, H. S. P. J., and and P. L. Farrell. 1980. Interferon, double-stranded RNA, and RNA degradation. Isolation of homogeneous pppA(2’p5’A)n-1 synthetase from Ehrlich ascites tumor cells. *J. Biol. Chem.* 255: 370–373.

221. Wathelet, M., S. Moutschen, A. Cravador, L. DeWit, P. Defilippi, G. Huez, and J. Content. 1986. Full-length sequence and expression of the 42 kDa 2-5A synthetase induced by human interferon. *FEBS Lett.* 196: 113–120.

222. Saunders, M. E., D. R. Gewert, M. E. Tugwell, M. McMahon, and B. R. Williams. 1985. Human 2-5A synthetase: characterization of a novel cDNA and corresponding gene structure. *EMBO J.* 4: 1761.

223. Hovanessian, A. G., A. G. Laurent, J. Chebath, J. Galabru, N. Robert, and J. Svab. 1987. Identification of 69-kd and 100-kd forms of 2-5A synthetase in interferon-treated human cells by specific monoclonal antibodies. *EMBO J.* 6: 1273–1280.

224. Hovanessian, A. G., J. Svab, I. Marié, N. Robert, S. Chamaret, and A. G. Laurent. 1988. Characterization of 69- and 100-kDa forms of 2-5A-synthetase from interferon-treated human cells. *J. Biol. Chem.* 263: 4945–9.

225. Hovnanian, A., D. Rebouillat, M. G. Mattei, E. R. Levy, I. Marié, A. P. Monaco, and A. G. Hovanessian. 1998. The human 2’,5’-oligoadenylate synthetase locus is composed of three distinct genes clustered on chromosome 12q24.2 Encoding the 100-, 69-, and 40-kDa forms. *Genomics* 52: 267–277.

226. Hartmann, R., H. S. Olsen, S. Widder, R. Jørgensen, and J. Justesen. 1998. p59OASL, a 2'-5' oligoadenylate synthetase like protein: A novel human gene related to the 2'-5' oligoadenylate synthetase family. *Nucleic Acids Res.* 26: 4121–4127.

227. Ibsen, M. S., H. H. Gad, L. L. Andersen, V. Hornung, I. Julkunen, S. N. Sarkar, and R. Hartmann. 2015. Structural and functional analysis reveals that human OASL binds dsRNA to enhance RIG-I signaling. *Nucleic Acids Res.* .

228. Perelygin, A. A., S. V. Scherbik, I. B. Zhulin, B. M. Stockman, Y. Li, and M. A. Brinton. 2002. Positional cloning of the murine flavivirus resistance gene. *Proc. Natl. Acad. Sci. U. S. A.* 99: 9322–9327.

229. Lin, R.-J., H.-P. Yu, B.-L. Chang, W.-C. Tang, C.-L. Liao, and Y.-L. Lin. 2009. Distinct Antiviral Roles for Human 2′,5′-Oligoadenylate Synthetase Family Members against Dengue Virus Infection. *J. Immunol.* 183: 8035–8043.

230. Hovnanian, A., D. Rebouillat, E. R. Levy, M. G. Mattei, and A. G. Hovanessian. 1999. The human 2',5'-oligoadenylate synthetase-like gene (OASL) encoding the interferon-induced 56-kDa protein maps to chromosome 12q24.2 in the proximity of the 2',5'-OAS locus. *Genomics* 56: 362–363.

231. Justesen, J., R. Hartmann, and N. O. Kjeldgaard. 2000. Gene structure and function of the 2'-5'-oligoadenylate synthetase family. *Cell. Mol. Life Sci.* 57: 1593–1612.

232. Kakuta, S., S. Shibata, and Y. Iwakura. 2002. Genomic Structure of the Mouse 2',5'-Oligoadenylate Synthetase Gene Family. *J. Interf. Cytokine Res.* 22: 981–993.

233. Kumar, S., C. Mitnik, G. Valente, and G. Floyd-Smith. 2000. Expansion and molecular evolution of the interferon-induced 2'-5' oligoadenylate synthetase gene family. *Mol. Biol. Evol.* 17: 738–750.

234. Steltz, T. A. 1998. A mechanism for all polymerases. *Nature* 391: 231–232.

235. Sarkar, S. N., A. Ghosh, H. W. Wang, S. S. Sung, and G. C. Sen. 1999. The nature of the catalytic domain of 2'-5'-oligoadenylate synthetases. *J. Biol. Chem.* 274: 25535–25542.

236. Hartmann, R., J. Justesen, S. N. Sarkar, G. C. Sen, and V. C. Yee. 2003. Crystal structure of the 2′-specific and double-stranded RNA-activated interferon-induced antiviral protein 2′-5′- oligoadenylate synthetase. *Mol. Cell* 12: 1173–1185.

237. Ibsen, M. S., H. H. Gad, L. L. Andersen, V. Hornung, I. Julkunen, S. N. Sarkar, and R. Hartmann. 2015. Structural and functional analysis reveals that human OASL binds dsRNA to enhance RIG-I signaling. *Nucleic Acids Res.* 43: 5236–5248.

238. Zhu, J., A. Ghosh, and S. N. Sarkar. 2015. OASL—a new player in controlling antiviral innate immunity. *Curr. Opin. Virol.* 12: 15–19.

239. Ghosh, A., L. Shao, P. Sampath, B. Zhao, N. V. Patel, J. Zhu, B. Behl, R. A. Parise,

J. H. Beumer, R. J. O'Sullivan, N. A. DeLuca, S. H. Thorne, V. A. K. Rathinam, P. Li, and S. N. Sarkar. 2019. Oligoadenylate-Synthetase-Family Protein OASL Inhibits Activity of the DNA Sensor cGAS during DNA Virus Infection to Limit Interferon Production. *Immunity* 50: 51-63.e5.

240. Sarkar, S. N., S. Pal, and G. C. Sen. 2002. Crisscross enzymatic reaction between the two molecules in the active dimeric P69 form of the 2′-5′ oligodenylate synthetase. *J. Biol. Chem.* 277: 44760–44764.

241. Sadler, A. J., and B. R. G. Williams. 2008. Interferon-inducible antiviral effectors. *Nat. Rev. Immunol.* 8: 559–568.

242. Ibsen, M. S., H. H. Gad, K. Thavachelvam, T. Boesen, P. Despres, and R. Hartmann. 2014. The 2'-5'-Oligoadenylate Synthetase 3 Enzyme Potently Synthesizes the 2'-5'-Oligoadenylates Required for RNase L Activation. *J. Virol.* 88: 14222–14231.

243. Lim, J. K., A. Lisco, D. H. McDermott, L. Huynh, J. M. Ward, B. Johnson, H. Johnson, J. Pape, G. A. Foster, D. Krysztof, D. Follmann, S. L. Stramer, L. B. Margolis, and P. M. Murphy. 2009. Genetic Variation in OAS1 Is a Risk Factor for Initial Infection with West Nile Virus in Man. *PLoS Pathog.* 5: e1000321.

244. Thamizhmani, R., and P. Vijayachari. 2014. Association of dengue virus infection susceptibility with polymorphisms of 2'-5'-oligoadenylate synthetase genes: A case-control study. *Brazilian J. Infect. Dis.* 18: 548–550.

245. Kristiansen, H., C. A. Scherer, M. McVean, S. P. Iadonato, S. Vends, K. Thavachelvam, T. B. Steffensen, K. A. Horan, T. Kuri, F. Weber, S. R. Paludan, and R. Hartmann. 2010. Extracellular 2′-5′ Oligoadenylate Synthetase Stimulates RNase L-Independent Antiviral Activity: a Novel Mechanism of Virus-Induced Innate Immunity. *J. Virol.* 84: 11898–11904.

246. Wu, S., Y. Wang, G. Chen, M. Zhang, M. Wang, and J.-Q. He. 2018. 2′-5′-Oligoadenylate synthetase 1 polymorphisms are associated with tuberculosis: a case-control study. *BMC Pulm. Med.* 18: 180.

247. Yan, W., L. Ma, P. Stein, S. A. Pangas, K. H. Burns, Y. Bai, R. M. Schultz, and M. M. Matzuk. 2005. Mice Deficient in Oocyte-Specific Oligoadenylate Synthetase-Like Protein OAS1D Display Reduced Fertility. *Mol. Cell. Biol.* 25: 4615–4624.

248. Elbahesh, H., B. K. Jha, R. H. Silverman, S. V. Scherbik, and M. A. Brinton. 2011. The Flvr-encoded murine oligoadenylate synthetase 1b (Oas1b) suppresses 2-5A synthesis in intact cells. *Virology* 409: 262–270.

249. Elkhateeb, E., H. T. Tag-El-Din-Hassan, N. Sasaki, D. Torigoe, M. Morimatsu, and T. Agui. 2016. The role of mouse 2′,5′-oligoadenylate synthetase 1 paralogs. *Infect. Genet. Evol.* 45: 393–401.

250. Beechey, C. V., M. C. Green, and International Committee on Standardized Genetic Nomenclature for Mice. 1981. *Genetic variants and strains of the laboratory mouse*,. Fischer.

251. Scherbik, S. V., K. Kluetzman, A. A. Perelygin, and M. A. Brinton. 2007. Knock-in of the Oas1br allele into a flavivirus-induced disease susceptible mouse generates the resistant phenotype. *Virology* 368: 232–237.

252. Scherbik, S. V., J. M. Paranjape, B. M. Stockman, R. H. Silverman, and M. A. Brinton. 2006. RNase L Plays a Role in the Antiviral Response to West Nile Virus. *J. Virol.* 80: 2987–2999.

253. Madden, J. C., D. Cui, and M. A. Brinton. 2019. RNase L Antiviral Activity Is Not a Critical Component of the Oas1b-Mediated Flavivirus Resistance Phenotype. *J. Virol.* 93.

254. Noguchi, S., E. Hamano, I. Matsushita, M. Hijikata, H. Ito, T. Nagase, and N. Keicho. 2013. Differential effects of a common splice site polymorphism on the generation of OAS1 variants in human bronchial epithelial cells. *Hum. Immunol.* 74: 395–401.

255. Kjær, K. H., J. Pahus, M. F. Hansen, J. B. Poulsen, E. I. Christensen, J. Justesen, and P. M. Martensen. 2014. Mitochondrial localization of the OAS1 p46 isoform associated with a common single nucleotide polymorphism. *BMC Cell Biol.* 15: 33.

256. Kjær, K., J. Pahus, M. Hansen, J. Poulsen, E. Christensen, J. Justesen, and P. Martensen. 2014. Mitochondrial localization of the OAS1 p46 isoform associated with a common single nucleotide polymorphism. *BMC Cell Biol.* 15: 33.

257. Rysiecki, G., D. R. Gewert, and B. R. g. Williams. 1989. Constitutive Expression of a 2′,5′-Oligoadenylate Synthetase cDNA Results in Increased Antiviral Activity and Growth Suppression. *J. Interferon Res.* 9: 649–657.

258. Coccia, E. M., G. Romeo, A. Nissim, G. Marziali, R. Albertini, E. Affabris, A. Battistini, G. Fiorucci, R. Orsatti, G. B. Rossi, and J. Chebath. 1990. A full-length murine 2-5A synthetase cDNA transfected in NIH-3T3 cells impairs EMCV but not VSV replication. *Virology* 179: 228–233.

259. Liu, X., H. Xing, W. Gao, D. Yu, Y. Zhao, X. Shi, K. Zhang, P. Li, J. Yu, W. Xu, H. Shan, K. Zhang, W. Bao, X. Fu, S. Yang, and S. Wang. 2017. A functional variant in the OAS1 gene is associated with Sjögren's syndrome complicated with HBV infection. *Sci. Rep.* 7: 1–9.

260. El Awady, M. K., M. A. Anany, G. Esmat, N. Zayed, A. A. Tabll, A. Helmy, A. Rahman El Zayady, M. S. Abdalla, H. M. Sharada, M. El Raziky, W. El Akel, S. Abdalla, N. G. Bader El Din, K. El Aini, and C. Liver Center. 2011. Single nucleotide polymorphism at exon 7 splice acceptor site of OAS1 gene determines response of hepatitis C virus patients to interferon therapy. .

261. Leisching, G., I. Wiid, and B. Baker. 2017. The Association of OASL and Type I Interferons in the Pathogenesis and Survival of Intracellular Replicating Bacterial Species. *Front. Cell. Infect. Microbiol.* 7.

262. Leisching, G., A. Ali, V. Cole, and B. Baker. 2020. 2′-5′-Oligoadenylate synthetase-like protein inhibits intracellular M. tuberculosis replication and promotes proinflammatory

cytokine secretion. *Mol. Immunol.* 118: 73–78.

263. De Toledo-Pinto, T. G., A. B. R. Ferreira, M. Ribeiro-Alves, L. S. Rodrigues, L. R. Batista-Silva, B. J. D. A. Silva, R. M. R. Lemes, A. N. Martinez, F. G. Sandoval, L. E. Alvarado-Arnez, P. S. Rosa, E. J. Shannon, M. C. V. Pessolani, R. O. Pinheiro, S. L. G. Antunes, E. N. Sarno, F. A. Lara, Di. L. Williams, and M. Ozório Moraes. 2016. STING-Dependent 2′-5′ Oligoadenylate Synthetase-Like Production Is Required for Intracellular Mycobacterium leprae Survival. *J. Infect. Dis.* 214: 311–320.

264. Sejvar, J. J. 2016. West Nile Virus Infection. *Microbiol. Spectr.* 4.

265. Hadfield, J., A. F. Brito, D. M. Swetnam, C. B. F. Vogels, R. E. Tokarz, K. G. Andersen, R. C. Smith, T. Bedford, and N. D. Grubaugh. 2019. Twenty years of West Nile virus spread and evolution in the Americas visualized by Nextstrain. *PLoS Pathog.* 15.

266. George, T. L., R. J. Harrigan, J. A. Lamanna, D. F. Desante, J. F. Saracco, and T. B. Smith. 2015. Persistent impacts of West Nile virus on North American bird populations. *Proc. Natl. Acad. Sci. U. S. A.* 112: 14290–14294.

267. Gould, L. H., and E. Fikrig. 2004. West Nile virus: a growing concern? *J. Clin. Invest.* 113: 1102–1107.

268. Kramer, L. D., A. T. Ciota, and A. M. Kilpatrick. 2019. Introduction, Spread, and Establishment of West Nile Virus in the Americas. *J. Med. Entomol.* 56: 1448–1455.

269. Komar, N., and G. G. Clark. 2006. West Nile virus activity in Latin America and the Caribbean. *Rev. Panam. Salud Publica/Pan Am. J. Public Heal.* 19: 112–117.

270. Napp, S., D. Petrić, and N. Busquets. 2018. West Nile virus and other mosquito-borne viruses present in Eastern Europe. *Pathog. Glob. Health* 112: 233–248.

271. Eybpoosh, S., M. Fazlalipour, V. Baniasadi, M. H. Pouriayevali, F. Sadeghi, A. Ahmadi Vasmehjani, M. H. Karbalaie Niya, R. Hewson, and M. Salehi-Vaziri. 2019. Epidemiology of West Nile Virus in the Eastern Mediterranean region: A systematic review. *PLoS Negl. Trop. Dis.* 13.

272. David, S., and A. M. Abraham. 2016. Infectious Diseases Epidemiological and clinical aspects on West Nile virus, a globally emerging pathogen Epidemiological and clinical aspects on West Nile virus, a globally emerging pathogen. .

273. Debiasi, R. L. 2011. West nile virus neuroinvasive disease. *Curr. Infect. Dis. Rep.* 13: 350–359.

274. Suthar, M. S., M. S. Diamond, and M. Gale. 2013. West Nile virus infection and immunity. *Nat. Rev. Microbiol.* 11: 115–128.

275. Brinton, M. A. 2002. THE MOLECULAR BIOLOGY OF WEST NILE VIRUS: A New Invader of the Western Hemisphere. *Annu. Rev. Microbiol* 56: 371–402.

276. Brinton, M. A. 2013. Replication cycle and molecular biology of the west nile virus. *Viruses* 6: 13–53.

277. Davis, C. W., H.-Y. Nguyen, S. L. Hanna, M. D. Sánchez, R. W. Doms, and T. C. Pierson. 2006. West Nile Virus Discriminates between DC-SIGN and DC-SIGNR for Cellular Attachment and Infection. *J. Virol.* 80: 1290–1301.

278. Bogachek, M. V., B. N. Zaitsev, S. K. Sekatskii, E. V. Protopopova, V. A. Ternovoi, A. V. Ivanova, A. V. Kachko, V. A. Ivanisenko, G. Dietler, and V. B. Loktev. 2010. Characterization of glycoprotein E C-end of west nile virus and evaluation of its interaction force with αvβ3 integrin as putative cellular receptor. *Biochem.* 75: 472–480.

279. Chu, J. J. H., and M. L. Ng. 2004. Infectious Entry of West Nile Virus Occurs through a Clathrin-Mediated Endocytic Pathway. *J. Virol.* 78: 10543–10555.

280. Jemielity, S., J. J. Wang, Y. K. Chan, A. A. Ahmed, W. Li, S. Monahan, X. Bu, M. Farzan, G. J. Freeman, D. T. Umetsu, R. H. DeKruyff, and H. Choe. 2013. TIM-family Proteins Promote Infection of Multiple Enveloped Viruses through Virion-associated Phosphatidylserine. *PLoS Pathog.* 9.

281. Shiryaev, S. A., I. A. Kozlov, B. I. Ratnikov, J. W. Smith, M. Lebl, and A. Y. Strongin. 2007. Cleavage preference distinguishes the two-component NS2B-NS3 serine proteinases of Dengue and West Nile viruses. *Biochem. J.* 401: 743–752.

282. Malet, H., M. P. Egloff, B. Selisko, R. E. Butcher, P. J. Wright, M. Roberts, A. Gruez, G. Sulzenbacher, C. Vonrhein, G. Bricogne, J. M. Mackenzie, A. A. Khromykh, A. D. Davidson, and B. Canard. 2007. Crystal structure of the RNA polymerase domain of the West Nile virus non-structural protein 5. *J. Biol. Chem.* 282: 10678–10689.

283. Samuel, G. H., Z. N. Adelman, and K. M. Myles. Antiviral immunity and virus-mediated antagonism in disease vector mosquitoes. .

284. Zhang, H.-L., H.-Q. Ye, S.-Q. Liu, C.-L. Deng, X.-D. Li, P.-Y. Shi, and B. Zhang. 2017. West Nile Virus NS1 Antagonizes Interferon Beta Production by Targeting RIG-I and MDA5. *J. Virol.* 91.

285. Liu, W. J., X. J. Wang, D. C. Clark, M. Lobigs, R. A. Hall, and A. A. Khromykh. 2006. A Single Amino Acid Substitution in the West Nile Virus Nonstructural Protein NS2A Disables Its Ability To Inhibit Alpha/Beta Interferon Induction and Attenuates Virus Virulence in Mice. *J. Virol.* 80: 2396–2404.

286. Angleró-Rodríguez, Y. I., P. Pantoja, and C. A. Sariol. 2014. Dengue virus subverts the interferon induction pathway via NS2B/3 protease-IκB kinase ε interaction. *Clin. Vaccine Immunol.* 21: 29–38.

287. Chan, Y. K., and M. U. Gack. 2016. A phosphomimetic-based mechanism of dengue virus to antagonize innate immunity. *Nat. Immunol.* 17: 523–530.

288. He, Z., X. Zhu, W. Wen, J. Yuan, Y. Hu, J. Chen, S. An, X. Dong, C. Lin, J. Yu, J. Wu, Y. Yang, J. Cai, J. Li, and M. Li. 2016. Dengue Virus Subverts Host Innate Immunity by Targeting Adaptor Protein MAVS. *J. Virol.* 90: 7219–7230.

289. Dalrymple, N. A., V. Cimica, and E. R. Mackow. 2015. Dengue virus NS proteins inhibit RIG-I/MAVS signaling by blocking TBK1/IRF3 phosphorylation: Dengue virus serotype 1 NS4A is a unique interferon-regulating virulence determinant. *MBio* 6: 1–12.

290. Muñoz-Jordán, J. L., M. Laurent-Rolle, J. Ashour, L. Martínez-Sobrido, M. Ashok, W. I. Lipkin, and A. García-Sastre. 2005. Inhibition of Alpha/Beta Interferon Signaling by the NS4B Protein of Flaviviruses. *J. Virol.* 79: 8004–8013.

291. Laurent-Rolle, M., E. F. Boer, K. J. Lubick, J. B. Wolfinbarger, A. B. Carmody, B. Rockx, W. Liu, J. Ashour, W. L. Shupert, M. R. Holbrook, A. D. Barrett, P. W. Mason, M. E. Bloom, A. García-Sastre, A. A. Khromykh, and S. M. Best. 2010. The NS5 Protein of the Virulent West Nile Virus NY99 Strain Is a Potent Antagonist of Type I Interferon-Mediated JAK-STAT Signaling. *J. Virol.* 84: 3503–3515.

292. Lubick, K. J., S. J. Robertson, K. L. McNally, B. A. Freedman, A. L. Rasmussen, R. T. Taylor, S. Tsuruda, M. Sakai, M. Ishizuka, E. F. Boer, E. C. Foster, A. I. Chiramel, C. B. Addison, R. Green, D. L. Kastner, M. G. Katze, S. M. Holland, A. Forlino, A. F. Freeman, M. Boehm, K. Yoshii, S. M. Best, and A. D. Walts. 2015. Flavivirus antagonism of type i interferon signaling reveals prolidase as a regulator of IFNAR1 surface expression. *Cell Host Microbe* 18: 61–74.

293. Best, S. M. 2017. The Many Faces of the Flavivirus NS5 Protein in Antagonism of Type I Interferon Signaling. *J. Virol.* 91.

294. Lim, P.-Y., M. J. Behr, C. M. Chadwick, P.-Y. Shi, and K. A. Bernard. 2011. Keratinocytes Are Cell Targets of West Nile Virus In Vivo. *J. Virol.* 85: 5197–5201.

295. Johnston, L. J., G. M. Halliday, and N. J. C. King. 2000. Langerhans cells migrate to local lymph nodes following cutaneous infection with an arbovirus. *J. Invest. Dermatol.* 114: 560–568.

296. Samuel, M. A., and M. S. Diamond. 2006. Pathogenesis of West Nile Virus Infection: a Balance between Virulence, Innate and Adaptive Immunity, and Viral Evasion. *J. Virol.* 80: 9349–9360.

297. Diamond, M. S., B. Shrestha, E. Mehlhop, E. Sitati, and M. Engle. 2003. Innate and adaptive immune responses determine protection against disseminated infection by West Nile encephalitis virus. *Viral Immunol.* 16: 259–278.

298. Lazear, H. M., and M. S. Diamond. 2014. New Insights into Innate Immune Restriction of West Nile Virus Infection. .

299. Szretter, K. J., B. P. Daniels, H. Cho, M. D. Gainey, W. M. Yokoyama, M. Gale, H. W. Virgin, R. S. Klein, G. C. Sen, and M. S. Diamond. 2012. 2′-O methylation of the viral mRNA

cap by West Nile virus evades Ifit1-dependent and -independent mechanisms of host restriction in vivo. *PLoS Pathog.* 8.

300. Cho, H., B. Shrestha, G. C. Sen, and M. S. Diamond. 2013. A Role for Ifit2 in Restricting West Nile Virus Infection in the Brain. .

301. Samuel, M. A., K. Whitby, B. C. Keller, A. Marri, W. Barchet, B. R. G. Williams, R. H. Silverman, M. Gale, and M. S. Diamond. 2006. PKR and RNase L Contribute to Protection against Lethal West Nile Virus Infection by Controlling Early Viral Spread in the Periphery and Replication in Neurons. *J. Virol.* 80: 7009–7019.

302. Szretter, K. J., J. D. Brien, L. B. Thackray, H. W. Virgin, P. Cresswell, and M. S. Diamond. 2011. The Interferon-Inducible Gene viperin Restricts West Nile Virus Pathogenesis. *J. Virol.* 85: 11557–11566.

303. You, F., P. Wang, L. Yang, G. Yang, Y. O. Zhao, F. Qian, W. Walker, R. Sutton, R. Montgomery, R. Lin, A. Iwasaki, and E. Fikrig. 2013. ELF4 is critical for induction of type i interferon and the host antiviral response. *Nat. Immunol.* 14: 1237–1246.

304. Schoggins, J. W., D. A. MacDuff, N. Imanaka, M. D. Gainey, B. Shrestha, J. L. Eitson, K. B. Mar, R. B. Richardson, A. V. Ratushny, V. Litvak, R. Dabelic, B. Manicassamy, J. D. Aitchison, A. Aderem, R. M. Elliott, A. García-Sastre, V. Racaniello, E. J. Snijder, W. M. Yokoyama, M. S. Diamond, H. W. Virgin, and C. M. Rice. 2014. Pan-viral specificity of IFN-induced genes reveals new roles for cGAS in innate immunity. *Nature* 505: 691–695.

305. Sun, B., K. B. Sundström, J. J. Chew, P. Bist, E. S. Gan, H. C. Tan, K. C. Goh, T. Chawla, C. K. Tang, and E. E. Ooi. 2017. Dengue virus activates cGAS through the release of mitochondrial DNA. *Sci. Rep.* 7: 1–8.

306. Aguirre, S., P. Luthra, M. T. Sanchez-Aparicio, A. M. Maestre, J. Patel, F. Lamothe, A. C. Fredericks, S. Tripathi, T. Zhu, J. Pintado-Silva, L. G. Webb, D. Bernal-Rubio, A. Solovyov, B. Greenbaum, V. Simon, C. F. Basler, L. C. F. Mulder, A. García-Sastre, and A. Fernandez-Sesma. 2017. Dengue virus NS2B protein targets cGAS for degradation and prevents mitochondrial DNA sensing during infection. *Nat. Microbiol.* 2.

307. van Gent, M., and M. U. Gack. 2017. Viral pathogenesis: Dengue virus takes on cGAS. *Nat. Microbiol.* 2: 17050.

308. Maekawa, H., T. Inoue, H. Ouchi, T. M. Jao, R. Inoue, H. Nishi, R. Fujii, F. Ishidate, T. Tanaka, Y. Tanaka, N. Hirokawa, M. Nangaku, and R. Inagi. 2019. Mitochondrial Damage Causes Inflammation via cGAS-STING Signaling in Acute Kidney Injury. *Cell Rep.* 29: 1261-1273.e6.

309. Byrne, S. N., G. M. Halliday, L. J. Johnston, and N. J. C. King. 2001. Interleukin-1β but not tumor necrosis factor is involved in West Nile virus-induced Langerhans cell migration from the skin in C57BL/6 mice. *J. Invest. Dermatol.* 117: 702–709.

310. Ramos, H. J., M. C. Lanteri, G. Blahnik, A. Negash, M. S. Suthar, M. M. Brassil, K.

Sodhi, P. M. Treuting, M. P. Busch, P. J. Norris, and M. Gale. 2012. IL-1β Signaling Promotes CNS-Intrinsic Immune Control of West Nile Virus Infection. *PLoS Pathog.* 8: e1003039.

311. Clarke, P., J. S. Leser, E. D. Quick, K. R. Dionne, J. D. Beckham, and K. L. Tyler. 2014. Death Receptor-Mediated Apoptotic Signaling Is Activated in the Brain following Infection with West Nile Virus in the Absence of a Peripheral Immune Response. *J. Virol.* 88: 1080–1089.

312. Samuel, M. A., J. D. Morrey, and M. S. Diamond. 2007. Caspase 3-Dependent Cell Death of Neurons Contributes to the Pathogenesis of West Nile Virus Encephalitis. *J. Virol.* 81: 2614–2623.

313. Wang, T., E. Scully, Z. Yin, J. H. Kim, S. Wang, J. Yan, M. Mamula, J. F. Anderson, J. Craft, and E. Fikrig. 2003. IFN-γ-Producing γδ T Cells Help Control Murine West Nile Virus Infection. *J. Immunol.* 171: 2524–2531.

314. Diamond, M. S., B. Shrestha, A. Marri, D. Mahan, and M. Engle. 2003. B Cells and Antibody Play Critical Roles in the Immediate Defense of Disseminated Infection by West Nile Encephalitis Virus. *J. Virol.* 77: 2578–2586.

315. Pinto, A. K., S. Daffis, J. D. Brien, M. D. Gainey, W. M. Yokoyama, K. C. F. Sheehan, K. M. Murphy, R. D. Schreiber, and M. S. Diamond. 2011. A Temporal Role Of Type I Interferon Signaling in CD8+ T Cell Maturation during Acute West Nile Virus Infection. *PLoS Pathog.* 7: e1002407.

316. Giordano, D., K. E. Draves, L. B. Young, K. Roe, M. A. Bryan, C. Dresch, J. M. Richner, M. S. Diamond, M. Gale, and E. A. Clark. 2017. Protection of mice deficient in mature B cells from West Nile virus infection by passive and active immunization. *PLoS Pathog.* 13.

317. Klein, R. S., E. Lin, B. Zhang, A. D. Luster, J. Tollett, M. A. Samuel, M. Engle, and M. S. Diamond. 2005. Neuronal CXCL10 Directs CD8+ T-Cell Recruitment and Control of West Nile Virus Encephalitis. *J. Virol.* 79: 11457–11466.

318. Koblischke, M., F. S. Spitzer, D. M. Florian, S. W. Aberle, S. Malafa, I. Fae, I. Cassaniti, C. Jungbauer, B. Knapp, H. Laferl, G. Fischer, F. Baldanti, K. Stiasny, F. X. Heinz, and J. H. Aberle. 2020. CD4 T Cell Determinants in West Nile Virus Disease and Asymptomatic Infection. *Front. Immunol.* 11: 16.

319. Sitati, E. M., and M. S. Diamond. 2006. CD4+ T-Cell Responses Are Required for Clearance of West Nile Virus from the Central Nervous System. *J. Virol.* 80: 12060–12069.

320. Veiga, E., and P. Cossart. 2006. The role of clathrin-dependent endocytosis in bacterial internalization. *Trends Cell Biol.* 16: 499–504.

321. Eisenreich, W., T. Rudel, J. Heesemann, and W. Goebel. 2019. How viral and intracellular bacterial pathogens reprogram the metabolism of host cells to allow their intracellular replication. *Front. Cell. Infect. Microbiol.* 9: 42.

322. Weddle, E., and H. Agaisse. 2018. Principles of intracellular bacterial pathogen spread

from cell to cell. *PLOS Pathog.* 14: e1007380.

323. Rayamajhi, M., J. Humann, K. Penheiter, K. Andreasen, and L. L. Lenz. 2010. Induction of IFN-αβ enables Listeria monocytogenes to suppress macrophage activation by IFN-γ. *J. Exp. Med.* 207: 327–337.

324. O'Connell, R. M., S. K. Saha, S. A. Vaidya, K. W. Bruhn, G. A. Miranda, B. Zarnegar, A. K. Perry, B. O. Nguyen, T. F. Lane, T. Taniguchi, J. F. Miller, and G. Cheng. 2004. Type I interferon production enhances susceptibility to Listeria monocytogenes infection. *J. Exp. Med.* 200: 437–445.

325. Hu, S., W. He, X. Du, J. Yang, Q. Wen, X. P. Zhong, and L. Ma. 2017. IL-17 Production of Neutrophils Enhances Antibacteria Ability but Promotes Arthritis Development During Mycobacterium tuberculosis Infection. *EBioMedicine* 23: 88–99.

326. Jones, J. W., N. Kayagaki, P. Broz, T. Henry, K. Newton, K. O'Rourke, S. Chan, J. Dong, Y. Qu, M. Roose-Girma, V. M. Dixit, and D. M. Monack. 2010. Absent in melanoma 2 is required for innate immune recognition of Francisella tularensis. *Proc. Natl. Acad. Sci. U. S. A.* 107: 9771–9776.

327. Rathinam, V. A. K., Z. Jiang, S. N. Waggoner, S. Sharma, L. E. Cole, L. Waggoner, S. K. Vanaja, B. G. Monks, S. Ganesan, E. Latz, V. Hornung, S. N. Vogel, E. Szomolanyi-Tsuda, and K. A. Fitzgerald. 2010. The AIM2 inflammasome is essential for host defense against cytosolic bacteria and DNA viruses. *Nat. Immunol.* 11: 395–402.

328. Kim, S., F. Bauernfeind, A. Ablasser, G. Hartmann, K. A. Fitzgerald, E. Latz, and V. Hornung. 2010. Listeria monocytogenes is sensed by the NLRP3 and AIM2 inflammasome. *Eur. J. Immunol.* 40: 1545–1551.

329. MacMicking, J. D. 2003. Immune Control of Tuberculosis by IFN- -Inducible LRG-47. *Science (80-.).* 302: 654–659.

330. Maric-Biresev, J., J. P. Hunn, O. Krut, J. B. Helms, S. Martens, and J. C. Howard. 2016. Loss of the interferon-γ-inducible regulatory immunity-related GTPase (IRG), Irgm1, causes activation of effector IRG proteins on lysosomes, damaging lysosomal function and predicting the dramatic susceptibility of Irgm1-deficient mice to infection. *BMC Biol.* 14: 33.

331. MacMicking, J. D., G. A. Taylor, and J. D. McKinney. 2003. Immune Control of Tuberculosis by IFN-γ-inducible LRG-47. *Science (80-.).* 302: 654–659.

332. Moreira-Teixeira, L., J. Sousa, F. W. McNab, E. Torrado, F. Cardoso, H. Machado, F. Castro, V. Cardoso, J. Gaifem, X. Wu, R. Appelberg, A. G. Castro, A. O'Garra, and M. Saraiva. 2016. Type I IFN Inhibits Alternative Macrophage Activation during Mycobacterium tuberculosis Infection and Leads to Enhanced Protection in the Absence of IFN-γ Signaling . *J. Immunol.* 197: 4714–4726.

333. Desvignes, L., A. J. Wolf, and J. D. Ernst. 2012. Dynamic Roles of Type I and Type II IFNs in Early Infection with Mycobacterium tuberculosis . *J. Immunol.* 188: 6205–6215.

334. Novikov, A., M. Cardone, R. Thompson, K. Shenderov, K. D. Kirschman, K. D. Mayer-Barber, T. G. Myers, R. L. Rabin, G. Trinchieri, A. Sher, and C. G. Feng. 2011. Mycobacterium tuberculosis Triggers Host Type I IFN Signaling To Regulate IL-1β Production in Human Macrophages . *J. Immunol.* 187: 2540–2547.

335. de Paus, R. A., A. van Wengen, I. Schmidt, M. Visser, E. M. E. Verdegaal, J. T. van Dissel, and E. van de Vosse. 2013. Inhibition of the type I immune responses of human monocytes by IFN-α and IFN-β. *Cytokine* 61: 645–655.

336. Bourigault, M. L., N. Segueni, S. Rose, N. Court, R. Vacher, V. Vasseur, F. Erard, M. Le Bert, I. Garcia, Y. Iwakura, M. Jacobs, B. Ryffel, and V. F. J. Quesniaux. 2013. Relative contribution of il-1α, il-1β and tnf to the host response to mycobacterium tuberculosis and attenuated m. Bovis bcg. *Immun. Inflamm. Dis.* 1: 47–62.

337. Thakur, A., H. Mikkelsen, and G. Jungersen. 2019. Intracellular Pathogens: Host Immunity and Microbial Persistence Strategies. *J. Immunol. Res.* 2019.

338. Adams, L. B., D. M. Scollard, N. A. Ray, A. M. Cooper, A. A. Frank, I. M. Orme, and J. L. Krahenbuhl. 2002. The Study of Mycobacterium leprae Infection in Interferon-γ Gene–Disrupted Mice as a Model to Explore the Immunopathologic Spectrum of Leprosy. *J. Infect. Dis.* 185: S1–S8.

339. Bao, S., K. W. Beagley, M. P. France, J. Shen, and A. J. Husband. 2000. Interferon-γ plays a critical role in intestinal immunity against Salmonella typhimurium infection. *Immunology* 99: 464–472.

340. Allerberger, F., and M. Wagner. 2010. Listeriosis: A resurgent foodborne infection. *Clin. Microbiol. Infect.* 16: 16–23.

341. Ahn, J. J., T. Selvanantham, M. A. Zhang, T. Mallevaey, and S. E. Dunn. 2016. Experimental infection with listeria monocytogenes as a model for studying host interferon-γ responses. *J. Vis. Exp.* 2016.

342. Bécavin, C., C. Bouchier, P. Lechat, C. Archambaud, S. Creno, E. Gouin, Z. Wu, A. Kühbacher, S. Brisse, M. Graciela Pucciarelli, F. García-del Portillo, T. Hain, D. A. Portnoy, T. Chakraborty, M. Lecuit, J. Pizarro-Cerdá, I. Moszer, H. Bierne, and P. Cossart. 2014. Comparison of widely used Listeria monocytogenes strains EGD, 10403S, and EGD-e highlights genomic differences underlying variations in pathogenicity. *MBio* 5.

343. Radoshevich, L., and P. Cossart. 2018. Listeria monocytogenes: Towards a complete picture of its physiology and pathogenesis. *Nat. Rev. Microbiol.* 16: 32–46.

344. Cossart, P. 2011. Illuminating the landscape of host-pathogen interactions with the bacterium Listeria monocytogenes. *Proc. Natl. Acad. Sci. U. S. A.* 108: 19484–19491.

345. Hoelzer, K., R. Pouillot, and S. Dennis. 2012. Animal models of listeriosis: A comparative review of the current state of the art and lessons learned. *Vet. Res.* 43: 18.

346. Bou Ghanem, E. N., T. Myers-Morales, and S. E. F. D'Orazio. 2013. A Mouse Model of Foodborne Listeria monocytogenes Infection. In *Current Protocols in Microbiology* John Wiley & Sons, Inc., Hoboken, NJ, USA. 9B.3.1-9B.3.16.

347. Cossart, P., and M. Lecuit. 2002. *Genetically-modified-animal models for human infections: the Listeria paradigm*,.

348. Conlan, J. W. 2011. Francisella tularensis: A Red-blooded Pathogen. .

349. Tempel, R., X. H. Lai, L. Crosa, B. Kozlowicz, and F. Heffron. 2006. Attenuated Francisella novicida transposon mutants protect mice against wild-type challenge. *Infect. Immun.* 74: 5095–5105.

350. Kieffer, T. L., S. Cowley, F. E. Nano, and K. L. Elkins. 2003. Francisella novicida LPS has greater immunobiological activity in mice than F. tularensis LPS, and contributes to F. novicida murine pathogenesis. *Microbes Infect.* 5: 397–403.

351. Moule, M. G., D. M. Monack, and D. S. Schneider. 2010. Reciprocal analysis of francisella novicida infections of a drosophila melanogaster model reveal host pathogen conflicts mediated by reactive oxygen and imdregulated innate immune response. *PLoS Pathog.* 6: 73–74.

352. Kraemer, P. S., A. Mitchell, M. R. Pelletier, L. A. Gallagher, M. Wasnick, L. Rohmer, M. J. Brittnacher, C. Manoil, S. J. Skerett, and N. R. Salama. 2009. Genome-wide screen in Francisella novicida for genes required for pulmonary and systemic infection in mice. *Infect. Immun.* 77: 232–244.

353. Conlan, J. W., W. Chen, C. M. Bosio, S. C. Cowley, and K. L. Elkins. Infection of Mice with Francisella as an Immunological Model. .

354. Pamer, E. G. 2004. Immune responses to Listeria monocytogenes. *Nat. Rev. Immunol.* 4: 812–823.

355. Bosio, C. M. 2011. The subversion of the immune system by Francisella tularensis. *Front. Microbiol.* 2.

356. Mitchell, G., and R. R. Isberg. 2017. Innate Immunity to Intracellular Pathogens: Balancing Microbial Elimination and Inflammation. *Cell Host Microbe* 22: 166–175.

357. Crotzer, V. L., and J. S. Blum. 2010. Autophagy and adaptive immunity. *Immunology* 131: 9–17.

358. Meunier, E., and P. Broz. 2016. Interferon-inducible GTPases in cell autonomous and innate immunity. *Cell. Microbiol.* 18: 168–180.

359. Sahoo, M., I. Ceballos-Olvera, L. del Barrio, and F. Re. 2011. Role of the Inflammasome, IL-1β, and IL-18 in Bacterial Infections. *Sci. World J.* 11: 2037.

360. Lasigliè, D., E. Traggiai, S. Federici, M. Alessio, A. Buoncompagni, A. Accogli, S.

Chiesa, F. Penco, A. Martini, and M. Gattorno. 2011. Role of IL-1 beta in the development of human TH17 cells: Lesson from NLPR3 mutated patients. *PLoS One* 6.

361. Saiga, H., S. Kitada, Y. Shimada, N. Kamiyama, M. Okuyama, M. Makino, M. Yamamoto, and K. Takeda. Critical role of AIM2 in Mycobacterium tuberculosis infection. .

362. Kim, S., F. Bauernfeind, A. Ablasser, G. Hartmann, K. A. Fitzgerald, E. Latz, and V. Hornung. Listeria monocytogenes is sensed by the NLRP3 and AIM2 Inflammasome. .

363. Zhu, Q., S. M. Man, R. Karki, R. K. S. Malireddi, and T. D. Kanneganti. 2018. Detrimental Type I Interferon Signaling Dominates Protective AIM2 Inflammasome Responses during Francisella novicida Infection. *Cell Rep.* 22: 3168–3174.

364. Gray, T. J., J. N. Burrow, P. G. Markey, P. I. Whelan, J. Jackson, D. W. Smith, and B. J. Currie. 2011. Case report: West nile virus (Kunjin subtype) disease in the Northern Territory of Australia - A case of encephalitis and review of all reported cases. *Am. J. Trop. Med. Hyg.* 85: 952–956.

365. Rawle, D. J., Y. X. Setoh, J. H. Edmonds, and A. A. Khromykh. 2015. Comparison of attenuated and virulent West Nile virus strains in human monocyte-derived dendritic cells as a model of initial human infection. *Virol. J.* 12: 46.

366. Hermance, M. E., and S. Thangamani. 2017. Powassan Virus: An Emerging Arbovirus of Public Health Concern in North America. *Vector-Borne Zoonotic Dis.* 17: 453–462.

367. Conlan, J. W., W. Chen, C. M. Bosio, S. C. Cowley, and K. L. Elkins. 2011. Infection of mice with francisella as an immunological model. *Curr. Protoc. Essent. Lab. Tech.* 2011: 1–16.

368. Bierne, H., and M. Hamon. 2020. Targeting host epigenetic machinery: The *Listeria* paradigm. *Cell. Microbiol.* 22.

369. Lecuit, M. 2020. <scp> *Listeria monocytogenes* </scp> , a model in infection biology. *Cell. Microbiol.* 22.

370. Noguchi, S., E. Hamano, I. Matsushita, M. Hijikata, H. Ito, T. Nagase, and N. Keicho. 2013. Differential effects of a common splice site polymorphism on the generation of OAS1 variants in human bronchial epithelial cells. *Hum. Immunol.* 74: 395–401.

371. Banerjee, I., B. Behl, M. Mendonca, G. Shrivastava, A. J. Russo, A. Menoret, A. Ghosh, A. T. Vella, S. K. Vanaja, S. N. Sarkar, K. A. Fitzgerald, and V. A. K. Rathinam. 2018. Gasdermin D Restrains Type I Interferon Response to Cytosolic DNA by Disrupting Ionic Homeostasis. *Immunity* 49: 413-426.e5.

372. Wei Huang, D., B. T. Sherman, and R. A. Lempicki. 2008. SURVEY AND SUMMARY Bioinformatics enrichment tools: paths toward the comprehensive functional analysis of large gene lists. *Nucleic Acids Res.* 37: 1–13.

373. Huang, D. W., B. T. Sherman, and R. A. Lempicki. 2009. Systematic and integrative

analysis of large gene lists using DAVID bioinformatics resources. *Nat. Protoc.* 4: 44–57.

374. Burke, J. M., S. L. Moon, T. Matheny, and R. Parker. 2019. RNase L Reprograms Translation by Widespread mRNA Turnover Escaped by Antiviral mRNAs. *Mol. Cell* 75: 1203-1217.e5.

375. Panfil, A. R., J. Al-Saleem, C. M. Howard, N. Shkriabai, M. Kvaratskhelia, and P. L. Green. 2018. Stability of the HTLV-1 antisense-derived protein, HBZ, is regulated by the E3 ubiquitin-protein ligase, UBR5. *Front. Microbiol.* 9.

376. Burgess, H. M., and I. Mohr. 2015. Cellular 5′-3′ mRNA exonuclease Xrn1 controls double-stranded RNA accumulation and anti-viral responses. *Cell Host Microbe* 17: 332–344.

377. Praest, P., R. D. Luteijn, I. G. J. Brak-Boer, J. Lanfermeijer, H. Hoelen, L. Ijgosse, A. I. Costa, R. D. Gorham, R. J. Lebbink, and E. J. H. J. Wiertz. 2018. The influence of TAP1 and TAP2 gene polymorphisms on TAP function and its inhibition by viral immune evasion proteins. *Mol. Immunol.* 101: 55–64.

378. Chassé, H., S. Boulben, V. Costache, P. Cormier, and J. Morales. 2016. Analysis of translation using polysome profiling. *Nucleic Acids Res.* 45: gkw907.

379. Selth, L. A., C. Gilbert, and J. Q. Svejstrup. 2009. RNA immunoprecipitation to determine RNA-protein associations in vivo. *Cold Spring Harb. Protoc.* 4: pdb.prot5234.

380. Brien, J. D., S. Daffis, H. M. Lazear, H. Cho, M. S. Suthar, M. Gale, and M. S. Diamond. 2011. Interferon Regulatory Factor-1 (IRF-1) Shapes Both Innate and CD8+ T Cell Immune Responses against West Nile Virus Infection. *PLoS Pathog.* 7: e1002230.

381. Schoggins, J. W., D. A. MacDuff, N. Imanaka, M. D. Gainey, B. Shrestha, J. L. Eitson, K. B. Mar, R. B. Richardson, A. V. Ratushny, V. Litvak, R. Dabelic, B. Manicassamy, J. D. Aitchison, A. Aderem, R. M. Elliott, A. García-Sastre, V. Racaniello, E. J. Snijder, W. M. Yokoyama, M. S. Diamond, H. W. Virgin, and C. M. Rice. 2014. Pan-viral specificity of IFN-induced genes reveals new roles for cGAS in innate immunity. *Nature* 505: 691–695.

382. Hopfner, K.-P., and V. Hornung. 2020. Molecular mechanisms and cellular functions of cGAS–STING signalling. *Nat. Rev. Mol. Cell Biol.* 1–21.

383. Ni, G., Z. Ma, and B. Damania. 2018. cGAS and STING: At the intersection of DNA and RNA virus-sensing networks. *PLoS Pathog.* 14.

384. Courtney, S. C., H. Di, B. M. Stockman, H. Liu, S. V. Scherbik, and M. A. Brinton. 2012. Identification of Novel Host Cell Binding Partners of Oas1b, the Protein Conferring Resistance to Flavivirus-Induced Disease in Mice. *J. Virol.* 86: 7953–7963.

385. Donovan, J., M. Dufner, and A. Korennykh. 2013. Structural basis for cytosolic double-stranded RNA surveillance by human oligoadenylate synthetase 1. *Proc. Natl. Acad. Sci. U. S. A.* 110: 1652–1657.

386. Reid, D. W., and C. V. Nicchitta. 2012. Primary role for endoplasmic reticulum-bound ribosomes in cellular translation identified by ribosome profiling. *J. Biol. Chem.* 287: 5518–5527.

387. Lane, K. T., and L. S. Beese. 2006. Structural biology of protein farnesyltransferase and geranylgeranyltransferase type I. *J. Lipid Res.* 47: 681–699.

388. Kjaer, K. H., J. B. Poulsen, T. Reintamm, E. Saby, P. M. Martensen, M. Kelve, and J. Justesen. 2009. Evolution of the 2′-5′-oligoadenylate synthetase family in eukaryotes and bacteria. *J. Mol. Evol.* 69: 612–624.

389. Skrivergaard, S., M. S. Jensen, T. B. Rolander, T. B. N. Nguyen, A. Bundgaard, L. N. Nejsum, and P. M. Martensen. 2019. The Cellular Localization of the p42 and p46 Oligoadenylate Synthetase 1 Isoforms and Their Impact on Mitochondrial Respiration. *Viruses* 11: 1122.

390. Vanya, M. 2017. Prevention of Zika virus and related complications. *Rev. Med. Microbiol.* 28: 75–78.

391. Halstead, S. M. 2017. Dengue and dengue hemorrhagic fever. In *Handbook of Zoonoses, Second Edition, Section B: Viral Zoonoses* vol. 11. CRC Press. 89–99.

392. Diamond, M. S. 2003. Evasion of innate and adaptive immunity by flaviviruses. *Immunol. Cell Biol.* 81: 196–206.

393. Miorin, L., A. M. Maestre, A. Fernandez-Sesma, and A. García-Sastre. 2017. Antagonism of type I interferon by flaviviruses. *Biochem. Biophys. Res. Commun.* 492: 587–596.

394. Riedl, W., D. Acharya, J. H. Lee, G. Liu, T. Serman, C. Chiang, Y. K. Chan, M. S. Diamond, and M. U. Gack. 2019. Zika Virus NS3 Mimics a Cellular 14-3-3-Binding Motif to Antagonize RIG-I- and MDA5-Mediated Innate Immunity. *Cell Host Microbe* 26: 493-503.e6.

395. Ueno, T., Y. Taga, R. Yoshimoto, A. Mayeda, S. Hattori, and K. Ogawa-Goto. 2019. Component of splicing factor SF3b plays a key role in translational control of polyribosomes on the endoplasmic reticulum. *Proc. Natl. Acad. Sci. U. S. A.* 116: 9340–9349.

396. Bao, Y., X. Liu, C. Han, S. Xu, B. Xie, Q. Zhang, Y. Gu, J. Hou, L. Qian, C. Qian, H. Han, and X. Cao. 2014. Identification of IFN-γ-producing innate B cells. *Cell Res.* 24: 161–176.

397. Rothfuchs, A. G., C. Trumstedt, H. Wigzell, and M. E. Rottenberg. 2004. Intracellular Bacterial Infection-Induced IFN-γ Is Critically but Not Solely Dependent on Toll-Like Receptor 4-Myeloid Differentiation Factor 88-IFN-αβ-STAT1 Signaling. *J. Immunol.* 172: 6345–6353.

398. Two, J., S. Agent, and B. Level. Experimental listeriosis model in mice. 2–3.

399. Dussurget, O., H. Bierne, and P. Cossart. 2014. The bacterial pathogen Listeria monocytogenes and the interferon family: type I, type II and type III interferons. *Front. Cell. Infect. Microbiol.* 4: 50.

400. Pine, R. 2002. Irf and tuberculosis. *J. Interf. Cytokine Res.* 22: 15–25.

401. Menning, M., and T. A. Kufer. 2013. A role for the Ankyrin repeat containing protein Ankrd17 in Nod1- and Nod2-mediated inflammatory responses. *FEBS Lett.* 587: 2137–2142.

402. Rausch, M. P., and K. T. Hastings. 2015. Diverse cellular and organismal functions of the lysosomal thiol reductase GILT. *Mol. Immunol.* 68: 124–128.

403. Lee, H.-C., E.-S. Lee, M. B. Uddin, T.-H. Kim, J.-H. Kim, K. Chathuranga, W. A. G. Chathuranga, M. Jin, S. Kim, C.-J. Kim, and J.-S. Lee. 2018. Released Tryptophanyl-tRNA Synthetase Stimulates Innate Immune Responses against Viral Infection. *J. Virol.* 93.

404. Kano, S., K. Sato, Y. Morishita, S. Vollstedt, S. Kim, K. Bishop, K. Honda, M. Kubo, and T. Taniguchi. 2008. The contribution of transcription factor IRF1 to the interferon-γ–interleukin 12 signaling axis and TH1 versus TH-17 differentiation of CD4+ T cells. *Nat. Immunol.* 9: 34–41.

405. Leisching, G., I. Wiid, and B. Baker. 2018. OAS1, 2, and 3: Significance During Active Tuberculosis? *J. Infect. Dis.* 217: 1517–1521.

406. Mello, F. C. de Q., D. R. Silva, and M. P. Dalcolmo. 2018. Tuberculosis: Where are we? *J. Bras. Pneumol.* 44: 82.

407. Kingry, L. C., and J. M. Petersen. 2014. Comparative review of Francisella tularensis and Francisella novicida. *Front. Cell. Infect. Microbiol.* 5.

408. Moreira, L. O., D. S. Zamboni, J. G. Filep, and J. C. Salazar. 2012. NOD1 and NOD2 signaling in infection and inflammation. .

409. West, L. C., and P. Cresswell. 2013. Expanding roles for GILT in immunity. *Curr. Opin. Immunol.* 25: 103–108.

410. Ahn, Y. H., S. Park, J. J. Choi, B. K. Park, K. H. Rhee, E. Kang, S. Ahn, C. H. Lee, J. S. Lee, K. S. Inn, M. La Cho, S. H. Park, K. Park, H. J. Park, J. H. Lee, J. W. Park, N. H. Kwon, H. Shim, B. W. Han, P. Kim, J. Y. Lee, Y. Jeon, J. W. Huh, M. Jin, and S. Kim. 2016. Secreted tryptophanyl-tRNA synthetase as a primary defence system against infection. *Nat. Microbiol.* 2: 1–13.

411. Liu, J., X. Guan, and X. Ma. 2005. Interferon Regulatory Factor 1 Is an Essential and Direct Transcriptional Activator for Interferon γ-induced RANTES/CCl5 Expression in Macrophages. *J. Biol. Chem.* 280: 24347–24355.

412. Abdullah, Z., M. Schlee, S. Roth, M. A. Mraheil, W. Barchet, J. Böttcher, T. Hain, S. Geiger, Y. Hayakawa, J. H. Fritz, F. Civril, K. P. Hopfner, C. Kurts, J. Ruland, G. Hartmann, T. Chakraborty, and P. A. Knolle. 2012. RIG-I detects infection with live Listeria by sensing secreted bacterial nucleic acids. *EMBO J.* 31: 4153–4164.

413. Pagliuso, A., T. N. Tham, E. Allemand, S. Robertin, B. Dupuy, Q. Bertrand, C. Bécavin, M. Koutero, V. Najburg, M. A. Nahori, F. Tangy, F. Stavru, S. Bessonov, A. Dessen, C. Muchardt, A. Lebreton, A. V. Komarova, and P. Cossart. 2019. An RNA-Binding Protein Secreted

by a Bacterial Pathogen Modulates RIG-I Signaling. *Cell Host Microbe* 26: 823-835.e11.

414. Schmolke, M., J. R. Patel, E. de Castro, M. T. A. Sánchez, M. B. Uccellini, J. C. Miller, B. Manicassamy, T. Satoh, T. Kawai, S. Akira, M. Merad, and A. García-Sastre. 2014. RIG-I detects mRNA of intracellular Salmonella enterica serovar typhimurium during bacterial infection. *MBio* 5.

415. Hagmann, C. A., A. M. Herzner, Z. Abdullah, T. Zillinger, C. Jakobs, C. Schuberth, C. Coch, P. G. Higgins, H. Wisplinghoff, W. Barchet, V. Hornung, G. Hartmann, and M. Schlee. 2013. RIG-I Detects Triphosphorylated RNA of Listeria monocytogenes during Infection in Non-Immune Cells. *PLoS One* 8.

416. Cheng, Y., and J. S. Schorey. 2018. Mycobacterium tuberculosis-induced IFN-β production requires cytosolic DNA and RNA sensing pathways. *J. Exp. Med.* 215: 2919–2935.

417. dos Santos, P. F., J. Van Weyenbergh, M. Delgobo, D. de Oliveira Patricio, B. J. Ferguson, R. Guabiraba, T. Dierckx, S. M. Menezes, A. Báfica, and D. S. Mansur. 2018. ISG15-Induced IL-10 Is a Novel Anti-Inflammatory Myeloid Axis Disrupted during Active Tuberculosis. *J. Immunol.* 200: 1434–1442.

418. Kimmey, J. M., J. A. Campbell, L. A. Weiss, K. J. Monte, D. J. Lenschow, and C. L. Stallings. 2017. The impact of ISGylation during Mycobacterium tuberculosis infection in mice. *Microbes Infect.* 19: 249–258.

419. Heesterbeek Mathieu L Angelier Richard A Harrison Suzan HM Rooijakkers, D. A., and S. H. Rooijakkers. 2018. Complement and Bacterial Infections: From Molecular Mechanisms to Therapeutic Applications. .

420. Clay, C. D., S. Soni, J. S. Gunn, and L. S. Schlesinger. 2008. Evasion of Complement-Mediated Lysis and Complement C3 Deposition Are Regulated by Francisella tularensis Lipopolysaccharide O Antigen . *J. Immunol.* 181: 5568–5578.

421. Sorbara, M. T., E. G. Foerster, J. Tsalikis, M. Abdel-Nour, J. Mangiapane, I. Sirluck-Schroeder, I. Tattoli, R. van Dalen, D. E. Isenman, J. R. Rohde, S. E. Girardin, and D. J. Philpott. 2018. Complement C3 Drives Autophagy-Dependent Restriction of Cyto-invasive Bacteria. *Cell Host Microbe* 23: 644-652.e5.

422. Ferguson, J. S., J. J. Weis, J. L. Martin, and L. S. Schlesinger. 2004. Complement Protein C3 Binding to Mycobacterium tuberculosis Is Initiated by the Classical Pathway in Human Bronchoalveolar Lavage Fluid. *Infect. Immun.* 72: 2564–2573.

423. Liu, M., S. Guo, J. M. Hibbert, V. Jain, N. Singh, N. O. Wilson, and J. K. Stiles. 2011. CXCL10/IP-10 in infectious diseases pathogenesis and potential therapeutic implications. *Cytokine Growth Factor Rev.* 22: 121–130.

424. Alsleben, N., M. Ruhwald, H. Rüssmann, F. M. Marx, U. Wahn, and K. Magdorf. 2012. Interferon-gamma inducible protein 10 as a biomarker for active tuberculosis and latent tuberculosis infection in children: a case-control study. *Scand. J. Infect. Dis.* 44: 256–62.

425. Bhattacharyya, C., P. P. Majumder, and B. Pandit. 2018. CXCL10 is overexpressed in active tuberculosis patients compared to M. tuberculosis-exposed household contacts. *Tuberculosis* 109: 8–16.

426. Cole, A. M., T. Ganz, A. M. Liese, M. D. Burdick, L. Liu, and R. M. Strieter. 2001. Cutting Edge: IFN-Inducible ELR − CXC Chemokines Display Defensin-Like Antimicrobial Activity . *J. Immunol.* 167: 623–627.

427. Finethy, R., S. Luoma, N. Orench-Rivera, E. M. Feeley, A. K. Haldar, M. Yamamoto, T.-D. D. Kanneganti, M. J. Kuehn, and J. Coers. 2017. Inflammasome Activation by Bacterial Outer Membrane Vesicles Requires Guanylate Binding Proteins. *MBio* 8: e01188-17.

428. Sauer, J. D., S. Pereyre, K. A. Archer, T. P. Burke, B. Hanson, P. Lauer, and D. A. Portnoy. 2011. Listeria monocytogenes engineered to activate the Nlrc4 inflammasome are severely attenuated and are poor inducers of protective immunity. *Proc. Natl. Acad. Sci. U. S. A.* 108: 12419–12424.

429. Michalska, A., K. Blaszczyk, J. Wesoly, and H. A. R. Bluyssen. 2018. A positive feedback amplifier circuit that regulates interferon (IFN)-stimulated gene expression and controls type I and type II IFN responses. *Front. Immunol.* 9: 1135.

430. Briken, V., H. Ruffner, U. Schultz, A. Schwarz, L. F. Reis, I. Strehlow, T. Decker, and P. Staeheli. 1995. Interferon regulatory factor 1 is required for mouse Gbp gene activation by gamma interferon. *Mol. Cell. Biol.* 15: 975–982.

431. Li, X. Q., X. N. Li, J. J. Liang, X. Bin Cai, Q. Tao, Y. X. Li, Q. Qin, S. P. Xu, and T. R. Luo. 2018. IRF1 up-regulates isg15 gene expression in dsRNA stimulation or CSFV infection by targeting nucleotides −487 to −325 in the 5′ flanking region. *Mol. Immunol.* 94: 153–165.

432. Donovan, J., G. Whitney, S. Rath, and A. Korennykh. 2015. Structural mechanism of sensing long dsRNA via a noncatalytic domain in human oligoadenylate synthetase 3. *Proc. Natl. Acad. Sci. U. S. A.* 112: 3949–3954.

433. Ibsen, M. S., H. H. Gad, K. Thavachelvam, T. Boesen, P. Despres, and R. Hartmann. 2014. The 2'-5'-Oligoadenylate Synthetase 3 Enzyme Potently Synthesizes the 2'-5'-Oligoadenylates Required for RNase L Activation. *J. Virol.* 88: 14222–14231.

434. Liao, X., H. Xie, S. Li, H. Ye, S. Li, K. Ren, Y. Li, M. Xu, W. Lin, X. Duan, C. Yang, and L. Chen. 2020. 20, 50-oligoadenylate synthetase 2 (OAS2) inhibits Zika virus replication through activation of type I IFN signaling pathway. *Viruses* 12.

435. Zheng, S., D. Zhu, X. Lian, W. Liu, R. Cao, and P. Chen. 2016. Porcine 2′, 5′-oligoadenylate synthetases inhibit Japanese encephalitis virus replication in vitro. *J. Med. Virol.* 88: 760–768.

436. Schwartz, S. L., E. N. Park, V. K. Vachon, S. Danzy, A. C. Lowen, and G. L. Conn. 2020. Human OAS1 activation is highly dependent on both RNA sequence and context of activating RNA motifs. *Nucleic Acids Res.* .

437. Vachon, V. K., B. M. Calderon, and G. L. Conn. 2015. A novel RNA molecular signature for activation of 2-5 oligoadenylate synthetase-1. *Nucleic Acids Res.* 43: 544–552.

438. Schwartz, S. L., and G. L. Conn. 2019. RNA regulation of the antiviral protein 2′-5′-oligoadenylate synthetase. *Wiley Interdiscip. Rev. RNA* 10: e1534.

439. Lee, M. S., B. Kim, G. T. Oh, and Y. J. Kim. 2013. OASL1 inhibits translation of the type i interferon-regulating transcription factor IRF7. *Nat. Immunol.* 14: 346–355.

440. Skrivergaard, S., M. S. Jensen, T. B. Rolander, T. B. N. Nguyen, A. Bundgaard, L. N. Nejsum, and P. M. Martensen. 2019. The Cellular Localization of the p42 and p46 Oligoadenylate Synthetase 1 Isoforms and Their Impact on Mitochondrial Respiration. *Viruses* 11: 1122.

441. Michaelson, D., W. Ali, V. K. Chiu, M. Bergo, J. Silletti, L. Wright, S. G. Young, and M. Philips. 2005. Postprenylation CAAX processing is required for proper localization of ras but not Rho GTPases. *Mol. Biol. Cell* 16: 1606–1616.

442. Rath, S., E. Prangley, J. Donovan, K. Demarest, N. S. Wingreen, Y. Meir, and A. Korennykh. 2019. Concerted 2-5A-Mediated mRNA Decay and Transcription Reprogram Protein Synthesis in the dsRNA Response. *Mol. Cell* 75: 1218-1228.e6.

443. Chitrakar, A., S. Rath, J. Donovan, K. Demarest, Y. Li, R. R. Sridhar, S. R. Weiss, S. V. Kotenko, N. S. Wingreen, and A. Korennykh. 2019. Real-time 2-5A kinetics suggest that interferons β and λ evade global arrest of translation by RNase L. *Proc. Natl. Acad. Sci. U. S. A.* 116: 2103–2111.

444. Field, L. L., V. Bonnevie-Nielsen, F. Pociot, S. Lu, T. B. Nielsen, and H. Beck-Nielsen. 2005. OAS1 splice site polymorphism controlling antiviral enzyme activity influences susceptibility to type 1 diabetes. *Diabetes* 54: 1588–1591.

445. Li, H., T. R. Reksten, J. A. Ice, J. A. Kelly, I. Adrianto, A. Rasmussen, S. Wang, B. He, K. M. Grundahl, S. B. Glenn, C. Miceli-Richard, S. Bowman, S. Lester, P. Eriksson, M.-L. Eloranta, J. G. Brun, L. G. Gøransson, E. Harboe, J. M. Guthridge, K. M. Kaufman, M. Kvarnström, D. S. Cunninghame Graham, K. Patel, A. J. Adler, A. D. Farris, M. T. Brennan, J. Chodosh, R. Gopalakrishnan, M. H. Weisman, S. Venuturupalli, D. J. Wallace, K. S. Hefner, G. D. Houston, A. J. W. Huang, P. J. Hughes, D. M. Lewis, L. Radfar, E. S. Vista, C. E. Edgar, M. D. Rohrer, D. U. Stone, T. J. Vyse, J. B. Harley, P. M. Gaffney, J. A. James, S. Turner, I. Alevizos, J.-M. Anaya, N. L. Rhodus, B. M. Segal, C. G. Montgomery, R. H. Scofield, S. Kovats, X. Mariette, L. Rönnblom, T. Witte, M. Rischmueller, M. Wahren-Herlenius, R. Omdal, R. Jonsson, W.-F. Ng, G. Nordmark, C. J. Lessard, and K. L. Sivils. 2017. Identification of a Sjögren's syndrome susceptibility locus at OAS1 that influences isoform switching, protein expression, and responsiveness to type I interferons. *PLOS Genet.* 13: e1006820.

446. Fedetz, M., F. Matesanz, A. Caro-Maldonado, O. Fernandez, J. A. Tamayo, M. Guerrero, C. Delgado, J. A. López-Guerrero, and A. Alcina. 2006. OAS1 gene haplotype confers susceptibility to multiple sclerosis. *Tissue Antigens* 68: 446–449.

447. Ablasser, A., and S. Hur. 2020. Regulation of cGAS- and RLR-mediated immunity to

nucleic acids. *Nat. Immunol.* 21: 17–29.

448. Bonelli, M., K. Dalwigk, A. Platzer, I. Olmos Calvo, S. Hayer, B. Niederreiter, J. Holinka, F. Sevelda, T. Pap, G. Steiner, G. Superti-Furga, J. S. Smolen, H. P. Kiener, and T. Karonitsch. 2019. IRF1 is critical for the TNF-driven interferon response in rheumatoid fibroblast-like synoviocytes: JAKinibs suppress the interferon response in RA-FLSs. *Exp. Mol. Med.* 51: 1–11.

449. Robinson, A. P., C. T. Harp, A. Noronha, and S. D. Miller. 2014. The experimental autoimmune encephalomyelitis (EAE) model of MS. utility for understanding disease pathophysiology and treatment. In *Handbook of Clinical Neurology* vol. 122. Elsevier B.V. 173–189.

450. Constantinescu, C. S., N. Farooqi, K. O'brien, and B. Gran. 2011. Themed Issue: Translational Neuropharmacology-Using Appropriate Animal Models to Guide Clinical Drug Development Experimental autoimmune encephalomyelitis (EAE) as a model for multiple sclerosis (MS) LINKED ARTICLES. .

451. McGeachy, M. J., Y. Chen, C. M. Tato, A. Laurence, B. Joyce-Shaikh, W. M. Blumenschein, T. K. McClanahan, J. J. O'Shea, and D. J. Cua. 2009. The interleukin 23 receptor is essential for the terminal differentiation of interleukin 17-producing effector T helper cells in vivo. *Nat. Immunol.* 10: 314–324.

452. Sievers, F., A. Wilm, D. Dineen, T. J. Gibson, K. Karplus, W. Li, R. Lopez, H. McWilliam, M. Remmert, J. Söding, J. D. Thompson, and D. G. Higgins. 2011. Fast, scalable generation of high-quality protein multiple sequence alignments using Clustal Omega. *Mol. Syst. Biol.* 7.

453. Johnsen, Ø., P. Murphy, H. Prydz, and A.-B. Kolstø. 1998. *Interaction of the CNC-bZIP factor TCF11/LCR-F1/Nrf1 with MafG: binding-site selection and regulation of transcription*,.

454. Varshney, D., A.-P. Petit, J. A. Bueren-Calabuig, C. Jansen, D. A. Fletcher, M. Peggie, S. Weidlich, P. Scullion, A. V Pisliakov, and V. H. Cowling. 2016. Molecular basis of RNA guanine-7 methyltransferase (RNMT) activation by RAM. *Nucleic Acids Res.* 44: 10423–10436.

455. Plaschka, C., L. Larivière, L. Wenzeck, M. Seizl, M. Hemann, D. Tegunov, E. V. Petrotchenko, C. H. Borchers, W. Baumeister, F. Herzog, E. Villa, and P. Cramer. 2015. Architecture of the RNA polymerase II-Mediator core initiation complex. *Nature* 518: 376–380.

456. Takagi, Y., G. Calero, H. Komori, J. A. Brown, A. H. Ehrensberger, A. Hudmon, F. Asturias, and R. D. Kornberg. 2006. Head Module Control of Mediator Interactions. *Mol. Cell* 23: 355–364.

457. Fensterl, V., and G. C. Sen. 2015. Interferon-Induced Ifit Proteins: Their Role in Viral Pathogenesis. *J. Virol.* 89: 2462–2468.